CRANFIELD UNIVERSITY

EGBIGENIBO GENUINE SATURDAY

HOT SECTION COMPONENTS LIFE USAGE ANALYSES FOR INDUSTRIAL GAS TURBINES

SCHOOL OF AEROSPACE, TRANSPORT AND MANUFACTURING

PROPULSION ENGINEERING CENTRE

PhD
Academic Year: 2014 - 2015

Supervisor: DR. YI-GUANG LI

November 2015

CRANFIELD UNIVERSITY

SCHOOL OF AEROSPACE, TRANSPORT AND MANUFACTURING

PROPULSION ENGINEERING CENTRE

PhD

Academic Year: 2014 - 2015

EGBIGENIBO GENUINE SATURDAY

HOT SECTION COMPONENTS LIFE USAGE ANALYSES FOR INDUSTRIAL GAS TURBINES

Supervisor: DR. YI-GUANG LI

November 2015

ABSTRACT

Industrial gas turbines generally operate at a bit stable power levels and the hot section critical components, especially high pressure turbine blades are prone to failure due to creep. In some cases, plants are frequently shut down, thus, in addition to creep low cycle fatigue failure equally sets in. Avoiding failure calls for proper monitoring of how the lives of these components are being consumed. Efforts are thus being made to estimate the life of the critical components of the gas turbine, but, the accuracy of the life prediction methods employed has been an issue. In view of the above observations, in this research, a platform has been developed to simultaneously examine engine life consumption due to creep, fatigue and creep-fatigue interaction exploiting relative life analysis where the engine life calculated is compared to a reference life in each failure mode. The results obtained are life analysis factors which indicate how well the engine is being operated.

The Larson-Miller Parameter method is used for the creep life consumption analysis, the modified universal slopes method is applied in the low cycle fatigue life estimation while Taira's linear accumulation method is adopted for creep-fatigue interaction life calculation. Fatigue cycles counting model is developed to estimate the fatigue cycles accumulated in any period of engine operation. Blade thermal and stress models are developed together with a data acquisition and pre-processing module to make the life calculations possible. The developed models and the life analysis algorithms are implemented in PYTHIA, Cranfield University's in-house gas turbine performance and diagnostics software to ensure that reliable simulation results are obtained for life analysis.

The developed life analysis techniques are applied to several months of real engine operation data, using LM2500+ engine operated by Manx Utilities at the Isle of Man to test the applicability and the feasibility of the methods. The developed algorithms provide quick evaluation and tracking of engine life. The lifing algorithms developed in this research could be applied to different engines. The relative influences of different factors affecting engine life consumption were investigated by considering each effect on engine life consumtion at different engine operation conditions and it was observed that shaft power level has significant impact on engine life consumption while compressor degradation has more impact on engine life consumption than high pressure turbine degradation. The lifing methodologies developed in this work will help engine operators in their engine conditions monitoring and condition-based maintenance.

DEDICATION

This work is firstly dedicated to the Knowledge Reservoir (The Almighty God) through whom knowledge flows to all beings who seek for it, and secondly to the Memory of my Dad, Mr. Saturday, E. Ayemi, who never lived to see this day after severally praying for me to have good success in my PhD programme.

ACKNOWLEDGEMENTS

I am very grateful to the Almighty God for the gift of life and for giving me the grace to carry on with my PhD research to its conclusion. May His Name alone be praised.

My sincere thanks go to my supervisor, Dr. Yi-Guang Li, for giving me the necessary guidance and assistance throughout my PhD programme. Many thanks are also due to Prof. Pericles Pilidis and every other staff of the Propulsion Engineering Centre. Severall staff at the IT department is appreciated also.

I am also very thankful to the Niger Delta Development Commission (NDDC), Nigeria for providing me with part sponsorship for my PhD programme. Same thanks are due to the Manx Utilities (MU), Isle of Man, for part sponsorship of my research and also providing me with the industrial platform for my research. In the above regards, I wish to thank my big uncle, Mr. Lambert E. J. Konboye (former Executive Director of Finance and Administration, NDDC), Mr. Mike Newby, Plant Engineering Manager, Generation Division, MU, Mr Graham Stigant, Efficiency Engineer, MU, Mr. John Harper and many other staff of Pulrose Power Station, MU, who provided me with relevant information in the course of my PhD research.

Special thanks are due to my Pastor here in the UK at RCCG, NewGate Parish, Bedford, Pastor Olufemi Awoleye, for his prayers and sense of direction. Every other members of the church are acknowledged. Same thanks are due to the General Overseer of my home church, Miracle Life Bible Church, Okpokunou, Pastor Abednego Okorodas, and every other brethren. I wish to express my sincere gratitude to other PhD students I met at Cranfield University. To Dr. Diemuodeke, E. O. I say a very big thank you for giving me great introduction to Bedford/Cranfield University and making me felt at home. Drs. Abdullahi Obonyegba Abu, Isaiah Allison and Ebi Austin Ogiriki, all of the Nigerian military deserve special thanks; I am grateful to you all. I also extend my gratitude to my students and colleagues in the University of Port Harcourt, acquaintance and friends back in Nigeria for your wonderful wishes.

To my parents, siblings and other family members, I say many thanks for your prayers and great wishes. Your good thoughts towards me are properly acknowleged. Finally, I wish express my heartfelt and sincere gratitude to my amiable, beautiful, caring and loving wife, Pereokosuafa for your understanding, care, love and prayers. Your unparalleled show of love and understanding led to the success in my research. My son, Ebipade (Ebison) who just arrived gave me tremendous joy and additional zeal in the defence of my PhD degree. You came at the right time and Daddy sincerely appreciates and loves you.

PUBLICATIONS

E.G. Saturday, Y. G. Li, E.A. Ogiriki, M. Newby and G. Stigant," Creep Life Usage Analysis and Tracking for Industrial Gas Turbine", Journal of Propulsion and Power, AIAA, Submitted for Publication.

E.G. Saturday, Y. G. Li and E.A. Ogiriki, "Effects of Ambient Temperature, Shaft Power and Degradation on Creep Life Consumption of Industrial Gas Turbine Blades", In Preparation.

Ebi A Ogiriki, Yiguang G Li, Theoklis Nikolaidis and Ebigenibo G Saturday, "Prediction of Environmental Effects on Gas Turbine Engine Creep Life", Proceedings of the Institution of Mechanical Engineers, Part O: Journal of Risk and Reliability, Submitted for Publication.

E.G. Saturday and Y. G. Li, "Development and Application of Fatigue Cycles Accumulation Model for Industrial Gas Turbines Operation", In Preparation.

E.G. Saturday and Y. G. Li, "Low Cycle Fatigue Life Estimation and Tracking for Industrial Gas Turbine Components Using Fatigue Factor Approach", In Preparation.

TABLE OF CONTENTS

LIST OF FIGURES

LIST OF TABLES

LIST OF SYMBOLS

Symbol	Description
A_{cs}	Cross-sectional area of blade
A_n	Total annulus flow area of the gases
$A_{n,\sec i}$	Annulus area of the blade section
B_{ht}	Blade mean height
BM_A	Bending moments on the turbine (machine) axial direction
BM_T	Bending moments on the turbine (machine) tangential direction
$BM_{P,i}$	Sum of the pressure change bending moments about the base of section i
BM_{XX}	Bending moments on the blade axial direction
BM_{YY}	Bending moments on the blade tangential direction
$BM^V_{Ax,i}$	Sum of the velocity change bending moments in the axial axis of the turbine
$BM^V_{T,i}$	Sum of the velocity change bending moments in the tangential axis of the turbine
C	Constant in LPM method
CF_{CE}	Creep factor of clean engine
CF_{DE}	Creep factor of degradaed engine
CFF_{CE}	Creep-fatigue factor of clean engine
CFF_{DE}	Creep-fatigue factor of degradaed engine
CFF	Creep-fatigue interaction factor
$CL_{\mathrm{Re}f}$	Creep life at reference engine operation point
$C_{p,g}$	Specific heat capacity of hot gases
$C_{p,m}$	Specific heat capacity of mixture of gases at blade exit
C_{p_ca}	Specific heat capacity of the cooling air
D	Damager parameter representing sum of life fractions
D_c	Creep damage parameter
$D_{c,\mathrm{Re}f}$	Creep life damage parameter at a reference engine operation point
D_{c+f,d_j}	Sum of creep and fatigue damage parameters for j days of engine operation
$D_{c+f,i}$	Sum of creep and fatigue damage parameters at the i^{th} point of engine operation
$D_{c+f,s}$	Sum of creep and fatigue damage parameters for a given period
D_f	Fatigue damage parameter
$D_{f,i}$	Fatigue damage parameter at the i^{th} point of engine operation
$D_{f,\mathrm{Re}f}$	Fatigue damage parameter at a reference engine operation point
$D_{f,s}$	Sum of fatigue damage parameters for a given period of engine operation

D_{f,d_j}	Sum of fatigue damage parameters for j days of engine operation
$D_{f,ti}$	Sum of fatigue damage parameters for time t_i of engine operation
E	Young's Modulus
ECL_{Tot}	Equivalent creep life at total time of engine operation
FoS	Factor of safety
$F_{\sec i}$	Centrifugal force at blade section i
$F_{P,\sec i}$	Pressure change force on each section of the blade
$F^{V}_{Ax,\sec i}$	Axial velocity change force at section i of the blade
$F^{V}_{T,\sec i}$	Tangential velocity change force at section i of the blade
G	Stands for any of LE, TE and SB
I	Second moment of area about neutral axis
I_{XX}	Second moment of area about the blade axial direction. The same as I_{MAX}
I_{YY}	Second moment of area about the blade tangential direction. The same as I_{MIN}
M	Bending moment about neutral axis; Mach number
M_{Guess_ex}	Guess Mach number satisfying non-dimensional flow condition at blade exit
M_{Guess_in}	Guess Mach number satisfying non-dimensional flow condition at blade inlet
$M_{P,i}$	Pressure bending moment about the base of section i
$M^{V}_{Ax,i}$	Bending moment of the velocity change force about the base of section i of the blade about the turbine axial axis
$M^{V}_{T,i}$	Tangential counterpart of $M^{V}_{Ax,i}$
N	Rotational speed of the compressor shaft (in rpm); Stress Cycles
N_b	Number of blades
$\overline{N}_a$	Mean number of fatigue cycles accumulated in a given period of engine operation
$N_{a,\mathrm{Re}f}$	Fatigue cycles accumulated at a reference engine operation point
N_d	Design speed of engine performance model
N_{eq}	Equivalent fatigue cycles
$N_{eq,a}$	Equivalent fatigue cycles accumulated in a given period of engine operation
$N_{eq,j}$	Equivalent fatigue cycles accumulated in j days of engine operation
N_f	Fatigue life
$2N_f$	Stress reversals
$N_{f,eq}$	Equivalent fatigue cycles to failure
$N_{f,i}$	Number of cycles to failure corresponding to the i^{th} block of load
$N_{f\_j,i}$	Number of cycles to failure for the j^{th} day and at the i^{th} operation point
$N_{f,\mathrm{Re}f}$	Fatigue cycles to failure at a reference engine operation point

$N_{f,\mathrm{Re}\,f}$	Number of cycles to failure at a reference point
N_f^{creep}	Number of cycles to failure under creep
$N_f^{fatigue}$	Number of cycles to failure under fatigue
$N_f^{oxidation}$	Number of cycles to failure under oxidation
$\overline{N}_{j,i}$	Mean value of equivalent cycles for the j^{th} day and at the i^{th} operation point
N_s	Compressor shaft rotational speed at a set power level
NGV_{PR}	Nozzle guide vane pressure recovery
Nu_g	Nusselt number of the gas
Nu'_g	Nominal mean Nusselt number
$Nu_{g,\mathrm{sec}\,i}$	Nusselt number of gas at section i of the blade
OT_{Tot}	Total time of engine operation
PCN	Relative rotational speed of the compressor shaft
PD_{CF}	Percentage decrease in creep factor
PD_{CF_m}	Mean percentage decrease in creep factor
PD_{CFF}	Percentage decrease in creep-fatigue factor
PD_{FF}	Percentage decrease in fatigue factor
P_{ex}	Total pressure at turbine exit
P_{in}	Total pressure at turbine inlet
$P_{in,i}$	Total pressure at stage i of turbine inlet
$P_{\mathrm{sec}\,i}$	Perimeter of blade section
ΔP_{cc}	Combustor pressure loss
$\dot{Q}_{in}$	Energy input to the blade
$\dot{Q}_{out}$	Energy removed from blade
R	Ratio of $\sigma_{\min}$ to $\sigma_{\max}$; Gas constant
Re_g	Reynolds number of hot gases
R_{btp}	Blade tip radius
R_{brt}	Blade root radius
$R_{LE,Rt}$	Leading edge root radius
$R_{LE,Tip}$	Leading edge tip radius
$R_{TE,Rt}$	Trailing edge root radius
$R_{TE,Tip}$	Trailing edge tip radius
SB	Furthest point at the suction side of blade
T	Temperature in Kelvin

T_{bm}	Bulk temperature of the blade material
T'_{bm}	Bulk temperature of the blade material with TBC
T_{Bur_In}	Burner inlet temperature
T_{Bur_Mean}	Burner mean exit temperature
T_{c_in}	Coolant flow inlet temperature
T_{c_ex}	Coolant flow exit temperature
T_{dp_stg}	Temperature drop per stage
T_{ex}	Temperature at exit of turbine stage
T_{Exit_i}	Temperature at the exit of stage i
T_g	Bulk gas temperature
$T_{g,ex}$	Gas temperature at exit of turbine stage
$T_{g,i}$	Gas temperature at node i of blade
$T_{g,\sec i}$	Gas temperature at section i of blade
$T_{\max}$	Maximum gas temperature
$T_{\min}$	Minimum gas temperature
$T_{m,i}$	Temperature of the blade material at node i
$T'_{m,i}$	Temperature of the blade material at node i for blades with TBC
$T_{m,\sec i}$	Temperature of the blade material at section i
$T'_{m,\sec i}$	Temperature of the blade material at section i for blades with TBC
T_{NGV}	Nozzle guide vane temperature
T_o	Reference temperature in Kelvin (in dynamic viscosity estimation)
T_{tbc_s}	TBC material surface temperature
$T_{tbc,\sec i}$	TBC material surface temperature at section i
$T^c_{ex,i}$	Coolant exit temperature at stage i
$T^c_{In,i}$	Coolant inlet temperature at stage i
$T^c_{ex\_NGV,i}$	NGV coolant exit temperature at stage i
$T^c_{in\_NGV,i}$	NGV coolant inlet temperature at stage i
$T^g_{ex\_NGV,i}$	Temperature of gas at NGV exit in stage i
$T^g_{ex,i}$	Temperature of gas at blade exit, stage i
$T^g_{in\_B}$	Temperature of gas at blade inlet, first stage
$T^g_{in,i}$	Temperature of gas at blade inlet, stage i
$T^g_{in\_NGV,i}$	Temperature of gas at NGV inlet in stage i

ΔT_{cc}	Combustor temperature loss
U_{ex}	Blade speed at exit
U_{in}	Blade speed at inlet
V_{Abs_ex}	Absolute speed of gas at blade exit
V_{Abs_in}	Absolute speed of gas at blade inlet
V_{Ax_ex}	Axial velocity of gas at blade exit
V_{Ax_in}	Axial velocity of gas at blade inlet
V_{ω_ex}	Whirl velocity of gas at blade exit
V_{ω_in}	Whirl velocity of gas at blade inlet
ΔV_{Ax}	Change in axial velocities of gas
$\Delta V_{T,\sec i}$	Change in tangential or whirl velocities of gas at section i of the blade
$X_{G,i}$	Distance from centre of gravity in the axial direction at blade section i to blade location defined by G
$Y_{G,i}$	Distance from centre of gravity in the tangential direction at blade section i to blade location defined by G
atm	Atmosphere
b	Fatigue strength exponent or Basquin exponent
c	Fatigue ductility exponent; blade chord
c_{Seci}	Chord of each blade section
$h_{CG,i}$	Distance from centre of gravity of blade section i to the turbine axis of rotation
h_g	External heat transfer coefficient
$h_{g\,'\sec i}$	External heat transfer coefficient at section i of blade
$h_{\sec}$	Height of each blade section
$h_{n,i}$	Distance from node i to the turbine axis
k	Cycles determining exponent
k_g	Thermal conductivity of gas
$k_{g,Seci}$	Thermal conductivity of gas at given blade section
k_{tbc}	Thermal conductivity of TBC material
l_{Seci}	Height of blade section
$\dot{m}_{c\_B}$	Mass flow rate of the cooling air for cooling each blade
$\dot{m}_{ca}$	Total mass of cooling air
$\dot{m}_{c\_NGV}$	Mass flow rate of the cooling air for cooling NGV
$\dot{m}_f$	Mass flow rate of fuel
m_{f_B}	Mass fraction of air for blade cooling

$m^{g}_{f\_in}$	Mass fraction of hot gases at blade NGV exit
m_{f_NGV}	Mass fraction of air for NGV cooling
$m^{c}_{f\_NGV}$	Mass fraction of air at NGV exit for mixing chamber
$\dot{m}_{t\_in}$	Mass flow rate of gases at turbine inlet
$m_{\sec i}$	Mass of section i of blade
$\dot{m}_{sp}$	Specific mass flow rate of the gases
m^*	Coolant mass flow function
m^*_{NGV}	NGV coolant mass flow function
n	Number of stages
n_i	Number of cycles corresponding to the ith block of load
p	Static pressure
p_{in}	Static pressure at the inlet of each blade stage
p_{ex}	Static pressure at the exit of each blade stage
Δp	Change in the static pressure across the rotor stage
t_{ex}	Static temperature at turbine exit
t_f	Stress rupture time or time to creep failure
$t_{f,i}$	Time to creep failure at the ith engine operation point
$t_{f,\mathrm{Ref}}$	Time to creep failure at a reference operation point
t_{ff}	Time to fatigue failure
$t_{ff,d}$	Time to fatigue failure in days of engine operation
$t_{ff,eq}$	Equivalent time to fatigue failure for given periods of engine operation
$t_{ff,h}$	Time to fatigue failure in hours of engine operation
$t_{ff,\mathrm{Ref}}$	Time to fatigue failure at a reference engine operation point
$t_{f,c+f}$	Time to creep-fatigue interaction failure
$t_{f,c+f\_d}$	Time to creep-fatigue interaction failure in days of engine operation
$t_{f,c+f\_eq}$	Equivalent time to creep-fatigue interaction failure for given periods of engine operation
$t_{f,c+f\_h}$	Time to creep-fatigue interaction failure in hours of engine operation
$t_{f,c+f\_\mathrm{Ref}}$	Time to creep-fatigue interaction failure at a reference operation point
$t_{h,j}$	Number of hours engine was operated in day j
$\bar{t}_h$	Mean number of hours the engine was operated in a number of days
t_i	Engine operation time at the ith operation point
$t_{i,\mathrm{Ref}}$	Engine operation time at reference operation point
x	Reynolds number exponent in Nusselt number estimation

y	Temperature exponent in Nusselt number estimation
ε_c	Creep strain
$\dot{\varepsilon}_c$	Creep strain rate
ε_{ff}	Overall cooling effectiveness
ε_{ff_NGV}	NGV cooling effectiveness
ε_f	True fracture ductility
ε'_f	Fatigue ductility coefficient
$\Delta\varepsilon$	Total strain range
$\frac{\Delta\varepsilon}{2}$	Total strain amplitude
$\frac{\Delta\varepsilon_e}{2}$	Elastic strain amplitude
$\frac{\Delta\varepsilon_p}{2}$	Plastic strain amplitude
η_c	Convection cooling efficiency
η_{cc}	Combustion efficiency
η_{c_NGV}	NGV convection cooling efficiency
η_{ci}	Compressor isentropic efficiency
η_{CTi}	Compressor turbine isentropic efficiency
η_p	Polytropic efficiency
η_{PTi}	Power turbine isentropic efficiency
θ	Blade stagger angle
κ	A constant, equivalent to $m_{\text{sec}} \times \omega^2$
ρ	Density of the blade material
ρ_g	Density of hot gases
σ	Bending stress
σ_a	Stress amplitude
σ'_a	Alternating stress amplitude at zero mean stress
σ_{CF}	Centrifugal stress
$\sigma^i_{CF,d}$	Centrifugal stress at each blade node for the i^{th} data point
$\sigma^S_{CF,d}$	Centrifugal stress at each blade node for a set speed level
σ_e	Endurance limit or fatigue limit
$\sigma^{Tot}_{G,i}$	Total stress at a specified location denoted by G
$\sigma^{BM}_{G,i}$	Bending moment stress at a specified location denoted by G
σ_m	Mean stress

$\sigma_{\max}$	The maximum stress in the given load spectrum
$\sigma_{Max,i}$	Maximum stress at node i of blade
$\sigma_{\min}$	The minimum stress in the given load spectrum
$\sigma_{Tot,d}^{i}$	Total stress at each blade node for the i^{th} data point
$\sigma_{Tot,d}^{S}$	Total stress at each blade node for a set speed level
σ_u	Ultimate tensile strength
σ_y	Yield strength
$\Delta\sigma$	Stress range
σ'_f	Fatigue strength coefficient
ϕ_{NGV}	NGV coolant mass percentage
ω	Angular speed of the compressor shaft
α_2	Gas flow angle at blade exit
β_1	Blade inlet angle
β_{ex}	Blade exit angle
γ_g	Ratio of specific heat capacities of hot gases
μ_o	Reference dynamic viscosity
μ_{ex}	Dynamic viscosity of gas at blade exit

LIST OF ABBREVIATIONS

ASME	American Society of Mechanical Engineers
CCGT	Combined Cycle Gas Turbine
CDM	Continuum Damage Mechanics
CE	Clean Engine
CF	Creep Factor
CG	Centre of Gravity
CL	Creep Life
DE	Degraded Engine
DOD	Domestic Object Damage
DT	Destructive Testing
ECCFF	Equivalent Cycles to Creep-Fatigue Failure
ECF	Equivalent Creep Factor
ECFF	Equivalent Creep-Fatigue Factor
ECFL	Equivalent Creep-Fatigue Life
ECL	Equivalent Creep Life
EFF	Equivalent Fatigue Factor
ENSIP	Engine Structural Integrity Program
ETCFF	Equivalent Time to Creep-Fatigue Failure
FCR	Flow Capacity Reduction
FEA	Finite Element Analysis
FF	Fatigue Factor
FOD	Foreign Object Damage
GSP	Goldhoof-Sherby Parameter
GT	Gas Turbine
HCF	High Cycle Fatigue
HOT	Higher Order Terms
HP	High Pressure
HPT	High Pressure Turbine
ISA	International Standard Atmosphere
LCF	Low Cycle Fatigue
LDA	Linear Damage Accumulation

LHS	Left Hand Side
LE	Leading Edge
LF	Life fraction
LMP	Larson Miller Parameter
MEA	Manx Electricity Authority
MHP	Mason-Haferd Parameter
MPC	Material Properties Countil
MSP	Manson-Succop's Parameter
MU	Manx Utilities
NDI	Non-Destructive Inspection
NDT	Non-Destructive Testing
NGV	Nozzle Guide Vanes
ODTM	One-Dimemsional Temperature Model
OECFF	Overall Equivalent Creep-Fatigue Factor
OEFF	Overall Equivalent Fatigue Factor
OSDP	Orr-Sherby-Dorn Parameter
OT	Operation Time
OTDF	Overall Temperature Distribution Factor
PR	Pressure Ratio
RHS	Right Hand Side
RL	Remaining Life
RMS	Root Mean Square
RTDF	Radial Temperature Distribution Factor
SC	Single Crystal
TBC	Thermal Barrier Coating
TE	Trailing Edge
TET	Turbine Entry Temperature
TMF	Thermo-Mechanical Fatigue
UTM	Uniform Temperature Model

1 INTRODUCTION

1.1 Preamble

The gas turbine engine is an internal combustion engine and has found usage in three major areas, viz: military aviation, civil aviation, and power generation. In this regard, gas turbines (GTs) are classified as aircraft GTs and industrials GTs. Gas turbine which produces high amount of power for its size has broader applications. The gas turbine engine has found increasing usage in power industry, both among utilities and merchant plants as well as the petrochemical industries, marine and land transportation, and many other services throughout the world. The gas turbine is able to run with variety of fuels such as natural gas, diesel fuel, low-Btu gases, vapourized fuel oils and biomass gases [1], [2].

A brief history of this prime mover as presented by Razak [3] is necessary here. A first attempt at producing a gas turbine is credited to Englishman, John Barber in 1791. Although Barber's engine was not robust, it paved the way for many further researches. Aegiclius Elling, a Norwegian, built the first successful gas turbine in 1903. In 1930, Englishman, Frank Whittle had a patent for his gas turbine engine meant to be used on a jet. In 1936, Hans Von Ohan and Max Hahn equally developed and patented their design in Germany. A similar historical account [4] of the gas turbine engine also credited its origin to John Barber, but views a Slovak engineer, physicist and inventor, Prof. Aurel Stodola (1859-1942) as the man behind the early steam and gas turbine.

The gas turbine engine operates on the Brayton cycle, which is a closed cycle. Practical operating cycle of 'internal combustion' gas turbine is the Joule cycle [5]. Figure 1.1 shows the T-S diagrams of gas turbine operating cycles of a single spool engine. Most gas turbines operate on the open cycle basis. Different configurations of the gas turbine engine are available today. Some of these configurations are turboshaft- for electric power generation, turbojet, turboprop, high-bypass turbofan, low-bypass afterburning turbofan, etc. [6], [7].

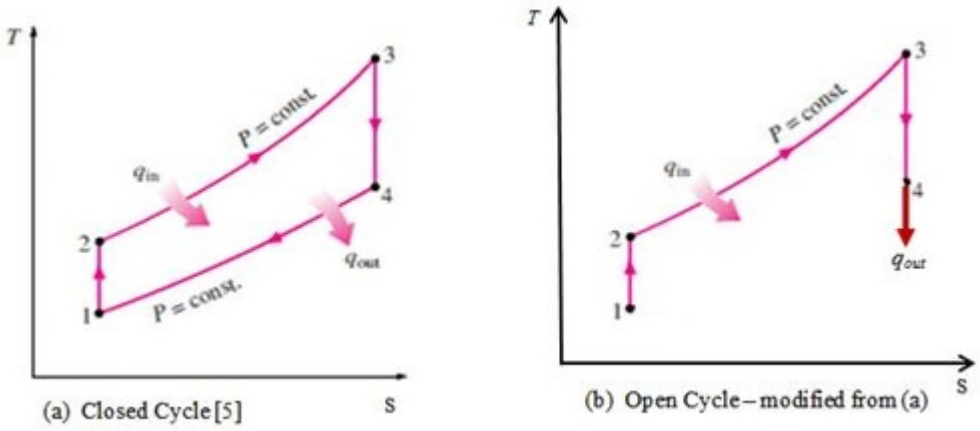

Figure 1.1: T-S Diagrams of Gas Turbine Engines ([5], pp.508)

The Brayton cycle engine in Figure 1.1 consist of a single shaft and it is referred to as simple cycle engine. This engine has been largely modified. The major modifications have led to regeneration cycle, cycle with intercooling, cycle with reheat and cycle with combination of any two of the three modification and all the three modifications combined [5], [7]. The gas turbine engine is also combined with a steam turbine for more efficient power generation; providing more power from steam turbines little additional fuel burnt. The resulting engine is the combined cycle plant [1], [5], [7]. Figure 1.2 shows the pictorial views of two different GT engines.

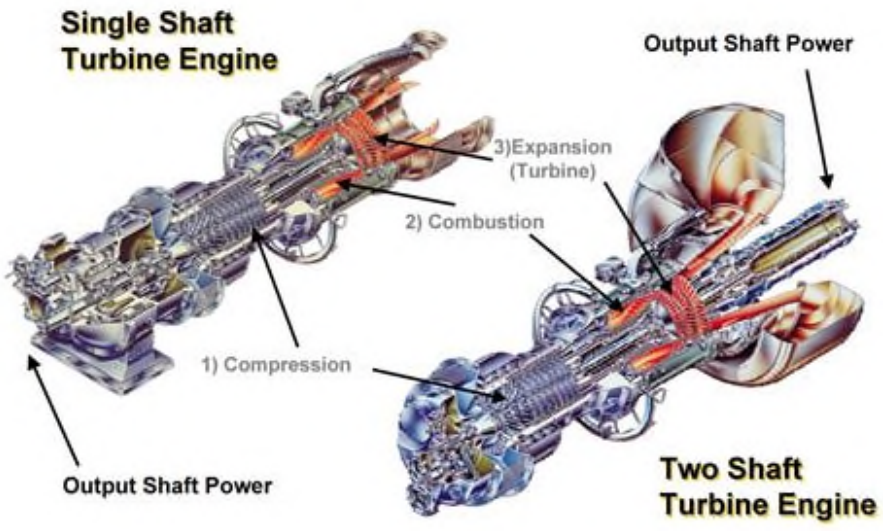

Figure 1.2: Various Gas Turbine Engines ([8] , pp.5)

In industrial applications, gas turbines are used for base load operation (continuous operation- operates for 6,000-8000 hours per year), peak load operation (operates during peak power demand period in the day- operates about 1,000 hours per year) or on stand-by basis where it is operated for less than 100 hours per year [8].

This work has to do with a two spool engine for combined cycle application. Manx Utilities' Pulrose power station combined cycle gas turbine (CCGT) is the focus here. Figure 1.3 shows a pictorial view of the steam generating unit of the plant [9]. The power station with a total output of 87 MW is located in the Isle of Man (an island between Great Britain and Ireland). The plant is being run by Manx Utilities (formerly by Manx Electricity Authority (MEA)) on behalf of the government and it comprises two 32MW gas turbines- GE's LM2500+ engines, in a combined cycle with a steam turbine which produces additional 23 MW of electricity [9]. At ISA conditions, the power output of each gas turbine is less than 32 MW. The power generated is used to service the island and the excess is sold to England. The possibility of monitoring the life consumption of the gas turbines in the station is the focus of this research. The basic performance parameters of the LM2500+ engine at 60Hz, sea level ISA condition is given in Table 1.1. More properties about the plant relating to engine operation results over time are explored in subsequent chapters.

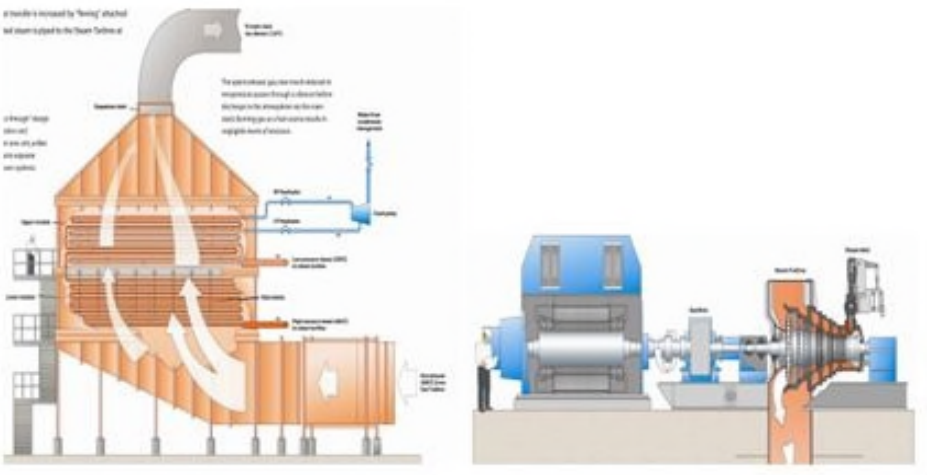

(a) Once through Steam Generator **(b) Steam Generator**

Figure 1.3: Pulrose Power Station Combined Cycle Gas Turbine- Steam Generating Unit ([9], p.22)

Table 1.1: Basic Engine Performance Parameters at Sea Level ISA condition [10]

S/N	Parameter	Unit	Value
1	Power Output	MW	30.2
2	SFC	g/kW-hr	212
3	Heat Rate	kJ/kWs-hr	9227
4	Exhaust Gas Flow	kg/s	85.9
5	Exhaust Gas Temperature	^{o}C	518
6	Power Turbine Speed	rpm	3600

The major advantage of the gas turbine engine over reciprocating engines is its high power to size ratio while high fuel cost is a major draw-back. But, the fact that the engine can operate on variety of fuels makes it attractive-although, the accompanying environmental effects should be considered in engine design, selection and usage [11]. Thermal output, fuel flexibility, reliability and life, size range and emissions are major design characteristics in gas turbines [11].

When operating on natural gas and the components (compressor, combustor and turbine) are working properly, relatively high efficiencies can be obtained, but, issues of degradation should be of concern to the operators especially. As in all human creations, nothing will last forever. Thus, how long will the gas turbine be in operation or how long some component of the engine will be in operation before they are replaced is good considering. For aircraft applications, the issue of lifing (process of determining the life of a component) is critical because any failure involves a catastrophe. In industrial application, lifing is still important as some practices involve replacing a component that still has reasonable useful life. This is cost on the part of the operators. Maintenance also involves cost. Too frequent maintenance with a view to avoiding failure implies waste of funds. Appropriate lifing techniques will lead to the application of proper maintenance schedule, avoid the disposal of useful components and avoiding failure at the same time [12], [13].

Another critical issue in managing industrial gas turbines is to consider running the machine at peak load condition or running at part load. Load has much negative influence on life [14], but high load means more income. Dropping load (shaft power)

in order to extend blade life may be contemplated. The influences of other engine operating conditions (such as ambient temperature and engine degradation) on engine life are also of interest to both the engine manufacturers and engine operators. The extent to which engine life is affected due to shaft power increase will be different at different power levels. But the effect of shaft power increase on engine life is often investigated at agiven ambient temperature level. Also, a degraded engine will lead to engine life comsumption faster but the rate depends on the power level and the ambient temperature considered. The effect of engine degradation on engine life is also often considered at a given power level and ambient temperature. Knowledge of how engine life consumption changes with degradation at different power levels and ambient temperatures will give engine operators a broader outlook of engine life consumption and this will help them in their condition-based maintenance decisions. Engine life estimation requires thermal and stress analysis employing Finite Element Analysis (FEA) and Computational Fluid Dynamics (CFD) tools, but the usage of these tools which are costly do not always give satisfactory results [15].

In the light of the above observations, it is paramount to investigate how the lives of failure-prone (critical) components of GT plants are being consumed. Different failure modes are in existence. The hot section components of gas turbines are more prone to failure under creep, one of the failure modes. In this work, the creep life of high pressure gas turbine blades is considered. Low cycle fatigue life and the creep-fatigue interaction are investigated also in this work. Since creep is the major failure mode while creep-fatigue interaction poses more danger, the influence of various operating conditions on the deviation of creep results from creep-fatigue interaction are examined. In essence, factors that warrant creep life estimation without considering creep-fatigue interaction life consumption are investigated. Ambient temperature, shaft and engine degradation affect engine life consumption as earlier pointed out. The effect of shaft power on engine life consumption is investigated at different ambient temperature levels in this work. The effect of ambient temperature on engine life consumption is also investigated at different power levels in this work. Finally, the effect of engine degaradtion on engine life consumption is investigated at different power levels and ambient temperatures. The above three sets of investigations are applied to each failure mode and this will provide relevant life-related results for engine operators.

Since continuous life consumption monitoring is envisaged and the usage of FEA and CFD tools (which though do not always give satisfactory results, but do give more accurate results) is not feasible, the life estimated in each failure mode should be compared with the life obtained at a reference engine operating condition, where the reference life is also estimated using the same models at a defined operating condition. The resulting relative life which is dimensionless will tell the degree of wellness of engine operation. The results obtained are based on the actual operating conditions of the engine for any given period of engine operation. Life analysis methodologies are thus developed in this research to help engine operators in making their condition-based engine maintenance decisions and make engine life monitoring/tracking feasible.

1.2 Aim and Objectives of the Research

The life of a gas turbine is of concern to both the designer/manufacturer and the operators of this machine. The aim of this work is thus to study and develop appropriate engine life estimation methods and apply same to industrial gas turbine hot section blades by making use of direct engine measurement data and make engine life tracking feasible and in less time, but at low cost to the operators of the engines. To achieve the above aim, appropriate lifing techniques are explored and same are applied to the LM2500+ engines operated by Manx Utilities at Pulrose Power Station, Isle of Man as a case study to investigate simultaneously different engine life consumption modes. The creep life consumption of the engine is carried out and a means of tracking the engine life is made possible. Further tasks are:

- To carry out low cycle fatigue life analysis on the engine.
- To carry out combined creep-fatigue interaction and see how results deviate from creep life in isolation in different engine operation conditions.

To ensure engine operators are aware of how engine life is being consumed at different conditions of engine operation, the effect of shaft power on engine life consumption is investigated at different ambient temperatures, the effect of ambient temperature on engine life consumption is investigated at different ambient temperatures while the effect of engine degradation on engine life consumption is investigated at different shaft power levels and ambient temperatures. Relative life analysis is carried out in each failure mode so that without too much reliance on the accuracy of the engine life

estimated at any engine operation period, engine operators will still have a better view of how engine life is consumed over any given period of engine operation in relation to a reference life (where reference life is also estimated using same algorithms at a particular operating condition of the engine). The life analysis will reveal how the engine life is being consumed and the dependence of life on engine operation properties. Also, the deviations of creep results from creep-fatigue interaction with engine operation conditions are obtained. The life analysis techniques are implemented into Cranfield in-house software, PYTHIA [16] (to obtain a new platform for appropriate engine life prediction) to ensure simultaneous estimation of the different life consumption modes of the high pressure turbine (HPT) blades of the engine, make engine life tracking feasible and quickly, and thus explore the possibility of extending the time between overhaul of hot section components.

1.3 Importance of the Research

The gas turbine is an expensive engine and effort should be made to extend its life. The extension of the life of a gas turbine means extending the life of its components (mainly the critical components) and this involves developing meaningful life trend and an aging characteristic for each material[17]. Proper engine life estimation and tracking will ensure that the life of the critical components of the engine are known and replacement of parts is carried out as at when due. Overestimation of engine life is detrimental; also, underestimation will lead to premature replacement of parts. Both ends are undesirable and imply undue costs to the operators. This work thus seeks to address this in the operation of industrial gas turbines. By ensuring simultaneous estimation of the life of critical components using different failure criteria, this work will thus give room for proper usage of lifing results. Although this work is targeted at the LM2500+ engines operated by Manx Utilities at Isle of Man, the developed models and adopted methodologies could be applied to other existing engines easily for appropriate life estimation and engine life tracking.

1.4 Scope and Limitations of the Research

The importance of predicting accurate life of gas turbines may lead one to explore all possible life deformation modes and relevant life estimation models in each failure mode. But this work is limited to

- Creep life analysis using Larson-Miller Parametric Method
- Low cycle fatigue life analysis using the Modified Universal Slopes Method
- Creep-fatigue interaction analysis using Taira's Linear Accumulation Method.

The effects of engine operation conditions and engine degradation on life consumption are analyzed. The models are implemented in PYTHIA so as to enable similar analysis on other existing engines.

1.5 Contributions to Knowledge

So much has been done in gas turbine life analysis. Most of the existing works centres mainly on any of the failure modes. For gas turbine hot section components, creep life has been the main focus, several works on creep-fatigue interaction though abound. This work tends to contribute to the existing knowledge base in the following areas:

- Creation of a platform for simultaneously determining creep life, low cycle fatigue life, creep-fatigue interaction analysis using relative life analysis.
- Creation of a means of quick assessment of engine life consumption and tracking of engine life using direct engine measurement data.
- Development and application of low fatigue cycles counting model in industrial gas turbines operations.
- Development of safety margins (obtained from investigating the low cycle fatigue contributions to creep-fatigue interaction life consumption at different engine operation conditions) in applying creep models without considering creep-fatigue interaction.
- In-depth analysis of the relative extent in which various factors affect engine life thus providing results that will meet several needs of engine operators.

1.6 Report Outline

Chapter One – This chapter presents an overview of what the research is about, makes a case of how the research is necessary, defines the scope and limitations of the research and presents contributions the research has made to the existing body of knowledge.

Chapter Two – Related literatures are reviewed and engine degradation/failure modes are identified. Relevant lifing models are also identified and the models to be used for the lifing analysis and the reasons for using such models are adduced.

Chapter Three – The research methodologies is presented in this chapter. Algorithm for creep-life consumption is presented. Relative creep life analysis at each engine operation point is ensured by making use of creep factors while life consumption for a complicated engine operation process is carried out by introducing equivalent creep factor. Low cycle fatigue counting model suitable for industrial gas turbine operation is developed. Relative life analysis for both fatigue life consumption and creep-fatigue interaction life consumption are developed- the concepts of fatigue factor, equivalent fatigue factor, creep-fatigue interaction factor and equivalent creep-fatigue interaction factor are introduced. Lifing models adopted for the various failure modes identified are presented, and the procedure to be used in carrying out the lifing analysis is presented using a flow diagram. Methodologies for engine model adaptation are presented together with design point simulation and off-design point calculation techniques.

Chapter Four – The major life analysis sub-models are presented in this chapter. These include data acquisition and pre-processing module, blade thermal model and blade stress model. The data acquisition and pre-processing module accepts the real engine operation data, pre-processes the data and sends the data to the engine performance model for simulations to obtain various gas path properties needed in the blade thermal and stress models. The blade thermal model estimates the temperature of the blade material at different sections along the span of the blade while the blade stress model calculates the stresses at same locations where temperatures are determined.

Chapter Five – In this chapter, engine performance model is created in PYTHIA and adapted to the real engine operating conditions to ensure accurate simulation of engine

performance. Design point simulation and off-design point simulations techniques are also presented.

Chapter Six - Creep life analysis is carried out in this chapter. The creep life analysis algorithms developed in Chapter 3 are applied to 8 months of engine operation to ascertain the feasibility of creep life tracking process. The effects of ambient temperature, shaft power, and engine components degradation on creep life consumption are examined.

Chapter Seven - Fatigue life analysis is presented in this chapter. The developed fatigue life analysis methodologies are applied to fatigue life tracking using data for 8 months of engine operation as a case study. The effects of ambient temperature, shaft power and engine degradation on fatigue life consumption are investigated. Relative fatigue life analysis is carried out.

Chapter Eight - In this chapter, creep-fatigue interaction life analysis is presented. Creep-fatigue interaction life tracking algorithms developed in Chapter 3 are applied to 8 months of engine operation. The contributions of fatigue to creep-fatigue interaction under different engine operation conditions are presented. Also, the effect of ambient temperature, shaft power and engine degradation on creep-fatigue life consumption are thoroughly investigated.

Chapter Nine - Conclusions about the work done so far are presented together with the major findings made in the research. Also, areas of future research relating to this work are presented. In essence, improvements required in the present work are presented while future research areas are identified.

A rich appendix is provided at the end where details of some parameters used in the work, especially life analysis sub-models in Chapter 4 are given. Various input data required in the work is also given in the appendices. The appendices also include sequential solution-algorithm trees (SSAT) of the life analysis sub-models and the lifing models. Using the SSAT, implementing the models in computer programs is easy. The entire life analysis module incorporated in PYTHIA and the various forms created and how the life analysis could be carried out with the developed algorithms is given in the appendix as program details and functionalities.

2 LITERATURE REVIEW

2.1 Gas Turbine Performance

Generally, industrial gas turbine applications involve either an air compressor driven by a gas generator with a separate power turbine (two-shaft engine), or an air compressor and a turbine on one shaft, where part of the turbine output is used to run the compressor and the other part available for the load (single-shaft engine). Combined cycle configuration (where the exhaust gases from the turbine exit are used to fire a boiler to generate steam for a steam turbine) could be gotten in both cases.

Industrial gas turbines are designed to provide a required power at specified operating conditions (fuel flow rate, pressure ratio, turbine entry temperature (TET) etc.). Part load operation is common. When operating at the design point, the performance analysis is simple and it is referred to as the design point performance analysis [1], [3]. When operating at part load, off-design performance analysis is carried out. In this, component maps (compressor map, combustor map and turbine map) are used and matching of parameters or components is required [1], [3], [18], [19]. In the use of component maps for off-design performance analysis, adiabatic conditions are assumed in most cases and the performance parameters predicted are not completely accurate or are only approximates as should be expected [20]. The performance discussion here is more or less design point performance and emphasis is on how effectively the fuel energy is utilized to produce shaft power. In other words, the focus is on the thermal efficiency and how operating conditions, mainly compressor pressure ratio and TET impact on the efficiency of gas turbines. The performance parameters of gas turbine engines are dependent on the type of the engine.

For industrial gas turbines, shaft power and efficiency are two major parameters easily identified [21]. Efficiency is viewed as the driving force in the design of all power generating units. The reason is not far-fetched: higher efficiency translates to lower operating costs [22]. In gas turbines, higher efficiency is brought about by high TET which means higher fuel flow rate. The TET value is limited by the metallurgical properties of the gas turbine materials, especially, the hot section components [1], [3], [23], [24]. Higher fuel flow rate equally translates to higher fuel cost aside the limit

imposed by the hot section turbine components. A balance thus needs to be struck. Higher pressure ratio also leads to higher efficiency but there is a limit to the pressure ratio at which efficiency will be on the increase for practical plants [1], [3]. An efficient engine may equally be viewed as a plant producing the designed power output with required fuel flow rate and other operating conditions. Figure 2.1 shows the variations of both efficiency and power with pressure ratio and turbine entry temperature.

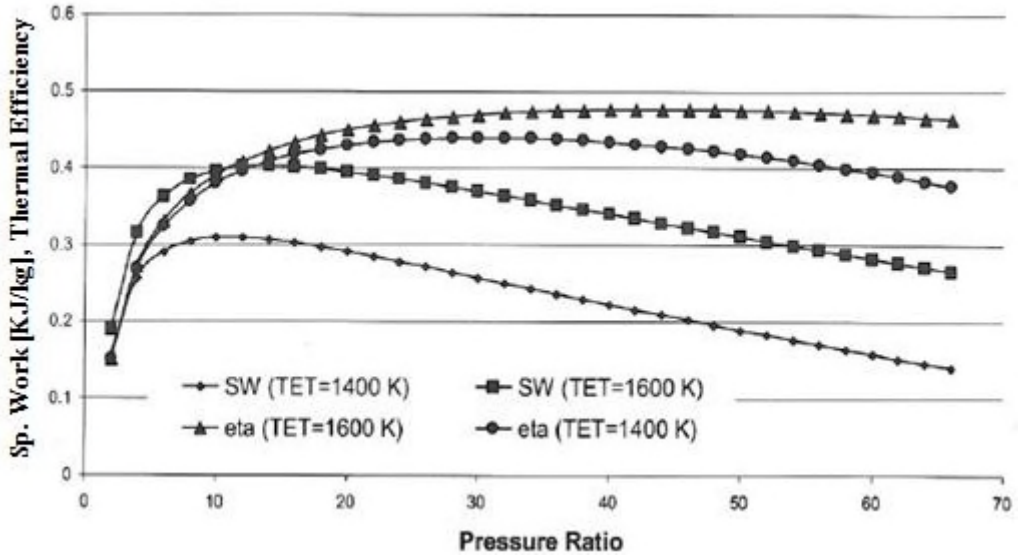

Figure 2.1: Variation of Turbine Thermal Efficiency and Specific Work with Pressure Ratio and Turbine Entry Temperature (TET) [7], pp.124

As it can be seen clearly from Figure 2.1, both thermal efficiency and specific work increase with TET at a given pressure ratio. For a given TET, the thermal efficiency increases with pressure ratio and attains a maximum value at a particular pressure ratio. Further increase in pressure ratio leads to decrease in the thermal efficiency. This decrease in thermal efficiency is due to decrease in component efficiencies [3]. The point of maximum efficiency increases with the TET. The specific work, like the thermal efficiency, increases with pressure ratio and gets to a peak value, but at a lower pressure ratio compared to that of the thermal efficiency for a given TET. The point of maximum specific work increases with TET as in the case of thermal efficiency. Increasing TET with a view to increasing the plant efficiency may be contemplated, but the life of the hot section gas turbine blades will be put at risk. Thus, in this research, the effect of TET on the hot section blades under different failure modes is investigated.

Gas turbine life cycle cost is another important parameter usually considered by power plant owners. It is evident the profitability of power plants for industrial purposes do depend on this parameter [12]. Generally, factors affecting gas turbine performance with no regard to degradation are compressor inlet conditions, pressure ratio and turbine inlet conditions. Since performance is of benefit to the gas turbine operators, efforts at improving gas turbine performance abound. Compressor inlet cooling is one proven way that increases gas turbine performance [25]–[30]. Other efforts at improving gas turbine performance include upgrading gas turbine components as presented below:

- Inlet guide vanes to allow for more airflow
- Improved seals to ensure tighter clearances
- Combustor liners, turbine blades and vanes and transmission pieces to enable higher turbine entry temperature values [31]. The benefits associated with the various upgrade techniques as presented in Table 2.1.

Table 2.1: The Benefits of Various Upgrade Techniques in Gas Turbines [31]

Option	MW Impact, %	Heat Rate Impact, %	Capital Cost, $/KW
Comprehensive Upgrade	+10 to +20	1 to 5	150 to 250
High -Flow IGVs	+4.5	1	<100
Hot Section Coatings	+5 to +15	0.5 to 1	50 to 100
Compressor Coatings	+0.5 to +3	0.5 t0 3	50
Inlet-Air Fogging	+5 to +15	1 to 5	50 to 100
Supercharging plus Fogging	+15 to +20	4	200

A reduction or drop in the performance of gas turbines, known as performance deterioration stems from degradation of engine components. Sometimes, absolute failure occurs and this is the subject of the next few sections.

2.2 Degradation and Failure of Gas Turbine Components

The hot section components of gas turbines, especially the compressor turbine blades and discs are prone to failure. The degradation of these and other components is common. There is need to draw a thin line between degradation and failure. The word degradation is Latin origin, derived from 'degradatio', literally meaning reduction. It is

"*the process of deteriorations of characteristics of an object with time; moving back; gradual decline; decline in quality; break down of matter due to the impact of the external forces in conformity with the laws of nature and time"* [32].

From the above definition, it is clear that when an engine component undergoes degradation, it will likely still perform its designed function but at a reduced level, meaning performance reduction or deterioration.

Saravanamutto et al.([1], *pp.391*) defined failure as
"a change of component configuration, size, surface or material properties that precludes further functioning of the component".

Failure is thus a more serious issue compared to degradation and the two terms are not inter-changeable. Gas turbine degradation is often classed as recoverable and non-recoverable degradation [33]. Recoverable degradation leads to performance loss which can be recovered by operation procedures. These include among others keeping the inlet and outlet pressures low, compressor washing (offline or online) [33]. Non-recoverable degradation on the other hand leads to performance deterioration which cannot be recovered. Meher-Homji et al. [34] classed performance deterioration/degradation as recoverable, non-recoverable and permanent. Irrespective of any terminology employed, degradation of components may lead to failure and it definitely brings about performance reduction.

The major gas turbine degradation modes are Compressor Fouling, Foreign Object damage (FOD), Domestic Object Damage (DOD), Erosion, Fretting and Wear. Another degradation mode is environmental attack in the form of hot corrosion (oxidation and Sulphidation) [35]–[38]. All the degradation modes mentioned above actually lead to performance deterioration and may lead to component failure except Domestic Object Damage which in most cases results in permanent damage of component and hence forces replacement of components. Aside degradation of components, other factors may lead to performance deterioration. One of these factors is poor inlet filtration [39]. The degradation modes highlighted above are briefly considered below.

- **Compressor Fouling-** Compressor fouling stems from deposition of debris in the airstream on compressor blades and discs thereby leading to drop in compressor performance. Compressor fouling is caused by tiny particles such as smoke, oil mists, carbon, sea salts, etc., and the adherence of particles to compressor blade surface is made possible by the presence of water mists or oil [40]. Fouling may equally result from oil vapours or chemical processes in industrial locations[1]. Compressor fouling leads to change in the shape and inlet angle of the aerofoil, increases the roughness of the compressor blade surface, and reduces the aerofoil throat area [40], [41]. Fouling can also occur in the turbine section [34]. Fouling is a recoverable degradation and it is corrected by either on-line washing or off-line washing [42]–[45].

- **Foreign Object Damage (FOD) -** Foreign Object damage (FOD) results from the impact of hard objects such as stones, hardware and pavement fragments on the rotating blades. This may lead to localized damage to the blades in the form of a notch or dent, thus affecting the microstructure and the surrounding residual stress field [38]. Foreign object damage often occurs in aircraft engines [46], and in these aircraft engines, objects such birds entering the compressor blades do occur. This also lead to performance reduction especially if large birds are involved [1].

- **Domestic Object damage (DOD) -** Domestic Object damage (DOD) is a more serious issue compared to Foreign Object damage (FOD) because DOD usually lead to damage of engine components as earlier pointed out. In DOD, materials such as loosen bolts or nuts enter the rotating blades/discs and the result is permanent damage of engine components. The damage may also result from debris and components from another location, but within same engine [47].

- **Erosion-** Erosion is common to components in the airstream, mainly compressor blades. It is caused by small objects in the airstream striking the blades. Erosion is common to aircraft routinely operated in dusty/sandy conditions [48]. Industrial gas turbines operated in desert areas are equally prone to erosion issues. Erosion does lead to removal of materials from blade tips thus changing the aerofoil shape of the blades and hence reduces performance.

Erosion may not lead to catastrophic blade failures but can contribute to other failure modes [49].

- **Fretting and Wear** - Fretting refers to removal of materials (wear) which occurs between mating surfaces, in this case, between the disc and blade root of compressors and turbines as a result of vibration [50] . Fretting leads to performance deterioration which can only be corrected during overhaul by replacement of affected parts. Fretting is a non-recoverable degradation and all non-recoverable degradation issues could be solved completely by the replacement of the affected parts if design performance values are to be achieved. In practice, this is costly and parts are only changed when it is economically unviable to use such degraded parts or the failure of such parts is clearly foreseen. Fretting may be mitigated by surface treatments or coatings [51].

- **Corrosion**- Corrosion comes in two major forms in the hot section of gas turbine operation. These are oxidation and sulphidation. The hot section materials are made of super-alloys and often coated with corrosion- resistance materials. At very high temperatures, these materials react with oxygen (oxidation) to form oxide films that wear off with time [49]. This is corrosion resulting from oxidation. Sulphur from the fuel may react with sodium chloride from the air at high combustion temperatures to form sodium sulphate which is deposited in hot section components leading to accelerated oxidation or sulphidation [52]. The sodium sulphate has a weakening effect on the coating materials. Like oxidation, oxide films are formed which breaks off with time. Corrosion (through oxidation or sulphidation) degrades materials fast.

2.3 Failure Mechanisms of Gas Turbine Components

In the previous section, gas turbine component degradation and failure were considered. A thin line was drawn between degradation and failure and the major modes of gas turbine degradation were presented. It is pertinent at this point to present the mechanisms of gas turbine failure. The hot section components of gas turbine are more likely to fail and these components are referred to as critical components. Other

components in rotating assemblies such as spacers, cover plates and seals may also be designated as critical [53]. The high pressure (HP) compressor turbine blades are the focus in this work. Gas turbine critical components are made of super-alloys to prevent failure and while in service, special inspection techniques are employed to assess the reliability of the materials at various stages in the life cycle and also for failure analysis [54].

Abdul Ghafir [37] identified fatigue, high temperature corrosion/oxidation and creep as the major failure modes common to gas turbine hot section components. Corrosion/oxidation is already discussed in the previous section as a degradation mode. Fatigue and creep are also treated as modes of degradation in many literatures but these are the two failure modes ascribed to gas turbine components. They equally occur in the combined form as creep-fatigue interaction/ thermo-mechanical fatigue. Creep failure, fatigue failure and failure in the combined modes are discussed in the following sub-sections.

2.3.1 Creep

Failure of materials (or plastic deformation of materials) is generally assumed to occur when the applied load on the material exceeds the ultimate tensile strength of the material. When the applied load is below the ultimate tensile strength of the material, the material can only undergo elastic deformation. Failure can equally occur if the applied load is below the ultimate tensile strength of the material and it is not fluctuating in nature but applied at high temperature levels. In this case, it will take a long time for the material to fail, depending on the magnitude of the applied stresses and the operating temperature. This time-dependent deformation of materials under non-fluctuating loading at high temperature is known as creep [36], [55], [56]. The rate of creep deformation depends on the properties of the material, the exposure time, the operating temperature and the magnitude of the applied load [36]. The mechanism of creep in metals is characterized by the flow of material (at elevated temperatures and for long period of time) due to defects in the material which may be localized point defects, also known as vacancies, line defects (dislocations), or defects in planes or grain boundaries [57]. Elongating the grains of materials in the direction of the applied load

tends to resist creep. Also the removal of the grain boundaries/increasing the size of the grains increases the material resistance to creep [58]. Nickel-based superalloys, single crystal (SC) super-alloys and nickel-based single crystal super-alloy materials are now vigorously used in high temperature operations as they give the highest resistance to creep failure [59]–[62].

The temperature at which creep deformation becomes a problem is material dependent. Generally, creep should be a concern when the temperature measured in Kelvin (K) or Rankine (R) is about 30% of the melting point of the material for metals and between 40% to 50% for ceramics [63]. For most gas turbine materials, Saravanamutto et al. [1] put this value as 50% (0.5). Creep deformation is gradual and is made up of three distinguishable phases. These are primary creep or phase I, secondary creep or phase II and tertiary creep or phase III [1], [64], [65]. These phases are shown in Figure 2.2. The creep deformation of a material is measured by the amount of strain deformation the material undergoes with time under constant stress condition. A material is assumed to fail due to creep damage if it undergoes 0.2% plastic deformation [66]. Generally, creep rate of materials increases with temperature [67]–[70], thus in gas turbine operation, the life of the hot section blades depends on the temperatures of the hot gases traversing the blades.

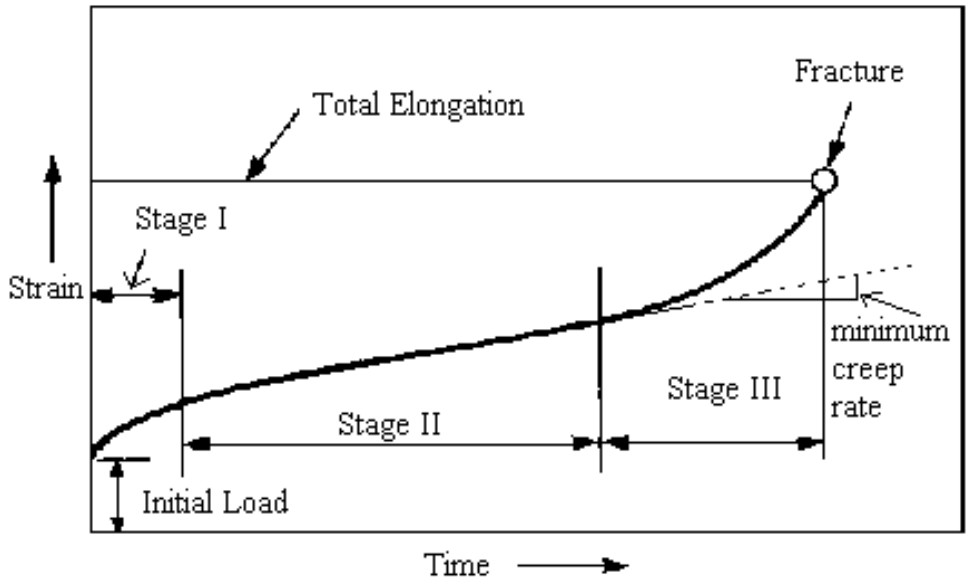

Figure 2.2: Creep Curve Showing Creep Phases [71]

2.3.2 Fatigue

When a material is under tensile or compressive loading and the load does not vary with time, the material will remain for infinite time without failing if the applied load (stress) is below the ultimate tensile strength of the material. The ultimate tensile strength (or ultimate strength or tensile strength for short) is the maximum stress that a material can withstand under the given load condition before failing [72]. But if the applied stress is cyclic or repetitive in nature, failure will occur when the applied stress is less than the ultimate tensile strength of the material. This failure resulting from the application of cyclic load or stress is known as fatigue [48], [73]–[75]. In gas turbines, the materials undergo repetitive loading due to centrifugal forces and vibration in some cases hence failure due to fatigue can occur.

The operating environment and the nature of the material in question may influence the failure of the material under cyclic loading. The cyclic load may be mechanical, thermal or both. Fatigue failure usually starts with crack initiation, crack propagation and then failure which is characterized by unstable crack propagation. These stages are termed primary, secondary and tertiary stages of fatigue [48]. Crack initiation occurs at sites of stress concentration such as surface imperfections, grain interfaces and persistent slip bands [76].

Fatigue loading of gas turbine members can be seen in compressor and turbine blades. In turbine blades, the hot gas path in contact with the rotating blades causes the blades to bend as a result of high pressure. But the stress level is usually in the elastic region. Each blade gets to the gas path and escapes from it at a regular time interval because of stator blades which causes intermittent blockade for each rotation. Thus, the loading of the blades is repetitive [1], [18], [48]. At elevated temperatures, the load is both mechanical and thermal as high temperature gradient is created. The number of cycles a material will experience under fatigue loading before failure depends largely on the stress level. At very large stress level, a material will fail under few fatigue cycles. Thus, in investigating the fatigue behaviour of materials, Stress-Number of cycles to failure (S-N) curves are used. A given S-N curve for a given material shows the number

of cycles a material will experience before it will fail under different stress levels. Figure 2.3 shows a typical S-N Curve.

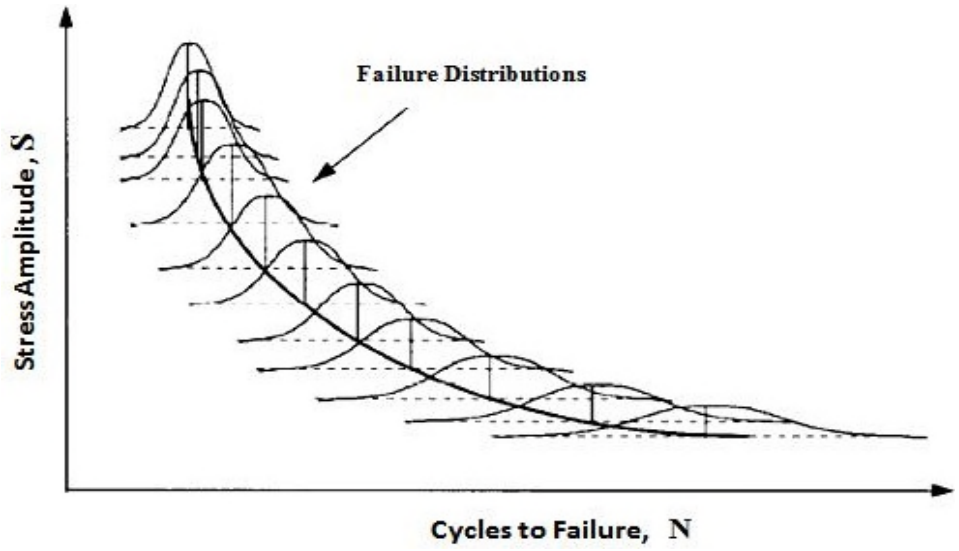

Figure 2.3: S-N Diagram ([48] , p.4-4)

Although, one can predict the number of cycles a material will experience under fatigue loading for a given stress level before failure from the S-N curve, these values may not be very precise because fatigue failure is stochastic in nature[48], [77]. The number of cycles to failure and the type of fatigue loading necessitates the categorization of fatigue as low cycle fatigue (LCF), high cycle fatigue (HCF) and thermo-mechanical fatigue (TMF). Each of these is briefly considered below.

2.3.2.1 Low Cycle Fatigue (LCF)

Low cycle fatigue is characterized by low number of cycles to failure and very high amplitude of applied load. The stress amplitude is high and the material gets to the plastic region (not all the time)[78] in each cycle. That is, in LCF, the material undergoes repetitive plastic deformation[1], [48], [77]. LCF thus involves high amplitude low frequency strains. In gas turbine blades, large strains occur in areas of stress concentration [79].

In aircraft engine operations, one low cycle may constitute quick take off from one point at high power level and landing at another point within a short while, especially

for military operations. In industrial engines, accelerating the engine from standstill to maximum engine rotational speed and then returning to standstill constitutes one low cycle operation [48]. Also, peak operation of engine on daily basis constitutes a low cycle operation for each day. The manner of evaluating the number of low cycles in industrial turbine operation with no recourse to the actual stresses the rotating components experienced will give quite misleading or inaccurate results. For instance, in running the engine to maximum speed level and then returning to standstill, if the speed fluctuates highly within the period, the number of fatigue cycles the rotating components experienced is more than the fatigue cycles that will be experienced for smooth transition to maximum speed and then smooth transition to standstill. In both cases, the convention provided above allocates one fatigue cycle to either process. In this research, a fatigue cycles counting model is developed to address the shortcoming highlighted above. The number of hours making up one cycle in the LCF analysis has to be properly spelt out. There is no clear distinction of the number of cycles to failure used in differentiating between LCF and HCF. In LCF, failure occurs when a material is subjected to $< 10^3$ stress cycles [48]; between 10^4 and 10^5 cycles [1]. Traditionally, if a material fails below 10^4 stress cycles, it is ascribed to LCF but if it fails above 10^4 stress cycles, it is said to fail under HCF [37].

2.3.2.2 High Cycle Fatigue (HCF)

High cycle fatigue is characterized by low amplitude high frequency repetitive stress application. As mentioned in the previous sections, fatigue failure due to large number of stress cycles, $> 10^4$ is traditionally taken as HCF failure. Unlike LCF, in HCF, the stress amplitude is small and hence repetitive plastic deformation is the cause of failure. The Engine Structural Integrity Program (ENSIP) specification requires HCF limit to correspond to10^9 cycles. Although the number of stress cycles to failure may be very high in HCF but in gas turbines vibratory loads generated at low stresses and at high frequencies could build up several million cycles in few hours [1]. HCF is the largest single cause of component failures in modern military gas turbine engines [80].

2.3.2.3 Thermo-Mechanical Fatigue (TMF)

Thermo-mechanical fatigue (TMF) is the result of the combination of the induced stresses due to temperature gradient and repetitive external loads [72], [81]–[83]. That is, it is characterized by both cyclic mechanical loading and fluctuating temperature (non-isothermal condition). Gas turbine components such as turbine discs and blades are subjected to TMF during start-up and shut down [84]. This is because at the start of the engine, especially for uncooled HP turbine blades, the blades experience high temperature on their outer surfaces, much higher than that of the core which takes some time to attain operating temperature [48]. During shut down, the outer surface equally cools faster thus creating another temperature gradient between the outer surface and the core.

Two stress cycles, thermal and mechanical stress cycles are identified in thermo-mechanical fatigue. TMF loading is said to be in- phase (IP) or out-of-phase (OP) depending on whether maximum temperature and maximum stress occur at the same time [72]. Failure prediction due to TMF is more difficult when the loading is out-of-phase than when it is in-phase [83]. Damage of components due to TMF is accelerated by harsh operating environment. This also applies to LCF and HCF. Some literatures view TMF as a combination of creep, fatigue and oxidation[72]. Fatigue results from oscillatory mechanical stress, but if thermal stresses vary as well, the combined effect leads to thermo-mechanical fatigue failure.

2.3.3 Combined Failure Mechanisms

Failure of gas turbine components may not be singly due to any of the failure mechanisms discussed in the previous sections (fatigue- LCF and HCF, and creep). TMF is one combined mode of failure. Besides these failure modes, it has been noted that the operating environment acts as a catalyst for failure to occur in any of the failure modes. The combination of individual failure modes will reduce the life of a component faster than each of the individual failure modes could do [85]. Failure due to combined mode is complex and this accounts for a reasonable number of engine component failures. Villasante [86] put the contribution of combined cycle fatigue, CCF (failure due to the combined influence of LCF, HCF, creep, oxidation etc.) to the total number

of issues that arise during an engine development at 40%. This, according to him, costs the industry millions of dollars as should be expected.

LCF/HCF interactions are very common and their combination has given rise to two-phase crack growth process. In this, crack initiation and growth may occur under LCF and continue in this for a while. Crack growth is then taken over by HCF until the component finally fails [38]. When blades suffer foreign object damage (FOD), failure due to fatigue or creep may occur earlier. In this case, initial crack growth may be due to HCF as a result of the high stress concentration at the point of impact. The crack growth reverses to LCF before HCF takes over later [38]. Two groups of FOD-induced failures have been identified. These are fatigue crack initiation directly at the point of contact (as discussed above) which causes failures within 10^5 to 10^6 cycles and crack initiation at regions of high tensile residual stresses which may be remote from the point of impact causing failures at 10^7 to 10^8 cycles [87].

There are minor combinations of failure modes regarding the environment the major failure mode occurs. For instance, fatigue in the presence of a corrosive environment is known as corrosive fatigue, if the fatigue load (repeated or repetitive load) is applied with sliding contact between materials, then we have sliding contact fatigue. The application of fatigue load together with rolling contact gives rise to rolling contact fatigue while the application of fatigue load with relative frictional sliding motion between surfaces results in fretting fatigue [47].

The dominance of a particular failure mode depends on the mode of operation of the turbine. For industrial gas turbines operated at uniform operating conditions, creep is the dominant failure mode [37]. For engines operated at peak loads for a few hours daily, LCF contribution will be significant.

Because of the implications associated with failure, efforts at preventing/reducing it abound. Proper design, diagnostics and maintenance efforts are employed over the years to ensure these important prime movers for various operations are not only available for use but also perform effectively and are reliable[1], [88], [89].

2.4 Life Prediction of Gas Turbine Components

In the last section, the various failure modes of gas turbine components were considered. Since several failure modes exist and they interact in most cases, the life of gas turbine components, especially the hot section components depend on a complex interaction of factors such as stress, creep, metal temperature, fatigue excitation and environmental effects [17]. Final failure of gas turbine components is avoided, and before failure, every component has a usable life. The process of determining or predicting/estimating the usable life of a gas turbine component is known as lifing [1].

In estimating the life of a component, the prevalent failure mode(s) is/are taken into consideration. If a material is predominantly under creep load condition, the number of hours the material will spend before failure is known as the creep life of the material. Also, if a material is adjudged to operate under fatigue loading condition, it will fail under a number of fatigue cycles, be it LCF, HCF or TMF. The number of cycles a component can undergo at a given load level before failure or before a crack of defined magnitude occur is known as the fatigue life of the component. The fatigue life is load specific. Thus, in life prediction, we consider creep life prediction and fatigue life prediction of a given component depending on the prevailing failure mode. In some cases, the failure modes interact and the combined mode life prediction is considered in such cases. The combined modes take the form of LCF/HCF, TMF and creep-fatigue failure [38], [87], [90], [91]. The life prediction methodologies under the various failure modes are considered next.

2.4.1 Creep Life Prediction Methods

There are several approaches to creep life prediction or estimation of creep life of components, including those of gas turbines especially the hot section components. Several models exist for determining creep life of a component and the life determining approaches have been classed in various ways. Any classification of creep life estimation approach makes use of the model involved and the technique used. Generally, creep life estimation approaches could be put into two groups: Total life approach and Damage mechanics approach involving crack growth rate. Abdul Ghafir [37] identified four (4) creep life estimation approaches. These are model based

approach, service based approach, statistical/probabilistic approach and soft computing approach. Eshati [92] in working on creep life estimation of stationary gas turbine engine identified design approach which is model based, post service approach, and statistical/probabilistic approach as some creep life estimation approaches. Faridani [93] pointed out that more than sixty-two creep relations (models) are in use with thirty-three of these models describing creep process using power law and twenty-eight of them addressing creep using exponential expressions. He further classified creep models into three categories- strain-time models, stress models and temperature dependency models. Strain-time models are creep models which consists of creep strain and time terms (t, ε or ε_c),where the time may be time to rupture or failure , t_f or time to reach a pre-defined strain value. Stress models include stress term σ in their formulation while temperature dependency models consist of temperature term. The major temperature dependency models are the time-temperature parametric models. The time-temperature parameters commonly used for creep life estimation are Orr-Sherby-Dorn parameter (OSDP), Goldhoof-Sherby parameter (GSP), Mason-Haferd parameter (MHP), Manson-Succop's parameter (MSP) and Larson Miller parameter (LMP) [37], [92].

Not all creep relations can model creep for the three regions of the creep curve. Most relations can only deal with creep in the secondary region while few can model the entire creep curve. Thus creep relations can be classified based on the region of the creep curve they can handle. From the foregoing, it is clear that there are various ways in which creep life estimation approaches can be categorized. In this work, no attempt is being made to classify the creep life estimation approaches, but some creep life estimation approaches will be discussed which fall in the category of total life approach. First, some general creep models will be presented, followed by the time-temperature parameters which find widespread usage. The last set of creep models to be considered are those which tend to address creep for the entire creep curve. This will be followed by a review of the classification of creep life estimation approaches due to design-based, post service, statistical/probabilistic-based and soft computing approaches as in Abdul Ghafir [37] and Eshati [92] to show that they equally make use of relations presented in the previous sections.

2.4.1.1 Basic Creep Life Prediction Models and Creep Curves

One of the general creep equations is given in the form [94],

$$\frac{d\varepsilon_c}{dt} = \frac{C\sigma^m}{d^b} e - \frac{Q}{kT} \tag{2.1}$$

where ε_c is the creep strain, $\frac{d\varepsilon_c}{dt} = \dot{\varepsilon}_c$ is the creep strain rate, C is a constant which is dependent on the material and the particular creep mechanism, the exponents m and b are constants which depend on the creep mechanism, Q is the activation energy of the creep mechanism, σ is the applied stress, d is the material grain size, k is Boltzmann's constant and T is the absolute temperature of the material. This is the power law equation of creep which can be cast in various forms.

The primary and secondary stages of creep are of interest in design and Bailey-Norton law, also called power law creep law is often used in the form [95],

$$\varepsilon_c = A\sigma^n t^m \tag{2.2}$$

In terms of creep strain rate, Equation (2.2) becomes,

$$\dot{\varepsilon}_c = A\sigma^n m t^{m-1} \tag{2.3}$$

where A, m and n are temperature dependent material constants. Equation (2.3) is the time hardening formulation of the power law creep. The strain hardening formulation is obtained by solving for t in Equation (2.2) and substituting in Equation (2.3). This is given as [95],

$$\dot{\varepsilon}_c = A^{1/m} m \sigma^{n/m} m t^{(m-1)/m} \tag{2.4}$$

The strain hardening formulation of the power law creep produces results that are in good agreement with actual test results under variable stress condition [95]. Some other creep rate laws are enumerated below, all obtained from [93] and [95]:

Kelvin- Voigt (visco-plastic creep) model: $\varepsilon(t) = \frac{\sigma_o}{E}\left[1 - \exp\left(-\frac{E}{\eta}\right)t\right]$ (2.5)

where η, E and σ_o are the viscosity, the elastic modulus, and the applied initial stress respectively.

Exponential Law: $$\dot{\varepsilon}_c = \varepsilon_c \exp\left(\frac{\sigma}{\sigma_e}\right) \quad (2.6)$$

where ε_c and σ_e are constants.

Phillips model: $$\varepsilon = \varepsilon_0 + A\log(1+Bt) \quad (2.7)$$

where A, B and ε_0 are constants.

Hyperbolic Sine law: $$\dot{\varepsilon}_c = 2\varepsilon_c \sinh\left(\frac{\sigma}{\sigma_e}\right) \quad (2.8)$$

where ε_c and σ_e are constants.

Graham-wall's simple polynomial model: $$\varepsilon_f = a_1.t^{\frac{1}{3}} + a_2.t + a_3.t^3 \quad (2.9)$$

where a_1, a_2 and a_3 are constants.

Andrade's law: $$\dot{\varepsilon}_c = \frac{\beta}{3}\frac{1}{t^{2/3}+\beta t} + K \quad (2.10)$$

where β and K are constants.

Mukharsee-Bird-Dorn equation is useful for expressing creep rate in terms of stress, temperature and grain size under steady state creep in the form [95],

$$\dot{\varepsilon}_c^s = \frac{AGb}{kT} D\left(\frac{b}{d}\right)^p \left(\frac{\sigma}{G}\right)^n = A'\exp\left(\frac{Q}{kT}\right) \quad (2.11)$$

where A is a dimensional constant, D is the diffusion coefficient given by Equation (2.12),

$$D = D_0 \exp\left(-\frac{Q}{RT}\right) \quad (2.12)$$

D_0 is a frequency factor, Q is activation energy, $R = N_A k$ is the gas constant, N_A is Avogadro's number, k is Boltzmann's constant, d is grain size, and p and n are

material constants. Experimental data is represented by plotting $\dot{\varepsilon}_c^s kT/DGb$ against σ/G [95]. Schuh and Dunand [96] developed a constitutive equation for power law creep of polycrystalline $\beta - T_i$ after collecting data generated by several researchers.

Creep life analysis requires the use of experimental data. Creep curves are generated from available data by plotting data from creep tests in various ways. The parameters often used for obtaining creep curves are stress, strain, time and temperature. The data usually used for plotting creep curves are often obtained during short time creep testing: some at very high temperature levels, others at very high stress levels to rupture, where rupture time will be short. At other times, data is generated at perceived operating conditions until strain of desired level is obtained. Such data has to be extrapolated to failure time since it will take too long for the test to be carried out until failure occurs. Collins and Daniewicz [97] identified three commonly used methods for extrapolating short term creep data to long term applications. These are the abridged method, mechanical acceleration method and thermal acceleration method. In the abridged method, the tests are carried out at a particular temperature but at different stress levels and creep curve is obtained by plotting creep strain against time. The curves are extrapolated to the desired design life. In the mechanical acceleration method, tests are carried out at a defined temperature level but at high stress levels compared to contemplated design levels in order to obtain desired strain level in short time. Creep curve is obtained by plotting stress against time and a family of constant strain/constant temperature curves are generated. In the thermal acceleration method, creep data is obtained by carrying out test at comparatively higher temperature levels to obtain a required creep strain. The creep curve is is a plot of stress against time and a family of constant temperature lines are gotten. In extrapolating the curves to obtain the creep design life, the possibility of potential failure due to creep rupture before reaching the creep design life cannot be predicted [97]. Figure 2.4 shows creep curves obtained under constant stress and at a given temperature [98].

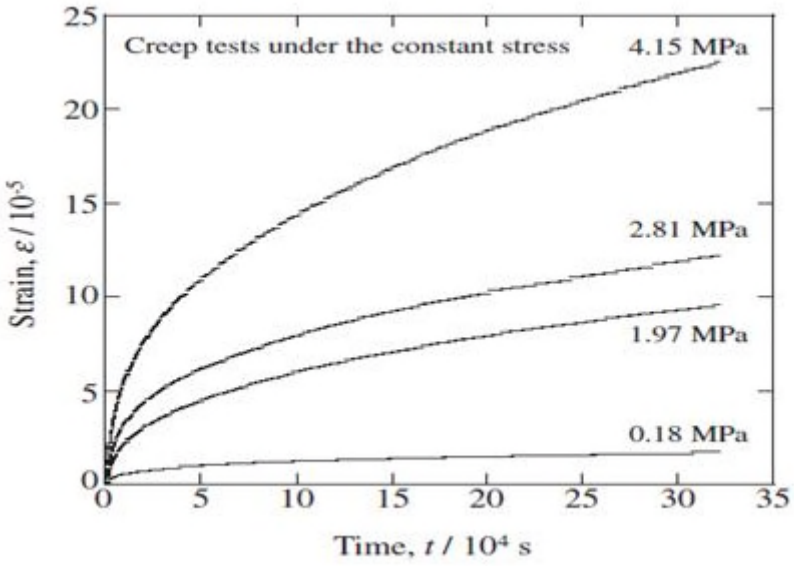

Figure 2.4: Creep Curves Obtained by Creep Tests Under Constant Stress ([98], p.1886)

The use of creep curves for life estimation seems not to be reliable since data for such tests are obtained in short time. Test period less than 1 % of expected life do not give good results. For reasonable results, test periods should extend to 10 % of expected life [97]. Also, the test temperature should be close to actual operating conditions. The apparent limitations in the use of creep curves has led to the emergence of several other methods for correlating short term test results at elevated temperatures to long term actual operating conditions. The time-temperature parametric method, the theta projection method, and the Monkman-Grant method are some methods widely used. These methods are considered below.

2.4.1.2 Creep Life Estimation Using Time-Temperature Parameters

Different parameters have been formulated for creep life determination. These parameters are temperature, time, and stress dependent. The commonly used time-temperature parameters as already pointed out are Larson Miller parameter (LMP), Orr-Sherby-Dorn parameter (OSDP), Goldhoof-Sherby parameter (GSP), Mason-Haferd parameter (MHP), and Manson-Succop's parameter (MSP). These parameters come into usage because experimental data is not available for all ranges of stress and temperature. Often interpolation/extrapolation techniques are used to account for insufficient data. The limit to the interpolation and extrapolation techniques is the melting point of the material. There is difficulty in obtaining results when the

temperature involved is up to 40% of the absolute melting point of the material. The use of the time-temperature parameters thus takes care of data insufficiency [37], [92].

The parameters are read from a master curve at the estimated temperature and stress levels [99]. In using some of these parameters, aside reading the parameter value, certain constants have to be obtained for the creep model to be applied [92]. The master curves are plots of the creep stress rupture data of the material concerned; often plotted as log of stress to rupture against a combination of log of time to rupture and temperature. Eno et al. [100] viewed these parameters as special cases of a general creep life analysis procedure which is anchored on linear statistical model. Using this approach, they fit the models to a statistical database efficiently and also compared the models to one another. The parameters are considered below.

Larson-Miller Parameter (LMP)

The Larson-Miller Parameter (LMP) is one of the time-temperature parameters for representing creep data and hence creep life estimation. It is the most widely used and useful for low stress and thus long time rupture condition. LMP is given as [101], [102],

$$LMP = T\left[\log t_f + C\right] \tag{2.13}$$

where T is the temperature in Kelvin[K] or Rankine [R], t_f is stress rupture time or time to failure in [hrs], and C is a constant usually of the order of 20; it varies with material and applications. The Larsson-Miller Parametric method which was developed during the 1950s by Miller and Larson while they were employed by GE performing research on turbine blade life is derived from the Arrhenius equation [103]. Appendix B shows how the Larsson-Miller Equation is obtained from the Arrhenius Equation. In the usage of LMP method, temperature which is one of the two variables that can be controlled in creep test (the other variable is stress) is eliminated and a master curve of the material is prepared using (STRESS AND TIME). Figure 2.5 shows LMP master curves of some materials [104]. The LMP value depends on the stress and it is read from the master curve of the material based on the stress value. The value of the LMP decreases with increase in stress.

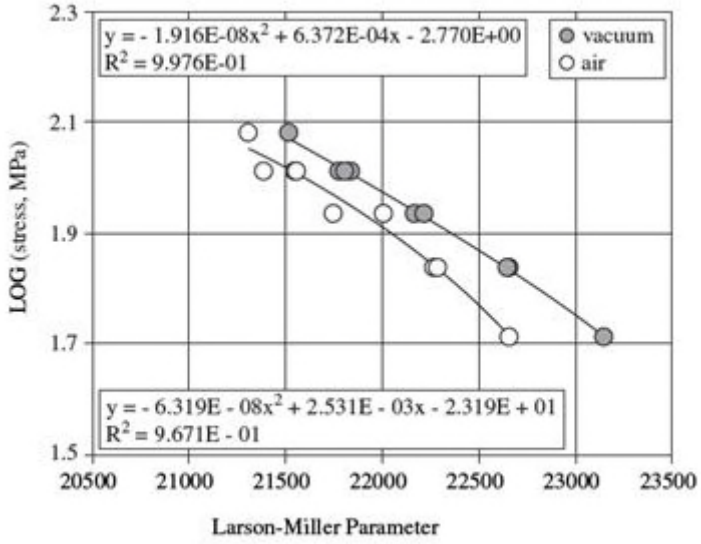

Figure 2.5: Larson-Miller Parameter (LMP) Master Curves ([104] , pp.407)

In using the LMP method, the stress level and temperature have to be determined using various techniques. Finite element analysis (FEA) is often employed in the determination of the temperature and stresses in the body under consideration. ANSYS and ABACUS also enable the determination of these parameters. Thus, a creep life estimation platform making use of LMP method has a way of determining these parameters probably from other known input data. At a given stress level and constant temperature, LMP value is read. To evaluate the creep life at another temperature value but same stress level, the LMP and temperature (T) are introduced into Equation (2.13) to calculate the time to failure, t_f . From Equation (2.13), it is obvious a plot of log of t_f against $1/T$ will be a straight line which slope is LMP and intercept C. Thus, all iso-stress lines will pass through point C.

The LMP method has been used extensively for creep life analysis [37], [92], [105]–[109]. Vaezi [110] used the LMP method in carrying out the life prediction of Inconel738 gas turbine blade, Oloyede [106], in analyzing the fundamental impact of firing syngas in gas turbines used the LMP method to estimate the life of Siemens SGT 6-5000F first stage nozzle and rotor blades using manufacturer's recommended replacement interval as a basis. Eno et al. [100] applied a number of time-temperature parameters to alloy 617 (a Ni-Cr-Mo useful for high temperature applications) and discovered that the Larson-Miller model was only second to an M-R-M model in fitting

the data. Abdul Ghafir et al.[109] used the Larson-Miller Parametric method, exploiting a creep factor approach in assessing the impact of operating and health conditions on aero gas turbine hot section creep life. In a furtherance to this work, Abdul Ghafir et al. [14] equally employed the LMP method in determining how the various performance parameters affect the creep life of hot section blades.

The Larson-Miller parameter remains the most widely and generally used in analyzing creep rupture data. This view has been held by several researchers including Chathopadhyaly and Gbosh [108], who introduced the LMP, OSDP and MHP in their creep life prediction software and Taminger [111] in his master's thesis on analysis of creep behaviour and parametric models for some materials. Being the mostly widely used method with appreciable accuracy relatively, the Larson-Miller Parametric method is used for creep life analysis in this research. The availability of material properties is another reason for using the Larson-Miller Parametric method. The premise of the usage of the Larson-Miller parametric method is that the logarithm of the stress applied to the material at any given point is a function of the material temperature in Kelvin, the Larson-Miller Parameter constant, C and the logarithm of the time, where the time is the stress rupture life or the time to accumulate a certain amount of creep strain [112]–[114].

Orr-Sherby-Dorn Parameter OSDP

The Orr-Sherby-Dorn Parameter (OSDP) is given as [115],

$$OSDP = \log t_f - \frac{Q}{RT} \tag{2.14}$$

where Q is the characteristic activation energy and R is the universal gas constant. From Equation (2.14), a plot of $\log t_f$ against $1/T$ at a defined stress level will be a straight line which intercept on the $\log t_f$ axis is the value of the parameter (OSDP). Parallel iso-stress lines with the same gradient will be obtained [92], [100]. The OSDP approach is thus used to fit creep data produced at different stress levels. This parameter fit data obtained from pure metals and dilute alloys more appropriately at $T > 0.5T_m$ (homologous temperature greater than 0.5), but satisfactory results are not feasible at other conditions [92].

The OSDP method is applied by obtaining the OSDP for different stress levels and plotting a creep rupture master curve. This curve together with Equation (2.14) enables the determination of a component life at a given stress and temperature level. The OSDP method, although viewed to be less satisfactory in fitting creep data but has found widespread use as shown in the works of Kurata et al. [105] and Nonaka et al. [107]. This method is not used in this research as it is less accurate and has less widespread usage compared to the Larson-Miller Parameter method. The condition imposed by the homologous temperature is another set-back in the usage of the OSDP method. The OSDP method is also easy to use as it requires knowledge of only the parameter (OSDP) for its application.

Goldhoof-Sherby Parameter (GSP)

The Goldhoof-Sherby Parameter (GSP) is given as [92],

$$GSP = \frac{\log t_f - \log t_a}{\left(\frac{1}{T} - \frac{1}{T_a}\right)} \tag{2.15}$$

where t_a is a time constant and T_a temperature constant. Two constants have to be evaluated here as against one constant for the LMP approach. In this approach, iso-stress lines obtained by plotting $\log t_f$ against $1/T$ are not parallel but converge at the point $\log t_a, \frac{1}{T_a}$, defining the two constants in the equation. The GSP has not found widespread use compared to the LMP and OSDP. The evaluation of two constants before usage is one set-back of the GSP method.

Manson-Haferd Parameter (MHP)

The Manson-Haferd Parameter (MHP) is given as [116], [117]

$$MHP = \frac{\log t_f - \log t_a}{T - T_a} \tag{2.16}$$

Like in the GSP, t_a is a time constant while T_a is temperature constant. Iso-stress lines in this case are obtained by plotting $\log t_f$ against T and all iso-stress lines converge at the point defined by the two constants $(\log t_a, T_a)$ [111]. A plot of stress against MHP yields a master curve. From the master curve, MHP for any stress level could be obtained and the time to failure for a particular temperature is evaluated using Equation (2.16). The MHP method seems to be a bit conservative and tends to predict shorter life compared to the LMP and OSDP methods [111].

Manson-Succop Parameter (MSP)

The Manson-Succop Parameter (MSP) is given as [92], [118],

$$MSP = f\left(\sigma \text{ or } \frac{\sigma}{E}\right) = \log t_f - BT \qquad (2.17)$$

where B is a material constant. MSP method is similar to the MHP method in terms of the variables used in generating the iso-stress lines ($\log t_f$ is plotted against T). It is equally likened to the LMP method for having one constant and hence parallel iso-stress lines. The gradient of each iso-stress line corresponds to the constant B. The MSP is also similar to the OSDP method in terms of parallelism of the iso-stress lines. A master curve can be generated from which time to failure due to creep of a given component can be determined for given stress and temperature levels. The MSP approach is also widely used for creep life determination.

Although, the LMP is the most frequent used of the time-temperature parameters, the choice of the parameter to be used is material and application dependent. This is because different parameters fit different data more appropriately. Agale-Khafri and Noori [119] in carrying out life prediction of Ni-based super alloy (Rene 80) between 1144 and 1255K at various stress levels using the time-temperature parameters, OSDP, LMP and MSP discovered that the MSP method offered the highest degree of fit.

The time-temperature parameters could be used by introducing a general form of the master curve equation which may be a representation of all parameters [117]. Such an equation has constants which can be solved depending on the parameter used. A general creep parameter is given as by Equation (2.18) [120],

$$P(\sigma) = \frac{\frac{\log t}{\sigma^q} - \log t_a}{(T - T_a)^r} \tag{2.18}$$

where T_a, t_a, q and r are material constants. These constants are to be determined from available experimental data. Various values of q and r determine the type of parameter in use. For instance, the Manson-Haferd Parameter is obtained when $q = 0$ and $r = 1$. Table 2.2 shows the parameter constants for some of the parametric methods while Figure 2.6 shows the graph of the various parameters considered here.

Table 2.2: Some Values of Constants for Time-Temperature Parameters ([121], p.5)

Material	Sherby–Dorn Q, kJ/mol	Larson–Miller C	Manson–Haferd	
			T_a K	log t_a
Various steels and stainless steels	≈400	≈20	-----	-----
Pure aluminum and dilute alloys	≈150	-----	-----	-----
Nimonic 81A (Ni-based)	380	18	311	16
1% Cr–1% Mo–0.25%V steel	460	22	311	18
A-286 stainless steel	380	20	367	16

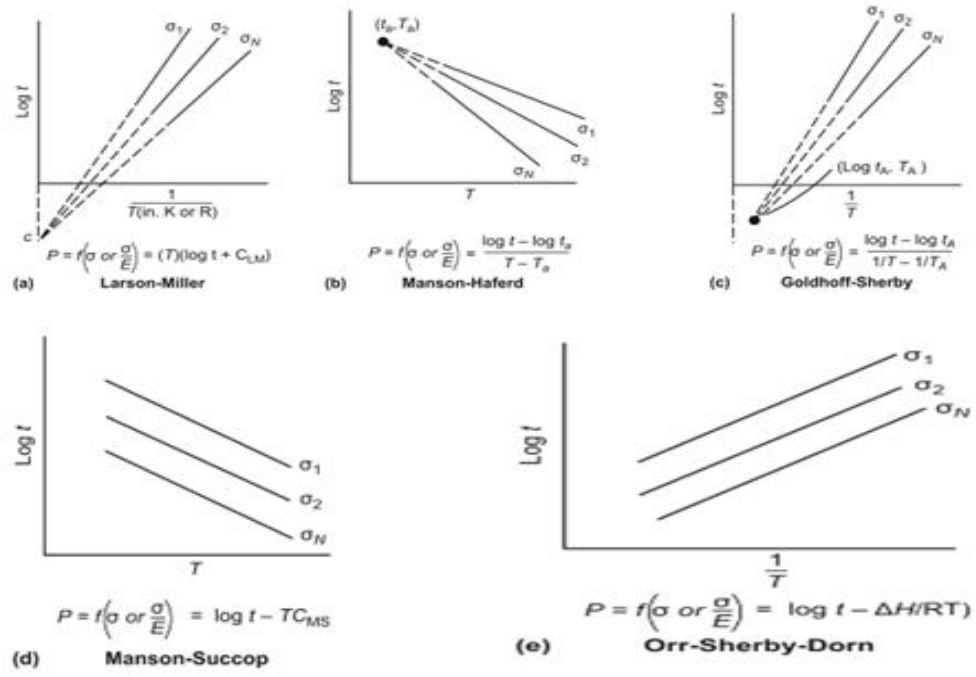

Figure 2.6: Graphs of various Time-Temperature Parameters ([118], p.26)

Minimum Commitment Method

In an attempt to bring all the time-temperature parameters under single and similar analysis, Manson and Ensign introduced the Manson-Ensign minimum commitment method [118]. In this, an equation is formulated which contain constants and falls into any of the parameters in use by determining the constants from the data obtained for a given material. This appears like a similar treatment compared to the creep general equation in [120]. The equation adopted for this method after several trials takes the form of Equation (2.19) [118],

$$\log(t) + A.P.\log(t) + P = G \tag{2.19}$$

where

$$P = R_1 T + \frac{R_2}{T} \tag{2.19a}$$

and

$$G = B + C.\log(\sigma) + D\sigma + E\sigma^2 \tag{2.19b}$$

The resemblance of the minimum commitment equation to any of the parameters is actually revealed when the constants R_1 and R_2 are determined from the actual data [118].

2.4.1.3 Other Creep Life Estimation Relations

Three other relevant creep relations for life estimation are considered here. These are the Monkman-Grant Method, the theta Projection Method and the Omega method.

Monkman-Grant Method

The steady state creep rate and rupture time is also modelled by the Monkman-Grant relationship given by Equation (2.20) [100],

$$\dot{\varepsilon}_c^s = \frac{C}{t_f} \; or \; t_f.\dot{\varepsilon}_c^s = C \tag{2.20}$$

where $\dot{\varepsilon}_c^s$ is the steady state creep rate and C is a constant. But $\dot{\varepsilon}_c^s = A\exp\left(\frac{Q}{kT}\right)$, thus Equation (2.20) can be put in the form of Equation (2.21),

$$t_f = \frac{C}{A}\exp\left(\frac{Q}{kT}\right) \tag{2.21}$$

Or

$$\log t_f - m_{NG} = 0.43\left(\frac{Q}{RT}\right) \tag{2.22}$$

where $m_{NG} = \frac{C}{A}$ is the Monkman-Grant constant [100]. The relationship between t_f and the steady creep rate, $\dot{\varepsilon}_c^s$, which is actually the minimum or secondary creep rate, $\dot{\varepsilon}_{\min}$ is equally represented by the Monman-Grant relationship as in Equation (2.23) [122],

$$t_f \dot{\varepsilon}_{\min}{}^m = C \tag{2.23}$$

m and C are constants. the exponent, m has value between 0.8 and 0.95 while C varies between 3 and 20 for the metals and alloys Monkman and Grant evaluated originally [122]. The Monkman-Grant relationship has been modified by the introduction of

failure strain ε_f in order to obtain better fit of many materials. This modified form is [122]

$$\frac{t_f \dot{\varepsilon}_{\min}^{\ m'}}{\varepsilon_f} = C' \tag{2.24}$$

where m' is close to unity and C' is a constant which is temperature dependent. The Monkman-Grant relationship shows that the time to failure or overall rupture life t_f of a material in long term tensile creep tests is inversely proportion to the power function of the minimum creep rate and the relationship holds for heat resistant structural materials such as ferritic steels and nickel-based alloys [69].

Theta Projection Method

The theta projection method is one of the creep relations that can model the three stages of creep. It considers for the primary creep, secondary creep (steady state creep) and tertiary creep [37]. Two concepts about the theta projection method have evolved. These are the 4-theta projection and the 6-theta projection methods and these are given by Equations (2.25) and (2.26) respectively [37], [48], [123]–[125],

$$\varepsilon_c = \theta_1\left(1 - e^{-\theta_2 t}\right) + \theta_3\left(e^{\theta_4 t} - 1\right) \tag{2.25}$$

$$\varepsilon_c = \theta_1\left(1 - e^{-\theta_2 t}\right) + \theta_3\left(e^{\theta_4 t} - 1\right) + \theta_5\left(1 - e^{-\theta_6 t}\right) \tag{2.26}$$

where θ_1, θ_2, ..., θ_6 are the theta projection parameters (constants) which are temperature and stress dependent and obtained from experimental data [37], [48]. The last term in the 6-theta projection presentation, $\theta_5\left(1 - e^{-\theta_6 t}\right)$ is introduced to ensure proper creep modelling at low creep strain, ε_c and time, t [37]. The creep strain rate $\dot{\varepsilon}_c$ is obtained by differentiating the expression for ε_c when the theta values are known.

According to Law, et al. [123], the theta method, Equation (2.25) models the primary and tertiary creep stages and views the secondary creep stage as an inflexion on the creep curve where strain hardening and strain softening effects are equal. θ_1 and θ_2 take care of primary creep while θ_3 and θ_4 address tertiary creep [48]. The temperature and stress dependent theta terms are expressed as in Equation (2.27) [123],

$$\log \theta_i = A_i + B_i\sigma + C_iT + D_i\sigma T \tag{2.27}$$

where $i = 1, 2, 3, 4.$ A modified theta projection method which uses one rate constant has been proposed [126]. The theta projection method, although models the three stages of creep, the heavily experimental data dependence on the evaluation of creep data makes it unsuitable for the creep life analysis in this research.

Omega Method

The omega method was developed by the Materials Properties Council (MPC) hence in some cases it is referred to as the MPC omega method [127], [128]. The omega method is expressed as [129],

$$\dot{\varepsilon}_c = \dot{\varepsilon}_0 . e^{\Omega \varepsilon_c} \tag{2.28}$$

where $\dot{\varepsilon}_0$ is an imaginary initial strain rate and Ω is the omega method parameter which is a variable that depends on temperature and stress and it is determined experimentally. $\dot{\varepsilon}_0$ approximates the minimum creep rate $\dot{\varepsilon}_{\min}$ when the primary creep region is small [129]. The expression is put in terms of strain and time by integrating Equation (2.28). Also, Equation (2.28) could be put in logarithmic form before integrating it. The relevant equations are given below [37], [129]:

$$\frac{1}{\dot{\varepsilon}_0 \Omega}\left(1 - e^{\Omega . \varepsilon_c}\right) = t_f \tag{2.29}$$

$$\ln \dot{\varepsilon}_c = \ln \dot{\varepsilon}_0 + \Omega \varepsilon_c \tag{2.30}$$

$$\varepsilon_c = \left(\frac{1}{\Omega}\right) \ln \left[\frac{1}{1 - \Omega \dot{\varepsilon}_0 t_f}\right] \tag{2.31}$$

Equations (2.29) and (2.31) are equivalent but Equation (2.31) seems to be more appropriate as the rupture life is expressed in terms of the other parameters. The exponential term in Equation (2.29) becomes negligible for large values of $\Omega\varepsilon_c$ and the rupture time under this condition is expressed by Equation (2.32) [129],

$$t_f = \frac{1}{\Omega \dot{\varepsilon}_0} \tag{2.32}$$

From the above, it is clear that with an estimate of $\dot{\varepsilon}_0$ and Ω, the rupture time t_f can be computed and this is an advantage of using the omega method. The omega method has been widely used, although its shortcoming has also been pointed out [127]–[129].

2.4.1.4 Review of Some Classifications of Creep Life Estimation Approaches

Several creep life estimating approaches have been explored so far but no attempt has so far being made to put these approaches in classified form. When the work of Faradani [93] is placed side by side with the works of Abdul Ghafir [37] and that of Eshati [92], one can conclude that there are no hard and fast rules covering the classification of creep lifing techniques, any approach adopted may be a matter of choice or convenience. Nonetheless, a great deal of work was done in classifying the creep life estimation approaches in the above literatures, thus, the creep life classification approaches from the perspectives of Abdul Ghafir [37] and Eshati [92] are summarized below.

Four categories of creep life estimation approaches could be identified. These are model based approach, service based approach, statistical/ probabilistic based approach, and soft computing approach [37] . Each of the approaches involves creep relations discussed directly or indirectly in previous sections, except the service based approach where little exposition will be done here. The model based approach involves the creation of a model- empirical, analytical or numerical and it divided into total life approach and damage tolerance approach. It is pertinent to point out here that all creep life estimation approaches could be put into two major divisions- total life approach and damage tolerance approach. In some cases, the statistical/ probabilistic approach is brought out to form a third group under this classification. Continuing with the classifications in the cited literatures, the total life approach is divided into life-based, strain-based and damage-based approaches. The life-based approach involves the determination of the life t_f of the component concerned using mainly the time-temperature parameters. The strain-based approach involves estimation of life using creep strain ε_c or creep strain rate $\dot{\varepsilon}_c$. The Monkman-Grant creep relation and the Omega method fall into this category. In damage-based models, creep damage is viewed as occurring progressively and accumulatively from zero damage level and reaches

failure with time depending on the material and the loading. Two theories are widely used under this context. These are the linear damage accumulation (LDA) theory and the continuum damage mechanics (CDM) theory. The LDA theory which views damage as linearly cumulative is mainly used in creep life assessment of steam turbine blades [130]. In both theories, Damage assessed using a damage parameter D which value ranges from zero for a material with no amount of damage to unity at the point of failure. In CDM, a damage state variable is introduced which is an internal variable and represents an irreversible damage accumulation with time [92], [130].The CDM gives more accurate results [130].

In the service-based approach, direct assessment of material in service is required using either non-destructive testing (NDT) techniques (where the material is tested while in service place) or destructive testing (DT) techniques (where the material is removed for testing). Non-destructive testing methods include among others visual inspection, magnetic particle inspection, radiographic examination, ultrasonic testing, liquid penetrant testing, etc.[131]–[134]. Non-destructive testing of materials which principally involves surface and volume examinations is less accurate in creep life prediction compared to destructive testing techniques [37], [131]. The statistical / probabilistic approach is mainly used in conjunction with other approaches, especially the model-based approaches to account for the uncertainties in the parameters that affect creep life in a given model or to develop the relationship between creep life and the parameters affecting it or as a substitute of an existing model [37], [92]. Eshati[92] tend to incorporate the soft computing techniques in the statistical and probabilistic category but Abdul Ghafir[37] put it in a class of its own. The soft computing techniques involve among others artificial neural network (ANN), fuzzy logic and evolution algorithm. These techniques which are widely used today are employed to overcome the complexities and limitations inherent in the model-based and service-based approaches [37].

2.4.2 Fatigue Life Prediction Methods

There are two major approaches to the determination of the life of a component due to fatigue. These are total life approach and defect-tolerance approach. The total life approach technique is divided into stress-based approach and strain-based approach

[47]. In the total life approach, the number of fatigue cycles (stress-based or stran-based) that a component undergoes before failure is determined. The total life approaches are the classical approaches to fatigue design and do involve the use of the S-N curve. The defect-tolerant approach is the fracture mechanics approach to fatigue design. It involves the determination of an initial (dominant) crack in a material and the number of cycles required to propagate this initial crack to some critical dimension (size). In this approach, the prediction of the crack propagation life involves empirical crack growth laws based on fracture mechanics [47]. This approach is thus also referred to as fracture mechanics approach.

There are also ‘safe-life’ and ‘fail-safe’ concepts in designing materials against fatigue. These concepts or approaches were developed by aerospace engineers. In the safe-life approach, the load under which a critical component is operating is estimated. Tests are then carried out in laboratory on a similar component, under the same loading conditions to determine the number of cycles the component undergoes before failure. Using an appropriate factor of safety, the fatigue life of the component in terms of the number of cycles in safe operation is obtained. The real component in operation is retired once this life is approached even if the component still performs its designed function. In this approach, several unknowns has to be accounted for but a safe operating life can be guaranteed by using a large factor of safety, but it may not be desirable from the economic and performance perspectives [47].

In the fail-safe approach, as the name implies, the component can fail but no catastrophe before replacement. The component is assumed to contain flaws and the critical flaw size is determined. Inspection techniques are put in place to check the size of the crack at regular intervals or on ‘continuous basis’ as the crack propagates. The component is replaced when it is no longer safe for usage depending on the size of the crack [135]. A critical look at the safe-life and fail-safe concepts will reveal that the safe-life concept is about the total life approach and the fail-safe concept is about the defect-tolerant approach. The stress-based, strain-based and defect-tolerant approaches to fatigue life estimation are considered next.

2.4.2.1 Stress-Life Approach

The stress life approach to fatigue life determination is applicable to high cycle fatigue (HCF) [47], [136]. This method involves the testing of flawless materials under fatigue loading. The number of fatigue cycles the component undergoes before failure at the applied stress amplitude is noted. An S-N curve for the material can then be generated for the material from which the life of the material (number of cycles to failure) at each stress amplitude can be determined [47], [136]. An S-N curve is given in Figure 2.3 which shows the probabilistic nature of fatigue. Figure 2.7 shows an S-N curve which shows the various cycle ranges that pertains to LCF and HCF respectively and the condition for infinite life.

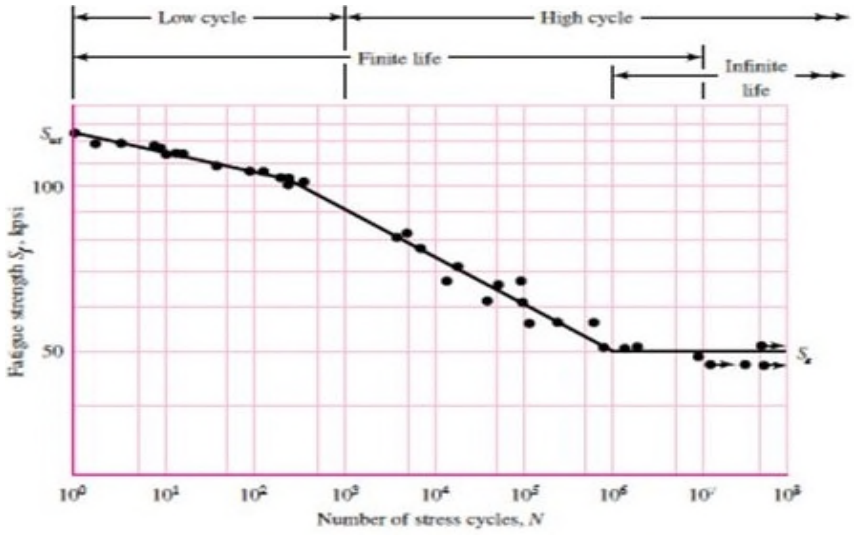

Figure 2.7: S-N Diagram showing LCF and HCF Ranges and Condition for Finite Life ([136] , p.266)

Some parameters need to be defined at this stage. These are maximum stress, minimum stress, mean stress, load ratio, stress amplitude, stress range, endurance limit or fatigue limit and stress cycle.

- ***Maximum stress***, σ_{max} - This is the maximum stress in the given load spectrum. It is tensile in nature.
- ***Minimum stress***, σ_{min} - This is the maximum compressive stress. It is negative by convention. For fully reversed loading, $\sigma_{min} = -\sigma_{max}$.

- ***Load ratio***, R - This is the ratio of $\sigma_{\min}$ to $\sigma_{\max}$. That is,

$$R = \frac{\sigma_{\min}}{\sigma_{\max}} \tag{2.33}$$

For fully reversed loading, $R = -1$ since $\sigma_{\min} = -\sigma_{\max}$. Similarly, $R = 0$ for zero tension fatigue, and $R = 1$ for static load [47].

- ***Stress amplitude*** σ_a - This is given by the relation below:

$$\sigma_a = \frac{\sigma_{\max} - \sigma_{\min}}{2} \tag{2.34}$$

Stress Range, $\Delta\sigma$ - This is expressed as,

$$\Delta\sigma = \sigma_{\max} - \sigma_{\min} = 2\sigma_a \tag{2.35}$$

The stress range is twice the stress amplitude.

- ***Mean Stress***, σ_m - This is expressed as the mean value of $\sigma_{\min}$ and $\sigma_{\max}$. Thus,

$$\sigma_m = \frac{\sigma_{\min} + \sigma_{\max}}{2} \tag{2.36}$$

- ***Endurance limit or fatigue limit***, σ_e - This is the stress amplitude below which a material will undergo infinite number of cycles without failing. Some materials do not have endurance limit.

- ***Stress Cycle,*** N - This corresponds to one set of the application and removal tensile and compressive load. If a material has a fatigue life of N_f, this is equivalent to $2N_f$ stress reversals; that is, stress changing from tensile to compressive and vice-versa. Thus, cycles to failure is in most cases replaced with number of reversals to failure which is $2N_f$.

Further work on fatigue requires knowledge of the loading types usually encountered in practice.

Fatigue Loading Types

There are four classes of fatigue loading as presented in [137]. These are constant amplitude proportional loading, constant amplitude non-proportional loading, non-constant amplitude proportional loading, and non-constant amplitude non- proportional loading. In fatigue life analysis, the type of loading is important in estimating the life of the material.

Fatigue Life Estimation Relations

A linear relationship exists between the stress amplitude, σ_a and the number of reversals to failure, $2N_f$ on a log-log scale. This is given by Basquin equation in the form below for uniaxial loading and zero mean stress [47],

$$\sigma_a = \sigma'_f \left(2N_f\right)^b \tag{2.37}$$

where σ'_f is the fatigue strength coefficient and b is known as the fatigue strength exponent or Basquin exponent. Taking the logarithm of both sides of Equation (2.37), a linear relationship is obtained as given by Equation (2.38),

$$\ln\sigma_a = \ln\sigma'_f + b\ln\left(2N_f\right) \tag{2.38}$$

For most metals, b is in the range -0.05 to -0.12 [47].

Mean Stress Effect in Stress-Based Fatigue

Basquin equation is applicable for zero mean stress condition. In real life loading conditions, situations of non-zero mean stress are very common. The stress amplitude for non-zero mean stress is estimated using mainly three relations of (old). These are the Soderberg relation, modified Goodman relation, and Gerber relation. These relations are presented in Equations (2.39) to (2.41) [47], [138],

Soderberg relation: $$\frac{\sigma_a}{\sigma_a'} + \frac{\sigma_m}{\sigma_y} = 1 \tag{2.39}$$

Modified Goodman relation: $$\frac{\sigma_a}{\sigma_a'} + \frac{\sigma_m}{\sigma_u} = 1 \tag{2.40}$$

Gerber relation: $$\frac{\sigma_a}{\sigma_a'}+\left(\frac{\sigma_m}{\sigma_u}\right)^2=1 \qquad (2.41)$$

σ'_a is the alternating stress amplitude at zero mean stress and fully reversed loading, σ_u is the tensile strength of the material while σ_y is the material yield strength. Equations (2.39) to (2.41) can be cast in the form,

$$\sigma_a=\sigma'_a\left[1-\left(\frac{\sigma_m}{\sigma_u}\right)^x\right] \qquad (2.42)$$

where $x=1$ for the modified Goodman relation, $x=2$ for the Gerber relation and $x=1$ and $\sigma_u=\sigma_y$ for the Soderberg relation [138].

The Soderberg relation provides a conservative estimate of fatigue life for most engineering alloys. It provides no room for material to even yield. The modified Goodman relation gives results that approximate experimental data for brittle metals but conservative for ductile alloys. The Gerber line provides the best fit to the failure points of test data and it is for ductile alloys under tensile mean stresses [47], [139]. Generally, for a given material, as the mean stress increases, the fatigue life decreases. The plot of the three relations is shown in Figure 2.8. The three lines intersect the ordinate axis at $\sigma_e=\sigma'_a$ where the mean stress is zero. On the abscissa, the Gerber line and the Goodman line intersect at σ_u, the tensile strength of the material, while the Soderberg line cuts the abscissa at the yield strength of the material, σ_y. At zero stress amplitude, the material undergoes purely static loading and failure will occur when the load exceeds the tensile strength of the material for the Goodman and Gerber relations. In the same vein, failure will occur when the yield strength is exceeded for the Soderberg relation. These facts are employed in plotting the lines. In the diagram, a yield line, known as limit on 'first circle' is constructed which intersects the yield strength on both axes.

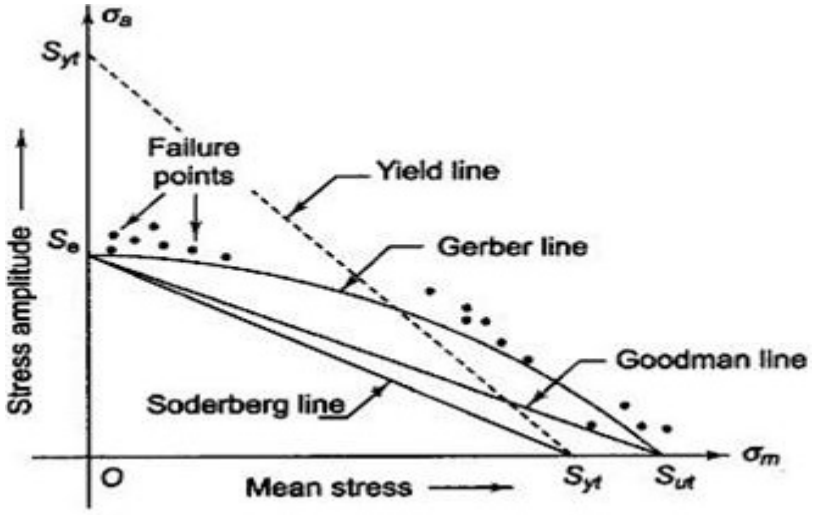

Figure 2.8: Soderberg, Goodman and Gerber Lines ([139], p.167)

Shigley [136] presented ASME relation, Langer (static yield) relation together with an equation for the three lines presented above. The ASME relation and the Langer (static yield) relation are given by Equations (2.43) and (2.44) respectively,

ASME-elliptic relation: $$\frac{\sigma_a}{\sigma_a'} + \left(\frac{\sigma_m}{\sigma_y}\right)^2 = 1 \qquad (2.43)$$

Langer (static yield) relation: $\sigma_a + \sigma_m = \sigma_y$ (2.44)

A factor of safety may be included in the above relations to reduce the limiting stresses- σ_e, σ_y and σ_u . The ASME-elliptic relation, like the Gerber relation, fits experimental data points to a good degree. The five relations are shown in Figure 2.9. Every point on each of these lines may be viewed as consisting of pans of points of σ_a and σ_m. Based on a given failure relation, any point below a line is safe while a point above a line depicts failure under the given load condition. A load line which slope is $\frac{\sigma_a}{\sigma_m}$ is obtained by drawing a straight line through a given point. One of such points through the modified Goodman line passes through point A in Figure 2.9.

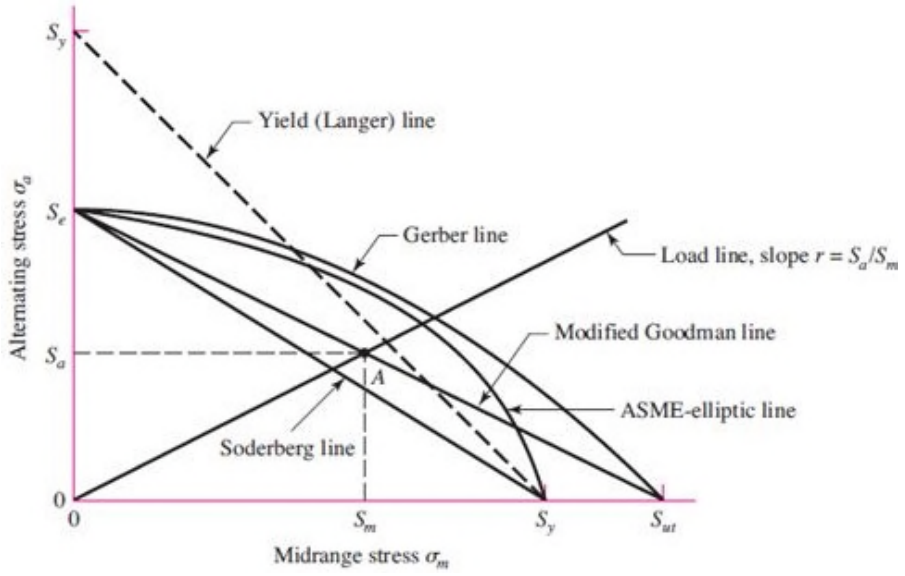

Figure 2.9: Fatigue Diagram Showing Various Failure Criteria ([136] , p.297)

Many other researchers have accounted for the mean stress effect in stress-based fatigue life analysis in their works. Some of these works are those of Morrow, Walker, and Smith, Watson and Topper (SWT) as presented by Ince and Glinka [140]. Their relations are presented in Equations (2.45) to (2.47),

Morrow relation: $$\frac{\sigma_a}{\sigma_a'} + \frac{\sigma_m}{\sigma_f} = 1 \qquad (2.45)$$

Walker relation: $$\sigma_a' = \sigma_{\max}^{\,1-\gamma}\sigma_a^{\,\gamma} = \sigma_{\max}\left(\frac{1-R}{2}\right)^{\gamma} = \sigma_a\left(\frac{2}{1-R}\right)^{\gamma} \qquad (2.46)$$

SWT relation: $$\sigma_a' = \sqrt{\sigma_{\max}\sigma_a} = \sigma_{\max}\sqrt{\frac{1-R}{2}} = \sigma_a\sqrt{\frac{2}{1-R}} \qquad (2.47)$$

where σ_f is the true fracture strength (applicable to Morrow relation only and γ is a material constant. All the fatigue life estimation relations considered so far, beside the Basquin relation, account for the mean stress. Morrow's relation is actually a modification of the Basquin relation as presented by Suresh [47] . Probably, the best relation that accounts for mean stress effect in stress-based fatigue life analysis is

Smith-Watson-Topper relation as it generally gives good agreement with test data for many engineering materials [141].

Other Effects in Stress-Based Fatigue Life Approach

Other effects aside mean stress effect in stressed-based fatigue life analysis are effects of surface treatment/surface finish effects, frequency, stress concentration due to the presence of notches and the nature of the loading in the case of multi-axial loading. Surface treatment includes among others nitriding, carburizing, flame hardening, induction hardening and shot peening. Surface treatment leaves the surface of the material with residual stresses, which if compressive is beneficial in terms of fatigue life but detrimental if tensile. Shot peening as a manufacturing process induces high compressive residual stresses on the surface of a material thus increases the fatigue life of a material [47], [142].

Stress Concentration and Notch sensitivity

The presence of discontinuities such as holes, groves or notches in materials lead to increase in stresses in the parts they are found. They are referred to as stress concentrators. Fatigue failure is almost always perceived to start at regions of discontinuities. Plastic strain occurs when the stress at the site of stress concentration exceeds the elastic limit [136]. The existence of cyclic plastic strain leads to fracture of the material. An elastic stress concentration factor K_t is introduced to account for the induced stresses. Some materials do not respond to the presence of notches fully, hence, the elastic stress concentration factor is replaced with a fatigue stress concentration factor K_f which is given as,

$$K_f = \frac{\max imum\ stress\ in\ notched\ specimen}{stress\ in\ notch\ \ free\ specimen} \qquad (2.48)$$

OR

$$K_f = \frac{un\ notched\ \ bar\ endurance\ \ \lim it}{notched\ bar\ endurance\ \lim it} \qquad (2.49)$$

$K_f < K_t$.

A notch sensitivity index is used to show how the elastic stress concentration factor agrees with the fatigue stress concentration factor in the form below [47], [137],

$$q = \frac{K_f - 1}{K_t - 1} \tag{2.50}$$

The parameter q varies from zero to unity. $q = 0$ when $K_f = 1$. In this case, there is no notch effect. $q = 1$ when there is full notch effect and $K_t = K_f$. In fatigue life estimation using the stress life approach for a material with a notch, K_f has to be determined. This involves the determination of K_t first which is a function of the geometry and loading mode only. The material is then specified and q is read from notch sensitivity charts. Figure 2.10 shows notch sensitivity charts for two different materials. K_f is the obtained from Equation (2.51) [47], [137],

$$K_f = 1 + q(1 + K_t - 1) \tag{2.51}$$

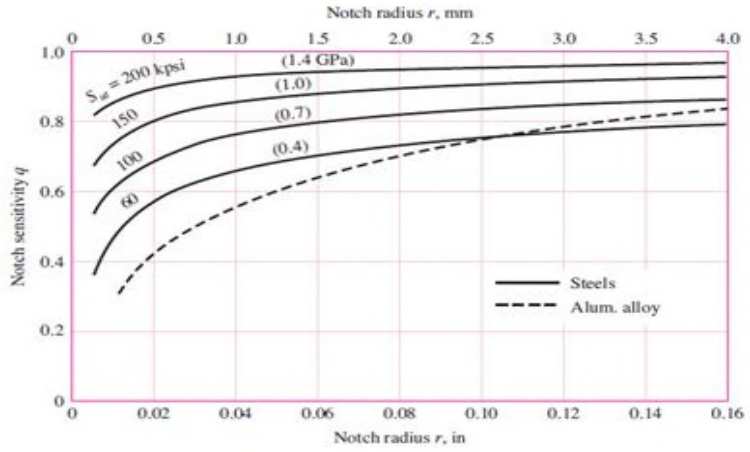

Figure 2.10: Notch Sensitivity Charts ([136], p.287)

Stress-Based Fatigue Life Prediction for Multi-axial Cyclic Stresses

The Basquin equation for zero mean stresses and all the other equations considered that account for mean stresses are all restricted to uniaxial stress application. For multi-axial stress application involving zero mean stress, Basquin equation is applied in the form below [47],

$$\sigma_{a,e} = \sigma'_f \left(2N_f\right)^b \tag{2.52}$$

where $\sigma_{a,e}$ is the amplitude of the effective stress defined based on the Von Mises Criterion as,

$$\sigma_{a,e} = \sigma_e = \frac{1}{\sqrt{2}}\sqrt{\left(\sigma_x - \sigma_y\right)^2 + \left(\sigma_y - \sigma_z\right)^2 + \left(\sigma_z - \sigma_x\right)^2 + 6\left(\tau_{xy}{}^2 + \tau_{yz}{}^2 + \tau_{zx}{}^2\right)} \tag{2.53}$$

σ_x, σ_y and σ_z are the three normal stresses while τ_{xy} , τ_{yz} and τ_{zx} are the three shear stress components.

For fluctuating multi-axial stresses, the effective stress is given in terms of the stress amplitudes of the principal stresses σ_{1a}, σ_{2a} and σ_{3a} where $\sigma_{1a} > \sigma_{2a} > \sigma_{3a}$; this is given by Equation (2.54),

$$\sigma_{a,e} = \sigma_e = \frac{1}{\sqrt{2}}\sqrt{\left(\sigma_{1a} - \sigma_{2a}\right)^2 + \left(\sigma_{2a} - \sigma_{3a}\right)^2 + \left(\sigma_{1a} - \sigma_{3a}\right)^2} \tag{2.54}$$

Liu and Malzdevan [143] gave a method of predicting fatigue life for multi-axial loading with non-zero mean stress.

Damage Summation for Uniaxial Loading

Tests about fatigue are usually conducted under constant stress amplitude and constant frequency. In practice, members are subjected to a range of fluctuating loads [144]. Damage summation rule provided by Palmgren and Miner [145], the Palmgren-Miner rule , is used in this case [47], [144]. In this, blocks of loads are generated from the entire load spectrum. Each block of load is of the same load amplitude and mean stress. The damage summation is given by Equation (2.55),

$$D = \sum_{i=1}^{m} \frac{n_i}{N_{fi}} \tag{2.55}$$

where m is the number of blocks of load formed, n_i is the number of cycles corresponding to the i^{th} block, N_{fi} is the number of cycles to failure corresponding to

the stress amplitude at the i^{th} block. $\frac{n_i}{N_{fi}}$ represents a fraction of damage. Failure is assumed to be cumulative and failure occurs when $D=1$. This linear damage rule does provide incorrect results [47]. It is pertinent to point out here that the Palmgren-Miner damage summation rule is applicable to creep-fatigue interactions and LCF-HCF interactions, etc.

2.4.2.2 Strain Life Approach

The strain-life approach to fatigue life estimation or fatigue design is reserved for low cycle fatigue, where a component is believed to undergo plastic deformation before failing. In getting to the plastic region, the material first experiences elastic strain. Thus, the total strain the material experiences is the sum of the elastic strain and the plastic strain expressed in terms of the strain amplitude as given by Equation (2.56) [136]**,**

$$\frac{\Delta\varepsilon}{2}=\frac{\Delta\varepsilon_e}{2}+\frac{\Delta\varepsilon_p}{2} \tag{2.56}$$

$\Delta\varepsilon$ is the total strain range, $\frac{\Delta\varepsilon}{2}$ is the total strain amplitude, $\frac{\Delta\varepsilon_e}{2}$ is the elastic strain amplitude and $\frac{\Delta\varepsilon_p}{2}$ is the plastic strain amplitude. The elastic strain is taken care of by Basquin equation, noting that the elastic strain amplitude relates with the stress amplitude in the form of Equation (2.57) [144],

$$\frac{\Delta\varepsilon_e}{2}=\frac{\Delta\sigma}{2E}=\frac{\sigma_a}{E} \tag{2.57}$$

E is the Young's Modulus of the material. The elastic stress amplitude is thus given by Equation (2.58),

$$\frac{\Delta\varepsilon_e}{2}=\frac{\sigma'_f}{E}\left(2N_f\right)^b \tag{2.58}$$

The plastic strain amplitude is given by Coffin-Manson relation in the form of Equation (2.59) [144],

$$\frac{\Delta\varepsilon_p}{2} = \varepsilon'_f \left(2N_f\right)^c \tag{2.59}$$

where $\frac{\Delta\varepsilon_p}{2}$ is the plastic strain amplitude, ε'_f is the fatigue ductility coefficient and c is the fatigue ductility exponent. The total strain amplitude is thus given by Equation (2.60),

$$\frac{\Delta\varepsilon}{2} = \frac{\sigma'_f}{E}\left(2N_f\right)^b + \varepsilon'_f \left(2N_f\right)^c \tag{2.60}$$

Equation (2.60) is for uniaxial fatigue loading. For torsional fatigue loading, the relation takes the form of Equation (2.61) [144],

$$\frac{\Delta\gamma}{2} = \frac{\tau'_f}{E}\left(2N_f\right)^{bo} + \gamma'_f \left(2N_f\right)^{co} \tag{2.61}$$

τ'_f, γ'_f , *bo* and *co* are the torsional fatigue properties. In the plastic region under fatigue loading, the relationship between stress and strain is no longer linear, rather, the responses are more complex and form hysteresis loop [136], [144].

Mean Stress Effects in Strain-Based Fatigue Life Analysis

The mean stress of the elastic strain term of the total strain amplitude may not be zero. Morrow provided a method which accounts for the mean stress as given by Equation (2.62) [47],

$$\frac{\Delta\varepsilon}{2} = \frac{\sigma'_f - \sigma_m}{E}\left(2N_f\right)^b + \varepsilon'_f \left(2N_f\right)^c \tag{2.62}$$

σ_m is the mean stress. In Equation (2.62), only the elastic term is affected by mean stress. Another version of Morrow's equation where both the elastic and plastic terms are affected by mean stress is given by Equation (2.63) [140],

$$\frac{\Delta\varepsilon}{2} = \frac{\sigma'_f - \sigma_m}{E}\left(2N_f\right)^b + \varepsilon'_f \left(\frac{\sigma'_f - \sigma_m}{\sigma'_f}\right)^{\frac{c}{b}} \left(2N_f\right)^c \tag{2.63}$$

Smith-Watson-Topper also provided a relation which accounts for the mean stress as given by Equation (2.64)[140], [146],

$$\sigma_{\max}\varepsilon_a = \sigma_{\max}\frac{\Delta\varepsilon}{2} = \frac{\left(\sigma'_f\right)^2}{E}\left(2N_f\right)^{2b} + \sigma'_f\,\varepsilon'_f\left(2N_f\right)^{b+c} \qquad (2.64)$$

‘‘*The SWT equation predicts that no fatigue damage occurs when the maximum stress is zero or negative (i.e., compressive), which is not always true. Therefore the Morrow correction should be used for loading sequences that are predominantly compressive. In cases of predominantly tensile loading, the SWT approach is more conservative than the Morrow approach and is thus recommended*’’[147], pp.10.

In the analysis of fatigue failure using the strain-life approach, the major effort is at obtaining the four ‘*fatigue parameters*’ which are σ'_f, ε'_f, b and c. Many researchers have made some inroads in obtaining these parameters. Some of these works will be reviewed after considering transition life, N_t.

Transition Life

The total strain amplitude consists of elastic strain amplitude and plastic strain amplitude as given in Equation (2.60). Both the elastic strain amplitude and the plastic strain amplitude are expressed in terms of the number of reversals to failure in exponential form. Taking the logarithms of both sides of Equations (2.58) and (2.59) give straight line equations as given by Equations (2.65) and (2.66) respectively,

$$\ln\frac{\Delta\varepsilon_e}{2} = \ln\left(\frac{\sigma'_f}{E}\right) + b\ln\left(2N_f\right) \qquad (2.65)$$

$$\ln\frac{\Delta\varepsilon_p}{2} = \ln\varepsilon'_f + c\left(2N_f\right) \qquad (2.66)$$

This implies a plot of the respective strain amplitude against the number of reversal to failure on a log-log scale will give straight lines with slopes b and c respectively. The transition life is the number of reversals to failure at which the elastic strain amplitude is equal to the plastic strain amplitude [147]. This is shown in Figure 2.11. Equating $\frac{\Delta\varepsilon_e}{2}$

and $\frac{\Delta\varepsilon_p}{2}$, the transition life in terms of number of reversals to failure is obtained as in Equation (2.67),

$$2N_t = \left(\frac{\varepsilon'_f E}{\sigma'_f}\right)^{\frac{1}{(b-c)}} \tag{2.67}$$

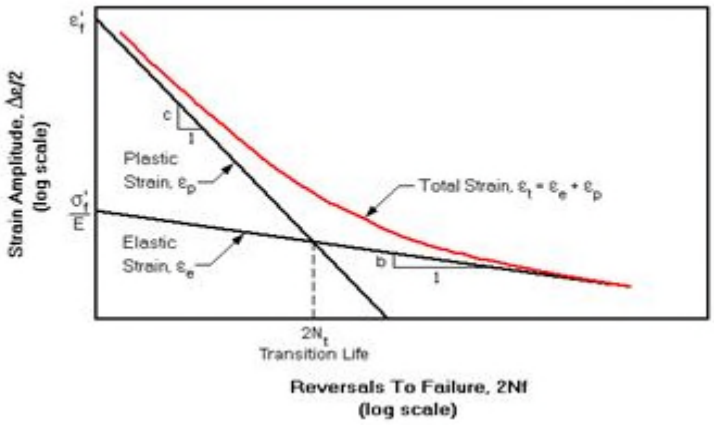

Figure 2.11: Transition Life ([147], p.8)

Other Strain-Life Approach Relations

Park and Song [148] , and Kim et al. [144] reviewed several works revealing different ways of addressing low cycle fatigue. These methods and their findings about the methods are summarized below. The underlying principle is the determination of the four 'fatigue parameters' $\sigma'_f, \varepsilon'_f, b$ and c.

Original Four-Point Correlation Method by Mansion

In this method, the total strain is given by Equation (2.68),

$$\frac{\Delta\varepsilon}{2} = \frac{\sigma'_f}{E}\left(2N_f\right)^b + \varepsilon'_f\left(2N_f\right)^c \tag{2.68}$$

The constants $\sigma'_f, \varepsilon'_f, b$ and c are obtained using the four points P_1, P_2, P_3 and P_4 in Figure 2.12. Two of the points are on the plastic strain curve while the other two are on the elastic strain curve. The fatigue properties are related to monotonic tensile test properties as presented below [144],

$$b = \frac{\log\left[\frac{2.5(1+\varepsilon_f)}{0.9}\right]}{\log\left[\frac{1}{4\times 10^5}\right]} \tag{2.69a}$$

$$c = \frac{1}{3}\left\{\log\left(\frac{0.0132 - \Delta\varepsilon_e^*}{1.91}\right) - \log\left(\frac{1}{4}\varepsilon_f^{\frac{3}{3}}\right)\right\} \tag{2.69b}$$

$$\sigma'_f = \frac{E}{2}\times 10^{b\log 2+\log\left[\frac{2.5\sigma_u(1+\varepsilon_f)}{E}\right]} \tag{2.69c}$$

$$\varepsilon'_f = \frac{1}{2}\times 10^{c\log\frac{1}{20}+\log\left(\frac{1}{4}\varepsilon_f^{\frac{3}{3}}\right)} \tag{2.69d}$$

where ε_f is true fracture ductility, and $\Delta\varepsilon_e^*$ is the value of the elastic strain range at 10^4 cycles on the elastic curve. It is estimated by Equation (2.69e),

$$\Delta\varepsilon_e^* = 10^{b\log(4\times 10^4)+\log\left[\frac{2.5\sigma_u(1+\varepsilon_f)}{E}\right]} \tag{2.69e}$$

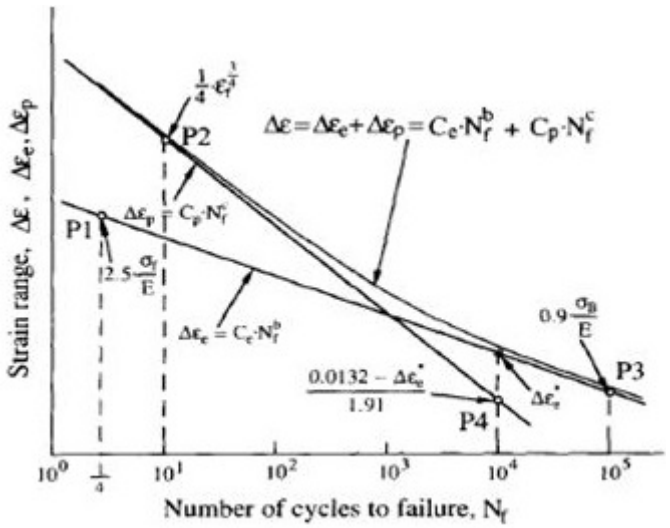

Figure 2.12: Four -Point Correlation Method by Mansion ([148], p.366)

Universal Slopes Method by Mansion

In this method, the total fatigue amplitude is as given by Equation (2.68) while the four fatigue parameters are as follows:

$$b = -0.12; c = -0.16; \quad (2.70a, b)$$

$$\sigma'_f = 1.9018\sigma_u \quad (2.70c)$$

$$\varepsilon'_f = 0.7579\varepsilon_f^{0.6} \quad (2.70d)$$

The fatigue equation is thus given by Equation (2.71),

$$\frac{\Delta\varepsilon}{2} = \frac{1.9018\sigma_u}{E}\left(2N_f\right)^{-0.12} + 0.7519\varepsilon_f\left(2N_f\right)^{-0.16} \quad (2.71)$$

Mitchell's Method

In this method, the four fatigue parameters in use for steels with hardness below 500 HB are given as follows:

$$b = -\frac{1}{6}\log\left[\frac{2\left(\sigma_u + 345\right)}{\sigma_u}\right] \quad (2.72a)$$

$$c = -0.6 \quad (2.72b)$$

$$\sigma'_f = \sigma_f = \sigma_u + 345[MPa] \quad (2.72c)$$

$$\varepsilon_f = \ln\left(\frac{100}{100 - RA}\right) \quad (2.72d)$$

where σ_f is the true fracture stress, and RA is the percentage reduction in area. Mitchell's equation is given as,

$$\frac{\Delta\varepsilon}{2} = \frac{\sigma_u + 345}{E}\left(2N_f\right)^{-\frac{1}{6}\log\left[\frac{2(\sigma_u+345)}{\sigma_u}\right]} + \varepsilon_f\left(2N_f\right)^{-0.6} \quad (2.73)$$

Modified Universal Slopes Method by Maralidharan and Manson

This method is an improvement on the universal slopes method and it shows that the tensile strength of the material also affects the life of the material in low cycle fatigue [144]. It is given by Equation (2.74),

$$\frac{\Delta\varepsilon}{2} = 0.623\left(\frac{\sigma_u}{E}\right)^{0.832}\left(2N_f\right)^{-0.09} + 0.0196\varepsilon_f^{\,0.155}\left(\frac{\sigma_u}{E}\right)^{-0.53}\left(2N_f\right)^{-0.56} \quad (2.74)$$

This the low cycle fatigue life analysis method adopted in this work. The modified universal slopes method is adopted for fatigue life analysis in this research because it provides the best results in fitting fatigue data [148].

Uniform Material Law

This method was proposed by Baumel and Seeger and it employs two different fatigue life expressions for two categories of materials: viz (i) unalloyed and low-alloy steels, and (ii) aluminium and titanium alloys [144], [148]. The respective fatigue relations are given below:

(I) Unalloyed and low-alloy steels:

$$\frac{\Delta\varepsilon}{2} = 1.50\frac{\sigma_u}{E}\left(2N_f\right)^{-0.087} + 0.59\psi\left(2N_f\right)^{-0.58} \qquad (2.75)$$

$$\text{where } \psi = \begin{cases} 1 \ for \ \frac{\sigma_u}{E} \le 0.003 \\ \\ 1.375 - 125.0\frac{\sigma_u}{E} \ for \ \frac{\sigma_u}{E} > 0.003 \end{cases} \qquad (2.76)$$

(II) Aluminum and Titanum alloy:

$$\frac{\Delta\varepsilon}{2} = 1.67\frac{\sigma_u}{E}\left(2N_f\right)^{-0.095} + 0.35\left(2N_f\right)^{-0.69} \qquad (2.77)$$

Modified Four-Point Correlation Method

This method proposed by Ong is an improvement on the original four-point correlation method [144]. The four points used in this metod are shown in Figure 2.13. The fatigue parameters are as follows:

$$\sigma'_f = \sigma_f = \sigma_u\left(1+\varepsilon_f\right) \qquad (2.78a)$$

$$b = \frac{1}{6}\left\{\log\left[0.16\left(\frac{\sigma_u}{E}\right)^{0.89}\right] - \log\left(\frac{\sigma_u}{E}\right)\right\} \qquad (2.78b)$$

$$\varepsilon'_f = \varepsilon_f \tag{2.78c}$$

$$c = \frac{1}{4}\log\left(\frac{0.00737 - \frac{\Delta\varepsilon_e^*}{2}}{2.074}\right) - \log\varepsilon_f \tag{2.78d}$$

where $\Delta\varepsilon_e^*$ is the value of the elastic strain range at 10^4 cycles on the elastic curve and it is given in this case as,

$$\Delta\varepsilon_e^* = 2\frac{\sigma_f}{E}\left[10^{\frac{2}{3}\left\{\log\left[0.16\left(\frac{\sigma_u}{E}\right)^{0.81}\right]-\log\left(\frac{\sigma_f}{E}\right)\right\}}\right] \tag{2.78e}$$

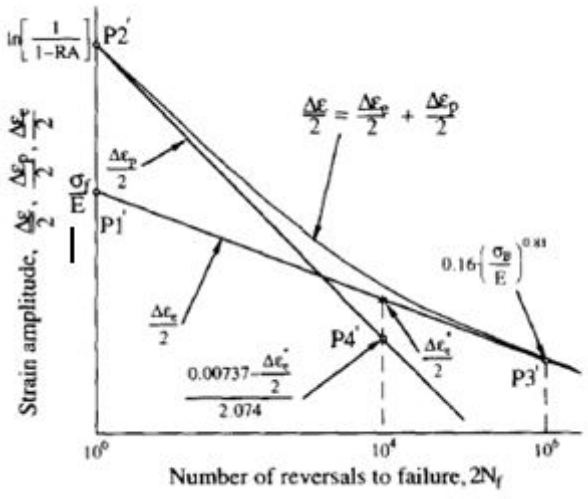

Figure 2.13: Modified Four- Point Correlation Method by Ong ([148], p.367)

Roessle and Fatemi also proposed a method which uses Brinnel Hardness (HB) and Young modulus, a method which Kim et al [144] referred to as hardness method. This method which exponents, b and c, are the same as those of universal slopes method is given by Equation (2.79),

$$\frac{\Delta\varepsilon}{2} = \frac{4.25(HB)+225}{E}(2N_f)^{-0.09} + \frac{0.32(HB)^2 - 487(HB) + 191000(2N_f)^{-0.56}}{E} \tag{2.79}$$

It was pointed out in the previous sections that compressive mean stress leads to life extension while tensile mean stress shortens life. This is shown in Figure 2.14. The effect of tensile stress on fatigue life using Morrow equation is illustrated in Figure 2.15.

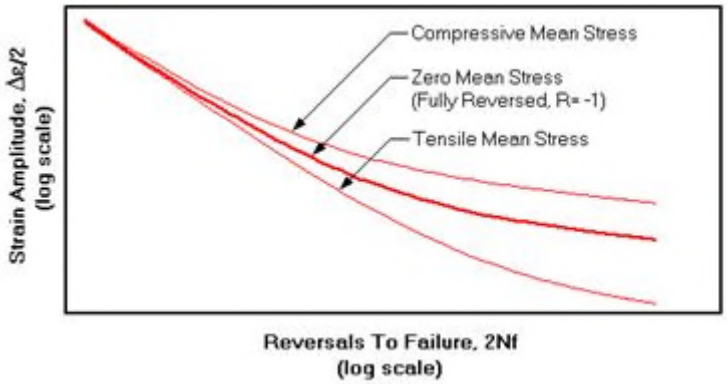

Figure 2.14: Effect of Mean Stress on Fatigue-Life Curve ([147], p.9)

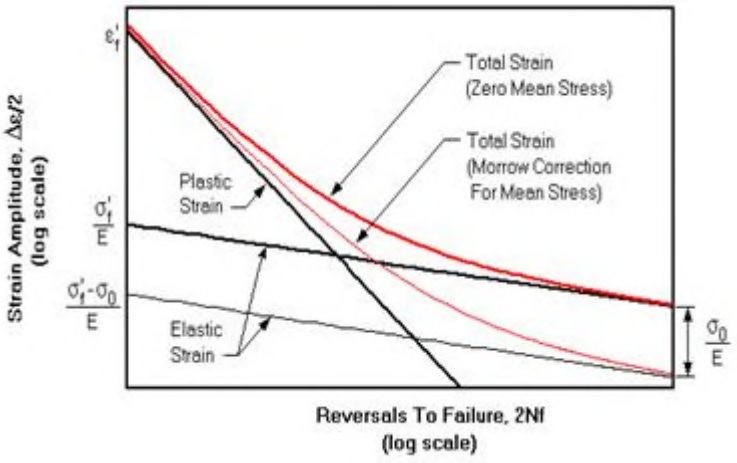

Figure 2.15: Effect of Mean Stress on Fatigue Life Using Morrow Equation ([147], p.10)

2.4.2.3 Defect-Tolerant Approach

The defect-tolerant approach to fatigue life analysis is the fracture mechanics approach where fatigue failure involves crack initiation, crack propagation and rapid crack acceleration to final failure. Crack initiation occurs at points of stress concentrations which are discontinuities or persistent slip bands, and the initial crack size is critical and its determination is one problem with the fracture mechanics approach [138], [149]. Several techniques have been developed to determine the initial crack size including

non-destructive inspection (NDI). The term defect-tolerant is used to portray the fact that a member is allowed to remain in service even if it contains detectable crack provided there is periodic inspection [138]. The total life approaches (stress-based and strain-based) to fatigue life estimation do not specify any damage caused to the material [150]. Although, the total life approaches do represent crack initiation life in smooth specimen, but do not take into cognizance the inherent defects in engineering materials, thus, life may be overestimated [151]. Also, the total life approaches do not yield accurate result or not proper for non-proportion loading condition. The fracture mechanics approach is useful in this case as well as for multiaxial loading [152]. In this research, engine life consumption determination on continuous basis is sought, thus, the defect-tolerant approach is not suitable for such life consumption tracking process.

Other Fatigue Life Prediction Approaches

There are other approaches in fatigue life determination. These are energy based approach, critical plane approaches and continuum damage mechanics approaches [141], [152]. In the energy based approach, products of stress and strain are used to quantify fatigue damage; but this approach does not reflect fatigue damage nucleation and growth observed on specific planes [152]. Critical plane approaches are based on the premise that crack nucleation and growth occurs at specific planes known as critical planes which are planes of maximum shear or maximum tensile stresses. Critical plane models predict the orientation of the crack or failure plane or tend to reflect the physical nature of fatigue damage in addition to predicting fatigue life; One critical plane model is the Fatemi-Socie model [152].

Continuum damage mechanics (CMD) has to do with the mechanical behaviour of deteriorating mediums at the continuum scale. It is a relatively new subject in engineering mechanics and models developed on its basis are mainly for uniaxial fatigue loading[141]. Schutz pointed out six important examples of many unresolved problems in metal fatigue as presented by Cui [141]. These are prediction of fatigue life under variable amplitude loading is still being unsatisfactory, and difficulty in representing actual conditions with experimental data. Also, issues of corrosion fatigue and fatigue-creep interaction are unresolved. The last two unresolved issues are

multiaxial fatigue stresses in variable amplitudes and obtaining fatigue life at very low probabilities of failure.

In this research, low cycle fatigue life consumption of the compressor turbine blades of the LM2500+ engine is considered in addition to creep life and creep-fatigue interaction life of same components. Continuous engine life consumption and hence engine life tracking is required. The modified universal slopes method, one of the total life strain-based low cycle fatigue life estimation techniques, is thus chosen for its accuracy in fitting fatigue data and suitability in being easily programmed for the low cycle fatigue life consumption monitoring needed in this research.

2.4.3 Creep-Fatigue Interaction Life Prediction Methods

Creep-fatigue interaction can be presented in the form of thermo-mechanical fatigue (TMF). TMF may entail creep-fatigue interaction in addition to failure due to oxidation. Failure due to TMF could be expressed by Equation (2.80) [72],

$$\frac{1}{N_f} = \frac{1}{N_f{}^{fatigue}} + \frac{1}{N_f{}^{oxidation}} + \frac{1}{N_f{}^{creep}} \tag{2.80}$$

where N_f, $N_f{}^{fatigue}$, $N_f{}^{oxidation}$, and $N_f{}^{creep}$ are the numbers of cycle to failure, numbers of cycle to failure due to fatigue, numbers of cycle to failure due to oxidation and numbers of cycle to failure due to creep respectively. Depending on the loading and operating environment, one damage mechanism is dominant [72].

Mao and Mahadevan [153] proposed a reliability model for creep and fatigue in materials with the creep-fatigue failure expressed in terms of D_c and D_f in the form,

$$F\left(D_c + D_f\right) = 2 - e^{\theta_1 D_c} + \frac{e^{\theta_1} - 2}{e^{\theta_2} - 1}\left(e^{\theta_2 D_c} - 1\right) - D_f \tag{2.81}$$

where θ_1 and θ_2 are parameters obtained from experimental results. D_c and D_f are the creep and fatigue failure parameters respectively. This model which is said to be continuous also presumes the cumulative nature of creep and fatigue failure terms present in a given materials.

Creep-fatigue interactions can be modelled exploiting two widely used approaches. These are the isothermal method and the linear time and cycle fraction rule by Taira in 1962 as presented by Zhuma and Swanson [83]. The isothermal method does not take creep and other effects into account [154] . Creep-fatigue interaction modelling using the Taira rule is more or less combining the Palmgren-Miner (P-M) rule for fatigue [47] and the Robinson's rule for creep [155] under various combination of stress and temperature. This is the linear damage accumulation rule and it is given by Equation (2.82) [156],

$$D = \sum \frac{N_i}{N_{fi}} + \sum \frac{t_i}{t_{fi}} \tag{2.82}$$

where N_i is the number of cycles at stress amplitude σ_{ai}, N_{fi} is the number of cycles to failure at stress amplitude σ_{ai}, t_i is the time spent at stress-temperature combination corresponding to σ_{ai} while t_{fi} is creep fracture life at stress-temperature combination corresponding to σ_{ai}. D is a parameter which value ranges from zero to unity. When D is unity, failure occurs. The value of D hence shows the level of damage a material has undergone and materials should be replaced when D approaches unity. Smaller values of D portrays more life of the component in question. Under failure, Equation (2.82) takes the form of Equation (2.83),

$$\sum \frac{N_i}{N_{fi}} + \sum \frac{t_i}{t_{fi}} = 1 \tag{2.83}$$

Each of $\sum \frac{N_i}{N_{fi}}$ and $\sum \frac{t_i}{t_{fi}}$ is viewed as separate damage terms- fatigue and creep (rupture) respectively. In this light , we can write [157]

$$D_{fatigue} + D_{rupture} = 1 \tag{2.84}$$

This linear summation rule/model predicts linear behaviour and thus makes unsafe prediction for cyclical work-softening materials and conservative prediction for cyclical work-hardening materials, but, different behaviours are often exhibited by actual

materials [156]. The limitations of the linear accumulation of creep and fatigue [78] notwithstanding, Equation (2.84) will be explored further and used for creep-fatigue interaction analysis in this work. Since creep will be estimated using LMP to give the number of hours to failure and fatigue will be analyzed to reveal the number of cycles to failure, the linear cumulative damage will only reveal the cumulative damage the material (in this case, HP compressor turbine blades) has undergone.

2.5 Basic Observations and Thesis Inputs

Much has been done in life analysis of engineering materials, including those of gas turbine components as revealed in the literatures reviewed. For instance, in creep life estimation of gas turbine components, estimating the stresses and the temperatures imposed on the blades is paramount in obtaining reasonably accurate life prediction. Often, finite element analysis (FEA) and computational fluid dynamics (CFD) based softwares are used in stress analysis and temperature determination. Creep life estimation using these tools requires that geometry of the component will be supplied together with the loads, and the loading changes with engine operation conditions. In case of one-off analysis where the engine life is predicted based on a set of engine operation conditions, the time to failure could be estimated at various locations of the component. If the time to failure is to be estimated using fractional life accumulation techniques, the usage of FEA and CFD tools will not only be time-consuming, but also costly. Also, accurate transfer of real engine operation data to these tools is another issue. But the usage of the more elaborate finite element procedures adopted do not always give satisfactory results [15]. This thus calls for a means of monitoring engine life consumption where the accuracy of the method used is not too significant.

There are tools for engine diagnostics both on board of off-board especially in aircraft engines operation. Also there are tools for life usage monitoring of engine parts in aircraft operations. In industrial turbine operation, remote monitoring of engine operation is in practice. Engine life monitoring systems are now in use but in most cases, engine operators do rely on the design life provided by the original engine manufacturers (OEM) for changing critical parts. Where present, the accuracy of the life monitoring process will call for worry. It will therefore be proper for industrial turbine

operators to monitor the life consumption of the critical components of their engines by using tools which are not costly and which accuracy is of less concern. This calls for relative life analysis where the life estimated is compared with the life at a reference engine operating condition to obtain a relative dimensionless life which value indicates the degree of wellness of engine operation in any given period. Abdul Ghafir et al.[14], [109] introduced the concept of creep factor in assessing the impacts engine operation and engine health conditions have on the creep life consumption of Aero gas turbine hot section blades. Such analysis on fatigue life consumption has not been thoroughly carried out. In this research, the concept of equivalent creep factor is introduced to assess the wellness of engine operation over any given time spectrum. In addition, the concepts of fatigue factor/equivalent fatigue factor, and creep-fatigue factor/equivalent creep-fatigue factor are introduced for monitoring engine fatigue life consumption rate and creep-fatigue life consumption rate respectively at different periods of engine operation.

In fatigue life analysis, the numbers of stress cycles or fatigue cycles the engine experiences at different operating conditions in any period of engine operation are required to be able to estimate the fatigue life consumption of the engine using damage summation rules[145]. In aircraft engine, one fatigue cycle may constitute quick take-off from one point at high power level and landing at another point within a short while, especially for military operations. In industrial engines, accelerating the engine from standstill to maximum engine rotational speed and then returning to standstill constitutes one complete low cycle operation [48] **.** Also, operating the engine at peak power level and shut down on daily basis constitutes a low cycle operation for each day. In the actual sense, although smooth operation of the engine may be assumed in industrial turbines, but the power level and the shaft speed varies greatly within even a short while of engine operation. It will not be enough to say one low cycle will be counted if the engine is shut down after several days of operation. In the light of the above, a model is developed in this research to estimate the fatigue cycles accumulated in a given period of engine operation so as to obtain more accurate fatigue life estimation in industrial turbine operation. Several models are available and used for fatigue cycles counting in aircraft engine operation, the model developed here derives from one of such models used by the US Airforce [158].

Another aspect of engine operation often considered is the effect of engine operation conditions and engine health parameters on engine life consumption. Methods employed in the investigation of gas turbine components degradation have been studied extensively [159]–[162]. Also, several researchers [163], [164] have looked at the effects engine degradation has on engine performance. Jordal et al. [165] viewing from the thermo-economic perspective investigated the effect of compressor fouling on gas turbine blade life, observing that for advanced blade materials, fouling has less effect on blade life. Many other researchers [14], [166], [167] have looked at the effects of various engine operating conditions and design parameters on engine life, but the effect of any operation parameter in relation to other parameters on engine life is either often overlooked or loosely investigated. Such effects are usually carried out at engine design point or user defined point. For instance, the impact ambient temperature has on creep life may be investigated at a particular power level without considering the sensitivity of the impact on engine life at different power levels. In this research, the impact of ambient temperature variation on engine creep life, fatigue life and creep-fatigue interaction life consumption at different shaft power levels are investigated. The effect of shaft power on engine life consumption is also studied at different ambient temperatures. Also, the effect of engine degradation, expressed in terms of engine health parameters indices reduction [159], on engine life is investigated at different shaft power levels and ambient temperatures. These results together with those of engine life tracking will give engine operators a general picture of how engine life is consumed under different operation conditions and this will aid them in making decisions concerning part load operations and condition-based maintenance.

2.6 Chapter Conclusions

Gas turbine performance, cases of engine degradation, gas turbine failure mechanisms and methods of estimating engine components failures in different failure modes have been considered in this chapter. Several works have been carried out in the field of gas turbine lifing, ranging from creep life analysis to creep-fatigue life analysis. Some knowledge gaps were identified with respective to works that has been done and in this

research, an attempt is being made to fill some of the identified gaps- there will always be further areas of research in the field and improvement of existing works.

In industrial gas turbine operation, creep which is time dependent failure of a material at elevated temperatures under stresses below the ultimate tensile strength of the material is identified to be the major cause of failure. There are many models and methods for estimating creep life of gas turbine materials. The methods could be broadly classified into two approaches- the total life approach and the damage mechanics approach. The time-temperature parameters are widely used. The Larson-Miller Parametric method, one of the time-temperature parameters is found to be the most suitable for the creep life analysis in this research. Fatigue life estimation models could also be classed as total life approach and damage mechanics approach. Low cycle fatigue life is considered and the modified universal slopes method is adopted for the fatigue life analysis in this work. Also, a low fatigue cycle counting model suitable for accumulating fatigue cycles in industrial turbine operation is meant to be developed.

Failure of turbine blades may be due to combination of creep and fatigue in the form of creep-fatigue interaction failure. Several models used for analyzing creep-fatigue interaction failure have been identified. Taira's linear accumulation method is adopted for the creep-fatigue interaction life analysis, where its shortcomings are noted, and these will be reduced with the application of relative life analysis. Relative life analysis involves comparing the life obtained in each failure mode and at any point of engine operation to a reference life in each mode so as to obtain results which stand for how well the engine was operated in the period considered. Observations were made based on the literatures reviewed. These include among others estimation of absolute life and the difficulty in obtaining accurate results, low fatigue cycle assumptions, and determination of different factors affecting engine life consumption on a narrow scale. In this research, an attempt is being made to address some of these issues.

3 ENGINE LIFE ESTIMATION PROCEDURES

The various life analysis models and the methodologies adopted for the analysis of the various models are presented in this chapter. The relevant areas considered are the lifing models adopted for life analysis, the methodologies employed in engine life consumption analysis in the various failure modes, and integration of life estimation models and sub-models required for life estimation using a flow diagram. In carrying out the life analysis, an engine model is created in PYTHIA and the model is adapted to the operating conditions of the real engine using engine field data. Engine model creation and adaption are considered in the next chapter. The created and adapted engine model is able to predict the performance of the engine at different operating conditions. This is necessary because the output from the engine performance simulation is fed to the lifing models linked in PYTHIA to estimate the life consumption in the various failure modes.

Thermal and stress models of the blade are developed from first principles. These models are able to determine the temperatures and the stresses on the high pressure compressor turbine blades at various sections. Coupled with the lifing models, the life at each section of the blade is estimated. A means of capturing all the data from the real engine operation is ensured so that the life consumptions at several times within a day are evaluated. The blade thermal model, blade stress model and the data capturing module (data acquisition and pre-processing module) are presented in Chapter 4. To ensure that the severity of engine operation is ascertained, the life consumption in each mode is compared with a reference value. The concept of fatigue factor and creep-fatigue interaction factor are introduced to access severity of engine operation under fatigue analysis and creep-fatigue interaction analysis respectively. These parameters are used together with creep factor for creep life analysis to ensure relative life analysis in all failure modes.

In a day operation of the engine, or for any given period of engine operation, several creep factors can be evaluated and the equivalent of theses creep factors termed equivalent creep factor is used to represent the level of engine life consumption due to creep for the period. Equivalent fatigue factor and equivalent creep-fatigue interaction factor are used for assessing life consumption due to fatigue and due to creep-fatigue

interaction respectively for any given period of engine operation. Fatigue and creep-fatigue interaction comes into play when there is frequent shut down of engine. In shutting down the engine after operating the engine for some hours, engine life is consumed due to fatigue and when fatigue interacts with creep, engine life consumption is faster. The contribution of fatigue life to creep fatigue interaction is assessed under different operating conditions of the engine using equivalent fatigue and equivalent creep-fatigue interaction factor values.

3.1 Creep Life Estimation Model and Creep Life Analysis Methodology

The creep life of the high pressure turbine blades are estimated using the Larsson-Miller Parameter method given by Equation (3.1),

$$t_f = 10^{\left(\frac{LMP}{T} - C\right)} \tag{3.1}$$

All the parameters have their original meanings as presented in chapter 2. Depending on the value of the Larson-Miller Parameter, Equation (3.1) can be expressed as,

$$t_f = 10^{\left(\frac{1000 \times LMP}{T} - C\right)} \tag{3.2}$$

Accuracy, widespread usage and availability of material properties are some of the reasons why the Larson-Miller Parametric method is used for the creep life consumption analysis in this research.

The Larson-Miller parameter, LMP in Equation (3.2) is stress dependent. It is read based on the maximum stress obtained from the stress model in Chapter 4. The temperature of the blade material is obtained from the thermal model. At any given section of the blade under the operating condition of the engine, the temperature at the blade section and the stress are obtained. The Larsson-Miller Parameter is read from the LMP curve (the curve is converted to numerical values and the code written in this work interpolates to obtain the LMP value based on the stress value). The time to failure is thus estimated using Equation (3.2). The time to failure at each section of the blade is estimated and the lowest value is taken, and this value is divided by a factor of safety

(FoS) [168] to obtain the creep life CL under that operating condition. This is expressed by Equation (3.3),

$$CL = \frac{t_f}{FoS} \tag{3.3}$$

The factor of safety employed depends on the application. In this work, relative life analysis is carried out and hence the value of the factor of safety will not influence the lifing results. The creep life of the HP turbine blades is estimated using the data points available from the real gas turbine operation. The creep life at each engine operation point is given in the form,

$$CL_i = \frac{t_{f,i}}{FoS} \tag{3.4}$$

where CL_i is the creep life estimated at point i based on the data points available for each day operation of the engine. The real engine operation data is collected in every 5 minutes, thus, it is assumed that at each data point the engine operates for 5 minutes. It is possible to estimate the life consumption rate at any single data point; also life consumption could be estimated in a given period of engine operation by selecting that region of engine operation for analysis. To estimate the life consumption in a given stable period of engine operation, the data acquisition and pre-processing system developed in the course of this research guides one in selecting the region (see Figure 4.5 please).

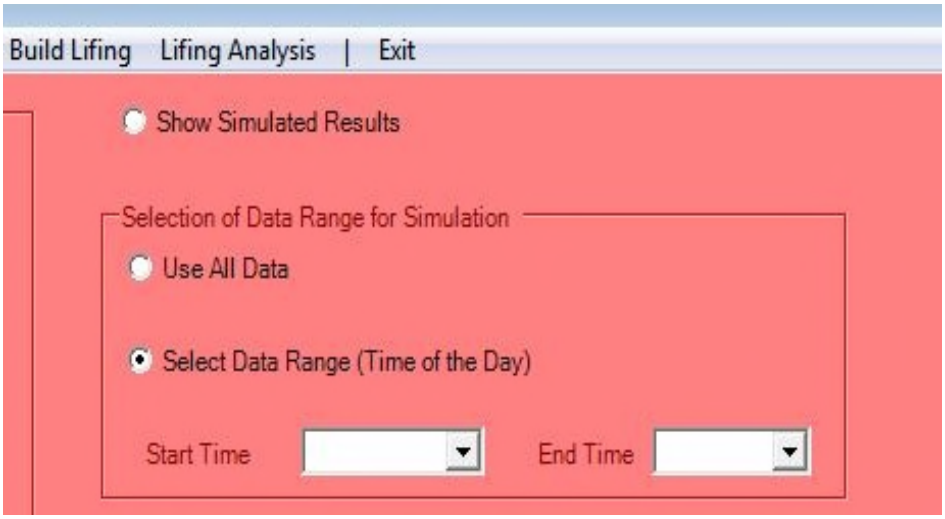

Figure 3.1: Selection of Data for Simulation and Life Analysis

Figure 3.1 shows how any region of the data supplied per day could be selected for life analysis. The data is supplied in excel sheet and two combo boxes are provided where data is selected by specifying the start time and the end time of the day operation of the engine. These two combo boxes are indicated as “Start Time” and “End Time” respectively. By default, all the data supplied which represents one day engine operation is used. To select any range, the “Select Data Range” radio button is checked and the “Start Time” and “End Time” combo boxes will be visible. A single engine operation point could be selecting by selecting the same time in the two combo boxes. To revert to using all the data for life analysis, the ‘Use All Data’ radio button is checked. Much about the program functionalities is given in Appendix A. The selected data is simulated using the engine performance model and the PYTHIA code to obtain gas path properties such as temperatures and pressures required in the blade thermal and stress models.

3.1.1 Life Fraction, Equivalent Creep Life and Remaining Life

The creep life estimated at each point of engine operation only tells how long it will take for the turbine blades to fail if engine operates at that condition continuously. In practice, the engine operates at many different conditions and both the power output and gas path properties which depend on power changes frequently from time to time (see Figures 4.8 to 4.12). The life estimated at the different points varies. The actual engine operation process is replaced by discrete steps based on the manner engine operation data is collected, and life consumption is estimated based on the discrete data points.

Figure 3.2 shows the discrete processes extracted from an actual engine operation period, the corresponding creep lives/equivalent creep life for the discrete processes, the life fractions consumed at each discrete step, and the total life fraction consumed for the entire period. The concept of life fraction is very useful for gas turbine users to assess the amount of creep life that has been consumed for a complicated operation process. The higher the creep life for a given discrete step or a given period of engine operation, the smaller the life fraction consumed as shown in Figure 3.2.

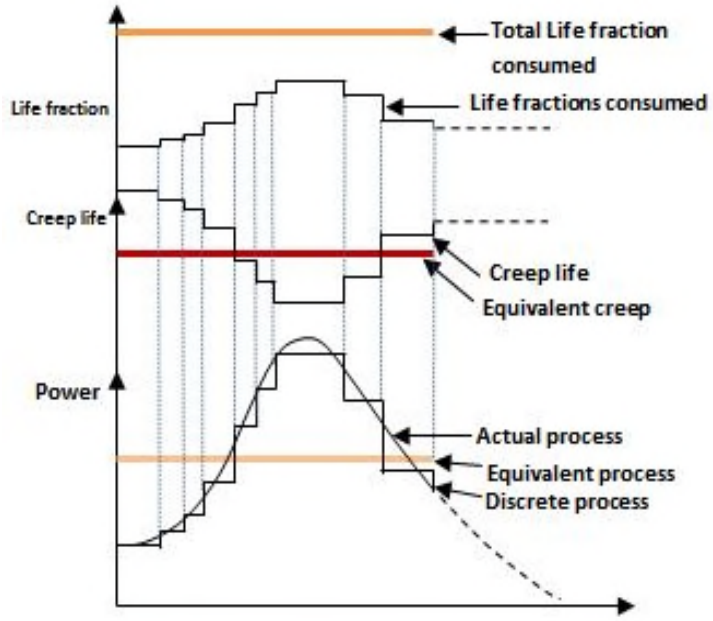

Figure 3.2: Actual and Equivalent Engine Operation Processes and Creep Life Consumption

The life fraction, LF at each operating point is the ratio of the time spent in that period to the creep life at that operating point and this is given by Equation (3.5),

$$LF_i = \frac{OT_i}{CL_i} \tag{3.5}$$

OT_i is the operating time in hours at each operating point. In this work, the operating time at each operating point is 5 minutes (5/60 hour). Based on individual operating points, the creep life is,

$$CL_i = \frac{OT_i}{LF_i} \tag{3.6}$$

Employing Robinsons life fraction rule [155], the sum of the life fractions can be expressed by Equation (3.7),

$$\sum_{i=1}^{m} LF_i = \sum_{i=1}^{m} \frac{OT_i}{CL_i} = x \tag{3.7}$$

m is the number of life fractions accumulated in time $OT = \sum_{i=1}^{m} OT_i$, and $x \leq 1$. Blade failure will occur when the sum of life fractions is accumulated to unity, i.e. $x = 1$. The time taken for the sum of the life fractions to be accumulated to unity is the equivalent

creep life (*ECL*). The equivalent creep life is estimated at any point from the sum of life fractions and the time taken to obtain the sum of life fractions. From Equation (3.7), in time $OT = \sum_{i=1}^{m} OT_i$, the sum of the life fractions is $x = \sum_{i=1}^{m} LF_i$. In a unit time, say 1 hour, the sum of the life fractions is given by Equation (3.8).

$$x = \frac{\sum_{i=1}^{m} LF_i}{OT} \tag{3.8}$$

In time t_f, the sum of the life fractions will be,

$$x = t_f \times \frac{\sum_{i=1}^{m} LF_i}{OT} \tag{3.9}$$

Assuming the sum of the life fractions is unity ($x = 1$) in time t_f, then t_f is the equivalent creep life and it is given by Equation (3.9),

$$t_f = ECL = \frac{OT}{\sum_{i=1}^{m} LF_i} \tag{3.10}$$

The equivalent creep life can be presented as in Equation (3.10),

$$ECL = \frac{OT}{\sum_{i=1}^{m} LF_i} = \frac{\sum_{i=1}^{m} OT_i}{\sum_{i=1}^{m} \frac{OT_i}{CL_i}} \tag{3.11}$$

The sum of the total operating hours for a day will be 24 hours if the engine is not shut down. If the engine is shut down, the programme automatically selects the period the engine was in operation for life estimation. It is pertinent to point out that the equivalent creep life based on one day engine operation will not be the same as the equivalent creep life representing a number of days. Results from the latter should be more relied on since many days operation of the engine is considered in the latter.

It is possible to also calculate the remaining life of the blades if the equivalent creep life and the time the engine has been in operation are known. The remaining life is the

difference between the equivalent creep life and the total time of engine operation. If the total time the engine has been in operation is OT_{Tot} and the equivalent creep life at that point is ECL, then the remaining life RL is simply,

$$RL = ECL - OT_{Tot} \tag{3.12}$$

3.1.2 Relative Creep Life Analysis

The absolute values of creep life and equivalent creep life obtained may not be absolutely accurate, as several assumptions were made in obtaining the life analysis sub-models. Also, the absolute equivalent creep life at any period of engine operation will not tell how well or unfavourable the engine has been operated for that period. By comparing the life obtained at each operating point or the equivalent creep life obtained for a day or a number of days of engine operation with a reference value, the impact of the engine operation on the creep life for that period will be appreciated. Ghafir [37] employed the concept of creep factor to assess the impact of engine operation on the creep life of the engine. The creep factor at a given operating point of the engine is given by Equation (3.13),

$$CF_i = \frac{CL_i}{CL_{\mathrm{Re}\,f}} \tag{3.13}$$

where CF_i is the creep factor at each point of engine operation while $CL_{\mathrm{Re}\,f}$ is a reference creep life. In this work, equivalent creep factor is introduced to assess the severity of engine operation for any given period. The equivalent creep factor ECF for the operation of the engine for any given period is the ratio of the equivalent creep life for the period to the reference creep life and it is given by Equation (3.14),

$$ECF = \frac{ECL}{CL_{\mathrm{Re}\,f}} \tag{3.14}$$

The equivalent creep factor is thus used to judge the fairness of engine operation for a given period. The reference life may not be the design life of the engine as may be provided by the OEM. It may be chosen at a steady operating condition where the operator of the engine wants the blade life to be. In this work, the reference life is

chosen at a particular engine operation point where the models developed in this work give the creep life which value is close to the time turbine blades failed due to creep in previous operations. If creep factor is greater than unity, then the engine is being operated at a more convenient condition with respect to the reference life, if it is less than unity, the engine is operated at worse conditions. The creep life analysis in this work will be based on the creep factor and the equivalent creep factor at any point and period of engine operation respectively. Since accurate equivalent creep life for a period of engine operation is difficult to estimate, the equivalent creep factor should be obtained from the creep factors of individual engine operating points. From Equations (3.11) and (3.14),

$$ECF = \frac{ECL}{CL_{\mathrm{Re}\,f}} = \frac{\sum_{i=1}^{m} OT_i}{\sum_{i=1}^{m} \frac{OT_i}{CL_i}} \times \frac{1}{CL_{\mathrm{Re}\,f}}$$

$$ECF = \frac{\sum_{i=1}^{m} OT_i}{\sum_{i=1}^{m} \frac{OT_i}{\left(\frac{CL_i}{CL_{\mathrm{Re}\,f}} \right)}} \tag{3.15}$$

But, $\frac{CL_i}{CL_{\mathrm{Re}\,f}} = CF_i$ (see Equation 3.13). Therefore,

$$ECF = \frac{\sum_{i=1}^{m} OT_i}{\sum_{i=1}^{m} \frac{OT_i}{CF_i}} \tag{3.16}$$

3.1.3 Integrated Creep Life Estimation System

In this work, an integrated creep life estimation system could be extracted from the entire life assessment algorithm by bringing the thermodynamic and adapted engine performance model together with the data acquisition and pre-processing model, the blade stress model, blade thermal model, and the creep life model. With the integration of the various models into one assembly, the creep life assessment of the targeted blades is feasible and could be carried out in any period of engine operation in a short time. It

accepts engine field data and pre-processes it and sends it to the thermodynamic model. The thermodynamic model carry out simulations using PYTHIA code and provides relevant data for the blade thermal and stress models. The blade thermal and stress models provide the temperatures and stresses required in the creep life model.

A Flow diagram of the integrated creep life estimation system is shown Figure 3.2. Five models make up the integrated creep life estimation system and they are enclosed in the dotted square, while the input data to the models and the output results from the system are placed outside the dotted square. At each point of engine operation, creep life estimation could be carried out and the outputs of the integrated creep life estimation system are the creep lives/creep factors at each point of engine operation and the equivalent creep life/equivalent creep factor for the entire period of engine operation. The equivalent creep factor for any period of engine operation could be obtained by simply providing all the engine operation data for that period for life analysis.

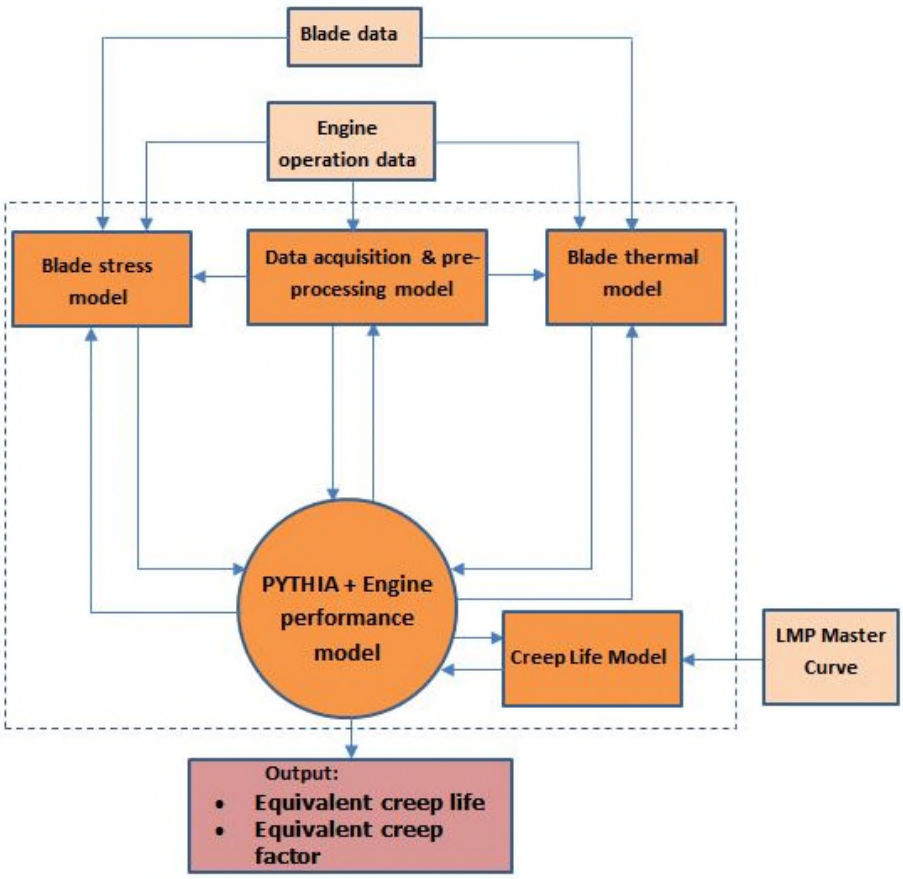

Figure 3.3: Integrated Creep Life Estimation System

The integrated life estimation system is incorporated in PYTHIA as a different program module. Also, modules for fatigue life calculation (considered in chapter 7) and creep-fatigue interaction life calculation (considered in chapter 8) are also developed and incorporated in PYTHIA. The details and the functionalities of the life analysis program modules developed in this research (using C-Sharp programming language) are given in Appendix A. A Sequential Solution-Algorithm Tree (SSAT) of the creep life estimation process is provided in Appendix E.1. SSAT is a tree-like representation of a given problem, similar to the solution trees employed in the solution tree problem solving procedure [169] , but the parameters are given wider representation in the SSAT approach. Details of the SSAT approach are given in Appendix D.

3.2 Low Cycle Fatigue Life Model and Fatigue Life Analysis Methodology

The fatigue life model adopted is the modified universal slopes method given by Equation (3.17),

$$\frac{\Delta\varepsilon}{2} = 0.623\left(\frac{\sigma_u}{E}\right)^{0.832}\left(2N_f\right)^{-0.09} + 0.0196\varepsilon_f{}^{0.155}\left(\frac{\sigma_u}{E}\right)^{-0.53}\left(2N_f\right)^{-0.56} \qquad (3.17)$$

where $\frac{\Delta\varepsilon}{2}$ is the total strain amplitude, σ_u is the ultimate tensile strength of the material, E is the Young's Modulus of the material, ε_f is the true fracture ductility, and N_f is the number of stress cycles to failure. The choice of the Modified Universal Slopes Method is due to the fact that it provides best results in fitting fatigue data [148]. Equation (3.17) could be expressed in terms of nominal alternating stress amplitude, σ_a by multiplying both sides of the equation by the modulus of elasticity, E as given by Equation (3.18),

$$\sigma_a = 0.623\sigma_u{}^{0.832}E^{0.168}\left(2N_f\right)^{-0.09} + 0.0196\varepsilon_f{}^{0.155}\sigma_u{}^{-0.53}E^{1.53}\left(2N_f\right)^{-0.56} \qquad (3.18)$$

The stress amplitude σ_a is obtained from the stress model in this work, and the number of stress cycles to failure N_f is estimated.

The failure of a component in fatigue depends on the stress amplitude and the mean stress about which the load fluctuates. In fatigue life estimation, test results showing

cycles to failure at different stress amplitudes are utilized. Tests about fatigue are usually conducted under constant stress amplitude and constant frequency. In practice, members are subjected to a range of fluctuating loads. Blocks of loads could be generated from the entire load spectrum, where each block consists of loads of the same stress amplitude and mean stress. The task is to determine how much damage each block of load will do. Damage summation rule provided by Palmgren and Miner [145], the Palmgren-Miner rule, is used in this case [47], [144]. The damage summation is given by Equation (3.19),

$$D = \sum_{i=1}^{m} \frac{n_i}{N_{f,i}} \tag{3.19}$$

where m is the number of blocks of load formed, n_i is the number of cycles corresponding to the i^{th} block, $N_{f,i}$ is the number of cycles to failure corresponding to the stress amplitude at the i^{th} block. $\frac{n_i}{N_{fi}}$ represents a fraction of damage. Failure is assumed to be cumulative and failure occurs when $D = 1$. From the above, two parameters are to be determined in fatigue life analysis. These are:

- The number of cycles to failure at a given stress amplitude, and
- The number of stress cycles corresponding to a given block of load defined by the stress amplitude.

Figure 3.3 shows the steps employed in carrying out fatigue life consumption of the gas turbine blades in this research. The load history in this research is obtained as stresses which are estimated from the compressor shaft speed and engine gas path properties gotten from the simulations in PYTHIA, and data provided in 24 hours of engine operation. The stresses are estimated using the stress model developed in Chapter 4. The program developed in this research and incorporated in PYTHIA enables the execution of the various steps in Figure 3.4. Also, estimation of fatigue life consumption and equivalent fatigue life in a given period of engine operation is carried out quickly.

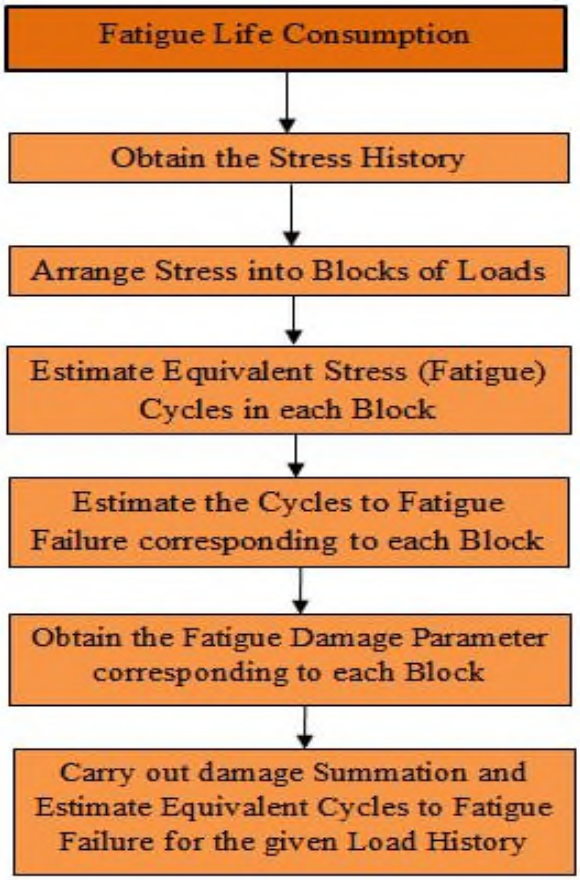

Figure 3.4: Algorithm for Fatigue Life Estimation

In this work, a low cycle fatigue model (Equation 3.17) is adopted to calculate the cycles to fatigue failure at a given stress amplitude (corresponding to each block of load) while a new cycle counting method is proposed to estimate the equivalent stress cycles (fatigue cycles) in each block of load.

3.2.1 Low Cycle Fatigue Idealization and Cycle Counting

In aero-engines, one low cycle may constitute quick take-off from one point at high power level and landing at another point within a short while, especially for military operations. In industrial engines, accelerating the engine from standstill to maximum engine rotational speed and then returning to standstill constitutes one complete low cycle operation [48] **.** Also, peak operation of engine on daily basis constitutes a low cycle operation for each day. In industrial engine operations, especially the LM2500+ engine under consideration, the stress amplitude reached even in maximum engine speed condition does not expose the hot section blade materials to fail under low cycle

fatigue regarding the stress the materials are exposed to; the number of cycles are far above the low cycle limit presented above. But in gas turbine blades, large strains occur in areas of stress concentration [79]**.** Bearing this in mind, low cycle fatigue idealization is formulated by assuming that areas of stress concentration might occur and hence the resulting stresses are increased to the low fatigue failure region. This is necessary because frequent engine shut down is practised in most gas turbine power plants. In essence, as the engine is operated for a long time, areas of stress concentration might occur in the compressor turbine blades and thus daily shut down with a view to extending life equally constitutes low cycle fatigue life consumption.

Low cycle fatigue of gas turbine materials, the compressor turbine blades in this case stems from the cyclic nature of the forces the blades are exposed to, and the cyclic nature of the forces results from variations in the power setting [48]. Although one low cycle is obtained per day for peak operation of industrial turbines, and the power level may be described as steady in many cases, but several different power values may be obtained within the operation period. Ambient temperature varies very often within a day and this alone leads to different shaft speed levels even if the range may be small. Figure 7.2 shows the required compressor shaft speed level and the actual shaft speed levels for one day operation of an industrial gas turbine. The compressor shaft speed is expressed in terms of compressor relative rotational speed *PCN*.

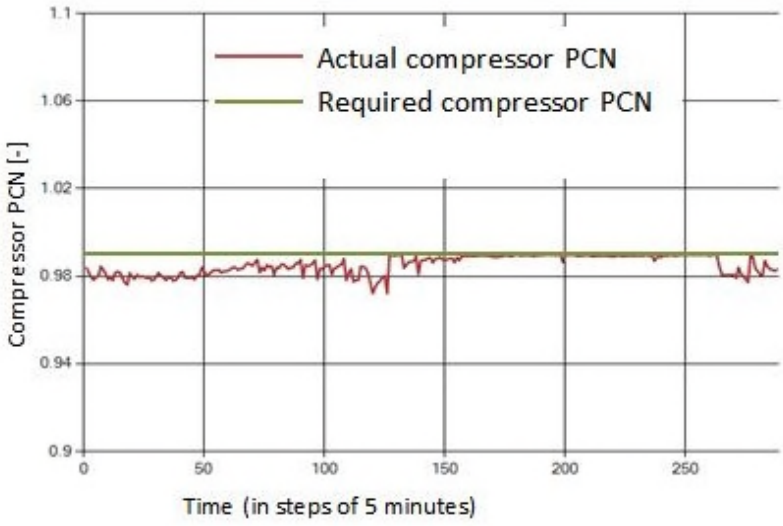

Figure 3.5: Actual and Required Shaft Speed Levels in a day Operation of an Industrial Gas Turbine

If in practice, the required compressor relative rotational speed level which is the compressor relative rotational speed level set for the engine operation is obtained at every point of the engine operation, one low cycle of engine operation could be counted from the start to the shutdown of the engine. The actual compressor relative rotational speed level varies in practice and this will lead to low fatigue failure in less time since the blades actually undergo more stress cycles. The equivalent number of low cycles in peak operation of the engine per day should be more than one as a result of shaft speed variation and this value should be estimated.

There are instruments for recording the cumulative low cycle fatigue damage rotating members in turbines undergo. One of such instruments patented by Meyer [170] records the rotational speed and provides a number of operating sequences each assigned with a predetermined constant life ratio. For a particular mission of engine operation, the effective or equivalent number of fatigue cycles consumed is estimated by accumulating fractional cycles from six different sequences based on speed and a unity cycle using Miner's rule put in the form of Equation (3.20),

$$N_{eq} = 1 + \varsigma N_{\varsigma} + \delta N_{\delta} + \alpha N_{\alpha} + \varepsilon N_{\varepsilon} + \beta N_{\beta} + \gamma N_{\gamma} \qquad (3.20)$$

N_{eq} is the equivalent number of cycles, $\varsigma, \delta, \alpha, \varepsilon, \beta$ and γ are the life ratio multiplicative constants for all six of the possible sequences, $N_i, i \equiv \varsigma, \delta, \alpha, \varepsilon, \beta$ and γ is the number of times a given sequence of operating region was traversed. Most of such equipment finds usage in aircraft engine operations and their shortcomings could be easily identified. In the above case, getting the operating ranges and providing appropriate life ratio multiplicative constants are some of the issues. Also, in low cycle fatigue life analysis, if the number of fatigue cycles are not recorded but the power or speed of the engine is recorded, one should device a means of getting the equivalent cycles from either the power data or speed data. Getting the equivalent cycles from the shaft speed data will be more appropriate noting that power variation does not always lead to speed variation in gas turbine operation. A case in point is when the inlet guide vanes are adjusted to vary the air intake leading to power output variation at constant shaft speed.

Knowing the history of engine operation, the several methods of engine cycle counting for low fatigue life analysis are available. Some of these methods are the peak count, mean crossing count, peak-trough count, level crossing count, range count, range pair count, range-mean count, markov matrix count, reservoir method, bathtub method, and rainflow cycle counting method. Of these, the rainflow counting method is predominantly used [171]–[175]. In these cycle counting methods, such as the rainflow technique, the stress time history is used. This means the stresses imposed in a given rotating component over a given period of engine operation are utilized to generate the equivalent number of fatigue cycles imposed on the component. The fatigue cycles are defined as closed stress/strain hysteresis loops. The stresses may be fully reversed or alternates about a mean stress value. One major advantage of the rainflow counting method is that it does not require knowledge of the entire load history [171], this make it possible for on-board application. The rainflow counting method makes use of a sequence of stress ranges which the fatigue damage procedure could not account for.

Operators of industrial turbines will likely have history of engine shaft power or compressor speed over time as against the stress values. In this research, the shaft speed of engine operation is available and techniques of generating the equivalent fatigue cycles from the shaft speed history are sought. In aircraft turbine engine operation, four sequences of engine operation are identified depending on transition from one speed level to another speed level. These are from zero to maximum speed (type 1 transitions), idle to maximum speed (type 2 transitions), intermediate to maximum speed (type 3 transitions), and transitions between any two speed levels except maximum speed (type 4 transitions) [158], [175]. The equivalent number of cycles from the given load history is given by Equation (3.21),

$$N_{eq} = N_1 + \frac{N_2}{4} + \frac{N_3}{40} \tag{3.21}$$

N_1 are number of the type 1 transitions, N_2 are number of the type 2 transitions, and N_3 are number of the type 3 transitions within the period of engine operation. Type 4 transitions do not contribute to the fatigue cycles for life analysis. This model is basically used by the US Air Force [158]. The issue with the above model is neglecting

the contributions of intermediate load transitions. With respect to Figure 3.4, going by the above model, very few type 3 transitions could be obtained together with one type 1 cycle if the engine is eventually shut down. Several type 4 transitions are obtainable in real engine operations and these will definitely contribute to the overall low cycles accumulated for a particular period of engine operation.

3.2.2 Proposed Fatigue Cycles Counting Model

The method presented in Equation (3.21) is widely used for aircraft engines. Several variations of speed which will definitely contribute to low cycle fatigue failure are left out. In industrial operations, a bit steady load is assumed, but the load varies a lot with time usually influenced by changes in ambient conditions. In aircraft engines, large changes in speeds could be recorded and such data over time can be subjected to cycle counting procedures such as the rain flow cycle counting method. In applying rain flow counting method, the available load history is first pre-processed and several minor load variations are smoothed out. Thus, the rain flow cycle counting method and the model presented in Equation (3.21) are ideal for estimating fatigue cycles undergone by aircraft engine rotating members. In industrial turbine operation, the speed variation is minimal and an alternative means of accumulating the fatigue cycles in rotating members is sought in this work. Though minor in most cases, the variation of each shaft speed from the set speed level contributes to fatigue failure and hence a fractional fatigue cycle is involved in such changes in shaft speeds. With shaft speed level set at N_S, when speed level changes from any level N_i to the next level N_{i+1}, the contribution to fatigue cycle is proportional to the difference between the two speed levels. That is, cycle contribution parameter (CCP) is proportional to the difference between N_i and N_{i+1} given by Equation (3.22),

$$CCP \propto N_{i+1} - N_i \tag{3.22}$$

The set speed level about which the actual speed levels revolve has much influence on the cycle contribution due to speed variation. Equation (3.22) is put in dimensionless form by dividing with the set speed level and is given by Equation (3.23),

$$CCP' = \frac{N_{i+1} - N_i}{N_S} \tag{3.23}$$

CCP' is the dimensionless cycle contributing parameter. Considering the type 1 load transitions in Equation (3.21), several different speed levels might have been traversed in raising the speed from 0 to maximum speed, depending on the time intervals in which the speed is recorded. Assuming n different speeds are recorded, 0 to maximum speed inclusive, then applying Equation (3.23) to the speeds, $(n-1)$ $CCP's$ will be obtained:

$$CCP'_1 = \frac{N_2 - N_1}{N_S};\ CCP'_2 = \frac{N_3 - N_2}{N_S};\ \ldots;\ CCP'_{n-2} = \frac{N_{n-1} - N_{n-2}}{N_S};\ CCP'_{n-1} = \frac{N_n - N_{n-1}}{N_S} \tag{3.24}$$

Summing all the $CCP's$, we obtain,

$$\sum_{i=1}^{n-1} CCP' = \frac{N_2 - N_1}{N_S} + \frac{N_3 - N_2}{N_S} + \ldots + \frac{N_{n-1} - N_{n-2}}{N_S} + \frac{N_n - N_{n-1}}{N_S} = \frac{N_n - N_1}{N_S} \tag{3.25}$$

But $N_n = N_S$, and $N_1 = 0$, therefore,

$$\sum_{i=1}^{n-1} CCP' = \frac{N_n - N_1}{N_S} = \frac{N_S - 0}{N_S} = 1 \tag{3.26}$$

The sum of the dimensionless cycle contributing parameters between successive speeds from zero to maximum gives one fatigue cycle, the same as type 1 load transition gives one fatigue cycle as given by Equation (3.21). Thus, intermediate speed transitions should be viewed as fractional contributions to the total fatigue cycles. Several different speed levels could be obtained in a given period of engine operation. The closer the difference between two adjacent speed levels, the smaller the cycle contributing parameter. The difference between two corresponding shaft speed levels may be positive or negative. Hence, the absolute value of the CCP' should be used for determining the equivalent cycles from the speeds obtained from engine operation. The equivalent number of cycles is as expressed by Equation (3.27),

$$N_{eq} = \sum_{i=1}^{n} \left(\left| \frac{N_{i+1} - N_i}{N_S} \right| \right)^k \tag{3.27}$$

where n is the number of different speed levels recorded in the course of engine operation, and k is the cycle determining exponent, which should be in the range $0.7 \le k \le 1$. In this range, the fractional cycle term in Equation (3.27) closely approximates the fractional cycles from the load transitions in Equation (3.21), and in addition, the value of k chosen depends on the frequency of load recording. If the load is recorded in short time intervals, k value very close to 1 will suffice, but if the time interval is large, then smaller value of k should be used to have larger values of cycle contributing parameters to account for the 'unrecorded speeds'. In this work, several engine shaft speeds are recorded in a day operation of the engine, but $k = 0.95$ is used in order to obtain more cycles and be a bit conservative. In this proposed model, the fractional cycles discarded using Equation (3.21) are accounted for, no matter how small. Alternatively, only increase in shaft speed could be used in estimating the cycle contributing parameters and the result multiplied by two to obtain the equivalent fatigue cycles. But it will be easier to provide a computer code to generate the equivalent fatigue cycles from data of engine operation using Equation (3.27) as against the alternative proposed.

The fatigue cycles actually result from stress variations and are also referred to as stress cycles. In this light, the fatigue cycles should be accumulated from the stress history of the blades. In this work, the centrifugal stress and the bending moment stresses the blades under study experience are considered. The centrifugal stresses contribute more to the total stresses and they could be easily obtained from the shaft speed and blade dimensions. Using the variation of centrifugal stress to accumulate the equivalent cycles, the stress cycles at different sections of the blade could be obtained and fatigue life estimation is thus carried out based on the stress accumulated at the various sections (see Figure 5.13). The equivalent stress cycles accumulated for each node of the blade, $N_{eq,d}$ using centrifugal stress variation is given by Equation (3.28),

$$N_{eq,d} = \sum_{i=1}^{n} \left(\left| \frac{\sigma_{CF,d}^{i+1} - \sigma_{CF,d}^{i}}{\sigma_{CF,d}^{S}} \right| \right)^{k} \tag{3.28}$$

where $\sigma_{CF,d}^{i}$, $\sigma_{CF,d}^{i+1}$ and $\sigma_{CF,d}^{S}$ are the centrifugal stresses at each node for the i^{th} data point, the next data point and the set speed level respectively. The total stress variation at each node could be used to accumulate the stress cycles. The total stress at each node of the blade consists of the centrifugal stress as well as the bending moment stresses. The equivalent stress cycles accumulated for a given period of engine operation due to variation of the total stress is given by Equation (3.29),

$$N_{eq,d} = \sum_{i=1}^{n} \left(\left| \frac{\sigma_{Tot,d}^{i+1} - \sigma_{Tot,d}^{i}}{\sigma_{Tot,d}^{S}} \right| \right)^{k} \tag{3.29}$$

$\sigma_{Tot,d}^{i}$, $\sigma_{Tot,d}^{i+1}$ and $\sigma_{Tot,d}^{S}$ are the total stresses at each node for the i^{th} data point, the next data point and the set speed level respectively. The equivalent stress cycles accumulated using Equations (3.28) and (3.29) are close because the centrifugal stress and the total stress at each node are close due to the low value of the momentum change stresses. The centrifugal stress model and the total stress models are given in Chapter 4. Although the cycles accumulated at each node $N_{eq,d}$ is evaluated, in this work this will be represented as N_{eq}. The model proposed in this research takes every shaft speed level into consideration, closely approximates the model for aircraft fatigue cycles counting used by the US Air Force, and it can be easily programmed; these make it more appropriate in this research

3.2.3 Low Cycle Fatigue Implementation

In low cycle fatigue life analysis, the equivalent number of fatigue cycles in a given period of engine operation is determined. Then, using an equivalent stress level of engine operation over the period, the number of cycles to failure is estimated. In this research, the number of cycles to failure is estimated using the modified universal slopes method. The estimation of the fatigue cycles to failure corresponding to each block of load using the Modified Universal Slopes Method is requires iteration process. For each block of load, the stress amplitude is obtained from the stress model developed in Chapter 4 while the number of fatigue cycles to failure, N_f is gradually increased until the right hand side (RHS) of the equation is equal to the value of the stress

amplitude (the left hand side- LHS). The N_f obtained at the point the RHS equals the LHS is the fatigue cycles to failure. The algorithm for estimating the fatigue cycles to failure corresponding to each block of load using the Modified Universal Slopes Method of low fatigue life analysis is given in Figure 3.6.

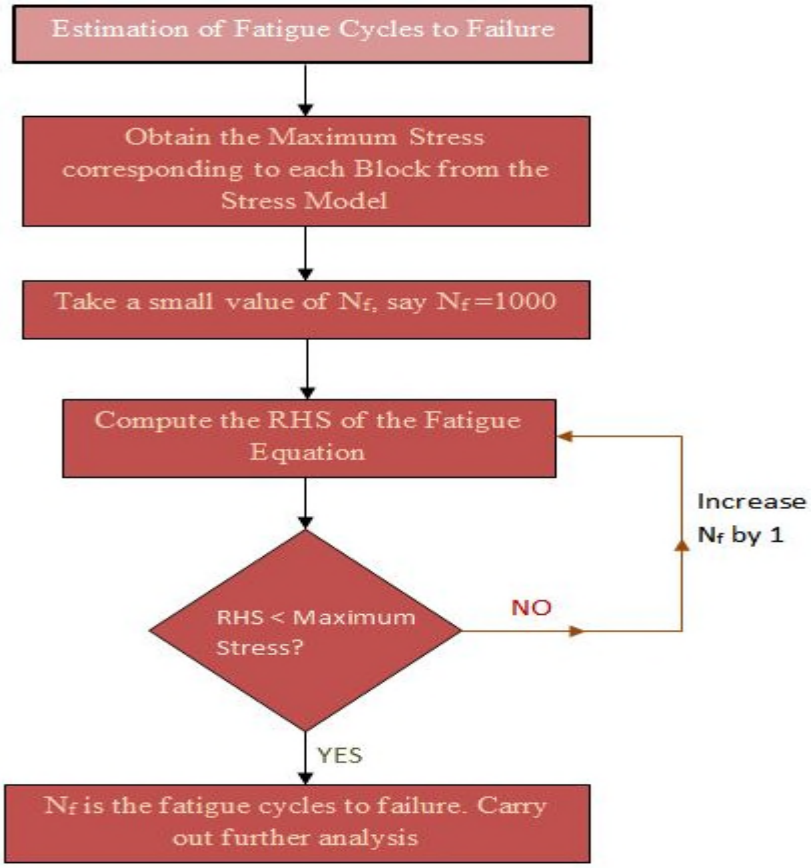

Figure 3.6: Algorithm for Estimating Fatigue Cycles to Failure

Further analysis involves estimation of fatigue factors and equivalent fatigue factor for a given period of engine operation. The effects of both shaft power level and ambient temperature on low cycle fatigue life is investigated in this work. Appendix E.2 shows a Sequential Solution-Algorithm Tree of the fatigue life estimation process.

The fatigue life consumed is estimated by dividing the equivalent cycles by the number of cycles to failure as given by Equation (3.30),

$$D_f = \frac{N_{eq}}{N_f} \tag{3.30}$$

D_f is the fatigue damage parameter which is a fraction of the fatigue life consumed during the period of engine operation. Fatigue failure is estimated at the nodal point in the blade where creep failure is most likely to occur. Since data for life analysis is supplied in days of engine operation, the fatigue life analysis will be carried out in days of engine operation as well as any period of engine operation. In a given day of engine operation, the number of stress cycles or fatigue cycles to failure N_f could be estimated using the average stress value experienced in the day. It could also be estimated using the maximum stress value for conservative fatigue life analysis. Fatigue failure is stochastic, thus, using the average stress value, the minimum stress value and the maximum stress value in estimating the cycles to failure and hence the fatigue damage parameter will give an appropriate region of fatigue failure results that will account for the probabilistic nature of fatigue. Instead of using Equation (3.30) where N_f is evaluated at a specified stress level, mean value of the equivalent stress N_{eq} could be obtained and the fractions of fatigue life consumed at each operation point (each engine operation point is assumed to last for 5 minutes, the interval within which engine operation properties are recorded) are evaluated and accumulated using Palmgren-Miner linear accumulation rule which assumes that the fractional fatigue damages are additive. This is given by Equation (3.31),

$$D_{f,i} = \frac{\overline{N}_j}{N_{f,i}} \tag{3.31}$$

$D_{f,i}$ is the fatigue damage parameter at each operation point, $\overline{N}_j$ is the mean value of the equivalent cycles accumulated per day of engine operation (the same for all operating points), and $N_{f,i}$ is the number of cycles to failure at each operation point. $\overline{N}_j$ is given by Equation (3.32).

$$\overline{N}_j = \frac{N_{eq,j}}{n} \tag{3.32}$$

$N_{eq,j}$ is the equivalent cycles for day j of engine operation, and n is the number of operation points recorded. In one day operation of the engine, the sum of the fatigue damage parameters D_{f,s_1} (represented generally for each day as D_{f,s_j}) will be,

$$D_{f,d\_j} = \sum_{i=1}^{n} D_{f,i} = \sum_{i=1}^{n} \frac{\overline{N}_j}{N_{f,i}} \tag{3.33}$$

$$D_{f,d\_1} = \sum_{i=1}^{n} D_{f,i} = \sum_{i=1}^{n} \frac{\overline{N}_1}{N_{f,i}} \tag{3.34}$$

In any period of engine operation, the sum of the fatigue damage parameters, $D_{f,s}$ is given by Equation (3.35),

$$D_{f,s} = \sum_{i=1}^{m} D_{f,i} = \sum_{i=1}^{m} \frac{\overline{N}_a}{N_{f,i}} \tag{3.35}$$

where $\overline{N}_a$ is the mean value of the equivalent cycles accumulated, $N_{eq,a}$ for the entire period of engine operation, and m is the total number of engine operation points where fatigue damage parameters are evaluated. The fatigue damage parameter for a day operation of the engine using Equations (3.30) and (3.35) respectively for several days of engine operation gives results that are almost the same with difference of about $7 \times 10^{-4}\,\%$. But Equation (3.35), which is similar to Equation (3.31), is used for the analysis here since the fatigue damage parameters of individual operating points are evaluated and accumulated. Based on the Palmgren-Miner rule, fatigue failure occurs when the fatigue damage parameter is unity, at which point the total fatigue life is consumed. That is, at the point of fatigue failure,

$$\sum_{i=1}^{m} D_{f,i} = 1 \tag{3.36}$$

For fatigue failure in practice, the damage parameter varies from 0.8 to 1.2, and in most industrial applications, failure is assumed when the damage parameter is 0.75 [175]. Failure at unity damage parameter is assumed in this work. The time to fatigue failure could be expressed in days or hours of engine operation, or in the number of fatigue cycles to failure where the average cycles consumed per day for the entire period of engine operation is used as the basis. The fatigue life at each point of engine operation depends on the maximum stress level and assuming that the engine is shut down from that stress level. For complicated engine operation, the equivalent fatigue life, $N_{f,eq}$ which is the number of fatigue cycles to failure for the period of engine operation, will

be used. The equivalent fatigue life is obtained from the accumulation of fatigue damage parameters and it is given by Equations (3.37) and (3.38),

$$D_{f,s} = \sum_{i=1}^{m} \frac{\overline{N}_a}{N_{f,i}} = \frac{\sum_{i=1}^{m} \overline{N}_a}{N_{f,eq}} \tag{3.37}$$

$$N_{f,eq} = \frac{\sum_{i=1}^{m} \overline{N}_a}{\sum_{i=1}^{m} \frac{\overline{N}_a}{N_{f,i}}} \tag{3.38}$$

The equivalent time to fatigue failure (ETFF) $t_{f,eq}$ could be estimated if the number of cycles accumulated $N_{eq,a}$, and the time taken to accumulate the cycles t_a are known. The cycles accumulated per unit time N_{a_t} is given by Equation (3.39),

$$N_{a\_t} = \frac{N_{eq,a}}{t_a} = \frac{\sum_{i=1}^{m} \overline{N}_a}{\sum_{i=1}^{m} t_i} \tag{3.39}$$

t_i is the time spent at each engine operation point. The equivalent time to fatigue failure is given by Equation (3.40),

$$t_{f,eq} = \frac{N_{f,eq}}{N_{a\_t}} \tag{3.40}$$

Making relevant substitutions from equations (3.38) and (3.39) in Equation (3.40), the equivalent time to fatigue failure is given by Equation (3.41),

$$t_{f,eq} = \frac{\sum_{i=1}^{m} t_i}{\sum_{i=1}^{m} \frac{\overline{N}_a}{N_{f,i}}} \tag{3.41}$$

The equivalent fatigue cycles to failure $N_{f,eq}$ and the equivalent time to fatigue failure are related in the form given by Equation (3.42),

$$t_{f,eq} = N_{f,eq} \times \frac{\sum_{i=1}^{m} t_i}{\sum_{i=1}^{m} \overline{N}_a} \tag{3.42}$$

Results of fatigue life analysis will be presented in terms of equivalent cycles of fatigue failure at any point of engine operation, but more generally in terms of relative life analysis, considered next. Further details of equivalent fatigue life expressed in any time frame of engine operation together with relative life analysis expressions are given in Appendix F.1.

3.2.4 Relative Fatigue Life Analysis- The Concept of Fatigue Factor

In the low cycle fatigue idealization, obtaining the equivalent number of fatigue cycles to failure at a given period of engine operation and estimating the fatigue damage parameter will only reveal the amount of fatigue life consumed, but this will not tell how well the engine is being operated for the period considered. Like the creep factor approach, if the number of cycles to failure is compared with the cycles to failure at a particular reference point, fatigue life will be obtained relative to the reference point, and this will give the operator of the engine an idea of the wellness of the operation of his engine. The fatigue factor (FF) is given by Equation (3.43),

$$Fatigue\ Factor\ (FF) = \frac{N_f}{N_{f,\mathrm{Re}f}} \tag{3.43}$$

where N_f is the number of cycles to failure at a given engine operation point (corresponding to a particular block of load), and $N_{f,\mathrm{Re}f}$ is the number of cycles to failure at the defined reference point. If $N_f < N_{f,\mathrm{Re}f}$, the engine is operated at a worse condition with respect to the reference point, if $N_f > N_{f,\mathrm{Re}f}$, the engine is operated at a favourable condition with respect to the reference condition. In a given period of engine operation, the equivalent fatigue factor will be estimated. This is the ratio of the equivalent fatigue life (equivalent cycles to fatigue failure) to the cycles to fatigue failure at the reference point; this is given by Equation (3.44),

$$EFF = \frac{N_{f,eq}}{N_{f,\mathrm{Re}\,f}} \tag{3.44}$$

EFF is the equivalent fatigue factor, and $N_{f,eq}$ is the equivalent cycles to failure based on the entire period of engine operation.

3.3 Creep-Fatigue Interaction Model and Creep-Fatigue Interaction Life Analysis Methodology

The creep-fatigue interaction life of the HP turbine blades in this work is estimated using linear accumulation law (Taira's method) which has both creep and fatigue damage terms as presented in Equation (3.45),

$$\sum \frac{N_i}{N_{f,i}} + \sum \frac{t_i}{t_{f,i}} = D \tag{3.45}$$

where N_i is the number of cycles at stress amplitude σ_{ai}, $N_{f,i}$ is the number of cycles to failure at stress amplitude σ_{ai}, t_i is the time spent at stress-temperature combination corresponding to σ_{ai} while $t_{f,i}$ is creep fracture life at stress-temperature combination corresponding to σ_{ai}. D is a parameter which value ranges from zero to unity. When D is unity, failure occurs. The value of D hence shows the level of damage a material has undergone and materials should be replaced when D approaches unity. Smaller values of D portrays more life of the component in question. The value of D lying between zero and unity makes the model linear. This linear summation rule/model predicts linear behaviour and thus makes unsafe prediction for cyclical work-softening materials but conservative prediction for cyclical work-hardening materials, but, different behaviours are often exhibited by actual materials [156]. The limitations of the linear accumulation of creep and fatigue [78] notwithstanding, Equation (3.45) will be explored further and used for creep-fatigue interaction analysis in this work. Figure 3.7 shows the nature of the model and how the two categories of materials highlighted above relate with it.

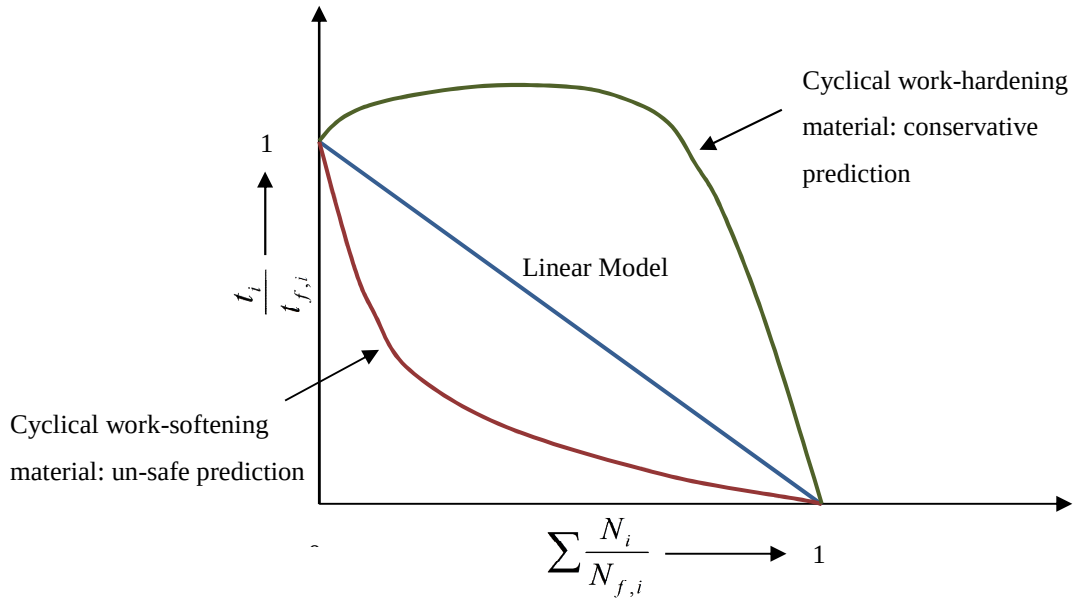

Figure 3.7: Nature of Creep-Fatigue Interaction Model [156]

In view of the behaviour of different materials to creep-fatigue interaction failure, different values of D should be applied to different materials under failure. For cyclical work-softening materials, the value of D at failure should be less than 1, hence using the linear model leads to un-safe prediction of material life. For cyclical work-hardening materials on the other hand, the value of D at failure should be greater than 1, thus the linear model leads to conservative life prediction. To evade the variance in the behaviour of different materials to the creep-fatigue interaction failure, the linear model is used in this research while the life obtained is compared to a reference life. This is considered later in this chapter. Using the linear model, under failure, Equation (3.45) takes the form of Equation (3.46),

$$\sum \frac{N_i}{N_{f,i}} + \sum \frac{t_i}{t_{f,i}} = 1 \qquad (3.46)$$

Each of $\sum \frac{N_i}{N_{f,i}}$ and $\sum \frac{t_i}{t_{f,i}}$ is viewed as separate damage terms- fatigue and creep (rupture) respectively. In this light , we can write [157],

$$D_{fatigue} + D_{rupture} = 1 \qquad (3.47)$$

Since creep is estimated using LMP to give the number of hours to failure and fatigue will be analyzed to reveal the number of cycles to failure, the linear cumulative damage will only reveal the cumulative damage the material (in this case, HP turbine blades) has undergone. Having knowledge of the history of engine operation, the creep-fatigue damage the material undergoes at various times could be evaluated and the time to creep-fatigue interaction failure can be estimated and presented either in days (or hours) of engine operation or cycles to failure.

Considering the creep term for each operation point, the creep damage parameter for each operation point $D_{c,i}$ is,

$$D_{c,i} = \frac{t_i}{t_{f,i}} \tag{3.48}$$

Considering the low cycle fatigue term for each engine operation point recorded, the fatigue damage parameter for each operation point $D_{f,i}$ is given by Equation (3.49),

$$D_{f,i} = \frac{N_i}{N_{f,i}} \tag{3.49}$$

$N_{f,i}$ is the fatigue cycles to failure for the i^{th} point of engine operation, which data is available. N_i is the number of cycles experienced at each point of engine operation. Designating the creep-fatigue damage parameter as D_{c+f}, at each engine operation point, it will be given by Equation (3.50),

$$D_{c+f,i} = \frac{t_i}{t_{f,i}} + \frac{N_i}{N_{f,i}} \tag{3.50}$$

Knowing the creep-fatigue damage parameter at any point of engine operation, the time to creep-fatigue failure could be obtained. The time to creep-fatigue failure $t_{f,c+f}$ is given by Equation (3.51),

$$t_{f,c+f} = \frac{t_i}{D_{c+f,i}} = \frac{t_i}{\frac{t_i}{t_{f,i}} + \frac{N_i}{N_{f,i}}} \tag{3.51}$$

In terms of cycles to failure, Equation (3.51) takes the form of Equation (3.52),

$$N_{f,c+f} = \frac{N_i}{D_{c+f,i}} = \frac{N_i}{\frac{t_i}{t_{f,i}} + \frac{N_i}{N_{f,i}}} \tag{3.52}$$

$N_{f,c+f}$ is the number of fatigue cycles to creep-fatigue interaction failure. From Equations (3.51) and (3.52), the relationship between time to fatigue failure and cycles to fatigue failure is obtained, and it is given by Equation (3.53),

$$N_{f,c+f} = \frac{N_i}{t_i} \times t_{f,c+f} \tag{3.53}$$

Considering one day operation of the engine, N_i is taken as the mean value of the equivalent fatigue cycles estimated per day as in the previous sections. Thus expressed for the j^{th} day with n operation points,

$$N_i = \overline{N}_a = \overline{N}_j = \frac{N_{eq,j}}{n} \tag{3.54}$$

The creep-fatigue damage parameter for the day, designated as $D_{c+f,d}$ with n operation points is given by Equation (3.55),

$$D_{c+f,d} = \sum_{i=1}^{n} \frac{t_i}{t_{f,i}} + \sum_{i=1}^{n} \frac{N_i}{N_{f,i}} \tag{3.55}$$

The time to creep-fatigue failure based on data for one day operation of the engine is given by Equation (3.56),

$$t_{f,c+f} = \frac{\sum_{i=1}^{n} t_i}{D_{c+f,d}} = \frac{\sum_{i=1}^{n} t_i}{\sum_{i=1}^{n} \frac{t_i}{t_{f,i}} + \sum_{i=1}^{n} \frac{N_i}{N_{f,i}}} \tag{3.56}$$

In terms of cycles to failure, Equation (3.56) takes the form of Equation (3.57),

$$N_{f,c+f} = \frac{\sum_{i=1}^{n} N_i}{D_{c+f,d}} = \frac{\sum_{i=1}^{n} N_i}{\sum_{i=1}^{n} \frac{t_i}{t_{f,i}} + \sum_{i=1}^{n} \frac{N_i}{N_{f,i}}} \tag{3.57}$$

Considering any period of engine operation, $N_i = \overline{N}_a$ is the mean value of the equivalent fatigue cycles accumulated in the period, and it is given by Equation (3.58),

$$N_i = \overline{N}_a = \frac{N_{eq,a}}{m} \tag{3.58}$$

$N_{eq,a}$ is the total number of fatigue cycles accumulated, and m is the number of engine operation points where fatigue damage parameters are estimated. The sum of the creep-fatigue damage parameters designated as $D_{c+f,s}$ for a given period of engine operation is given by Equation (3.59),

$$D_{c+f,s} = \sum_{i=1}^{m} \frac{t_i}{t_{f,i}} + \sum_{i=1}^{m} \frac{N_i}{N_{f,i}} \tag{3.59}$$

For such complicated engine operation process, the equivalent creep-fatigue life (ECFF) will be evaluated. The time to creep-fatigue interaction failure and the cycles to creep-fatigue interaction failure for daily operation of the engine are best expressed as equivalent values also, since several engine operation points are used in getting the creep-fatigue interaction life. The equivalent creep-fatigue life is the time taken for the sum of the damage parameters to be unity when the engine is operated in different conditions, and it is given by Equation (3.60),

$$ECFL = \frac{\sum_{i=1}^{m} t_i}{D_{c+f,s}} = \frac{\sum_{i=1}^{m} t_i}{\sum_{i=1}^{m} \frac{t_i}{t_{f,i}} + \sum_{i=1}^{m} \frac{N_i}{N_{f,i}}} \tag{3.60}$$

The time to creep-fatigue interaction failure in Equation (3.60) is in hours of engine operation. This could be expressed in cycles of engine operation when the equivalent cycles experienced in the period of engine operation are evaluated. This is given by Equation (3.61),

$$ECFL = \frac{N_{eq,a}}{D_{c+f,s}} = \frac{\sum_{i=1}^{m} N_i}{\sum_{i=1}^{m} \frac{t_i}{t_{f,i}} + \sum_{i=1}^{m} \frac{N_i}{N_{f,i}}} \tag{3.61}$$

3.3.1 Creep-Fatigue Interaction Life Analysis System

A creep-fatigue interaction life analysis system could be extracted from the overall life analysis system. The creep-fatigue interaction life analysis system gets inputs from the outputs of the creep life analysis system and the fatigue life analysis system as already pointed out. Figure 3.8 shows the creep-fatigue interaction life analysis system which is linked to PYTHIA and interacts with the other two life analysis systems considered in this research. To carry out the creep-fatigue interaction life consumption of the HP compressor turbine blades of the LM2500+ in any period of engine operation, the creep life consumption should be estimated first followed by the fatigue life consumption before implementing creep-fatigue interaction consumption. The results of the creep-fatigue interaction life output could be in terms of fatigue cycles to failure or time to failure. Results are generally presented in terms of relative life analysis values- creep-fatigue interaction factors at different engine operation points and equivalent creep-fatigue interaction factor for a given period of engine operation.

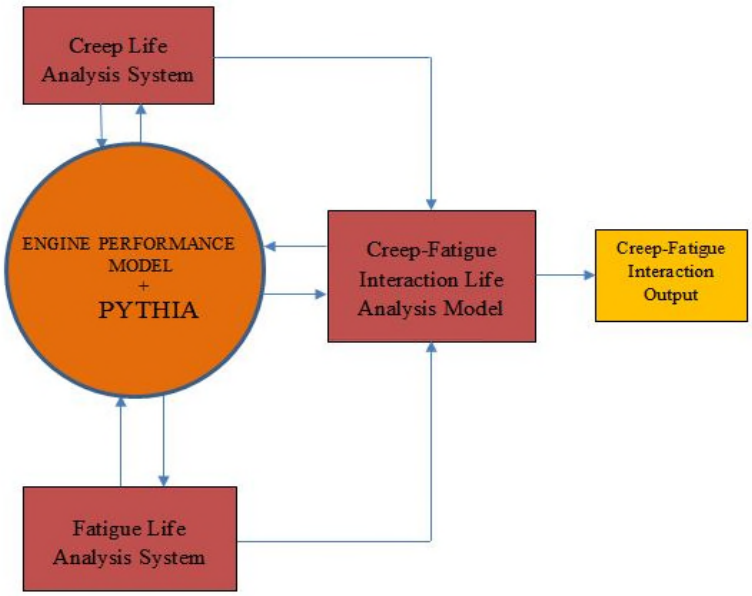

Figure 3.8: Creep-Fatigue Interaction Life Analysis System

3.3.2 The Concept of Creep-Fatigue Interaction Factor

Like the creep factor and the fatigue factor, the creep-fatigue interaction factor is used to assess the severity of engine operation under creep-fatigue interaction life consumption. The creep-fatigue interaction factor at any point of engine operation is expressed by Equation (3.62),

$$CFF = \frac{t_{f,c+f}}{t_{f,c+f\_\mathrm{Re}f}} \tag{3.62}$$

CFF is the creep-fatigue interaction factor or creep-fatigue factor for short, $t_{f,c+f\_\mathrm{Re}f}$ is the time to creep-fatigue interaction failure at a reference point. It can also be expressed in terms of cycles to failure as given by Equation (3.63),

$$CFF = \frac{N_{f,c+f}}{N_{f,c+f\_\mathrm{Re}f}} \tag{3.63}$$

$N_{f,c+f\_\mathrm{Re}f}$ is the number of cycles to creep-fatigue interaction failure at the reference point. From Equations (3.51) and (3.62), the creep-fatigue factor is as given by Equation (3.64),

$$CFF = \frac{t_{f,c+f}}{t_{f,c+f\_\mathrm{Re}f}} = \frac{1}{t_{f,c+f\_\mathrm{Re}f}} \times \frac{t_i}{\frac{t_i}{t_{f,i}} + \frac{N_i}{N_{f,i}}} \tag{3.64}$$

In terms of cycles to failure, from Equations (3.52) and (3.63), the creep-fatigue interaction factor is given by Equation (3.65),

$$CFF = \frac{1}{N_{f,c+f\_\mathrm{Re}f}} \times \frac{N_i}{\frac{t_i}{t_{f,i}} + \frac{N_i}{N_{f,i}}} \tag{3.65}$$

Equations (3.64) and (3.65) gives same result and the choice of which equation to use is based on availability of the required data and convenience.

For a complicated operation process, the equivalent creep-fatigue interaction factor (ECFF) is evaluated; it is the ratio of the equivalent creep-fatigue life to the creep-fatigue life at the reference operating condition and it is given by Equation (3.66),

$$ECFF = \frac{ECFL}{t_{f,c+f\_\mathrm{Re}f}} \tag{3.66}$$

And in terms of cycles to failure, the equivalent creep-fatigue interaction factor is given by Equation (3.67),

$$ECFF = \frac{ECFL}{N_{f,c+f\_\mathrm{Re}f}} \tag{3.67}$$

By making substitutions in Equations (3.66) and (3.67), the equivalent creep-fatigue factor for complicated operation using time to failure and cycles to failure are given respectively by Equations (3.68) and (3.69),

$$ECFF = \frac{ECFL}{t_{f,c+f\_\mathrm{Re}f}} = \frac{1}{t_{f,c+f\_\mathrm{Re}f}} \times \frac{\sum_{i=1}^{m} t_i}{\sum_{i=1}^{m} \frac{t_i}{t_{f,i}} + \sum_{i=1}^{m} \frac{N_i}{N_{f,i}}} \tag{3.68}$$

$$ECFF = \frac{ECFL}{N_{f,c+f\_\mathrm{Re}f}} = \frac{1}{N_{f,c+f\_\mathrm{Re}f}} \times \frac{\sum_{i=1}^{m} N_i}{\sum_{i=1}^{m} \frac{t_i}{t_{f,i}} + \sum_{i=1}^{m} \frac{N_i}{N_{f,i}}} \tag{3.69}$$

3.3.3 Relationship between Life Analysis Factors

At any point of engine operation, the creep factor (CF), fatigue factor (FF), and creep-fatigue interaction factor (CFF) could be expressed in a single relation. Considering individual operating points, from Equations (3.53) and (3.63) the creep-fatigue factor is given by Equation (3.70),

$$CFF = \frac{N_{f,c+f}}{N_{f,c+f\_\mathrm{Re}f}} = \frac{1}{N_{f,c+f\_\mathrm{Re}f}} \times \frac{N_i}{\frac{t_i}{t_{f,i}} + \frac{N_i}{N_{f,i}}} \tag{3.70}$$

But $t_{f,i} = CF \times t_{f,\mathrm{Re}f}$ and $N_{f,i} = FF \times N_{f,\mathrm{Re}f}$. Making these substitutions to Equation (3.70) and simplifying, we obtain the relation between the three life analysis factors at each engine operation point as,

$$CFF = \frac{N_i}{N_{f,c+f\_\mathrm{Re}f}} \times \frac{CF \times FF \times t_{f,\mathrm{Re}f} \times N_{f,\mathrm{Re}f}}{(FF \times N_{f,\mathrm{Re}f} \times t_i) + (CF \times t_{f,\mathrm{Re}f} \times N_i)} \tag{3.71}$$

In terms of time to failure, the relationship between the life analysis factors will be in the form given by Equation (3.72),

$$CFF = \frac{t_i}{t_{f,c+f\_\mathrm{Re}f}} \times \frac{CF \times FF \times t_{f,\mathrm{Re}f} \times N_{f,\mathrm{Re}f}}{(FF \times N_{f,\mathrm{Re}f} \times t_i) + (CF \times t_{f,\mathrm{Re}f} \times N_i)} \quad (3.72)$$

The creep-fatigue interaction factor / equivalent creep-fatigue interaction factor could also be expressed in terms of both time to failure and cycles to failure as shown above. Appendix F.2 shows further details of creep-fatigue interaction life expressions and expressions of creep-fatigue interaction factor in different time frames.

3.4 Integration of Life Estimation Models

The three life estimation models and the sub-models and data required for the life analysis are shown in the flow diagram in Figure 3.9, each set distinguished with different colours. The sequence of activities to be carried out to obtain life analysis results from the life estimation models could be derived from the flow diagram in Figure 3.8.

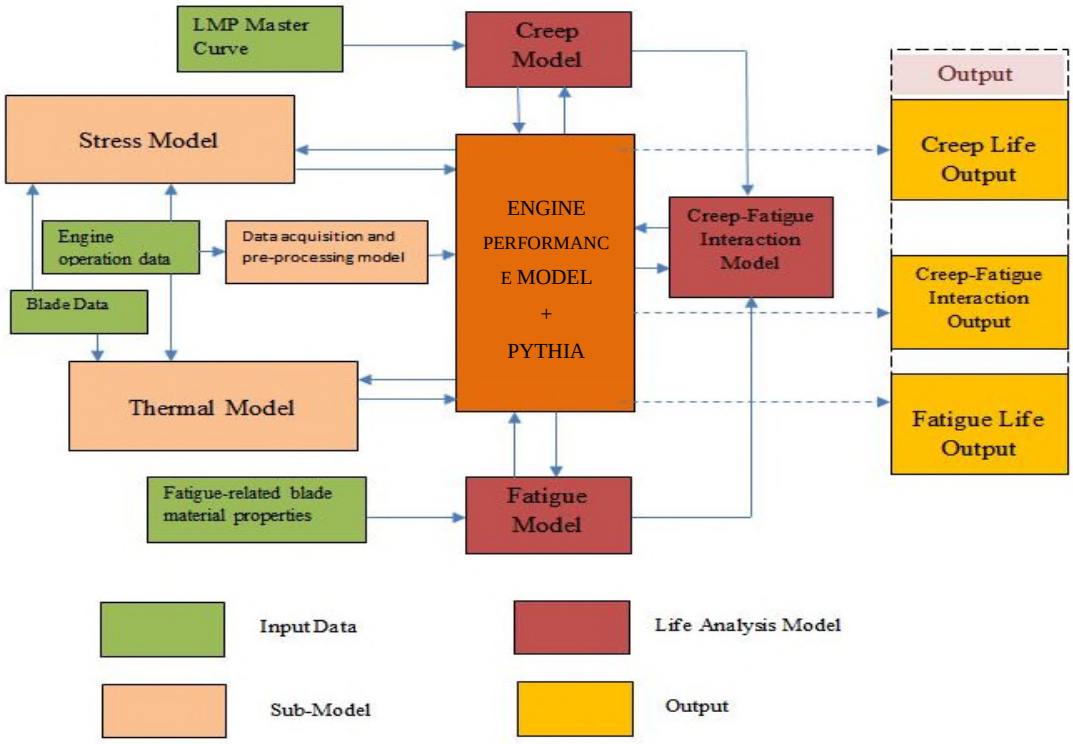

Figure 3.9: Flow Diagram of Life Estimation Models

The engine performance model is created in PYTHIA and together with PYTHIA they form the heart of the life analysis algorithm. The engine performance model is a thermodynamic model of the real engine which is made to produce results similar to the real engine by adapting the engine model to the real engine operation conditions. The creation and adaptation of the engine performance model is considered in Chapter 5, but the respective methodologies are presented later in this chapter. The engine performance model takes input from engine operation data and does performance analysis using PYTHIA code to get some data (gas path properties) required for the blade thermal and stress models. The blade thermal and stress models take further input from blade data and interacts with PYTHIA which in turn interacts with the creep model, fatigue model and creep-fatigue interaction model. Apart from the engine operation data and the blade data, the fatigue model requires fatigue-related material properties as input while LMP master curve is required for the creep life model.

For a given period of engine operation, the blade life is obtained from the results of individual engine operation points using life fraction accumulation rules. The output from the creep model is creep life in terms of number of hours to failure and life consumed in hours. Remaining life could also be presented. In terms of relative life analysis, the equivalent creep factor at any duration of engine operation could be obtained as an output. In this work, in any period of engine operation, the creep factor for each engine operation point and the equivalent creep factor for the entire period are presented. In the fatigue life model, the number of cycles to failure could be obtained as the output. Also, the output in terms of severity of engine operation could be given as the equivalent fatigue factor of engine operation for a given duration. Equivalent creep-fatigue interaction factor could be obtained from the creep-fatigue interaction model. The output in this model can equally be the number of hours to creep-fatigue interaction failure or the remaining life in hours due to creep-fatigue interaction. The relative life results are generally provided in each failure mode. Fatigue life analysis is usually considered if the engine is often shut down. Even if the engine is in continuous operation, fatigue failure will still set in because of the variation of shaft speed. The developed fatigue counting model will make the fatigue life analysis possible for any

period of engine operation; therefore, creep-fatigue interaction failure can also be carried out for any given period of engine operation.

From Figure 3.9, the basic tasks involved in this research could be identified, and these are summarized below:

- Development and analysis of blade thermal model - Considered in Chapter 4
- Development and analysis of blade stress model - Considered in Chapter 4
- Creation of engine performance model in PYTHIA- Considered in Chapter 5
- Adaptation of engine performance model - Considered in Chapter 5
- Validation of the engine performance model - Considered in Chapter 5
- Development of data acquisition and pre-processing module – required for single point life analysis, also serve as a subroutine in the main program developed in this research – Considered in Chapter 4
- Analysis of life estimation models
- Integration of various models in PYTHIA – the capabilities and the functionalities of the life analysis software developed is given in Appendix A.
- Estimation of blade life using various lifing models
- Validation of overall life estimation models by carrying out life consumption analysis for a number of months of engine operation. This shows both the feasibility of the life tracking process and how results compare with what is obtainable in real engine operation process.
- Further analysis of life estimation models to detect the influences of shaft power variation, ambient temperature variation and engine degradation on the various relative engine life analysis parameters employed and developed in this work. Sensitivity of the life analysis factors to each effect is carried out.
- Further investigation aimed at arriving at engine operation conditions that warrants only creep life estimation even if engine is shut down frequently.

3.5 Engine Performance Model Creation in PYTHIA

To carry out life analysis of an existing engine, the performance model of the engine is created in PYTHIA. The engine performance model is a thermodynamic model of the real engine. An engine model is created in PYTHIA by assembling component bricks, which are expressed as component icons[176]. The component icons include INTAKE, COMPRE (for compressor), BURNER (for combustor), TURBIN (for turbine), SPLITTER, MIXEE or MIXFUL, NOZCON (for convergent nozzle), DUCTER, etc. The last icon in any engine model created in PYTHIA is PERFOR, which is used for final calculation of performance. Each icon is clicked and the initial component performance parameters are supplied. The creation of the engine performance model of the LM2500+ engine used in this research is considered in Chapter 5.

3.6 Adaptation of Engine Performance Model

Adaptation is the tuning of the engine model through mathematical processes for the engine model to run at various operating conditions and produce results that are similar to those of the real engine operating in same conditions. There are two types of adaptation the engine model can be subjected to. These are design point performance adaptation and off-design performance adaptation. In setting up the engine model and providing data for each brick based on the available field data, it is noteworthy that not every relevant data could be obtained, for example, the high pressure turbine entry temperature. This and many other parameters are estimated. When the model is run, the estimated output performance parameters will not be the same as the actual output performance parameters from the real engine. That is, predicted engine performance may be slightly different from real engine performance [176]. With proper adaptation of the engine model, the difference between the predicted performance parameters and the engine field data can be minimized greatly. PYTHIA has the capabilities of carrying out both design point performance adaptation and off-design performance adaptation. Design-point adaptation and off-design adaptation procedures are presented in the following sub-sections.

3.6.1 Design Point Performance Adaptation

Design point performance adaptation is an inverse mathematical problem and involves the selection of *to-be-adapted component parameters* and *target performance parameters* [176], [177]. The to-be-adapted component parameters are also referred to as independent adaptation parameters or gas turbine design point parameters while the target performance parameters also termed dependent adaptation parameters or measurable or measured performance parameters[176]. As the name implies, the independent adaptation parameters (to-be-adapted component parameters) are to be provided by the user and are inputted in the bricks or icons in the engine model as initial component performance parameters; for example, compressor and turbine efficiencies. The measurable parameters (target performance parameters) depend on the values of the to-be-adapted parameters. There must be mathematical relationships between the two sets of parameters- the essence is that, values of the to-be-adapted component parameters combine in various ways to give rise to the values of the target performance parameters. The mathematical model for design point performance adaptation as presented by Li et al. [16], [176], [177] is summarized here.

Having M number of target performance parameters and N number of to-be-adapted component parameters, the relationship between the to-be-adapted performance parameters $\vec{z}$ and the target performance parameters $\vec{x}$ is given as,

$$\vec{z} = h(\vec{x}) \tag{3.73}$$

where $h(\vec{x})$ is a vector-valued function. Taking $\vec{z}_0, \vec{x}_0$ as initial design point (baseline), the Taylor series expansion of Equation (3.73) yields Equation (3.74),

$$\vec{z} = \vec{z}_0 + \left.\frac{\partial h(\vec{x})}{\partial \vec{x}}\right|_0 (\vec{x} - \vec{x}_0) + HOT \tag{3.74}$$

HOT stands for the higher order terms in the expansion. A linear relationship thus exists between the deviations of the respective parameters from the design point in the form,

$$\Delta\vec{z} = H \cdot \Delta\vec{x} \tag{3.75}$$

Three cases can be identified with respective to the values of M and N.

CASE I: $M = N$

Solution: $$\Delta\vec{x} = H^{-1} \cdot \Delta\vec{z} \tag{3.76}$$

CASE II: $M < N$: In this case, a pseudo inverse is defined in the form,

$$H^{\#} = H^{T}\left(HH^{T}\right)^{-1} \tag{3.77}$$

Solution: $$\vec{x} = H^{\#}\vec{z} \tag{3.78}$$

CASE III: $M > N$: A pseudo inverse is defined in this case as,

$$H^{\#} = \left(H^{T}H\right)^{-1}H^{T} \tag{3.79}$$

Solution: $$\vec{x} = H^{\#}\vec{z} \tag{3.80}$$

The root mean square (RMS) of the difference between the predicted and the target parameters is used as a convergence criterion expressed as [176],

$$RMS = \sqrt{\sum_{i=1}^{M}\left(Z_{i,\,predicted} - Z_{i,\,target}\right)^{2}} < \delta \tag{3.81}$$

where δ is chosen as 0.001 in most cases [16], [176]. The adaptation error of the i^{th} target performance parameter is expressed as [176],

$$\varepsilon_i = \frac{Z_{i,\,predicted} - Z_{i,\,target}}{Z_{i,\,target}} \times 100\,\% \tag{3.82}$$

PYTHIA makes use of the above algorithm in carrying out design point adaptation. This is applied to the LM2500+ engine used in this research in Chapter 5.

3.6.2 Off-Design Performance Adaptation

Gas turbines in practice operate in several off-design conditions. Off-design performance adaptation is thus carried out to ensure that the engine performance model produces results similar to the real engine in different off-design conditions of engine operation. This has been considered by several researchers including Li et al.[159], [178]–[180] and involves the application of scaling factors to the engine components characteristic maps. This is done in order to calibrate the components characteristic maps. Stamatis et al.[181] proposed a method that could ensure accurate simulation of

engines of same type which may differ due to manufacturing or assembly tolerances. Like the newer works, they equally exploit the modification of component maps, noting that accurate component maps may not be required from the onset since the maps are derived during the adaptation process. The off-design performance adaptation involving the use of linear scaling factors has been studied and presented by [180], and the basic methodology employed for compressor map calibration is summarized below.

In the off-design performance adaptation process, scaling factors are first obtained at the design point (usually with all characteristics known) and applied to the whole map. The results are then used in generating the scaling factors at a defined range of off-design points. The adapted component maps should be able to predict results similar to the real engine at off-design conditions. The components map scaling technique in the adaptation process could be applied to the compressors, combustors and turbines. Non-linear off-design scaling factors could be sought [179]. Optimal set of off-design scaling factors are obtained using genetic algorithm. This has been implemented in PYTHIA by Li[180], and it is applied to the engine performance model in this research.

3.7 Off-Design Performance Calculation

At the design point of an engine, most engine parameters such as pressure ratio, speed, mass flow rate and the power output are specified usually with the ambient conditions. Components efficiencies are also given at the design point. The task normally involved in design point calculation is to estimate the overall plant efficiency and the air flow rate required to obtain the design power. The gas turbine engine, in practice, operates at a wide range of speed and power output, coupled with wide changes in ambient conditions. Any operation of the engine aside the design point is known as off-design performance. This research involves the usage of direct engine measurement data obtained at different off-design conditions. Engine performance simulations are carried out using PYTHIA capabilities to estimate gas path properties at different locations of the engine and compare such with the real engine data before lifing is carried out. Thus, the off-design performance calculation process is presented here.

There are several methods employed in off-design performance calculations in gas turbines. These methods involve components matching, gas path analysis, artificial

intelligence based methods, fuzzy logic based methods, Kalman filtering methods, Wittenberg's method and computational fluid dynamics based methods. Suraweera [182] introduced core control method in predicting gas turbine off-design performance. Components matching method is the most widely used method, and it requires the usage of components characteristics- components maps. Generally, compressor characteristics, combustor characteristics and turbine characteristics are needed in components matching technique, knowing that turbine and nozzle characteristics are similar, thus the three characteristics could be applicable to both industrial and aircraft engines.

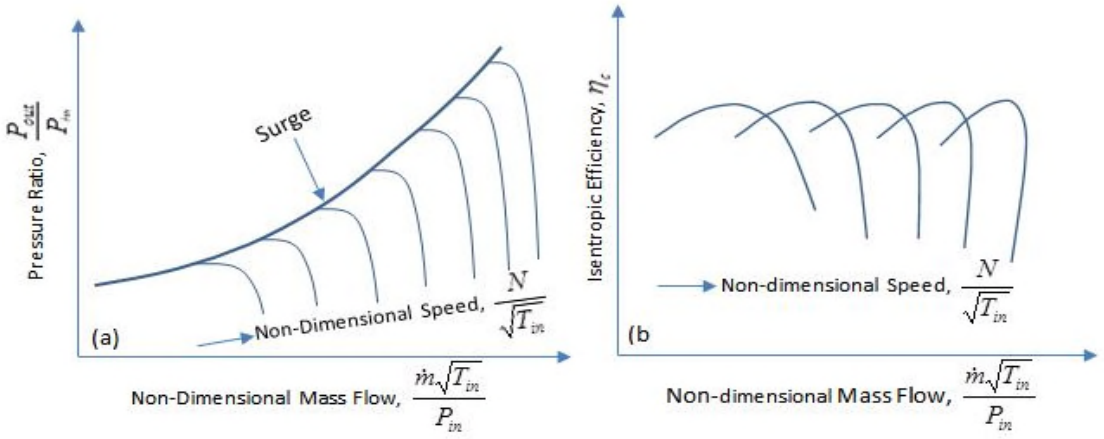

Figure 3.10: Compressor Characteristics: (a) Pressure Ratio vs Non-Dimensional Mass Flow, (b) Isentropic Efficiency vs Non-Dimensional Mass Flow

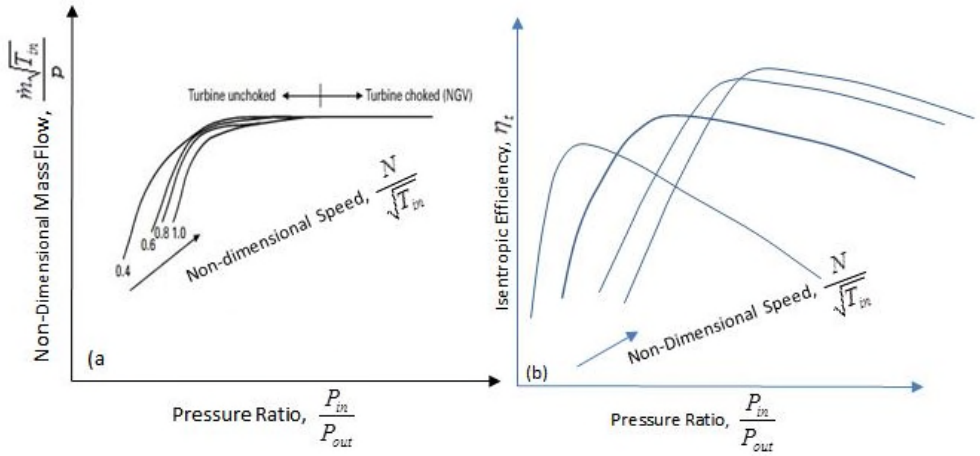

Figure 3.11: Turbine Characteristics: (a) Non-Dimensional Mass Flow vs Pressure Ratio- Modified From [3]**, (b) Isentropic Efficiency vs Pressure Ratio**

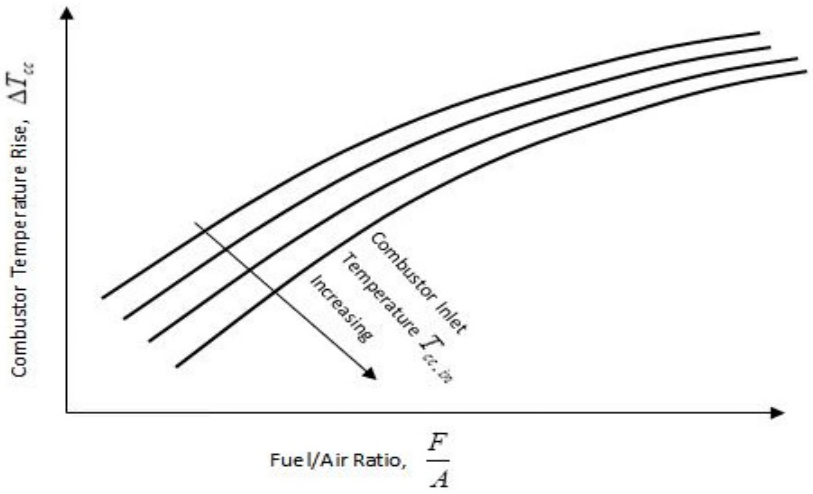

Figure 3.12: Combustor Characteristics – Temperature Rise vs Fuel/Air Ratio

Figures 3.10, 311 and 3.12 show the compressor characteristics, turbine characteristics and combustor characteristics respectively. The components characteristics specify a wide range of the variations of mass flow, pressure ratio, efficiency and rotational speed for compressor and turbine. The mass flow and rotational speed are expressed in dimensionless form. The combustor characteristics is expressed in terms of variations of combustor temperature rise ΔT_{cc} and fuel/air ratio F/A (theoretical values) at various combustor inlet temperatures $T_{cc,in}$ [19]. The actual combustor temperature rise and actual fuel/air ratio are obtained by defining combustion efficiency η_{cc} in any form of Equations (3.83) and (3.84),

$$\eta_{cc} = \frac{(F/A)_{theoretical}}{(F/A)_{actuall}} \tag{3.83}$$

$$\eta_{cc} = \frac{\Delta T_{cc,actual}}{\Delta T_{cc,theoretical}} \tag{3.84}$$

The value of the combustion efficiency is usually assumed in off-design performance calculations, and it is quite high, in the range 98.5% to 99.5% due to nearly stoichiometric combustion process [19].

The component matching technique calls for compatibility of mass flow, work and rotational speed between various components. It is an iterative process and parameters are guessed and compatibility checks are carried out. Also, a particular variable is selected as the engine 'handle' which determines the matching conditions of the engine. Commonly selected handles are speed, turbine entry temperature, and exhaust gas temperature. Shaft power could also be selected as engine handle, especially for an engine with free power turbine. The component matching technique is employed in off-design calculations in PYTHIA. The algorithm applied in this method to the LM2500+ engine type is presented in Chapter 5.

3.8 Blade Thermal and Stress Models

In analysing each of the lifing models, temperature and stress are to be estimated. This calls for the creation of blade thermal model and stress model respectively. The inputs to these models come from blade data and engine operation data. Further data is obtained from the engine performance model. The blade thermal and stress models are developed from first principles. These models are analytical and give quite accurate results compared to results from other stress and temperature analysis tools such as ABACUS, ANSYS. The finite element analysis (FEA) and computational fluid dynamics (CFD) tools employed in stress and thermal analysis are able to produce quite accurate results but they do not fit into this research because this research requires continuous determination of engine life consumption using data from the real engine operation. A one-off analysis of temperatures and stresses at various locations in the blade using FEA or CFD tools will enable the calculation of time to failure due to creep, but the loading has to be changed for any other data of engine operation. The results from these tools from previous works help to fine tune the results from the analytical thermal and stress models developed. Also, the data from the engine operation are fed in PYTHIA to estimate some input parameters required in the stress and thermal models. This necessitates the creation of analytical thermal and stress models that communicate with PYTHIA inner code to generate lifing results. By incorporating the thermal model, stress model, and lifing models in PYTHIA, it is possible to assess the life of the HP turbine blades at every section of available engine data and hence estimate the cumulative damage the blades suffer for the given period of engine operation. The life

of the engine is thus tracked using these developed algorithms. The development of blade thermal and stress models is considered in Chapter 4.

3.9 Life Prediction Points on the Blade

In order to determine the life of the blades, each blade is divided into n sections and temperatures are estimated at (n+1) nodes while stresses are estimated at the (n+1) nodes in three chord-wise sites- leading edge (LE), trailing edge (TE) and farthest point at the suction surface of the blade (indicated as SB). Figure 3.13 shows the division of the blade into n sections and the (n+1) nodes (N_1 to N_{n+1}) where temperatures and stresses are estimated are indicated. The temperature of the blade material is estimated at the (n+1) nodes by applying a radial temperature distribution factor to the combustor exit gases and assuming forced convection cooling of the blades. The temperature is assumed to be equal at every location across each nodal point. In the case of the stress value, at each node, the maximum stress at the three chord-wise sites is taken and used for life calculation.

In creep life consumption analysis, at each node, the estimated blade material temperature and the maximum stress at the node are used to estimate the creep life using the Larson-Miller Parameter method. The LMP value in the Larson-Miller equation is obtained by reading the value corresponding to the maximum stress level from the Larson-Miller Master curve of the blade material. The numerical equivalent of the master curve is provided and a code is written to obtain the LMP value through interpolation. The smallest value of creep life at the (n+1) nodes is used to represent the creep life of the blade. In fatigue life estimation, because creep-fatigue interaction analysis is also carried out, the fatigue cycles to failure are estimated at the same location where the smallest creep life was gotten. Creep-fatigue interaction life is thus estimated also at the same location where creep life as well as fatigue life was estimated.

In practice, the location of minimum creep life may not be the location where the largest stress value is obtained and where the smallest cycles to fatigue failure will occur. But in industrial turbine operation where a bit steady power levels are maintained over time, creep seems to dominate the failure modes. Thus, the location where creep failure is

likely to occur is the same location where creep-fatigue interaction failure may take place. Also, estimating fatigue life at each node and creep-fatigue interaction life at each node and selecting the smallest value in each case is quite involved considering computation time. These form the decision for carrying out fatigue life analysis and creep-fatigue interaction life analysis at the location where blade failure due to creep will likely occur.

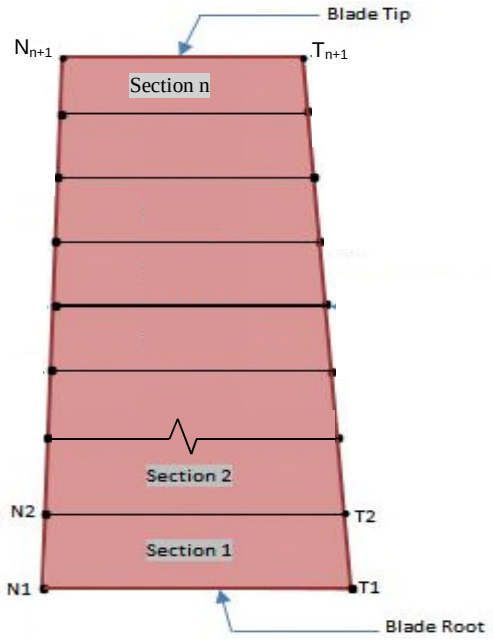

Figure 3.13: Blade Sections and Locations of Life Estimation

3.10 Software Development and Engine Life Calculations

The creep life model, fatigue life model and creep-fatigue interaction life models have been programmed and incorporated in PYTHIA using C-Sharp programming language. The engine life analysis sub-models- data acquisition and pre-processing module, the blade thermal model and the blade stress model are developed and incorporated as separate modules to make the life calculations feasible. The developed software thus has new features besides those originally developed in PYTHIA. In the new software, two sets of additional interfaces/windows are created. These are the “Life Setting Windows” and the “Life Analysis Windows”. The Life Setting Windows are three in number. They include the “Blade Life Setting Window”, “Creep Life Setting Window” and the “Fatigue and Creep-Fatigue Interaction Setting Window”. Input data to the blade is accessed through the “Blade Life Setting Window”. The “Creep Life Setting Window”

enables us to obtain the LMP master curve data of the blade material, while through the "Fatigue and Creep-Fatigue Interaction Setting Window" fatigue related input data are provided for life analysis. The Life Analysis windows on the other hand are two in number. These are the "Creep Life Analysis Window" and the "Fatigue and Creep-Fatigue Interaction Analysis Window".

The windows created to enable life calculation in this work are accessed through the "Engine Design Window" in PYTHIA. Here, the "Engine Design Window" is modified so as to communicate with the new windows created. Creep life analysis is carried out via the Creep Life Analysis Window while fatigue life analysis and creep-fatigue interaction life analysis are carried out through the Fatigue and Creep-Fatigue Interaction Analysis Window. To carry out the engine life consumption for a given period of engine operation, the real engine operation data is uploaded and simulations carried out to obtain related data required in the blade thermal and stress models. This is achieved through the "Engine Design Window" making using of the data acquisition and pre-processing module developed and PYTHIA off-design calculation capabilities. The windows developed, the basic functions of the software and how engine life consumptions are estimated are presented in Appendix A.

3.11 Chapter Conclusions

The lifing models and methodologies employed in engine life consumption analysis in each failure mode considered in this research have been highlighted in this chapter. At the heart of the work is PYTHIA and an engine performance model of the real engine is created and adapted to the real engine operation conditions to provide simulation results required by the blade thermal and stress models. The blade is divided into n sections and life is estimated at (n+1) nodal points, where the minimum life is taken to represent the time or cycles to failure at each engine operation condition. Results are generally presented in terms of life analysis factors which tell how well the engine was operated. The relevant basic tasks carried out in this research are also presented.

4 DEVELOPMENT OF ENGINE LIFE ANALYSIS SUB-MODELS

The creep life and the fatigue life models require input data. The creep life model requires blade metal temperature at various sections along the blade and stresses at same locations. The fatigue life model requires stress values as input while the creep-fatigue interaction model uses the outputs of the creep life model and fatigue life model as input. Thus, two basic models are required in engine life analysis. These are the blade thermal model and blade stress model. Both models require simulated data from PYTHIA as input data. A third model which felicitates the transfer of field data for simulation is the data acquisition and pre-processing model. All the life analysis models and the sub-models are integrated in PYTHIA. The linking of the model to PYTHIA is necessary because PYTHIA could carry out simulation of engine performance at any operating condition of the engine and provide results which are needed as inputs in the lifing sub-models. The linking of all the models to PYTHIA is also to ensure engine life calculations are carried out in a single platform.

The life analysis in this work makes use of all the data from the engine output for the whole day. Life consumption at every 5 minutes is carried out (amounting to 288 points of engine operation conditions in a day where engine life consumption is estimated). The overall or equivalent life consumption for the day could be obtained. Also, the equivalent life consumption for a number of days of engine operation or any period of engine operation in a day could be estimated. Calling 288 data points from the output of the real engine for performance simulation in PYTHIA and obtaining gas path properties for the blade thermal and stress models is paramount in this work. The data acquisition and pre-processing sub-model is thus developed to achieve this. Figure 4.1 shows the structure of the three sub-models together with their inputs and how they interact with the engine performance model.

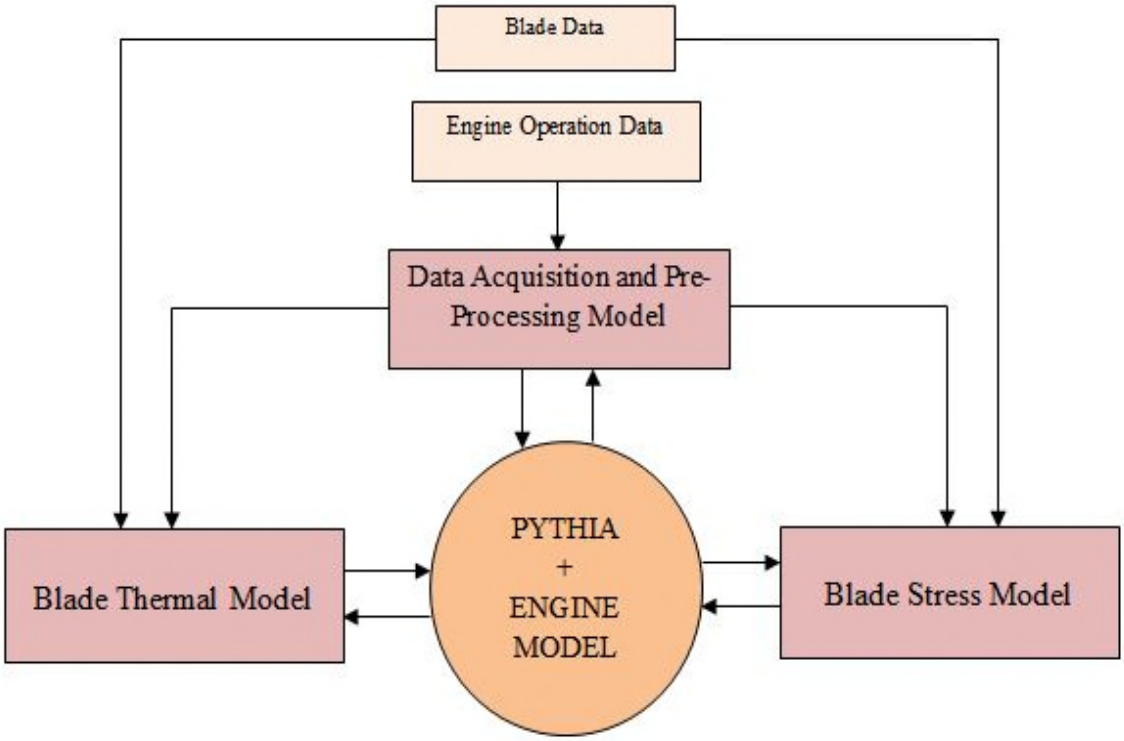

Figure 4.1: Structure of the Engine Life Analysis Sub-Models

Each of the models interacts with the engine (performance) model created in PYTHIA. The development and analysis of the life analysis sub-models is considered in this chapter.

4.1 Data Acquisition and Pre-Processing Module

In using PYTHIA for engine performance simulation or diagnostics analysis, one has to set up analysis interphase after obtaining the engine performance model. Off-design parameters are supplied manually. Also, engine degradation parameters under degraded engine condition are inputted manually. Degradation under off-design condition could be provided. Figures 4.2 and 4.3 show off-design set up and degradation under off-design condition set up respectively in PYTHIA. In the off-design setting, ambient temperature deviation is inputted. In the off-design under degradation setting, the off-design case is still ambient temperature deviation while 1% degradation is implanted in: compressor efficiency and flow capacity, combustor efficiency, and compressor turbine efficiency and flow capacity respectively.

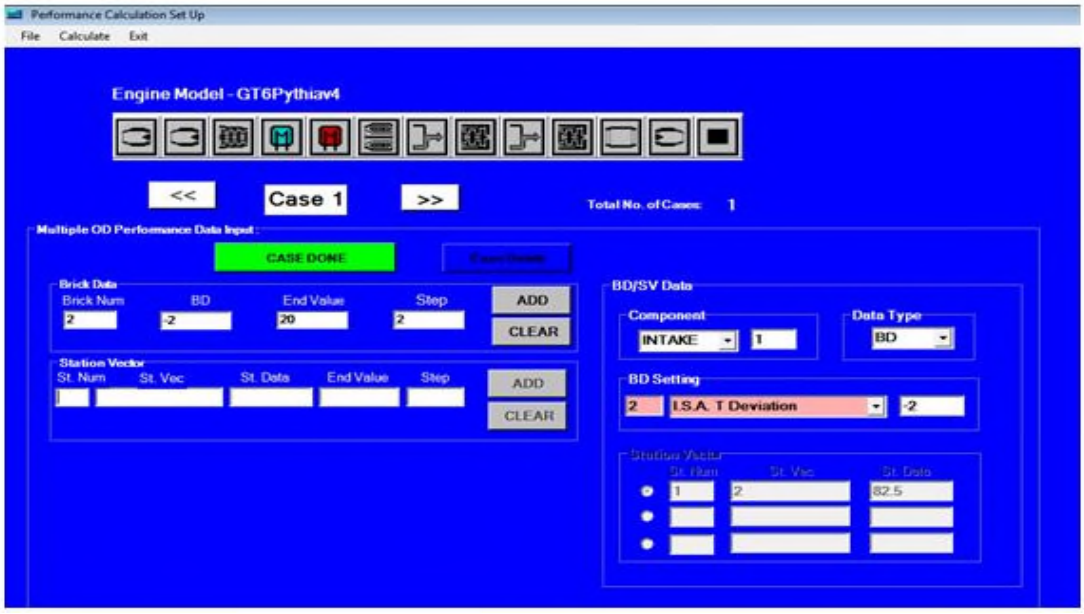

Figure 4.2: Off-Design Setting in PYTHIA

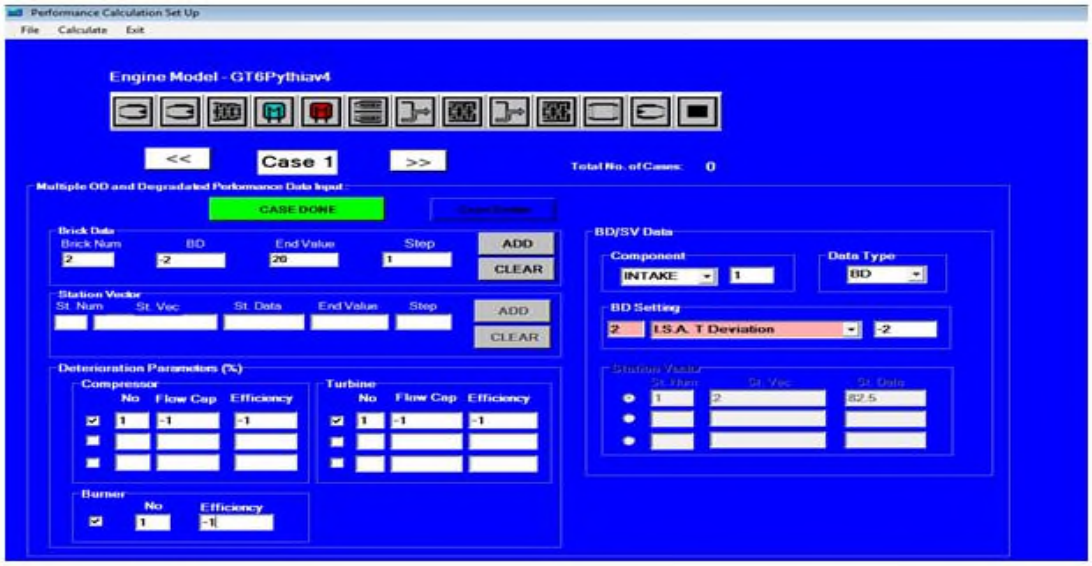

Figure 4.3: Degradation Under Off-Design Setting in PYTHIA

Assuming 288 data points are to be simulated and their outputs are to be used in the lifing model; this will be a tough task. This was one of the challenges before the author in this research. The way out is to set up data acquisition and pre-processing module which calls an excel sheet where data from the field for one day operation of the engine is available. The data acquisition and pre-processing model is a computer module which forms a separate module in PYTHIA. It selects the data for the day operation of the

engine, checks for periods the engine was not in operation using the results of the power output, sends processed data to PYTHIA for simulation, gets simulation results (gas path properties) from PYTHIA, and supplies same to the blade thermal and stress models. The code which is written in C-Sharp [183] has been included in PYTHIA , Figure 4.4.

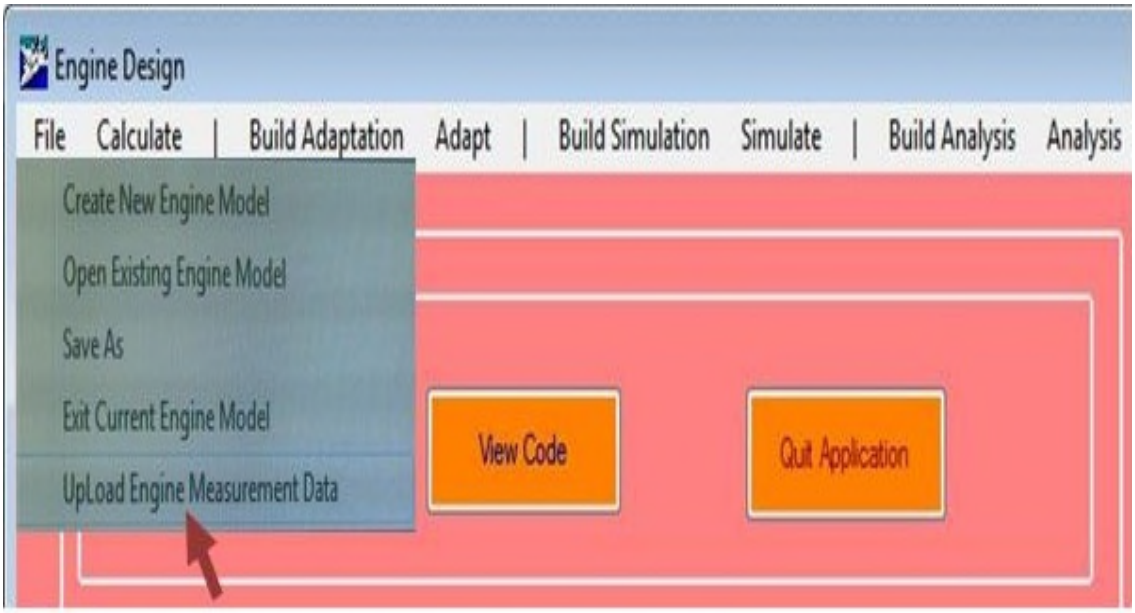

Figure 4.4: Uploading Data in PYTHIA for Simulation

Ambient temperature deviation and shaft power are used as off-design conditions in the performance simulations in this work to obtain gas path properties required in the blade thermal and stress models. Some of the parameters needed in the blade thermal and stress models are compressor shaft relative rotational speed (PCN), compressor exit temperature, compressor turbine efficiency, compressor turbine inlet temperature and pressure, compressor turbine exit temperature and pressure, coolant flow rate, and coolant temperature. Some of the simulated parameters could be viewed from the platform created for life analysis in this research, Figure 4.5.

Figure 4.5: Some Simulated Parameters from PYTHIA

These simulated parameters are used as inputs in the blade thermal and stress models. The blade thermal and stress models also require other input parameters aside the simulated parameters from the engine performance model. The blade thermal and stress models are considered next.

4.2 Blade Thermal Model

The blade thermal model helps in estimating the temperature of the blade at various sections of the blade. The blade could be divided into a number of sections, say n. Temperatures at the base of each section are then determined. In this work, the blade is divided into 8 equal sections, making available 7 intermediate sectional lines and a section at the blade root and tip respectively. Nine nodal points are thus available where blade material temperature is estimated. It is also possible to assume that temperatures at every point in the blade are the same, that is, uniform temperature distribution across the span of the blade. In both cases, the blades are cooled by convection, where cooling air is extracted towards the large stage of the compressor. This will lead to uniform temperature model and one-dimensional temperature model. To aid the development of the thermal model, the geometry of the blade and its associated parameters need to be reviewed. Figure 4.6 shows the geometry of the blade in different views and some parameters associated with blade geometry. In Figure 4.6(a), we can see two edges of the blade. These are the leading edge (LE) which faces the direction of the fluid flow and the trailing edge (TE). At the concave side of the blade (suction surface in Figure 4.6(b)), the farthest point from the axial axis is indicated as SB (see Figure 4.6(a)). This

point together with the leading and trailing edges are to be noted, since they act as points of likely highest mechanical stresses.

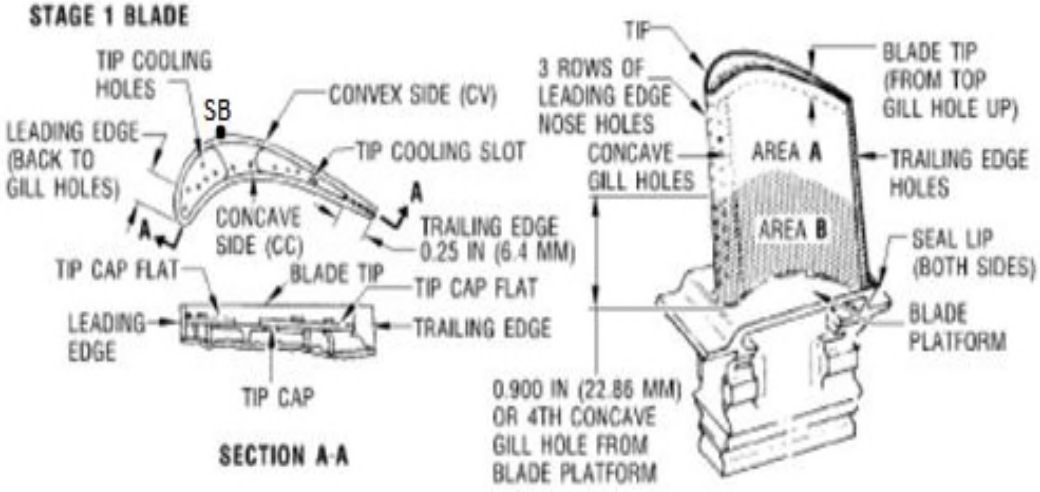

(a) First stage turbine blade in different views [184]

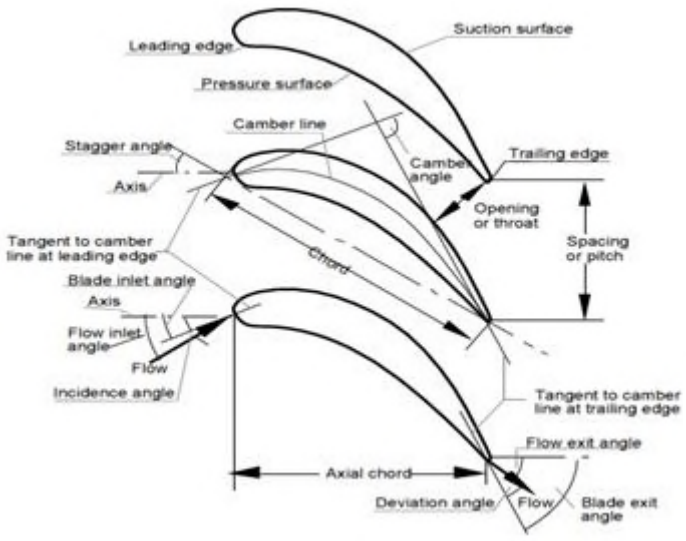

(b) Blade Parameters [185]

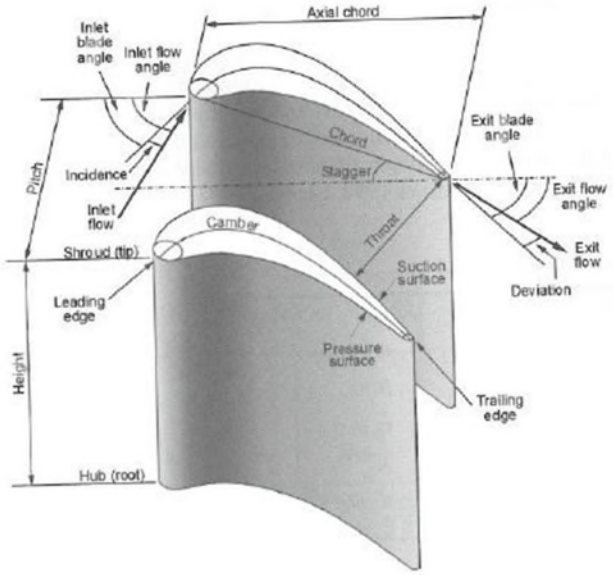

(c) Blading Terminology [186], pp.13

Figure 4.6: Blade Geometry and Parameters

Other parameters about the blade geometry are illustrated / defined with the aid of Figure 4.7.

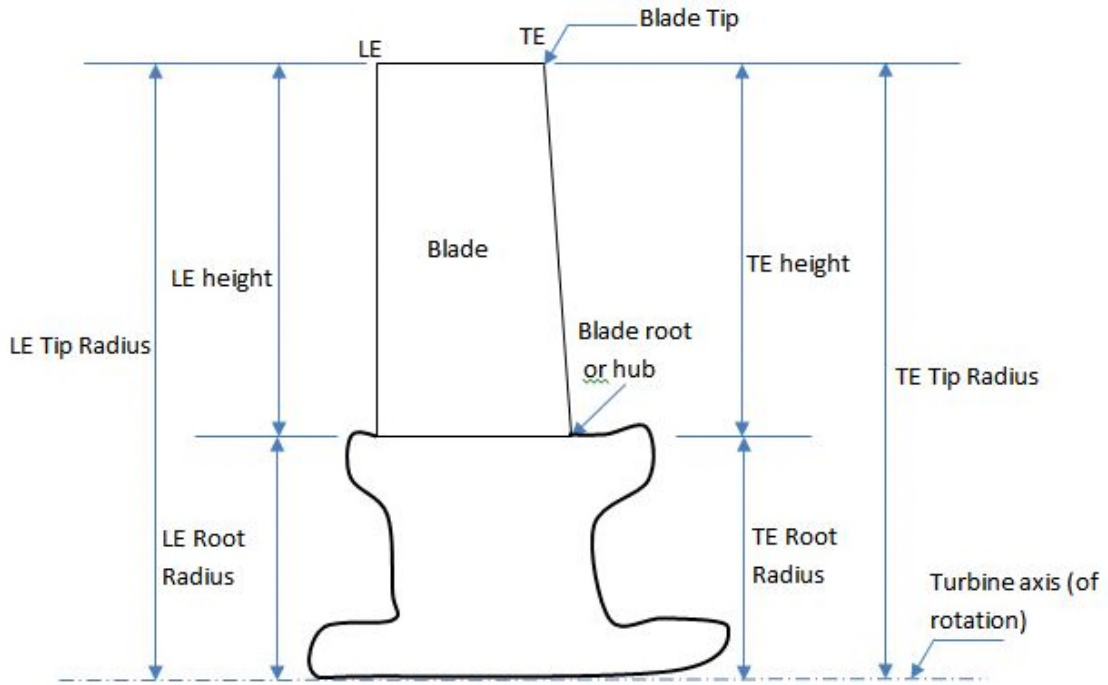

Figure 4.7: Blade Dimensions

The blade pressure surface (see Figure 4.6(a)) when projected to a plane surface may be rectangular or tapered. Rectangular blade surface is assumed in this case, since the actual blade profile is almost rectangular. In Figure 4.7, LE Tip Radius is the distance from the turbine axis of rotation to the blade tip at the leading edge while TE Tip Radius is the distance from the turbine axis of rotation to the tip of the blade at the trailing. These two dimensions may not be the same. Similarly, the leading edge root radius and the trailing edge root radius, designated as LE Root Radius and TE Root Radius respectively may not be equal. In view of this, in this work, the mean value at the LE and TE is used to represent the respective dimension. Thus, the blade tip radius R_{btp} is given as,

$$R_{btp} = \frac{1}{2}\left(R_{LE,Tip} + R_{TE,Tip}\right) \qquad (4.1)$$

where $R_{LE,Tip}$ and $R_{TE,Tip}$ are the leading edge tip radius and the trailing edge tip radius respectively. The mean root radius of the blade R_{brt}, where the LE root radius and TE root radius are designated as $R_{LE,Rt}$ and $R_{LE,Rt}$ respectively is given by Equation (4.2),

$$R_{brt} = \frac{1}{2}\left(R_{LE,Rt} + R_{TE,Rt}\right) \tag{4.2}$$

The blade height could be expressed in terms of the leading edge or the trailing. At any of the two positions, the blade height is the difference between the blade tip radius and the blade root radius. The mean blade height is,

$$B_{ht} = \frac{1}{2}\left(R_{btp} + R_{brt}\right) \tag{4.3}$$

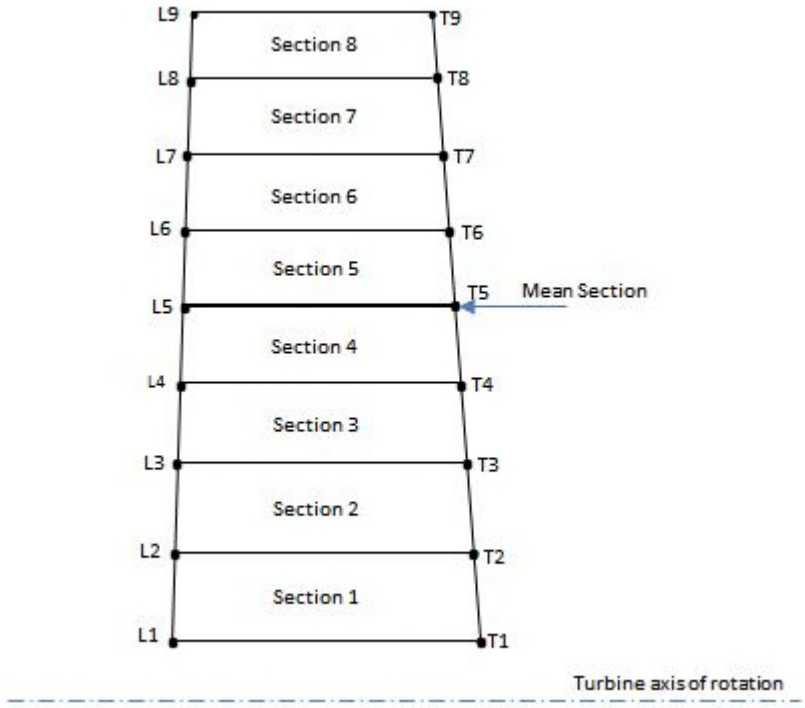

Figure 4.8: Blade Sections

Figure 4.8 shows the division of the blade along the span into 8 sections and the locations along which temperatures and stresses will be estimated. The blade is divided into 8 equal sections by using section lines L2T2 to L8T8. Two other sections lines are included to coincide with the root of the blade, L1T1 and the tip of the blade, L9T9. The section line, L5T5 which divides the blade into two equal halves is known as the mean section of the blade [185] . In the one-dimensional thermal model, temperatures at nodes L1 to L9 and at nodes T1 to T9 will be estimated, with the assumption that temperatures at nodes Li and Ti are the same, where i ranges from 1 to 9. That is, the temperature variation is only in the radial direction. The uniform temperature model

assumes that temperatures at every section of the blade are equal. This is not true in practice. In both models, two sub-models are derived-model for blades without thermal barrier coating and model for blades with thermal barrier coating. Thus, four thermal models are developed in all. The one-dimensional thermal model is more representative of real life situations, and since the engine under review in this study has blades that are cooled and with thermal barrier coatings, the one-dimensional thermal model with thermal barrier coatings is used for the life analysis in this work. The uniform temperature model is introduced for quick check of results and for comparison of results if the need arises. Figure 4.9 shows the four thermal models.

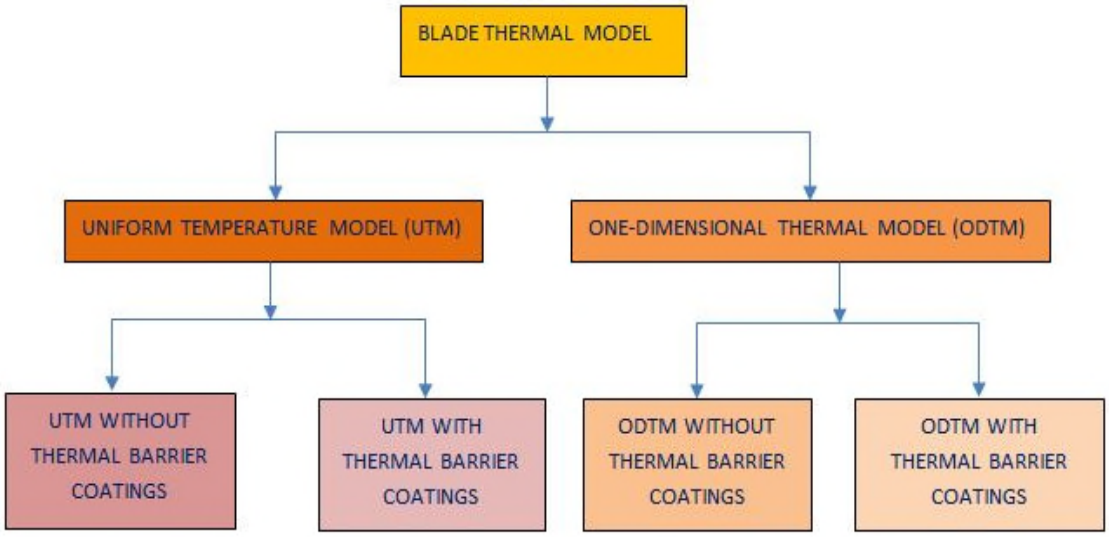

Figure 4.9: Blade Thermal Models Employed

The thermal models are considered in the following sub-sections.

4.2.1 Uniform Temperature Model

The uniform temperature model assumes uniform blade temperature at every point of the blade surface. Convection cooling is considered as a basis for obtaining the model. Three system design parameters are employed in arriving at the uniform temperature model. These parameters which are also employed in the one-dimensional thermal model are coolant mass flow function, overall cooling effectiveness and convective cooling efficiency. Each of these parameters which are adapted from [187] and could also be obtained from [188] is considered in turn.

I. Coolant mass flow function

Considering overall energy balance, as coolant flow at temperature T_{c_in} enters the blade through the blade hub or root and exits at the blade tip at temperature T_{c_ex} as in Figure 4.10, the following relations are obtained:

- The energy input to the whole blade, $\dot{Q}_{in}$ is,

$$\dot{Q}_{in} = h_g B_p B_{ht} \left(T_g - T_{bm}\right) \tag{4.4}$$

where h_g is the external heat transfer coefficient, B_p is the perimeter of the blade, T_g is the bulk gas temperature, and T_{bm} is the bulk temperature of the blade material.

- The energy removed from the whole blade is,

$$\dot{Q}_{out} = \dot{m}_{c\_B} C_{p\_ca} \left(T_{c\_ex} - T_{c\_in}\right) \tag{4.5}$$

where $\dot{m}_{c\_B}$ is the mass flow rate of the cooling air for cooling each blade, C_{p_ca} is the specific heat capacity of the cooling air. With $\dot{m}_{ca}$ as the total mass of cooling air, N_b the number of blades and m_{f_B} as the mass fraction of air for blade cooling, the cooling air per blade is given by Equation (4.6),

$$\dot{m}_{c\_B} = \frac{\dot{m}_{ca} \times m_{f\_B}}{N_b} \tag{4.6}$$

Under steady state, the energy input to the whole blade is equal to the energy removed from the blade, thus,

$$\dot{Q}_{in} = \dot{Q}_{out}$$

$$h_g B_p B_{ht} \left(T_g - T_{bm}\right) = \dot{m}_{c\_B} C_{p\_ca} \left(T_{c\_ex} - T_{c\_in}\right) \tag{4.7}$$

Rearranging Equation (4.7) yields,

$$m^* = \frac{\dot{m}_{c\_B} C_{p\_ca}}{h_g B_p B_{ht}} = \left(\frac{T_g - T_{bm}}{T_{c\_ex} - T_{c\_in}}\right) \tag{4.8}$$

where m^*, a non-dimensional representation of coolant mass flow, is referred to as *coolant mass flow function* [187]. This is the ratio of difference in temperature between the blade and the hot gases and increase in temperature of the cooling air.

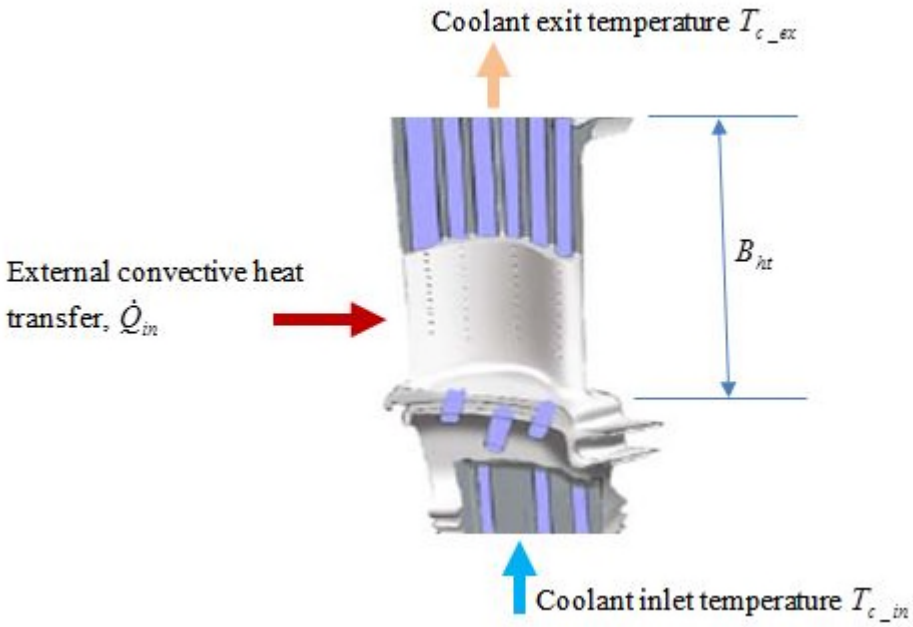

Figure 4.10: Heat Transfer and Coolant Temperatures in a Turbine Blade -Modified from [187]

II. Overall cooling effectiveness

The overall cooling effectiveness ε_{ff} is defined as the ratio of the difference in temperature between the blade and the hot gases and the difference in temperature between the hot gases and coolant inlet temperature. This is given by Equation (4.9),

$$\varepsilon_{ff} = \frac{T_g - T_{bm}}{T_g - T_{c\_in}} \tag{4.9}$$

III. Convection cooling efficiency

The convection cooling efficiency η_c is given as the ratio of the coolant temperature rise to the difference between the blade bulk material temperature and the coolant inlet temperature, given by Equation (4.10),

$$\eta_c = \frac{T_{c\_ex} - T_{c\_in}}{T_{bm} - T_{c\_in}} \tag{4.10}$$

Combining Equations (4.8) to (4.10), we express the cooling effectiveness in terms of the other two parameters in the form,

$$\varepsilon_{ff} = \frac{m * \eta_c}{1 + m * \eta_c} \tag{4.11}$$

From Equation (4.9), the blade metal bulk temperature could be expressed as,

$$T_{bm} = T_g - \varepsilon_{ff}\left(T_g - T_{c\_in}\right) \tag{4.12}$$

The high pressure turbine blades under study are in two-stage design. The first stage is exposed to much higher temperatures than the second stage, thus the first stage blades life is being focused in this work. The bulk gas temperature T_g is the temperature at the exit of the nozzle guide vanes, NGV or temperature at the inlet of the rotor stage. T_g is less than the temperature at the inlet of the high pressure compressor turbine, (turbine entry temperature, TET or T_5 in this work). The TET and the coolant inlet temperature are obtained from the performance simulations in PYTHIA. The overall cooling effectiveness, which value in practice is about 0.5 [187] is assumed in most cases, this value is also assumed in this work. For multi-stage analysis where the blade life of more than one stage is targeted, the coolant exit temperature at each stage has to be estimated. This will serve as the coolant inlet temperature of the subsequent stages. This is obtained from Equation (4.10) expressed in terms of the nozzle guide vanes in the form,

$$T^c_{ex\_NGV,i} = T^c_{in\_NGV,i} - \eta_{c\_NGV}\left(T_{NGV} - T^c_{in\_i}\right) \tag{4.13}$$

where $T^c_{in\_NGV,i}$ is the coolant inlet temperature at stage i, $T^c_{ex\_NGV,i}$ is the coolant exit temperature at stage i, T_{NGV} is the NGV bulk metal temperature , and η_{c_NGV} is the convective cooling efficiency of the NGV. For the first stage, Equation (4.13) takes the form of Equation (4.13a),

$$T^c_{ex\_NGV,1} = T^c_{in\_NGV,1} - \eta_{c\_NGV}\left(T_{NGV} - T^c_{in\_NGV,1}\right) \tag{4.13a}$$

The nozzle guide vane convective cooling efficiency, η_{c_NGV} is obtained from Equation (4.11) by assuming a value for the convective cooling effectiveness of the NGV, ε_{ff_NGV}. Denoting the NGV non-dimensional mass flow as m^*_{NGV}, we get,

$$\eta_{c\_NGV} = \frac{\varepsilon_{ff\_NGV}}{m^*_{NGV} - \left(m^*_{NGV} \times \varepsilon_{ff\_NGV}\right)} \tag{4.14}$$

The NGV non-dimensional mass flow is assumed to be about 40% of the NGV coolant mass percentage, ϕ_{NGV} [189] given as,

$$\phi_{NGV} = \frac{m_{f\_NGV} \times \dot{m}_{ca}}{\dot{m}_{t\_in}} = \frac{\dot{m}_{c\_NGV}}{\dot{m}_{t\_in}} \tag{4.15}$$

where m_{f_NGV} is the mass fraction of air for NGV cooling, $\dot{m}_{NGV\_c}$ is the mass flow rate of air for NGV cooling, $\dot{m}_{ca}$ is the total mass of cooling air, $\dot{m}_{t\_in}$ is the total mass flow rate of air at turbine inlet, it is the difference between the air flow rate at compressor inlet, $\dot{m}_{c\_in}$ and the cooling air flow rate $\dot{m}_{ca}$ plus the fuel flow rate $\dot{m}_f$:

$$\dot{m}_{t\_in} = \dot{m}_{c\_in} - \dot{m}_{ca} + \dot{m}_f \tag{4.16}$$

In theory, the fuel flow rate is usually assumed to be equal to that of the cooling air, thus the flow rate at turbine inlet is taken to be equal to the air flow at compressor intake. The nozzle guide vane metal temperature T_{NGV} is obtained from Equation (4.9) as,

$$T_{NGV} = T^g_{in\_NGV} - \varepsilon_{ff\_NGV}\left(T^g_{in\_NGV} - T^c_{in\_NGV}\right) \tag{4.17}$$

where $T^g_{in\_NGV}$ is the bulk gas temperature at the inlet of the NGV and $T^c_{in\_NGV}$ is the NGV coolant inlet temperature. This is assumed to be equal to the blade inlet coolant temperature. For stage 1, $T^g_{in\_NGV}$ is equivalent to the turbine entry temperature (TET) or T_5 in this work. This value, and the coolant inlet temperature, as already stated are obtained from performance simulations in PYTHIA. For subsequent stages, the nozzle NGV bulk gas temperature is estimated by considering the number stages and the

temperature drop per stage. Assuming n stages and equal temperature drop per stage, the temperature drop per stage T_{dp_stg} is,

$$T_{dp\_stg} = \frac{TET - T_{g,ex}}{n} \tag{4.18}$$

where $T_{g,ex}$ is the temperature of the gas at the exit of the turbine. The temperature at the exit of the first stage serves as the temperature at the NGV inlet in the second stage, and the sequence continues. The temperature at the exit of the i^{th} stage $T^{g}_{ex,i}$ is given by Equation (4.19),

$$T^{g}_{ex,i} = TET - i \times T_{dp\_stg} \tag{4.19}$$

Alternatively, with n stages, the product of the pressure ratios will give the overall pressure ratio PR, given by Equation (4.20),

$$PR = \frac{P_{ex}}{P_{in}} = PR_{stg1} \times PR_{stg2} \times PR_{stg3} \times ... \times PR_{stgn} \tag{4.20}$$

P_{ex} is the pressure at the exit of the (entire) turbine stage, P_{in} is the pressure at the inlet of the (entire) turbine stage, PR_{stg1}, PR_{stg2}, PR_{stg3}, … , and PR_{stgn} are the pressure ratios of the various stages of the turbine. Assuming equal pressure ratio per stage, denoted as PR_{stg} Equation (4.20) will be in the form,

$$PR = \left(PR_{stg}\right)^{n} \tag{4.21}$$

Thus, the pressure ratio per stage is obtained from the overall pressure ratio given by Equation (4.22),

$$PR_{stg} = PR^{\frac{1}{n}} \tag{4.22}$$

With the pressures at turbine inlet and turbine exit (P_{in} and P_{ex}) obtained from the simulations in PYTHIA, the intermediate pressures could be obtained using the pressure ratio per stage and the inlet and exit pressures. The pressure at the exit of stage 1,

denoted as $P_{ex,1}$ (denoted generally for stage i as $P_{ex,i}$) is given by Equation (4.23) where $P_{in,1}$ is the pressure at the inlet of stage 1 (obtained from simulations in PYTHIA),

$$P_{ex,1} = P_{in,1} \times PR^{\frac{1}{n}} \tag{4.23}$$

The pressure at the exit of stage 1 acts as the pressure at the inlet of stage 2, and following this sequence, all the intermediate pressure values could be obtained. Alternatively, the pressure at the exit of stage m, $(m \leq n)$, denoted as $P_{ex,m}$ could be obtained from Equation (4.24),

$$P_{ex,m} = P_{in,1} \times PR^{\frac{m}{n}} \tag{4.24}$$

When $m = n$, the pressure obtained will be the pressure at the exit of the (entire) turbine stage which is obtained from the simulations. P_{in} is actually the pressure at the inlet of the NGV, the pressure at the inlet of the turbine stage is obtained by applying a nozzle guide vane recovery pressure NGV_{PR}. Using the equations obtained so far will not introduce much error because NGV pressure recovery is usually close to unity. The TET and the temperature at the exit of the turbine are obtained from the simulations in PYTHIA. The corresponding intermediate temperatures could be estimated using Equation (4.25), assuming the polytropic efficiency η_p is the same for each stage,

$$T_{ex,i} = T_{in,i} \times \left(\frac{P_{ex,i}}{P_{in,i}} \right)^{\frac{(\gamma_h - 1)\eta_p}{\gamma_h}} \tag{4.25}$$

$T_{ex,i}$ and $T_{in,i}$ are the temperatures at the exit and the inlet respectively at stage i. The temperature at the inlet of a given stage is the nozzle guide vanes (NGV) inlet temperature, and since the blades are cooled, the actual temperature of the hot gases at the inlet of the rotor blades will be less than the temperature at the inlet of the NGV- this is considered later in this section. The temperature at the exit of a given stage forms the temperature at the inlet of the NGV of the next stage. The polytropic efficiency is obtained from Equation (4.26),

$$\eta_p = \frac{\ln\left\{1-\eta_t\left[1-\left(\frac{P_{ex}}{P_{in}}\right)^{\left(\frac{\gamma_h-1}{\gamma_h}\right)}\right]\right\}}{\left(\frac{\gamma_h-1}{\gamma_h}\right)\ln\left(\frac{P_{ex}}{P_{in}}\right)} \qquad (4.26)$$

Appendix C-1 shows how the polytropic efficiency given by Equation (4.26) is obtained.

In this work, the turbine has only two stages and the intermediate temperature is estimated assuming equal temperature drop per stage. The temperature at the exit of the HP compressor turbine is T_6 and this value is obtained from performance simulation results. The temperature at the exit of the first stage is obtained from Equations (4.18) and (4.19). The temperature at the inlet of the rotor blades in each stage is less than the temperature at the exit of the NGV. The blade inlet temperature at each stage is obtained by considering temperature of the gas at the NGV are cooled and then considering adiabatic mixing of the gases at the NGV exit and at the point of entering the rotor blades [37]. The mixing of the hot gases at the NGV exit with the NGV coolant exit gases is shown in Figure 4.11.

Considering the cooling of the NGV, the following relation is obtained,

$$\dot{m}_{c\_NGV} C_{p,ca}\left(T^{c}_{ex\_NGV} - T^{c}_{in\_NGV}\right) = \dot{m}_{t\_in} C_{p,g}\left(T^{g}_{in\_NGV} - T^{g}_{ex\_NGV}\right) \quad (4.27)$$

where $C_{p,g}$ is the specific heat capacity at constant pressure of the hot gases, and $T^{g}_{ex\_NGV}$ the bulk gas temperature at the exit of the NGV, and it is obtained from Equation (4.27) in the form,

$$T^{g}_{ex\_NGV} = T^{g}_{in\_NGV} - \frac{\dot{m}_{c\_NGV} C_{p,ca}}{\dot{m}_{t\_in} C_{p,g}}\left(T^{c}_{ex\_NGV} - T^{c}_{in\_NGV}\right) \quad (4.27a)$$

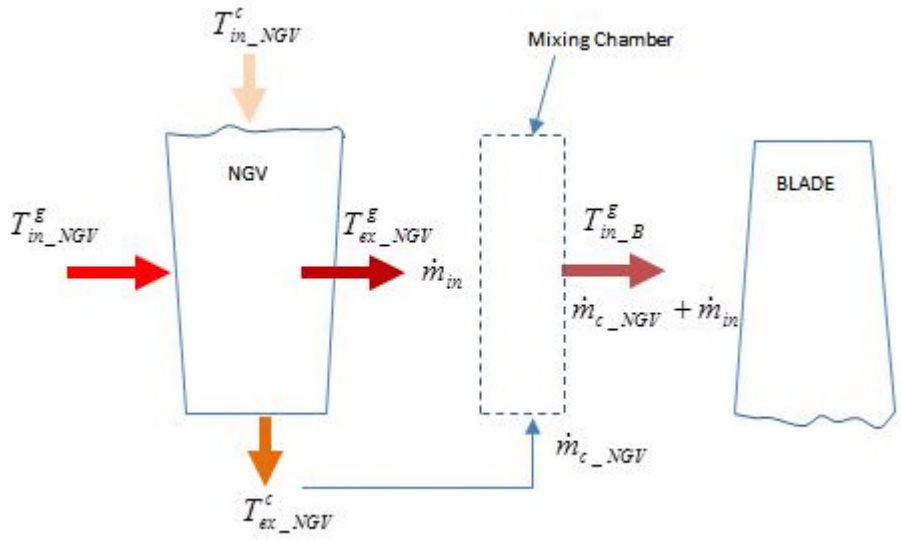

Figure 4.11: Determination of Turbine Inlet Temperature

The bulk gas temperature at the blade inlet $T^{g}_{in\_B}$ is obtained by considering adiabatic mixing of the cooling air at the exit of the NGV and the gas stream at the exit of the NGV. Taking $C_{p,m}$ as the specific heat capacity at constant pressure of the hot gas stream after mixing,

$$\left(\dot{m}_{NGV\_c} + \dot{m}_{t\_in}\right) \times C_{p,m} \times T^{g}_{in\_B} = \dot{m}_{NGV\_c} C_{p,ca} T^{c}_{ex\_NGV} + \dot{m}_{t\_in} C_{p,g} T^{g}_{ex\_NGV} \quad (4.28)$$

From Equation (4.22), $T^{g}_{in\_B}$ is obtained as,

$$T^{g}_{in\_B} = \frac{\dot{m}_{c\_NGV} C_{p,ca} T^{c}_{ex\_NGV} + \dot{m}_{t\_in} C_{p,g} T^{g}_{ex\_NGV}}{\left(\dot{m}_{c\_NGV} + \dot{m}_{t\_in}\right) \times C_{p,m}} \quad (4.29)$$

And $C_{p,m}$ is given as,

$$C_{p,m} = m^{c}_{f\_NGV} \times C_{p,ca} + m^{g}_{f\_in} \times C_{p,g} \quad (4.30)$$

where $m^{c}_{f\_NGV}$ and $m^{g}_{f\_in}$ are the mass fractions of the NGV cooling air and the hot gas stream at the exit of the NGV respectively which enter the mixing chamber. Because $m^{c}_{f\_NGV}$ is small compared to $m^{g}_{f\_in}$, $C_{p,m}$ is approximately equal to $C_{p,g}$.

For multi-stage design, we have obtained expressions for determining the temperatures at the various stages of the design: at NGV inlet and exit, and at blade inlet and exit. The corresponding pressures are determined under blade stress model. We now consider two cases- blade without thermal barrier coating and blade with thermal barrier coating.

CASE I: Blade without Thermal Barrier Coating

For blade without thermal barrier coating, the blade metal temperature T_{bm} is obtained using Equation (4.12), where the temperature of the gas at the blade inlet $T_{in\_B}^{g}$ is used in the place of T_g. It is also given here for convenience.

$$T_{bm} = T_{in\_B}^{g} - \varepsilon_{ff}\left(T_{in\_B}^{g} - T_{c\_in}\right) \qquad (4.12a)$$

The blade metal temperature is gotten by exploiting many other equations presented in this chapter. The temperature obtained is assumed to be the same at every section of the blade. A Sequential Solution-Algorithm Tree (SSAT) of this model, which shows the basic steps required in obtaining the required parameter (in this case, blade metal temperature for cooled blades without thermal coating with uniform temperature at every section) is given in Appendix D.1.

CASE II: Blade with Thermal Barrier Coating

Thermal barrier coatings coupled with air cooling leads to appreciable reduction in blade metal temperature. The thickness and the type of material used in thermal barrier coating depends on the structure desired and the application intended [190]. Thickness of thermal barrier coating (TBC) materials is usually in the order of 100μm to 2mm [191]. Cao et al.[192] gave the properties of different materials used for thermal barrier coatings. The property of interest in this work is the thermal conductivity of the thermal barrier coating material in addition to the thickness of the coating. If the blade has thermal barrier coating, the blade metal temperature in Equation (4.12) is equivalent to the temperature of the coating material. Equation (4.12a) will thus be put in the form of Equation (4.31) where T_{tbc_s} is the temperature at the outer surface (wall) of the TBC material.

$$T_{tbc\_s} = T^{g}_{in\_B} - \varepsilon_{ff}\left(T^{g}_{in\_B} - T_{c\_in}\right) \tag{4.31}$$

The temperature of the blade material is obtained by considering the energy transfer between the hot gases to the TBC surface and the energy transfer from the TBC material to the surface of the blade. The energy transfer from the hot gases to the TBC surface $\dot{Q}_{g\_tbc}$ is given by Equation (4.32),

$$\dot{Q}_{g\_tbc} = h_g A_{tbc\_s}\left(T_g - T_{tbc\_s}\right) \tag{4.32}$$

A_{tbc_s} is the surface area of the TBC material, the heat transfer surface area. The energy transfer from the TBC material to the blade surface $\dot{Q}_{tbc\_bm}$ is given by Equation (4.33),

$$\dot{Q}_{tbc\_bm} = \frac{k_{tbc} A_{tbc\_s}\left(T_{tbc\_s} - T_{bm}\right)}{\delta_{tbc}} \tag{4.33}$$

k_{tbc} is the thermal conductivity of the TBC material (in W/mK) and δ_{tbc} is the thickness of the TBC material (in m). Under steady state condition, the heat transfer rate from the hot gases to the TBC is equal to the heat transfer rate from the TBC to the blade material. Therefore Equating Equations (4.32) and (4.33) and re-arranging, the blade material temperature is obtained as given by Equation (4.34),

$$T_{bm} = T_{tbc\_s} - \left(\frac{\delta_{tbc}}{k_{tbc}}\right) \times h_g\left(T_g - T_{tbc\_s}\right) \tag{4.34}$$

T_g is the temperature of the gas at turbine inlet, same as $T^{g}_{in\_B}$. The only unknown parameter in Equation (4.34) is the external heat transfer coefficient h_g, and it is given as,

$$h_g = \frac{Nu_g \times k_g}{c} \tag{4.35}$$

where Nu_g, k_g and c are the Nusselt number of the gas, thermal conductivity of the gas and the average chord of the blade. k_g is read based on the average gas temperature, in this work the value is interpolated using property tables provided by The Engineering

ToolBox [193]. The blade chord c is estimated from the blade geometry while the Nusselt number is estimated using an empirical relationship in the form [194],

$$Nu_g = Nu'_g \left(\frac{\mathrm{Re}_g}{2\times10^5} \right)^x \left(\frac{T_g}{T_{tbc\_s}} \right)^y \tag{4.36}$$

where Nu'_g is the nominal mean Nusselt number, it is equal to Nu_g when the Reynolds number of the gas Re_g equals 2×10^5 and $\frac{T_g}{T_{tbc\_s}} \to 1$. The exponent y is estimated from the relation [194],

$$y = 0.14 \left(\frac{\mathrm{Re}_g}{2\times10^5} \right)^{-0.4} \tag{4.37}$$

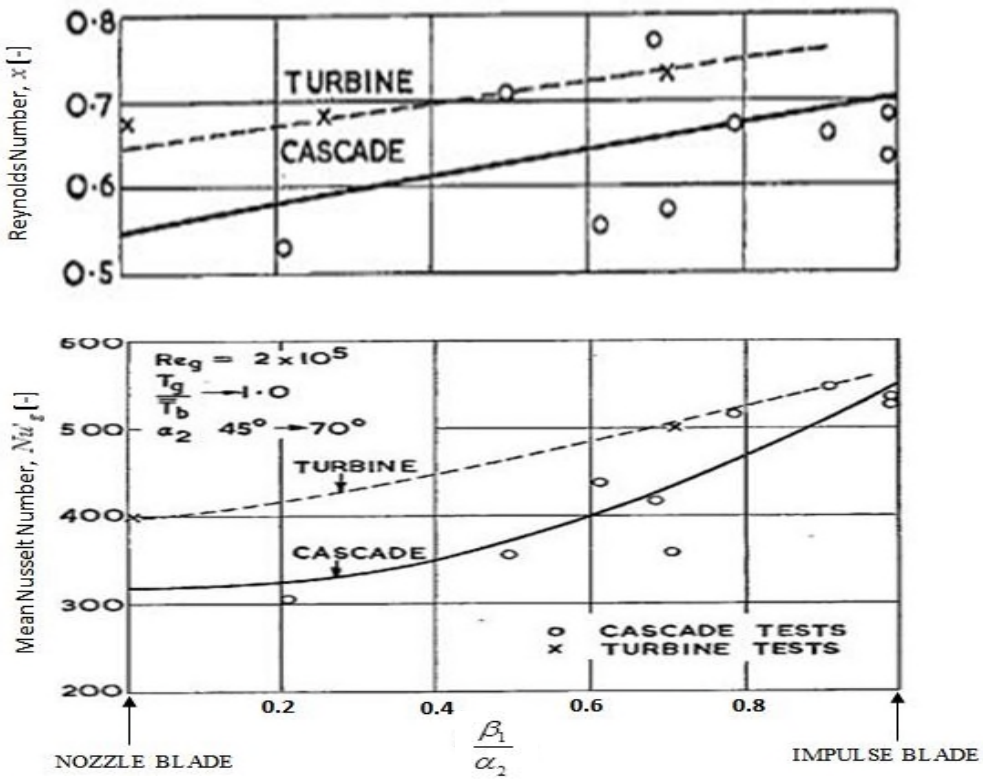

Figure 4.12: Heat Transfer Data for Turbine Blades ([194], pp.34)

Nu'_g and the Reynolds number exponent x could be obtained from data about correlation of heat transfer for wide range of turbine blades [194] . This is shown in Figure 4.12. The values of Nu'_g and x are read based on the ratio of the blade inlet

angle to the gas outlet angle (see Figure 4.6) both values which are obtainable and shown later in this work.

The Reynolds number is given as,

$$\mathrm{Re}_g = \frac{\rho_g \times V_{Abs\_ex} \times c}{\mu_{ex}} \tag{4.38}$$

where ρ_g is the gas density, V_{Abs_ex} is the absolute velocity of the gas at the exit of the blade, μ_{ex} is the blade exit gas viscosity. The viscosity at the exit of the blade is obtained using the Sutherland Equation given as [195],

$$\mu_{ex} = \mu_o \frac{T_o + C}{T + C}\left(\frac{T}{T_o}\right)^{\frac{3}{2}} \tag{4.39}$$

where μ_o is reference dynamic viscosity (in Pa.s or μ Pa.s; $\mu_o = 18.27 \mu Pa..s$), C is Sutherland's constant ($C = 120K$), T_o is reference temperature in Kelvin ($T_o = 291.15K$), $T \equiv T_{ex,i}^{g}$ is the input temperature in Kelvin. The gas density is expressed in terms of the blade exit static pressure p_{ex} and static temperature t_{ex} as,

$$\rho_g = \frac{p_{ex}}{R \times t_{ex}} \tag{4.40}$$

where R is the gas constant (in J/kgK). The static temperatures and the pressures at the exit of each blade stage will be obtained in the blade stress model considered later in this chapter. All the parameters required in estimating the external heat transfer coefficient of the hot gases are now known and the blade metal temperature could be estimated using Equation (4.34). It is pertinent to point out that the blade metal temperature obtained for blade with thermal coating will be much less than that obtained without thermal barrier coating, the value of the former much influence by the thermal conductivity and the thickness of the thermal barrier coating. The temperature reduces with increase in the thickness of the thermal barrier coating but increases with increase in the thermal conductivity of the thermal barrier coating used. The latter is usually assumed to be constant for a given material, thus an appropriate thickness of the thermal barrier is required to achieve a design temperature with other parameters known. A Sequential Solution-Algorithm Tree of this model is given in Appendix D.2.

4.2.2 One-Dimensional Blade Thermal Model

The one-dimensional blade thermal model is influenced by the temperature profile at the exit of the combustor which is characterized by two parameters. These parameters are the overall temperature distribution factor (OTDF), and the radial temperature distribution factor (RTDF) [196]. OTDF affects NGV while RTDF affects rotor blades. The RTDF is given by Equation (4.41),

$$RTDF = \frac{T_{\max} - T_{Bur\_Mean}}{T_{Bur\_Mean} - T_{Bur\_In}} \tag{4.41}$$

$T_{\max}$ is the maximum circumferential mean temperature anywhere in the combustor exit, commonly called the *streak temperature* [197] , T_{Bur_In} is the burner inlet temperature, while T_{Bur_Mean} is the mean burner exit temperature. T_{Bur_Mean} represents the mean temperature recorded around the span of the blade [198]. The location of the maximum temperature results from random hardware variations and it cannot be localized for a fleet of engines [197]. The RTDF determines the life of a rotor blade because as the rotor rotates, the blades experience the circumferential average of the temperatures at any radial plane [199]. The maximum temperature is gotten from Equation (4.41) as given by Equation (4.42),

$$T_{\max} = T_{Bur\_Mean} + RTDF\left(T_{Bur\_Mean} - T_{Bur\_In}\right) \tag{4.42}$$

The burner inlet and exit temperatures are obtained from the performance simulations in PYTHIA. The burner exit temperature obtained from the simulation is taken as the mean burner exit temperature in this work. Lower values of RTDF are recommended for uniform temperature profile [189], and it should be less than 20% [199]. RTDF of 0.12 is used in this work.

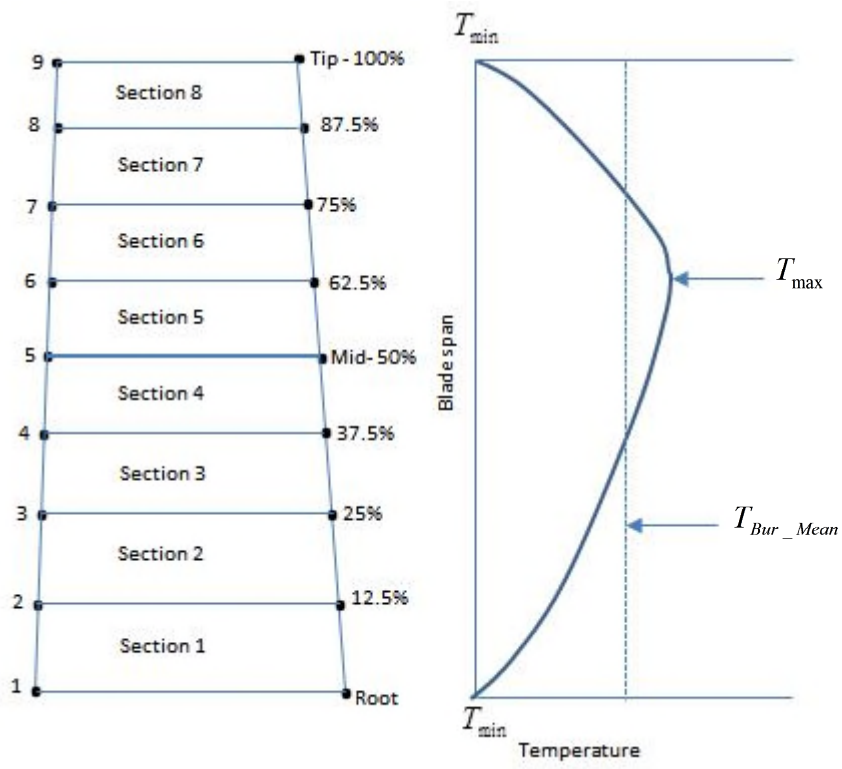

Figure 4.13: Blade Sections and Radial Temperature Distribution

The blade is divided into 8 equal sections and temperatures at the 9 nodes are to be determined (see Figure 4.13). The percentage distance of each section line from the root along the blade span or height is given. At the mean section, indicated as mid, the location is 50% distance along the span from the blade root. It is worthy of note that these nodes can be represented with numbers 1 to 9. The radial temperature distribution and locations of maximum and minimum temperatures are indicated. An arbitrarily line indicating the burner mean exit temperature is also included. In this work, the maximum radial temperature is assumed to be at a distance of 62.5% from the blade root (since peak profile occurs mostly above blade centre [197]), while the minimum temperature is assumed to be at the blade root and blade tip as in Figure 4.13. Also, assuming linear temperature distribution from the maximum temperature to the minimum temperature at the blade root and blade tip respectively, the hot gas temperatures at the 9 nodes are estimated as follows:

$$T_{g,Root} = T_{g,1} = T_{g,Tip} = T_{g,9} = T_{\min} \tag{4.43a}$$

$$T_{g,62.5\%Rt} = T_{g,6} = T_{\max} \tag{4.43b}$$

$$T_{g,12.5\%Rt} = \frac{4T_{\min} + T_{\max}}{5} \tag{4.43c}$$

$$T_{g,25\%Rt} = \frac{3T_{\min} + 2T_{\max}}{5} \tag{4.43d}$$

$$T_{g,37.5\%Rt} = \frac{2T_{\min} + 3T_{\max}}{5} \tag{4.43e}$$

$$T_{g,Mid} = \frac{T_{\min} + 4T_{\max}}{5} \tag{4.43f}$$

$$T_{g,75\%Rt} = \frac{T_{\min} + 2T_{\max}}{3} \tag{4.43g}$$

$$T_{g,87.5\%Rt} = \frac{2T_{\min} + T_{\max}}{3} \tag{4.43h}$$

$T_{g,Root}$ is the gas temperature at the root. This is the same as the temperature at node 1 denoted as $T_{g,1}$. $T_{g,Tip}$ is the temperature at the blade tip which is the same as the temperature at node 9, $T_{g,9}$. Since minimum gas temperatures $T_{\min}$ is assumed to occur at the blade tip and blade root, Equation (4.43a) is obtained. $T_{g,Mid}$ is the gas temperature at the mid-section of the blade. The other notations apply to the gas temperature at the indicated percentage distance from the root of the blade, thus $T_{g,87.5\%Rt}$ stands for the gas temperature at 87.5% distance from the blade root. Since T_{Bur_Mean} represents the mean temperature of all the nodal temperatures, the minimum temperature is obtained as,

$$T_{\min} = \frac{9T_{Bur\_Mean} - 4T_{\max}}{5} \tag{4.43i}$$

Appendix C.2 shows how the hot gas temperatures at the 9 nodes are obtained. In the analysis, temperatures at each blade section will be estimated (sections 1 to 8). To do this, the mean section gas temperature will be used to represent the temperature of the section. This is imperative because an element of distance is employed in the temperature estimation. For each section, the mean section gas temperature is the mean value of the gas temperatures of the two nodes bounding the section, and this is given as,

$$T_{g,Seci} = \frac{T_{g,i} + T_{g,i+1}}{2} \tag{4.44}$$

For section 1,

$$T_{g,Sec1} = \frac{T_{g,1} + T_{g,2}}{2} \tag{4.45}$$

The blade metal temperature at each section, $T_{m,Seci}$ is estimated using Equation (4.12) expressed in terms of the section as,

$$T_{m,Seci} = T_{g,Seci} - \varepsilon_{ff}\left(T_{g,Seci} - T^{c}_{In,i}\right) \tag{4.46}$$

where $T^{c}_{In,i}$ is the coolant inlet temperature at the section. For section 1,

$$T_{m,Sec1} = T_{g,Sec1} - \varepsilon_{ff}\left(T_{g,Sec1} - T^{c}_{In,1}\right) \tag{4.47}$$

For subsequent sections, the coolant exit temperature of the previous sections form the coolant inlet temperature of those sections. For instance, in section 1, $T^{c}_{Ex,1}$, which is the coolant exit temperature from section 1, is the coolant inlet temperature of section 2. This is illustrated in Figure 4.14.

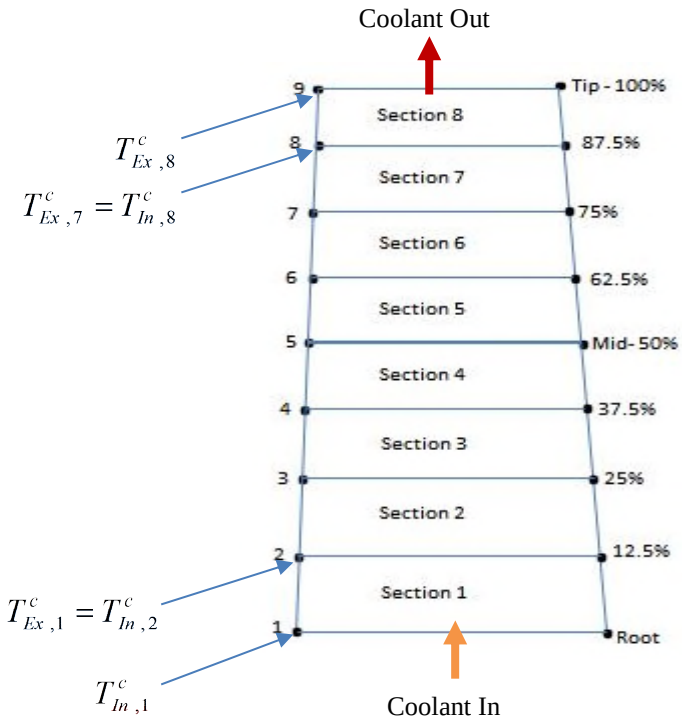

Figure 4.14: Blade Coolant Inlet and Exit Temperatures at Various Sections

The coolant exit temperature at each section, $T^{c}_{Ex,i}$ is obtained by considering overall energy balance at the section, exploiting Equation (4.7) put in the form,

$$h_{g,Seci} P_{Seci} l_{Seci} \left(T_{g,Seci} - T_{m,Seci}\right) = \dot{m}_{c\_B} C_{p\_ca} \left(T^{c}_{Ex,i} - T^{c}_{In,i}\right) \quad (4.48)$$

where $h_{g,Seci}$ is the external heat transfer coefficient for each section, P_{Seci} is the perimeter of the section, l_{Seci} is the height of the section and $\dot{m}_{c\_B}$ is the mass flow rate of air for cooling each blade. From Equation (4.48), the coolant exit temperature at each section is,

$$T^{c}_{Ex,i} = T^{c}_{In,i} + \frac{h_{g,Seci} P_{Seci} l_{Seci} \left(T_{g,Seci} - T_{m,Seci}\right)}{\dot{m}_{c\_B} C_{p\_ca}} \quad (4.49)$$

From Equation (4.9),

$$T_{g,Seci} - T_{m,Seci} = \varepsilon_{ff} \left(T_{g,Seci} - T^{c}_{In,i}\right) \quad (4.50)$$

Therefore, the coolant exit temperature at each section is,

$$T^{c}_{Ex,i} = T^{c}_{In,i} + \frac{h_{g,Seci} P_{Seci} l_{Seci} \times \varepsilon_{ff} \left(T_{g,Seci} - T^{c}_{In,i}\right)}{\dot{m}_{c\_B} C_{p\_ca}} \quad (4.51)$$

For section 1,

$$T^{c}_{Ex,1} = T^{c}_{In,1} + \frac{h_{g,Sec1} P_{Sec1} l_{Sec1} \times \varepsilon_{ff} \left(T_{g,Sec1} - T^{c}_{In,1}\right)}{\dot{m}_{c\_B} C_{p\_ca}} \quad (4.52)$$

The external heat transfer coefficient for each section $h_{g,Seci}$ is obtained as in the Equation (4.35), but this time expressed for each section in the form of Equation (4.53),

$$h_{g,Seci} = \frac{Nu_{g,Seci} \times k_{g,Seci}}{c_{Seci}} \quad (4.53)$$

$Nu_{g,Seci}$, is the Nusselt number of the hot gas for each section, $k_{g,Seci}$ is the thermal conductivity of the hot gas for each section (read from tables based on the average gas temperature of each section), and c_{Seci} is the chord of each blade section (the same for all sections since the blade is divided into 8 equal sections). The Nusselt number is

estimated for each blade section using Equation (4.36), but expressed for each blade section as in Equation (4.54),

$$Nu_{g,Seci} = Nu'_{g,Seci}\left(\frac{\mathrm{Re}_{g,Seci}}{2\times10^{5}}\right)^{x_{Seci}}\left(\frac{T_{g,Seci}}{T_{m,Seci}}\right)^{y_{Seci}} \qquad (4.54)$$

The nominal mean Nusselt number $Nu'_{g,Seci}$ and the exponent y_{Seci} are read from Figure 4.12 for each section. The exponent y_{Seci} is obtained from Equation (4.37) for each section. The Reynolds number for each blade section is estimated using Equation (4.55), similar to Equation (4.38),

$$\mathrm{Re}_{Seci} = \frac{\rho_{g,Seci}\times V_{Abs,Exi}\times c_{Seci}}{\mu_{Seci}} \qquad (4.55)$$

$\rho_{g,Seci}$ is the blade exit gas density in each section, it is as given by Equation (4.40) but expressed for each blade section in this case. $V_{Abs,Exi}$ is the absolute velocity at the exit of the section, μ_{Seci} is the blade exit gas viscosity at the section. The viscosity at the section is as given by Equation (4.39), but here $T \equiv T_{g,Seci}$. Like the temperature of the gases at each section (see Equation 4.44), the parameters used at the sections are taken as the mean parameter of the bounding nodes. Thus given any parameter at a section, λ_{Seci} where λ_{Seci} could stand for density, viscosity, chord, etc.it is evaluated using Equation (4.56),

$$\lambda_{Seci} = \frac{\lambda_i + \lambda_{i+1}}{2} \qquad (4.56)$$

λ_i and λ_{i+1} are the parameter at the two nodes bounding the section. The temperatures at the node will be estimated by taking the average temperature of the blade metal bounding the node. The temperature at the tip of the blade will be taken as the temperature at section 8 of the blade material while the blade material root temperature will be the temperature of the blade material at section 1. At every other node, the temperatures are estimated using Equation (4.57),

$$T_{m,i} = \frac{T_{m,Seci} + T_{m,Sec\,i+1}}{2} \qquad (4.57)$$

$T_{m,i}$ is the temperature of the blade material at node i. The two cases concerning blades without thermal barrier coating and blades with thermal barrier coating are now considered here.

CASE I: Blades without Thermal Barrier Coating

For blades without thermal barrier coating, the blade material sectional temperatures are estimated using Equation (4.47) while the nodal temperatures are obtained using Equation (4.57). These equations are given below for convenience.

- Blade sectional temperatures:

$$T_{m,Seci} = T_{g,Seci} - \varepsilon_{ff}\left(T_{g,Seci} - T^{c}_{In,i}\right) \tag{4.47}$$

- Blade nodal temperatures:

$$T_{m,i} = \frac{T_{m,Seci} + T_{m,Seci+1}}{2} \tag{4.57}$$

Appendix D.3 shows a Sequential Solution-Algorithm Tree of this model.

CASE II: Blades with Thermal Barrier Coating

If the blades have thermal barrier coating, the sectional and nodal metal temperatures are replaced by the temperatures of the thermal barrier coating material in Equations (4.47) and (4.57). These are given by Equations (4.58a) and (4.58b) respectively,

$$T_{tbc,Seci} = T_{g,Seci} - \varepsilon_{ff}\left(T_{g,Seci} - T^{c}_{In,i}\right) \tag{4.58a}$$

$$T_{tbc,i} = \frac{T_{tbc,Seci} + T_{tbc,Seci+1}}{2} \tag{4.58b}$$

$T_{tbc,i}$ is the temperature of the TBC material at each node while $T_{tbc,Seci}$ is the temperature of the TBC material at each section. The temperature of the blade material at each section is as in Equation (4.34), but here it is given in terms of each blade section as in Equation (4.59),

$$T_{m,Seci} = T_{tbc,Seci} - \left(\frac{\delta_{tbc}}{k_{tbc}}\right) \times h_{g,Seci}\left(T_{g,Seci} - T_{tbc,Seci}\right) \tag{4.59}$$

Here, it is assumed that the thickness of the TBC is the same for all the sections. The external heat transfer coefficient for each section is already obtained as given by Equation (4.53). Therefore, every parameter required in determining the blade material temperature at each blade section is known. The blade material temperature at each node is taken as the mean value of the temperature of the sections bounding the node as in Equation (4.56). The gas turbine blades analysed in this research have thermal barrier coatings and are cooled. Hence, the last thermal model developed is applied for the life analysis in this work. Blade material temperature estimated using this model clsely approximates results obtained from FEA models under similar loading in the works of Abu [200], Eshati [92] and other open literatures. A Sequential Solution Algorithm Tree of this model is given in Appendix D.4.

4.3 Blade Stress Model

The blade stress model considers the various stresses the blades encounter and evaluates the maximum stress at different locations along the span of the blade. There are different sources of stresses to turbine blades. These are stresses arising from the centrifugal forces acting at any section along the blade span, stresses from gas bending moments due to velocity and pressure change of the fluid passing across the blade, bending moments stresses due to centrifugal forces from blade leaning, shear loading stresses due to gas pressure or centrifugal twisting of blades, and stresses due to complex loading arising from temperature gradients [201]. In this work, stresses arising from centrifugal forces and bending moments due to pressure and velocity change of the fluid traversing the blades are considered and applied in arriving at the stresses at various sections of the blade. Bending moment due to blade leaning will not come into play when at every section of the blade the centres of gravity lie on a single radial line passing through the root to the tip of the blade, also shear stresses are negligible [201]. The major stresses are due to centrifugal loading, but pressure change and velocity change imposed stresses have to be considered.

In this work, the stress model is developed from [201] while the algorithm borrows a lot from [37]. Like in the blade thermal model, the blade is divided into 8 sections and the maximum stress arriving from the combination of the various stresses are estimated at

three chord-wise locations - the leading edge (LE), trailing edge (TE) and the farthest point at the suction surface of the blade, designated as SB (see Figure 4.6). The determination of stresses at these locations is necessary since these are the most likely sites for maximum stress (compression or tensile) [201]. The stresses to be considered are now reduced to centrifugal stresses, bending moment stresses due to pressure change, and bending moment stresses due to velocity change. The output of the stress model is the maximum stress at the various sections in any of the three chord-wise locations. Figure 4.15 shows the blade stresses to be estimated.

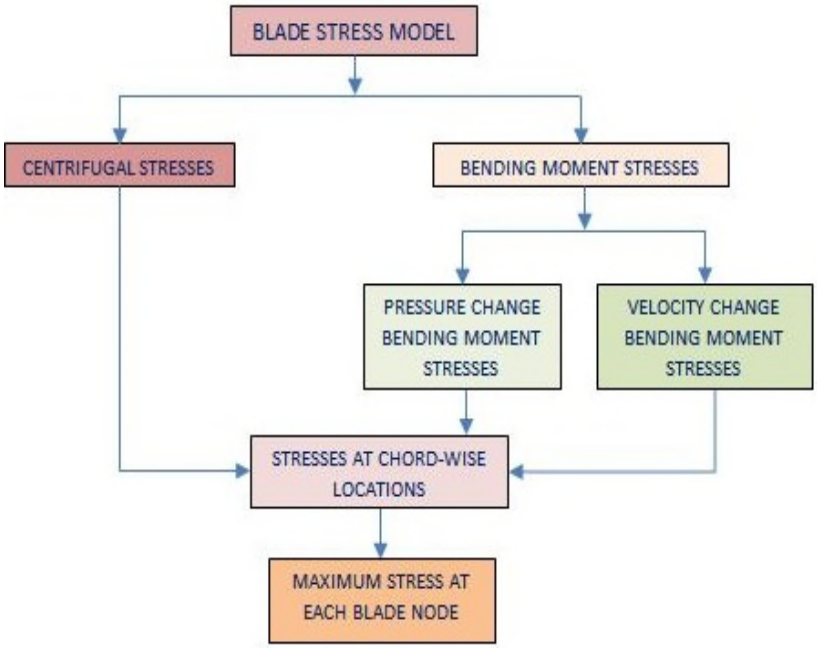

Figure 4.15: Various Stresses Estimated in Blade Stress Model

Before delving into each of these stresses, the sectioning of the blade with more detailed dimensioning is necessary and is given in Figure 4.16. From Figure 4.16, h_{sec} is the height of each blade section, it is the same for all 8 sections. Since the blade is divided into 8 equal sections,

$$h_{\text{sec}} = \frac{B_{ht}}{8} \tag{4.60}$$

where B_{ht} is the mean blade height. R_{brt} is the distance from the blade root to the turbine axis, $h_{CG,1}$ is the distance from the turbine axis to the centre of gravity of section 1. For section i, the respective distance will be denoted as $h_{CG,i}$ and it is given by Equation (4.61),

$$h_{CG,i} = R_{brt} + h_{\sec}\left(i - 0.5\right) \tag{4.61}$$

$h_{n,2}$ is the distance from node 2 to the turbine axis. Node 1 coincides with the blade root and its distance which can be denoted as $h_{n,1}$ is already denoted as R_{brt}. For node i, the respective distance from the turbine axis denoted as $h_{n,i}$ is given by Equation (4.62),

$$h_{n,i} = R_{brt} + i \times h_{\sec} \tag{4.62}$$

The above relations will aid in determining the stresses at the various nodes of the blade.

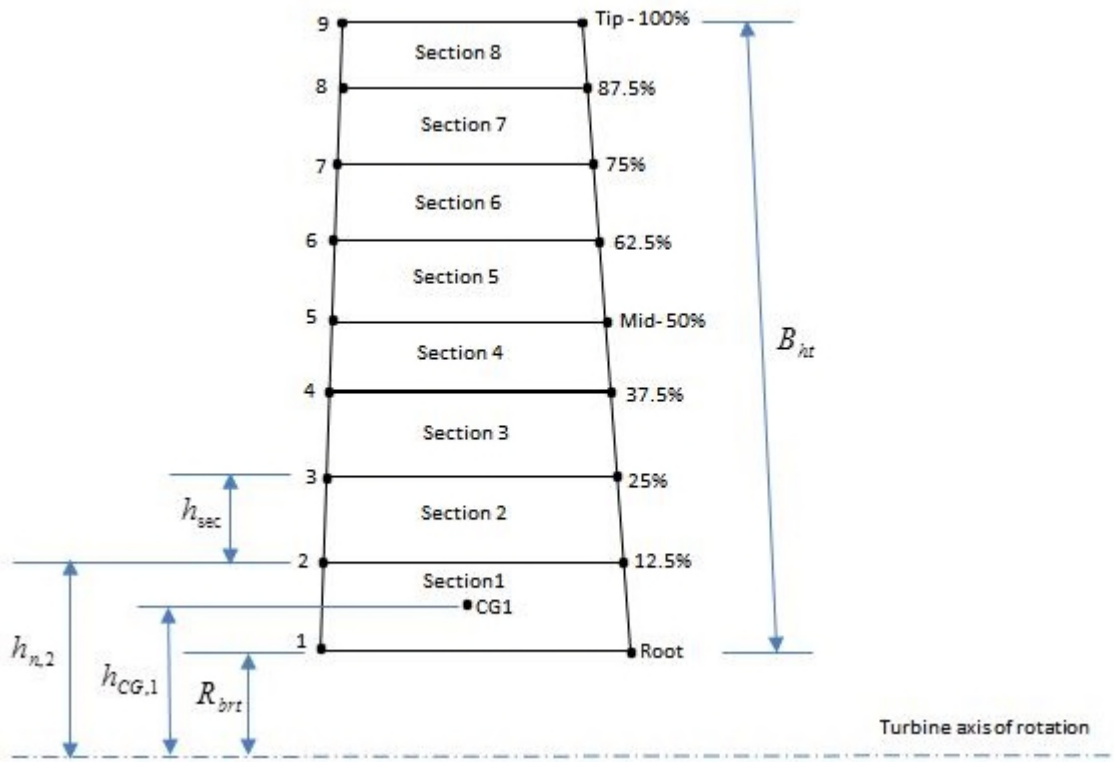

Figure 4.16: Blade Sections and Dimensions

4.3.1 Centrifugal Stresses

The centrifugal stresses arise from the centrifugal loading, and could be obtained from the centrifugal forces. These centrifugal forces will be estimated at each blade section. The centrifugal forces will be highest at the blade root. Assuming the centrifugal force at each blade section acts at the centre of gravity of the section, the centrifugal force, $F_{\sec i}$ will be,

$$F_{\sec i} = m_{\sec i} \times \omega^2 \times h_{CG,i} \tag{4.63}$$

where $m_{\sec i}$ is the mass of the section, ω is the angular speed of the compressor shaft, (in rad/s) and it is given as,

$$\omega = \frac{2\pi N}{60} \tag{4.64}$$

N is the rotational speed of the compressor shaft (in rpm). In this work, the rotational speed obtained from the performance simulations in PYTHIA is given as a relative value, thus N is given by Equation (4.65),

$$N = PCN \times N_d \tag{4.65}$$

PCN is the compressor relative rotational speed, and N_d is the design speed of the engine model created. The blades are not tapered and have almost uniform cross-sectional area along the blade span, thus assuming the cross-sectional areas A_{cs} at each section of the blade are the same, the mass of each blade section will be the same and will be given as,

$$m_{\sec i} = m_{\sec} = \rho \times A_{cs} \times h_{\sec} \tag{4.66}$$

where ρ is the density of the blade material. The centrifugal force at the centre of gravity of each blade section will now be given in the form,

$$F_{\sec i} = m_{\sec} \times \omega^2 \times h_{CG,i} = \kappa h_{CG,i} \tag{4.67}$$

where $\kappa = m_{\sec} \times \omega^2$ is a constant. The centrifugal force at the nodes of each blade section will be determined. Since the blade is shroud-less, the centrifugal force at the blade tip will be zero. The centrifugal force at the root of the blade (node 1) will be the sum of the centrifugal forces at the centres of gravity of each of the 8 blade sections. This is given as,

$$F_{Root} = F_1 = \sum_{i=1}^{i=8} F_{\sec i} \tag{4.68}$$

At node i, the centrifugal force F_i will be,

$$F_i = \sum_{i=i}^{i=8} F_{\sec i} \tag{4.69}$$

Thus, for shroud-less blades, $F_9 = 0$. The centrifugal stress at each node $\sigma_{CF,i}$ is given by Equation (4.70),

$$\sigma_{CF,i} = \frac{F_i}{A_{cs}} \tag{4.70}$$

4.3.2 Bending Moment Stresses

The bending moment stresses are due to pressure change and velocity change of the gases as they transverse the blade section. Thus, they are to be dealt with separately. The pressure change is in the axial direction while velocity change at each section of the blade will be resolved in the axial and the tangential directions, and the resultant velocity change force will be obtained. This resultant velocity change force when assumed to act at the centre of gravity of the blade section will produce a bending moment. Similarly, the pressure change when multiplied by the annulus area of a section will produce the pressure change force, and if this force is assumed to act at the centre of gravity of the section, it will produce a bending moment about any section of the blade. Thus, the bending moments due to pressure change and velocity change are determined first and the stresses they produce in any section are estimated using Equation (4.71),

$$\sigma_b = \frac{M \times y}{I} \tag{4.71}$$

where M is the bending moment about the neutral axis, I is the second moment of area about the neutral axis, y is the perpendicular distance from the point of the stress to the neutral axis, while σ_b is the bending stress to be evaluated. The sum of the bending moments due to pressure change and velocity respectively are resolved about the blade axis before applying in Equation (4.71).

4.3.2.1 Pressure Change Bending Moments

The change in pressure as the gases pass through the blade is estimated by determining the pressure at the inlet and the exit of the blade section. The change in the static pressure Δp is the same at each section of the blade and it is given as,

$$\Delta p = p_{in} - p_{ex} \tag{4.72}$$

where p_{in} is the static pressure at the inlet of each blade stage and p_{ex} is the static pressure at the exit of each blade stage. These parameters are obtained from their respective stagnation parameters represented with capital letters, P_{in} and P_{ex} respectively. The axial velocities at the inlet and the exit of each stage of the turbine are required in calculating these pressures. Details are given in the Appendix.

Taking the force to act at the centre of gravity of each blade section, the force on each section of the blade, $F_{P,\sec i}$ depends on the size of the annulus area of the section and it is given by Equation (4.73),

$$F_{P,\sec i} = \frac{\Delta p \times A_{n,\sec i}}{N_b} \tag{4.73}$$

$A_{n,\sec i}$ is the annulus area of the blade section. For section 1, the annulus area will be,

$$A_{n,\sec 1} = \pi\left(h_{n,2}{}^2 - R_{brt}{}^2\right) \tag{4.74}$$

For subsequent sections,

$$A_{n,\sec i} = \pi\left(h_{n,i+1}{}^2 - h_{n,i}{}^2\right) \tag{4.75}$$

where $1 < i \leq 8$. Since the force acts at the centre of gravity of each blade section, and the centre of gravity of each blade section is located at the centre of the section along the blade span, the moment of the pressure force about the base of the section will be,

$$M_{P,i} = F_{P,\sec i} \times \frac{h\sec}{2} \tag{4.76}$$

where $M_{P,i}$ is the pressure bending moment about the base of section i. The sum of the bending moments about each node could be accumulated. At the blade root, the pressure

change bending moment will be the sum of the bending moments at the base of all the 8 sections. Thus, at section i, the sum of the pressure bending moments about its base is,

$$BM_{P,i} = \sum_{i=i}^{i=8} M_{P,i} \tag{4.77}$$

where $BM_{P,i}$ is the sum of the pressure change bending moments about the base of section i of the blade. Details of the various parameters and the thermodynamic relations that will aid in the determination of properties used in the pressure change bending moments are given in Appendix C.3.

4.3.2.2 Velocity Change Bending Moments

The velocity change as the gases traverse the blades creates forces due to change in momentum. The forces could be estimated in both the axial and tangential directions at each blade section by considering the specific mass flow of the gases as given by Equation (4.78),

$$\dot{m}_{sp} = \frac{\dot{m}_{t\_in}}{A_n} \tag{4.78}$$

A_n is the total annulus flow area of the gases and it is given by Equation (4.79),

$$A_n = \pi\left(R_{btp}{}^2 - R_{brt}{}^2\right) \tag{4.79}$$

R_{btp} and R_{brt} are the mean blade tip radius and the mean blade root radius respectively. Thus, with ΔV_{Ax} as the axial velocity difference for the first turbine stage (the same for all sections of the blade), the axial velocity change force $F^{V}_{Ax,\sec i}$ for each section of the blade is as given by Equation (4.80),

$$F^{V}_{Ax,\sec i} = \frac{\dot{m}_{sp} \times A_{n,\sec i} \times \Delta V_{Ax}}{N_b} \tag{4.80}$$

The tangential velocity change for each section of the blade is different and is denoted as $\Delta V_{T,\sec i}$. For a given blade section, the tangential velocity change is evaluated at the two nodes bounding the section and the mean value is used to represent the tangential velocity change for the section. The tangential velocity change force for each section is given by Equation (4.81),

$$F_{T,\sec i}^{V} = \frac{\dot{m}_{sp} \times A_{n,\sec i} \times \Delta V_{T,\sec i}}{N_b} \tag{4.81}$$

where $F_{T,\sec i}^{V}$ is the tangential velocity change force at section i of the blade. The velocity change bending moment of section i of the blade about its base, taking the velocity change force to be acting at its centre of gravity is similar to Equation (4.76) and is given for the axial and tangential directions in Equations (4.82) and (4.83) respectively:

$$M_{Ax,i}^{V} = F_{Ax,\sec i}^{V} \times \frac{h\sec}{2} \tag{4.82}$$

$$M_{T,i}^{V} = F_{T,\sec i}^{V} \times \frac{h\sec}{2} \tag{4.83}$$

$M_{Ax,i}^{V}$ is the bending moment of the velocity change force about the base of section i of the blade about the turbine axial axis while $M_{T,i}^{V}$ is its tangential counterpart. The sum of the moments about the base of blade section i for the axial and tangential directions are given by Equations (4.84) and (4.85) respectively:

$$BM_{Ax,i}^{V} = \sum_{i=i}^{i=8} M_{Ax,i}^{V} \tag{4.84}$$

$$BM_{T,i}^{V} = \sum_{i=i}^{i=8} M_{T,i}^{V} \tag{4.85}$$

$BM_{Ax,i}^{V}$ and $BM_{T,i}^{V}$ are the sums of the bending moments in the axial and tangential axis of the turbine respectively. Steps at obtaining the axial velocities and the tangential velocities at blade inlet and exit at different sections of the blade are presented in Appendix C.3. The tangential velocity here is the tangential component of the absolute velocity of the flow, referred to as whirl velocity in Appendix C.3.

4.3.2.3 Bending Moments in Blade Direction

The axes (axial and tangential) of the aerofoil (of the blade) do not coincide with the axial and tangential axes of the machine. The axial and tangential moments arising from the pressure and velocity changes have to be resolved to the blade axial and tangential

directions (see Figure 4.17). In Figure 4.17, BM_A and BM_T are the axial and tangential bending moments on the turbine (machine) axial and tangential directions respectively. The corresponding bending moments on the blade axial and tangential directions are indicated respectively as BM_{XX} and BM_{YY}. $I_{XX} = I_{MIN}$ is the second moment of area about the blade axial direction, while $I_{YY} = I_{MAX}$ is the second moment of area about the blade tangential axis. θ is the blade stagger angle which may vary from the blade tip to the root, and hence from section to section of the blade.

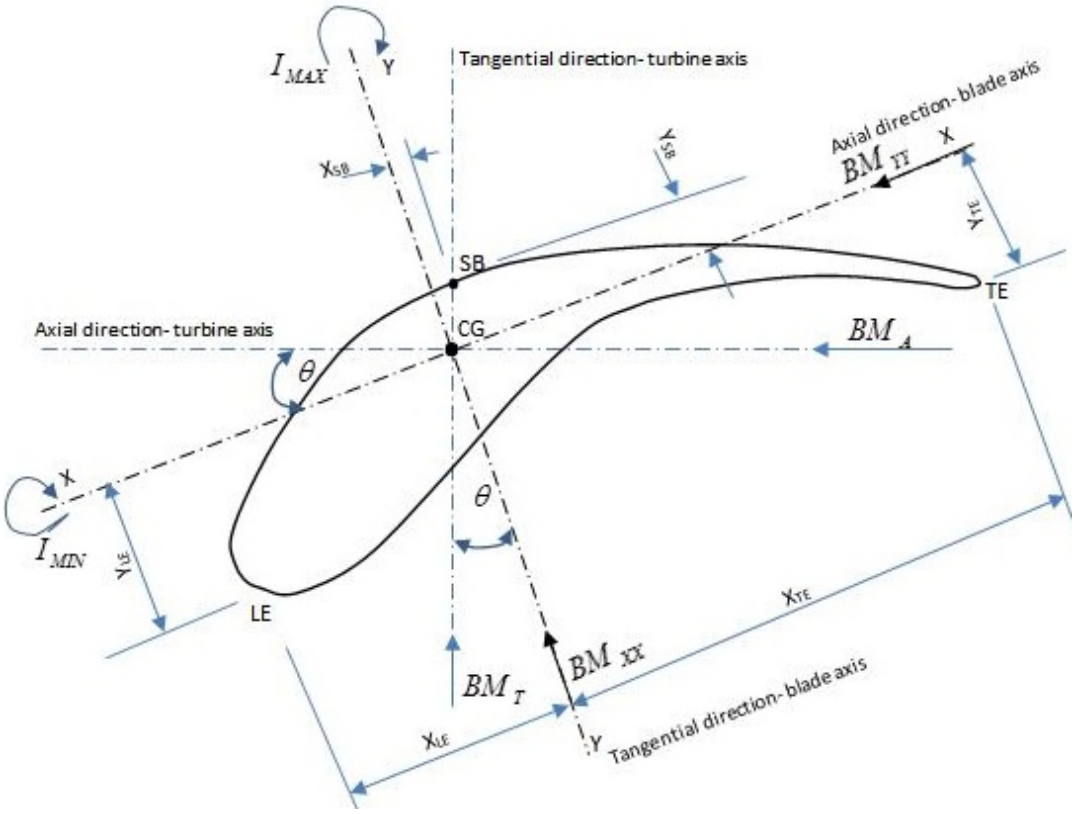

Figure 4.17: Bending Moments Relative to Machine and Blade Directions

For each section of the blade, the bending moments about the base of the section in the blade axial direction and tangential direction are as given by Equations (4.86) and (4.87), where θ_i is the blade stagger angle at the base of the section,

$$BM_{XX,i} = \left(BM_{P,i} + BM^{V}_{Ax,i}\right)\sin\theta_i + BM^{V}_{T,i}\cos\theta_i \qquad (4.86)$$

$$BM_{YY,i} = \left(BM_{P,i} + BM^{V}_{Ax,i}\right)\cos\theta_i - BM^{V}_{T,i}\cos\theta_i \qquad (4.87)$$

$BM_{XX,i}$ is the bending moment in the blade axial direction at the base of each section of the blade, $BM_{YY,i}$ is the corresponding moment in the blade tangential direction.

4.3.2.4 Bending Moment Stresses

The stresses due to bending moments resolved in the blade direction are computed at the blade leading edge (LE), trailing edge (TE) and farthest point at the suction surface of the blade (SB). In Figure 4.17, X_{LE} and X_{TE} are the distances from the centre of gravity (CG) of the blade to the blade LE and TE respectively in the blade axial direction, Y_{LE} and Y_{TE} are the corresponding distances in the tangential direction of the blade. X_{SB} and Y_{SB} are the distances from the CG to the farthest point at the suction surface of the blade in the axial and tangential directions respectively. These distances may vary from section to section along the span of the blade. At the base of any section, the stress in each of the three locations (LE, TE and SB) can be expressed with a general formula given by Equation (4.88),

$$\sigma_{G,i}^{BM} = \frac{BM_{XX,i} \times Y_{G,i}}{I_{MIN,i}} + \frac{BM_{YY,i} \times X_{G,i}}{I_{MAX,i}} \tag{4.88}$$

In Equation (4.88), $\sigma_{G,i}^{BM}$ is the bending moment stress, $G = LE$ at the leading edge, $G = TE$ at the trailing edge and $G = SB$ at the farthest point in the blade suction surface.

4.3.3 Total and Maximum Blade Stresses

The total stress at the base of each section of the blade in the three locations (LE, TE and SB) is the sum of the centrifugal stress and the bending moment stress. This is expressed as,

$$\sigma_{G,i}^{Tot} = \sigma_{CF,i} + \sigma_{G,i}^{BM} \tag{4.89}$$

where $\sigma_{G,i}^{Tot}$ is the total stress at each of the three locations at the base of each section of the blade. The maximum stress at the base of each section of the blades is used for the life analysis of the blades. It is the maximum value of the three stresses at the base of each section. Thus employing C-Sharp programming syntax, the maximum stress $\sigma_{Max,i}$ could be expressed as in Equation (4.90),

$$\sigma_{Max,i} = \left(\sigma_{G,i}^{Tot}\right).\max \tag{4.90}$$

The distribution of stresses along the blade chord is similar to what is obtained from finite element model presented in the work of Eshati [92] under similar loading; although, the blade life is calculated at various nodes of the blade and the least value is taken to represent the blade life in this work. A sequential Solution-Algorithm Tree of the blade stress model is provided in Appendix D.5.

4.4 Chapter Conclusions

The engine life analysis sub-models are considered in this chapter. Three models are developed to enable the engine life calculation feasible. The first is a computer module which collects the field data, pre-processes it and sends the processed data to PYTHIA for off-design performance calculations. Gas path properties are generated in the process and the results are compared with those of the field data where data from the field are available, such as compressor exit temperature and pressure. Some of the results obtained are sent to the two other models- blade thermal model and blade stress model as inputs. Four thermal models are developed- uniform temperature model with and without thermal barrier coatings, and one-dimensional temperature model with and without thermal barrier coatings. The one-dimensional temperature model with thermal barrier coatings is used later for life calculations in this work as it fits into the nature of the blades in the engine considered in this research. The thermal model estimates the temperature of the blade material at 9 different nodes of the blade, as the blade is divided into 8 equal sections. Radial temperature distribution is applied together with convective cooling in developing the thermal model. The stress model estimates the maximum stress at three chord-wise sites (leading edge, trailing edge, and furthest point at the back of the blade) in each of the 9 nodal points of the blade. The stress model considers centrifugal stress and bending moment change stresses arising from pressure change bending moments and velocity change bending moments. Other sources of stresses are minor and thus not considered in the model. The maximum stress at any of the chord-wise locations in each blade node is obtained in the blade stress model and this value is used for the life analysis.

5 ENGINE PERFORMANCE MODEL CREATION AND MODEL ADAPTATION

An engine performance model of the real engine is created in PYTHIA and adapted to the conditions of the real engine so as to make engine life calculation feasible and to ensure accurate estimation of engine performance parameters at any operating condition. This is necessary because the lifing models and sub-models created and integrated to PYTHIA make use of the some of the gas path properties, (especially temperatures and pressures at the inlet and exit of the high pressure turbine) from the performance model. The creation and adaptation of the LM2500+ engine model is considered here. The engine performance model is also validated here. Also, the algorithm for off-design performance calculation using components matching technique applicable to the LM2500+ engine model is presented.

5.1 Creation of LM2500+ Engine Model in PYTHIA

The creation of engine model in PYTHIA involves the assemblage of component icons. A pre-requisite for setting up accurate engine model is proper configuration of the components showing how the various components are related in graphical form. Figure 5.1 shows the configuration of the LM2500+ engine model.

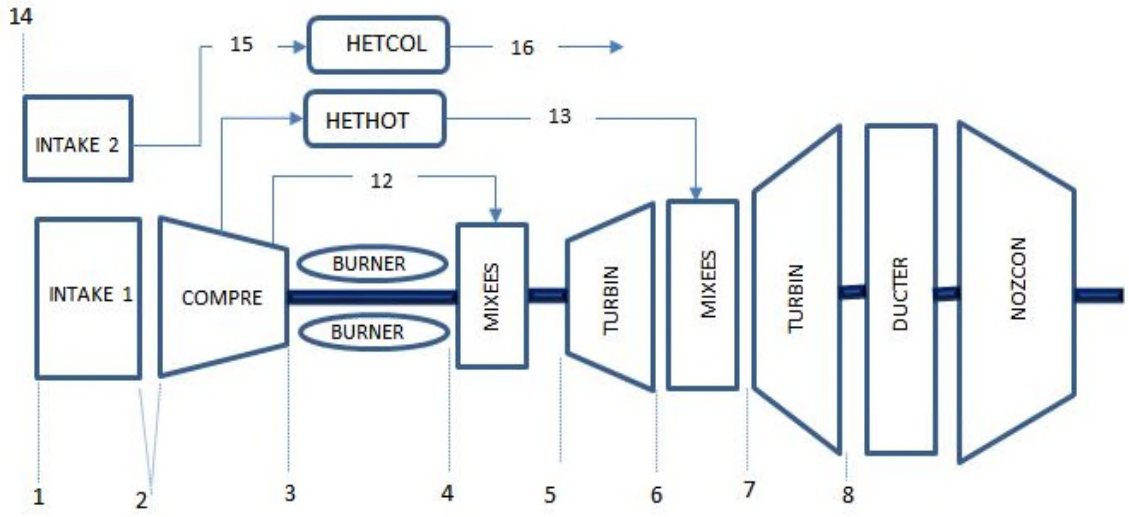

Figure 5.1: Engine Performance Model Configuration

The engine performance model in PYTHIA is shown in Figure 5.2 and the components are identified in Figure 5.3.

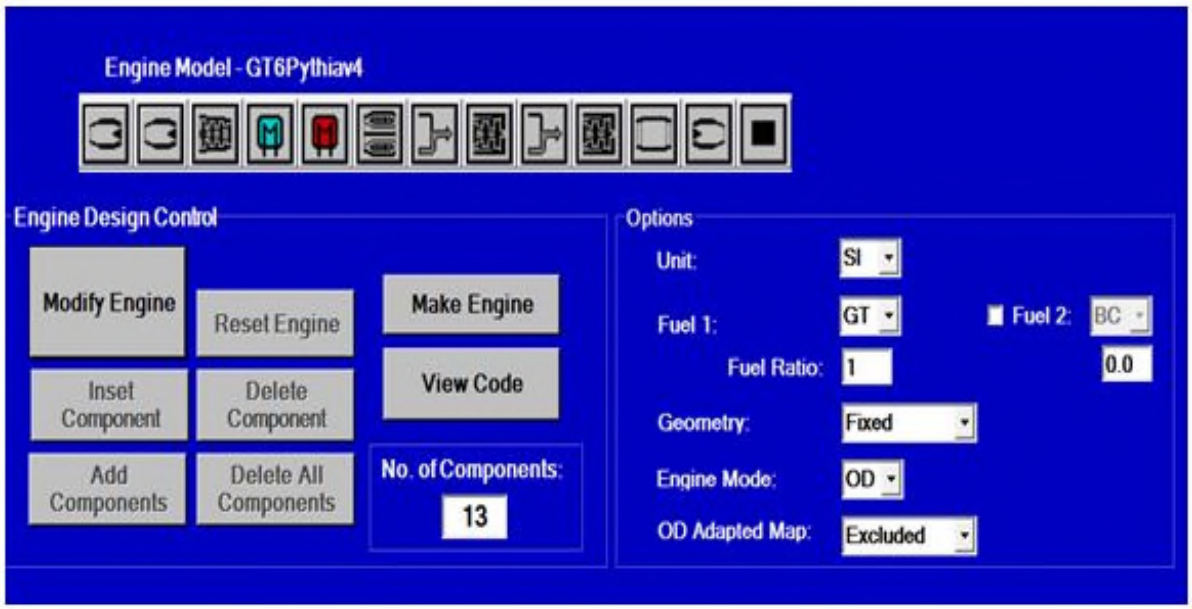

Figure 5.2: LM2500+ Engine Performance Model in PYTHIA

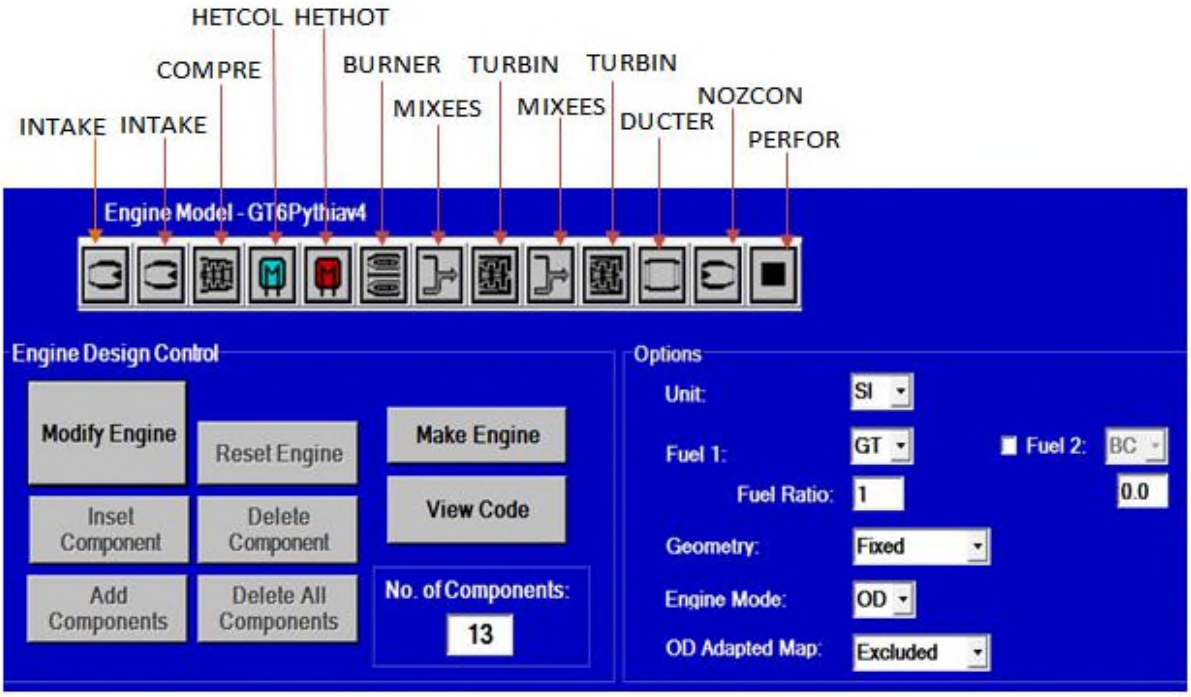

Figure 5.3: Identification of Engine Model icons in PYTHIA

The next stage of the engine model creation is to click on each icon and fill in the initial component performance parameters. For the INTAKE icon for instance, ISA T Deviation and ISA P Deviation, which are the deviations of the ambient temperature and pressure respectively from ISA conditions should be provided, together with other relevant parameters. In providing the initial component parameters, the engine operation data from the field is relied on. The initial component parameters for the INTAKE brick are shown in Figure 5.5.

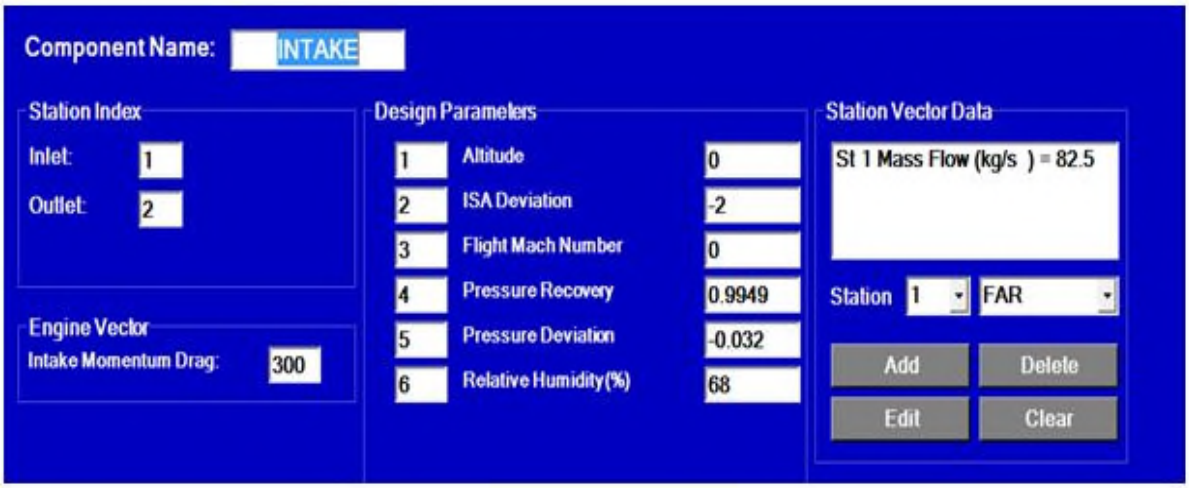

Figure 5.4: Parameters for Setting up INTAKE Brick in PYTHIA

All the required data are provided for each brick or icon, and the engine performance model is fully set up. The next step is to adapt the engine performance model to the real engine operation conditions.

5.2 Design Point Adaptation of the LM2500+ Engine Model

The created engine model is adapted to both the design-point and off-design point conditions. Here, only results of the design point adaptation are presented. As pointed out in Chapter 3, to do design-point adaptation on the engine model, to-be- adapted component parameters as well as target performance parameters are selected; these parameters for the LM2500+ engine model design popint adaptation are as shown in Tables 5.1 and 5.2 respectively.

Table 5.1: To-be-Adapted Component Parameters

No.	Parameter	Symbol	Unit
1	Mass flow at compressor inlet	$\dot{m}_a$	kg/s
2	Compressor pressure ratio	PR	–
3	Compressor isentropic efficiency	η_{ci}	–
4	Compressor turbine isentropic efficiency	η_{CTi}	–
5	Power turbine isentropic efficiency	η_{PTi}	–
6	Burner exit temperature	T_4	K

Table 5.2:Target Performance Parameters

No.	Parameter	Symbol	Unit
1	Compressor exit temperature	T_3	K
2	Compressor exit total pressure	P_3	atm
3	Compressor turbine exit temperature	T_6	K
4	Compressor turbine exit total pressure	P_6	atm
5	Power turbine exit temperature	T_8	K

In addition to the above parameters, condition parameters are defined for design point performance adaptation in PYTHIA. The condition parameters selected for this analysis are:

- Deviation of ambient temperature
- Deviation of ambient pressure, and
- Power turbine auxiliary work.

The to-be-adapted performance parameters are selected at a steady operating condition of the real engine. The selected point, which may be viewed as the design point, may not the actual design point provided by the original engine manufacturer (OEM). In fact, because of the constant changes in the environmental conditions from season to season, it is pertinent the engine model is adapted to the prevailing operating conditions before any further work is done, such as gas path analysis, diagnostics or life analysis.

Data Selection

To aid the selection of stable operating condition, data acquisition and pre-processing software was developed. A new data acquisition and pre-processing software similar to the existing one but with more capabilities was developed in the course of doing this work. More functions were added by MSc students who did adaptation and diagnostic works on the same engine. In this adaptation process, the selected data is in May 2014. The data selection process is shown in Figures 5.5 and 5.6 for the newly developed platform and the old platform respectively.

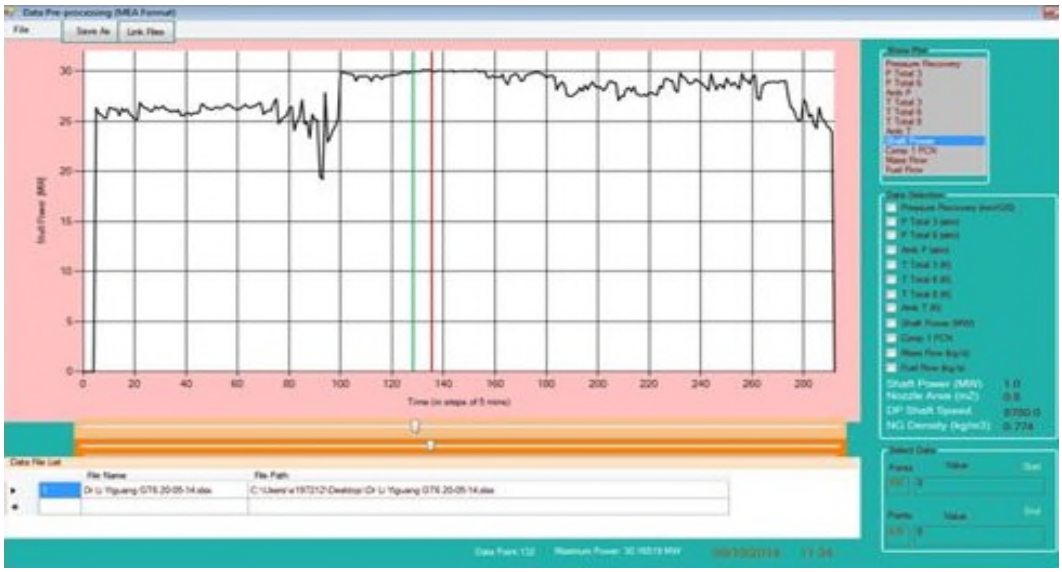

Figure 5.5: Data selection Window- New Platform

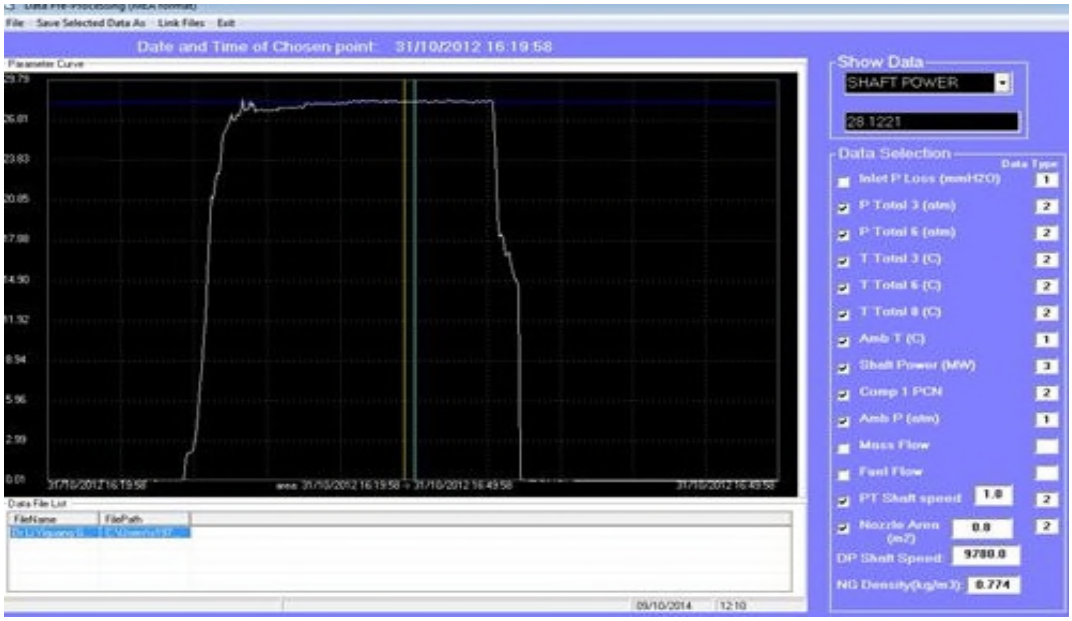

Figure 5.6: Data selection Window- Old Platform

One of the advantages of the new platform is that it could obtain the mean value of any range of selected data. This is more representative of all the values in any stable condition than choosing a single point as in the case of the old platform. The criteria for data selection can be easily identified. These are selecting data in an interval in which the power is in a steady state, and selecting data close to the nominal value in the engine, in this case 30MW [202]. In this work, the selected power was 30.1045MW in May 20 2014. Further capabilities of the data acquisition and pre-processing system and how data is selected for diagnostic analysis or adaptation processes are well explained in the works of Aziaka [203] and Buggins[204].

Set up of Adaptation Process in PYTHIA and Adaptation Results

The adaptation process is set up in PYTHIA by selecting the to-be-adapted component parameters and the target performance parameters from the appropriate windows as shown in Figure 5.7. Values of the target performance parameters and the condition parameters are provided. Once the set-up is completed, linear and non-linear design point performance adaptation can be done by pressing the respective menus under the Run main menu (See Figure 5.8). The non-linear adaptation results were adopted in this work.

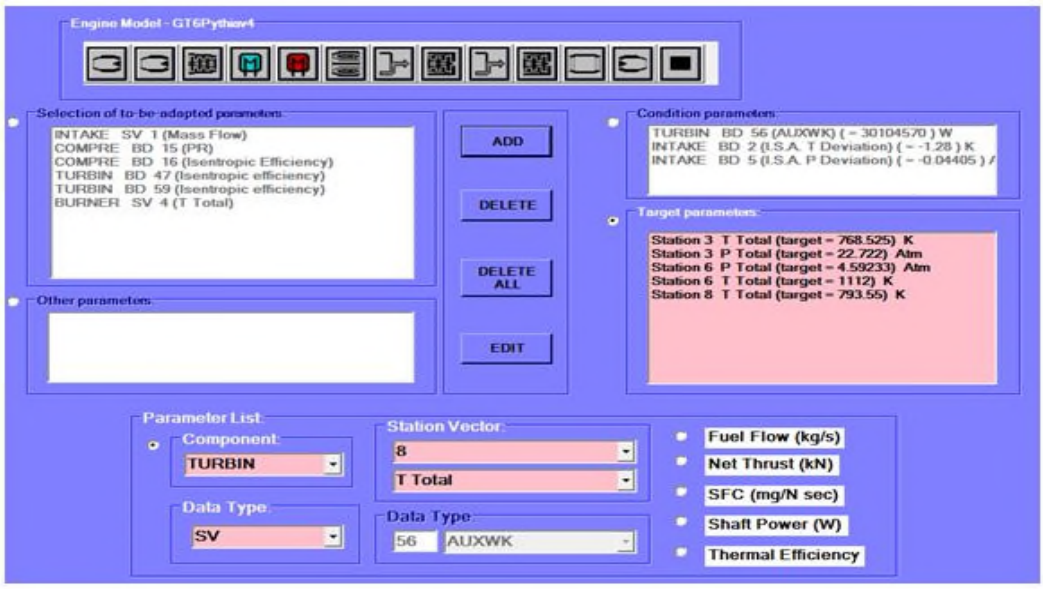

Figure 5.7: Adaptation Setting in PYTHIA

In carrying out design point adaptation, the process may be repeated several times. After each adaptation phase, the predicted parameters may be far from target parameters, meaning large RMS value. The initial parameters in the engine model have to be updated with the adapted parameters and the process is repeated. When the RMS value is less than 0.001, the adaptation process may be stopped and the engine model should be finally updated with the adapted parameters. In this work, RMS value of 6.55×10^{-4} was obtained as shown in the adaptation results in Figure 5.8.

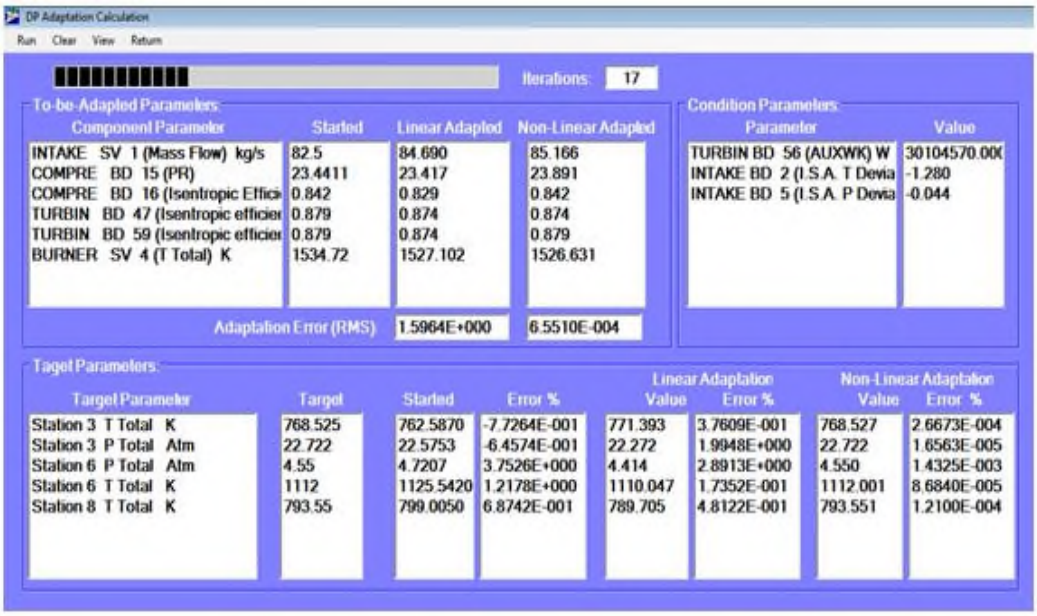

Figure 5.8: Design-Point Performance Adaptation Results

In this research, the engine model was adapted to both design and off-design conditions using the capabilities provided by PYTHIA.

5.3 Validation of Engine Performance Model

The adapted model ought to predict engine gas path parameters and performance parameters that are very close to those of the real engine at different operating conditions; especially shaft power levels and ambient conditions. The engine performance model is validated by running the model at different off-design conditions and comparing relevant simulated results from the engine model with those from the field. Power is used as the handle in the engine model and every gas path properties responds to power changes. The compressor exit temperature, T_3, and the power turbine

exit temperature T_8 for 288 data points for field data and simulated data from the engine model are compared in Figures 5.9 and 5.10 respectively.

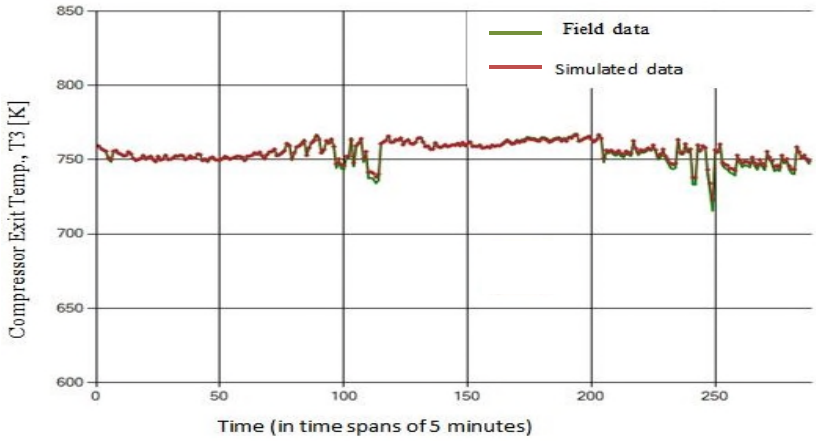

Figure 5.9: Comparison of Field Data and Simulated Data - Compressor Exit Temperature

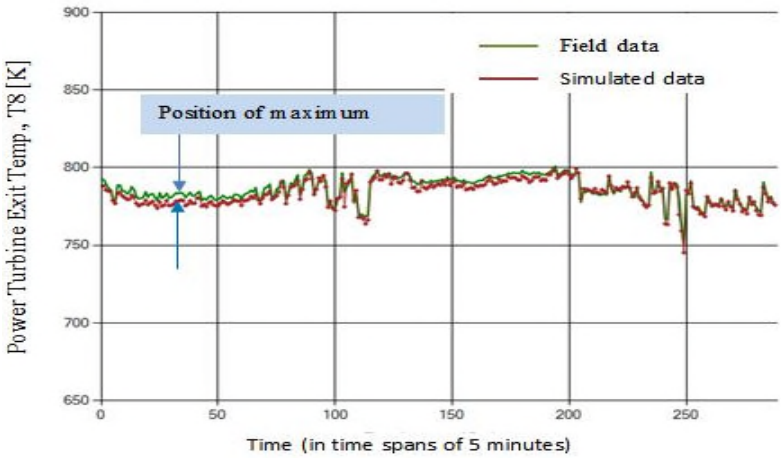

Figure 5.10: Comparison of Field Data and Simulated Data - Power Turbine Exit Temperature

The generation and comparison of relevant data is made possible by the author's newly developed life analysis model incorporated to PYTHIA which can collect data from the field in excel sheet as input directly. The developed platform admits 24 hours data, and using shaft power and ambient temperature deviation as off-design conditions, other gas path properties are calculated using the capabilities of PYTHIA. Data is collected in every 5 minutes from the real engine and saved in excel, this amounts to 288 data values in every 24 hours. In each of the graphs, the green line stands for field data while the brown line represents simulated data. For the above comparisons, the maximum

deviation between the field data and the simulated data occurs in the power turbine exit temperature as indicated on the graph and the value expressed in percentage is less than 0.02%. The code is able to predict these deviations at each point. In some days, the percentage deviation is very minimal as in Figure 5.11.

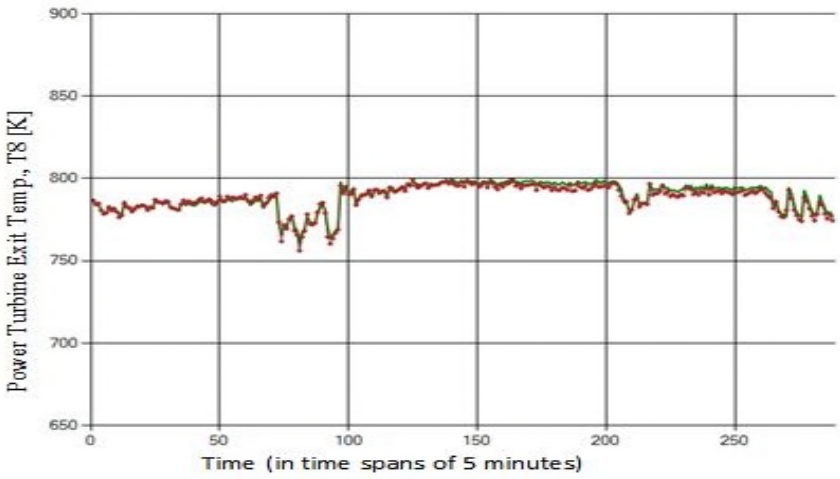

Figure 5.11: Close Matching of Field Data and Simulated Data

Another thing to look at is how other parameters respond to power variations. Figure 5.12 shows the shaft power output from the field while Figures 5.13 and 5.14 shows respectively the response of field data and simulated data to power changes.

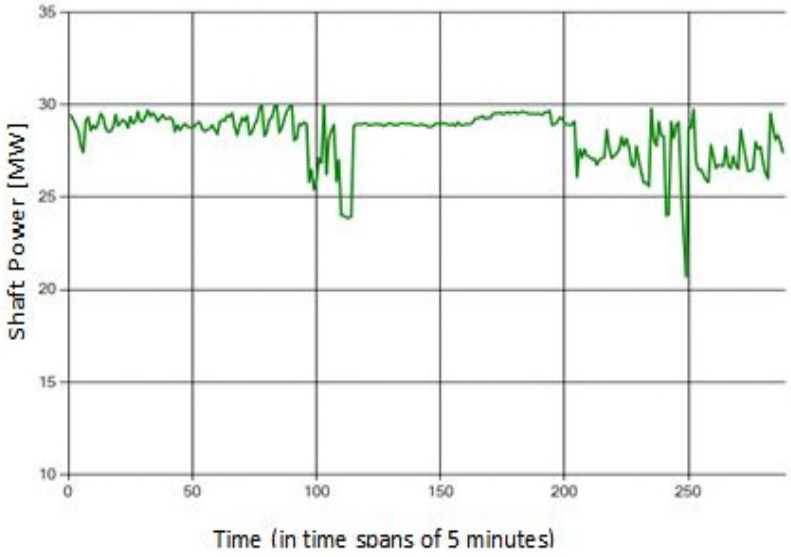

Figure 5.12: Shaft Power Variation of Engine over 24 hours

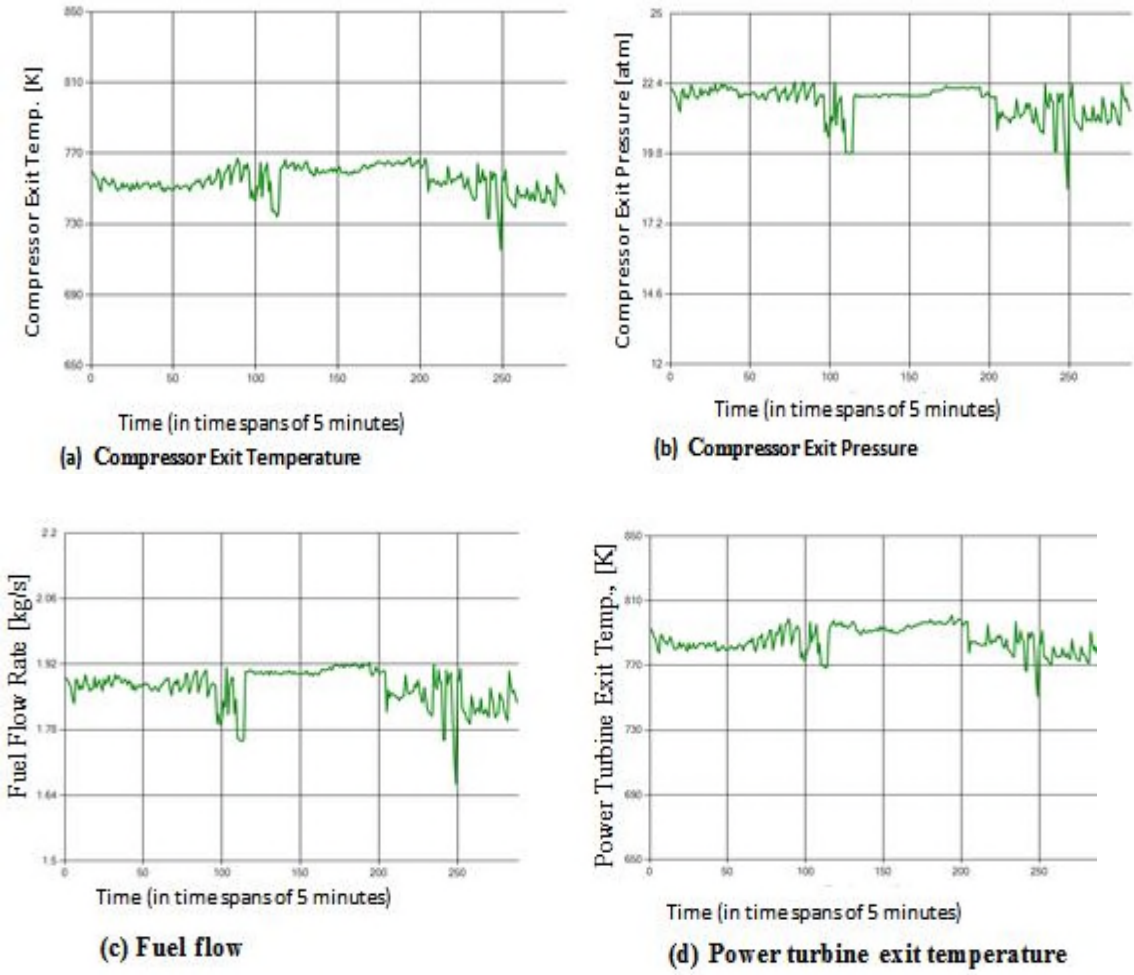

Figure 5.13: Response of some Field Data to Shaft Power Variation

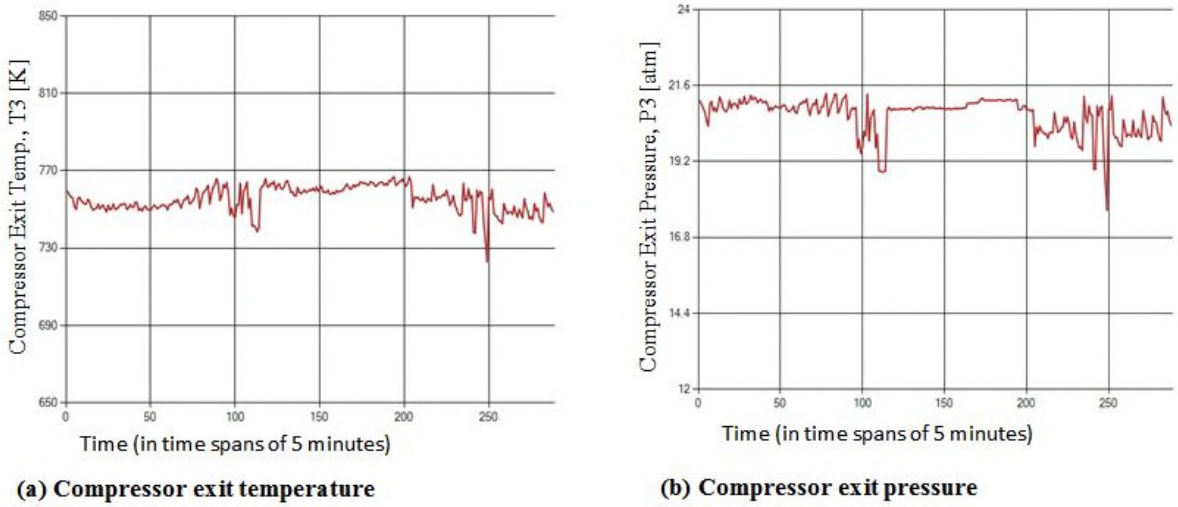

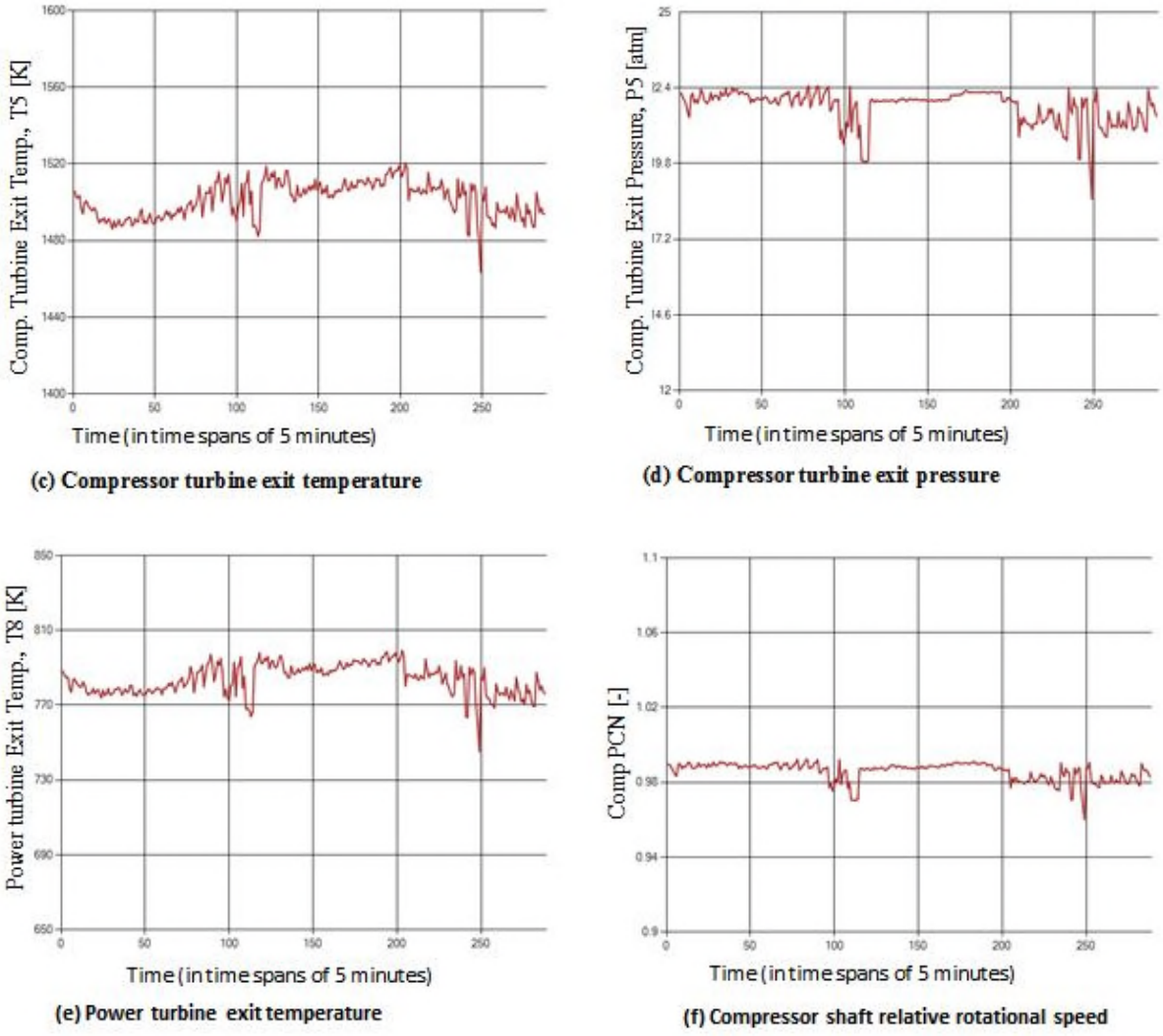

Figure 5.14: Response of Some Simulated Data to Shaft Power Variation

In Figure 5.13, all the four parameters vary in the same pattern as the power, showing that shaft power influences all gas path properties. Power is thus used as the handle in the engine model created in PYTHIA. The simulated results also respond in line with power variation as shown in Figure 5.14. Having tuned the engine performance model to the real engine condition, and all gas path properties from the simulations closely matching the real engine properties, and also varying proportionately with power changes, the output from the engine model could be trusted for further analysis such as life analysis as in this case.

5.4 Off-Design Performance Calculation of LM2500+ Type Engine

The components matching technique of off-design performance calculation could be applied to various engines. The application of this technique to an engine with gas generator and a free power turbine (similar to the engine used in this research) is presented below. A schematic diagram of the gas turbine unit is shown in Figure 5.15, where the gas generator is placed inside dotted rectangle. The compressor turbine drives the compressor, thus, the work output of the compressor turbine should be equal to the work absorbed by the compressor.

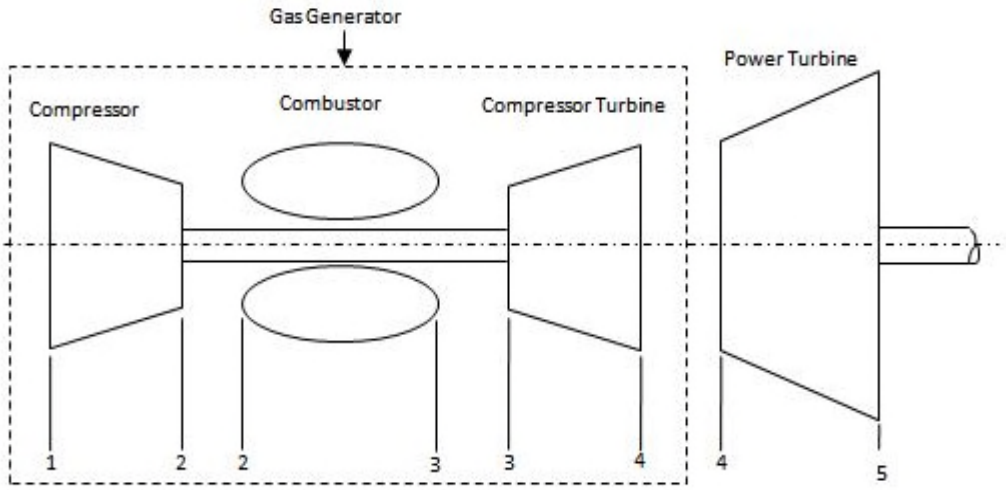

Figure 5.15:Gas Turbine Unit- Gas Generator with a Free Power Turbine

In carrying out off-design performance calculation using the matching technique, some basic assumptions have to be made. Some of these assumptions are given here.

- The mass flow rate at station 1, $\dot{m}_1$ is assumed to be the same as the mass flow rates at stations 3, 4 and 5 assuming fuel flow compensates the bleed air for cooling. Thus, $\dot{m}_1 = \dot{m}_3 = \dot{m}_4 = \dot{m}_5 = \dot{m}$
- The value of the pressure loss in the combustion process ΔP_{cc} is taken as a percentage of the compressor delivery pressure P_2 (stagnation values are used), and it is assumed.
- Ram effect in the intake process is negligible, also exhaust losses are negligible, thus, $P_a = P_1 = P_5$, also, $T_1 = T_a$; P_a and T_a are the ambient pressure and ambient temperature respectively.

Shaft speed is taken as the engine handle. The basic steps in the matching process are highlighted below.

STEP 1: IN THE COMPRESSOR

Assumptions: $P_1 = P_a$; $T_1 = T_a$

(i) Select compressor rational speed N, calculate $N/\sqrt{T_1}$

(ii) Guess pressure ratio, P_2/P_1 ($\equiv P_{out}/P_{in}$ in Figure 3.10(a))

(iii) From compressor map (Figure 3.10(a)), read the value of the non-dimensional mass flow, $\dot{m}\sqrt{T_1}/P_1$

(iv) From Figure 5.16(b), read the value of the compressor efficiency, η_c

(v) Calculate the compressor temperature rise; $\Delta T_{12} = \frac{T_1}{\eta_c}\left[\left(\frac{P_2}{P_1}\right)^{\frac{\gamma-1}{\gamma}} - 1\right]$, γ is the ratio of the specific heat capacities of the compressed air

(vi) Calculate the compressor work (specific work); $CW = Cp_a \Delta T_{12}$, Cp_a is the heat capacity of the compressed air

STEP 2: IN THE COMBUSTOR

(i) Assume values for the combustion efficiency , η_{cc} and pressure loss, ΔP_{cc}

(ii) Guess the combustor exit temperature, T_3

(iii) Obtain T_2 from STEP 1 (v) and calculate the combustor temperature rise; $\Delta T_{cc} = \Delta T_{23} = T_3 - T_2$

(iv) From the combustor map (Figure 3.12), read the theoretical fuel/air ratio and calculate the actual fuel/air ratio using Equation (3.83)

(v) Calculate: (a) P_3 from $P_3/P_2 = 1 - (\Delta P_{cc}/P_2)$; (b) $N/\sqrt{T_3}$; (c) non-dimensional mass flow at combustor exit; $\left(\dot{m}\sqrt{T_3}/P_3\right)_{CC,EXIT}$

STEP 3: IN THE (COMPRESSOR) TURBINE

(i) Guess turbine pressure ratio, P_3/P_4

(ii) From turbine characteristic map (Figure 3.11 (a)), read the value of the non-dimensional mass flow at turbine inlet, $\left(\dot{m}\sqrt{T_3}/P_3\right)_{T,INLET}$; from Figure 3.11(b), read the value of turbine isentropic efficiency, η_t

(iii) Calculate: (a) the temperature drop across the turbine, $\Delta T_{34} = \eta_t T_3\left[1-\left(\frac{P_3}{P_4}\right)^{\frac{1-\gamma_h}{\gamma_h}}\right]$, γ_h is the ratio of the specific heat capacities of the hot gases; (b) P_4: $P_4 = \frac{P_3}{\left(P_3/P_4\right)}$, T_4 from T_3 and ΔT_{34} (c) The non-dimensional mass flow at turbine exit, $\left(\dot{m}\sqrt{T_4}/P_4\right)_{T,EXIT}$

(iv) Calculate the turbine work, $TW = \eta_m Cp_h \Delta T_{34}$, Cp_h and η_m are the heat capacity of the hot gases and mechanical efficiency respectively

STEP 4: CARRY OUT CHECKS

(I) Check for work compatibility between compressor and turbine:
Is $TW = CW$?
If YES, go to (II); if NO, change the turbine pressure ratio P_3/P_4

(II) Check for compatibility of flow between combustor exit and turbine inlet:
Is $\left(\dot{m}\sqrt{T_3}/P_3\right)_{CC,EXIT} = \left(\dot{m}\sqrt{T_3}/P_3\right)_{T,INLET}$?
If YES, go to STEP 5; if NO, change the value of T_3

STEP 5: IN THE POWER TURBINE

(i) Calculate the turbine pressure ratio, P_4/P_5: $P_4/P_5 = P_4/P_a$; $P_5 = P_a$

(ii) From Figure 3.11(a), read the value of the non-dimensional mass flow at the power turbine inlet, $\left(\dot{m}\sqrt{T_4}/P_4\right)_{PT,INLET}$

STEP 6: CARRY OUT FINAL CHECK

Check for mass flow compatibility at the exit of the compressor turbine and the inlet of the power turbine:

Is $\left(\dot{m}\sqrt{T_4}/P_4\right)_{T,EXIT} = \left(\dot{m}\sqrt{T_4}/P_4\right)_{PT,INLET}$?

If NO, choose another compressor pressure ratio P_2/P_1; if YES, matching is completed. The calculation could be carried out for another value of N.

The calculation of power output, overall plant thermal efficiency, specific fuel consumption, etc. could be easily carried out when matching is completed. The algorithm of the matching technique presented here has nested-loop format and involves iterations. Other methods of components matching in off-design calculations are in use, and component matching algorithms of different engine configurations could be found in many literatures [1], [3], [19]. PYTHIA exploits components matching techniques in off-design performance calculations using the code provided by TURBOMACH [205], Cranfield in-house gas turbine performance and diagnostic software.

5.5 Chapter Conclusions

In this chapter, engine performance model creation, model adaptation, model validation, and off-design performance calculations are considered. The engine performance model is created in PYTHIA and adapted to both the design and off-design conditions. The creation of engine performance model requires the selection of component icons and providing relevant data for the icons. The engine performance model is a thermodynamic model of the real engine and made to behave like the real engine through adaptation. Design-point adaptation adaptation of the LM2500+ engine is carried out and the results are presented. PYTHIA has the capabilities of both design point adaptation and off-design point adaptation and these capabilities were exploited in adapting the created engine model. The adapted engine performance model is validated by comparing the simulation results from the engine performance model to the results from the real engine in the field. The simulation results closely matched the results from the real engine. Also, all gas path properties responds to power variation in the manner expected in practice. The engine performance model is thus adjudged to be appropriate for further work, such as life analysis in this case. The off-design performance calculation process applicable to the engine model used in this research is also presented.

6 CREEP LIFE ANALYSIS

The creep life consumption analysis of the HP turbine blades of the LM2500+ engine used in this research is presented in this chapter. Also, creep life tracking and factors affecting creep life consumption are considered. The creep life analysis sub-models-engine performance model, data acquisition and pre-processing model, blade thermal model, and blade stress model are presented in previous chapters. These models and the creep life estimation mmethodologies presented in chapter 3 are applied to real engine operation data for creep life consumption analysis. In this work, the engine performance model, the blade thermal and stress models, the data acquisition and pre-processing module and the creep life model are assembled to form an integrated creep life assessment system, where engine creep life at different periods of engine operation could be estimated separately and cumulatively to obtain the equivalent creep life consumption.

6.1 Creep Life Estimation for Daily Engine Operation

Figure 6.1 presents a comparison among the simulated creep life at each step, the equivalent creep life, and the creep life fraction for one day operation of the engine; the parameters evaluated using the models developed in this research.

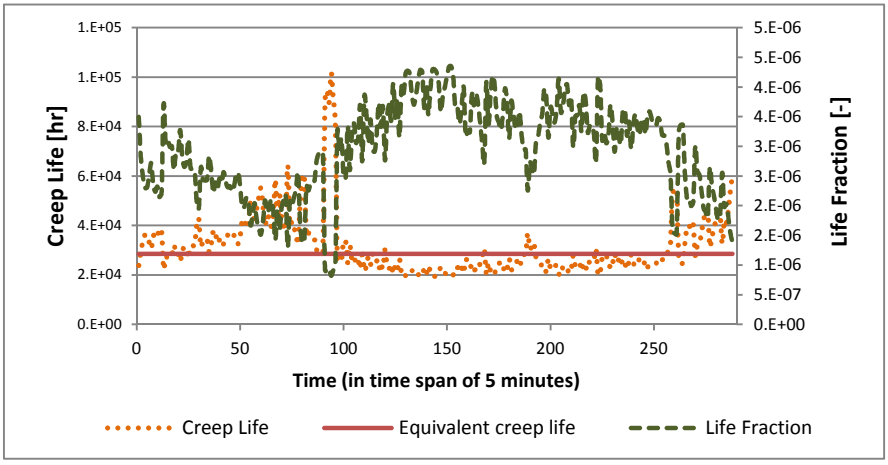

Figure 6.1: Predicted Creep Life, Equivalent Creep Life and Life Fractions for a typical Day Operation

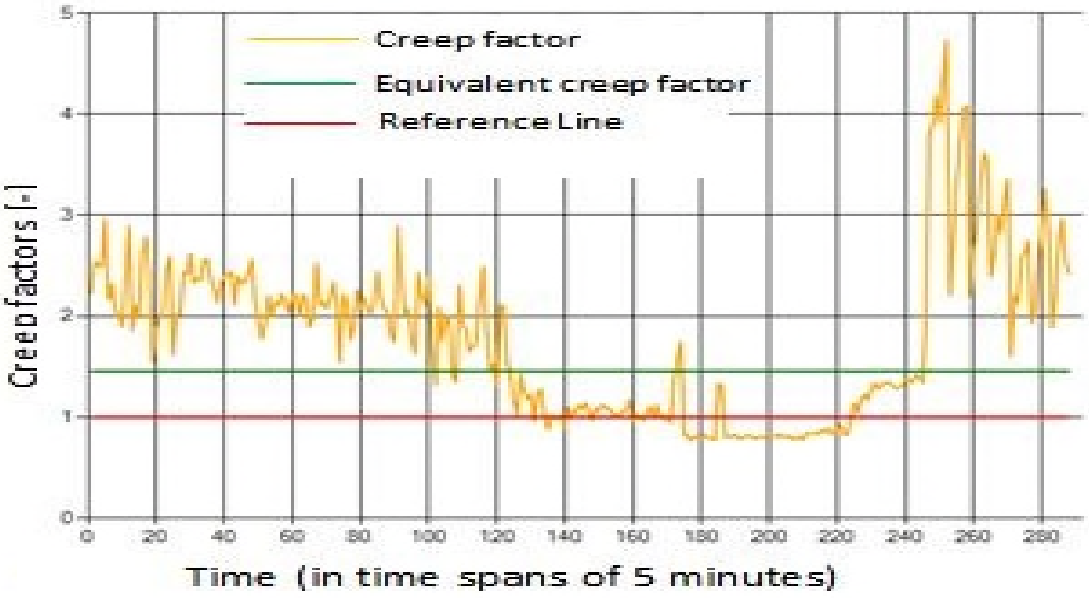

Figure 6.2: Creep Factors and Equivalent Creep Factors for Cold Day Engine Operation

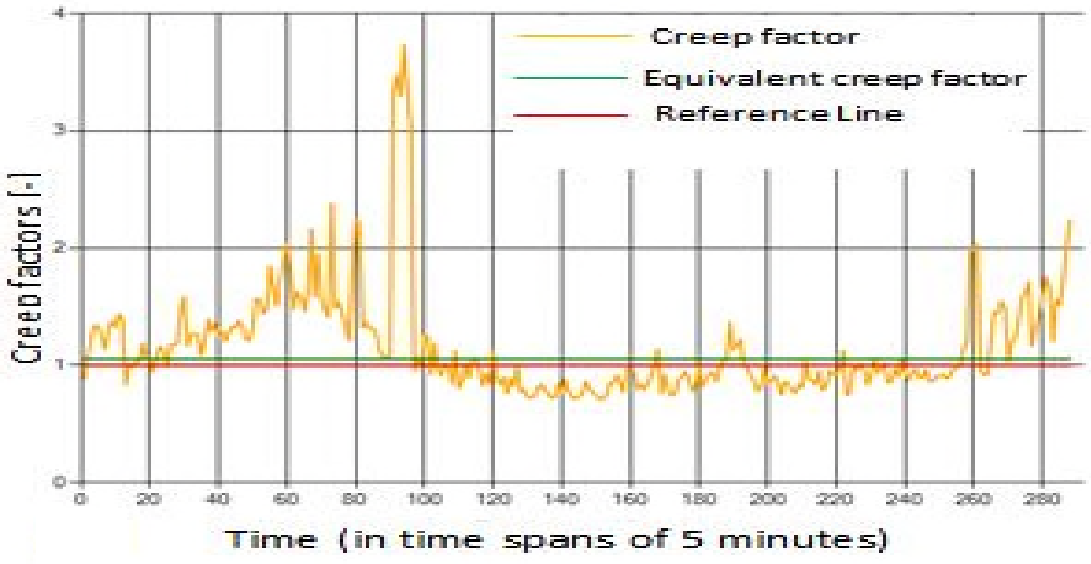

Figure 6.3: Creep Factors and Equivalent Creep Factors for Hot Day Engine Operation

Figure 6.2 shows the creep factors for all the engine operation points and their respective equivalent creep factors and reference line (equivalent to creep factor of unity) for one day operation of the engine. The creep factors are quite high and only few values are below the reference line which value is unity. The equivalent creep factor for the day is 1.4556, which is much higher than the reference value. Figure 6.2 was obtained from a day in January where temperatures were low (many of the recorded temperatures were lower than the engine model design point ISA deviation

temperature). Few creep factors are less than the reference value. In Figure 6.3 many creep factors are less than the reference value. The data was obtained from a hot day in June and quite a number of the recorded temperatures are above the engine model design point ISA deviation temperature. The equivalent creep factor for the day operation of the engine is 1.0545. Comparing the two days of engine operation, the creep life consumption in the second day is higher as the lower equivalent creep factor translates to smaller value of equivalent creep life and hence shorter time to creep failure (see Equation (3.14)).

The values of the creep factor at each point of engine operation depends largely on the power level and the ambient temperature- the two off-design conditions considered in engine off-design performance calculation. In Figure 6.3, if only temperature was considered, almost all the creep factors would have been less than the reference value. The power level at many points was lower than that of the engine performance model design point value hence the creep factors are pushed up. The high creep factor values recorded in Figure 6.3 is due to lower power output and this is shown in Figure 6.4.

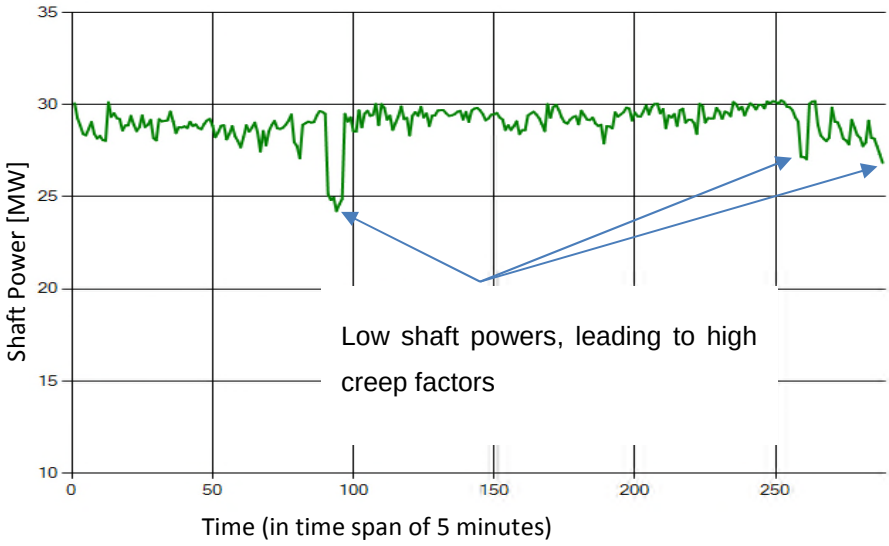

Figure 6.4: Influence of Shaft Power Variation on Creep Factor

6.2 Creep Life Tracking of Gas Turbine Components: A Case Study

In this work, it is possible to monitor the creep life consumption of the HP turbine blades quickly. This is done by analysing the daily life consumption of the engine to obtain the equivalent creep factor of the engine operation per day. The equivalent creep factor for a number of days of engine operation could be obtained as the code written automatically calculates the equivalent creep factor for all the data it captures to calculate the life consumption. By comparing the equivalent creep factors per day of engine operation over a period of time, the engine operator will clearly see how well the engine has been operated in that period. Also, an estimate of the life consumed in the period will be noted in addition to an estimate of the remaining life of the engine. If the equivalent creep factor over a given period is more than unity, then cumulatively, the engine has been operated in a favourable condition compared to the reference life of the engine.

To test the feasibility and the applicability of the developed algorithms for creep life tracking, the developed creep life anlysis/tracking methodology is applied to 8 months of real engine operation data to see how the engine life could be tracked. Figure 6.7 shows the equivalent creep factors per day for 8 different months of engine operation (January, February, March, June and July, August, November, and December 2014).

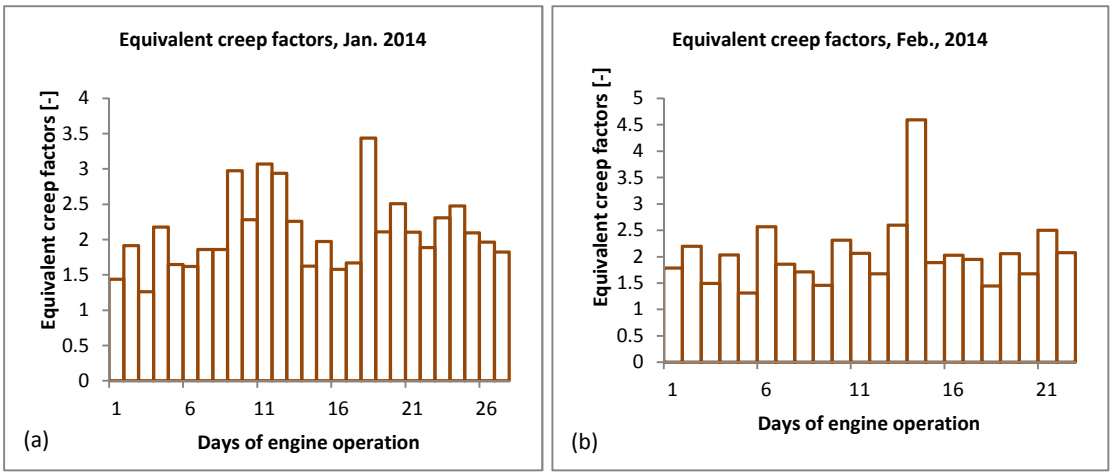

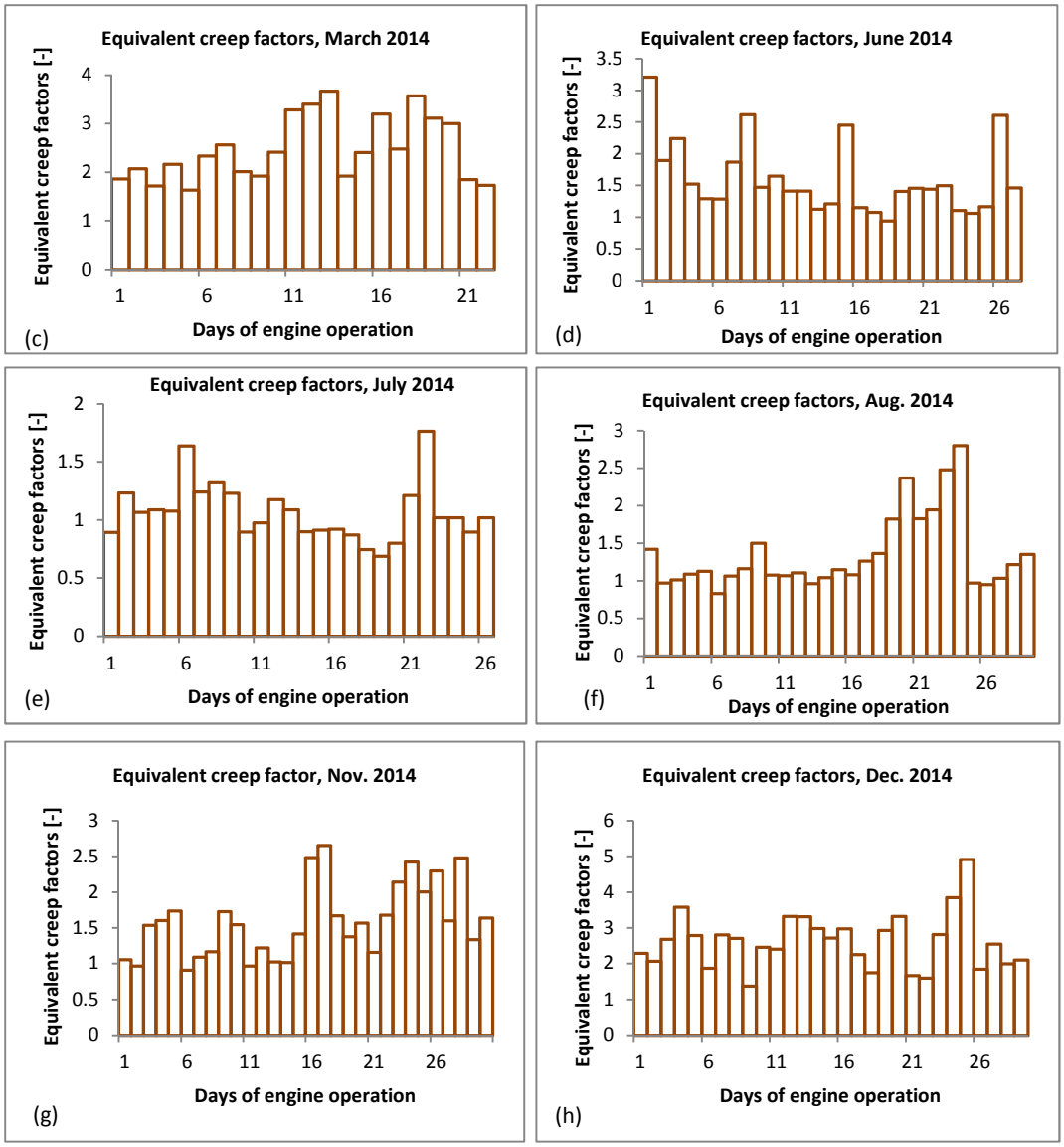

Figure 6.5: Equivalent Creep Factors in Eight Months of Engine Operation

From Figure 6.5 (a), (b) and (c), the equivalent creep factors per day of engine operation are all above 1. These months come with low ambient temperatures and hence low engine life consumption with power level not too high. Very high creep factor values in these three months result from very cold days. In Figure 6.5 (d), the equivalent creep factors are quite high, but in many days, the value not much greater than unity. This is because of a mixture of cold and hot days recorded in June while similar power levels of engine operation were maintained. In July, as depicted in Figure 6.5 (e), the engine was operated in a bit harsh conditions as the equivalent creep factors were lower than unity

in some of the days. In August, the ambient temperatures were a bit high from the beginning of the month up to the middle of the month and many equivalent creep factors are close to 1 in this period. Between the 20th and the 25th of the month, low temperatures crept in and the equivalent creep factors went up. In November, as shown in Figure 6.5 (g), engine operation was not favourable in some days but quite favourable in many other days. In December, temperatures were low generally and the equivalent creep factors were all above the reference value of unity as shown in Figure 6.5 (h). To mitigate fast consumption of engine life in hot days, the power level should be reduced if necessary. The effect of ambient temperatures and power level on creep life consumption is considered later in this chapter.

To compare the impact of engine operation on creep life consumption of each month considered, the equivalent creep factors estimated for each month of engine operation are used. The equivalent creep factor of engine operation for each month considered is given in Figure 6.6.

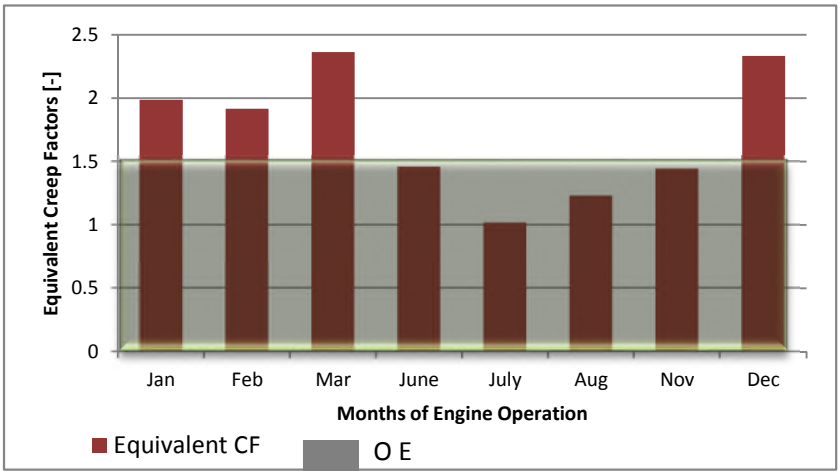

Figure 6.6: Equivalent Creep Factors for Each Month of Engine Operation

In Figure 6.6, the equivalent creep factor obtained for March and December are the highest while the value for July is lowest. In March and December, the temperatures were quite low in many days leading to favourable engine operation conditions and hence high equivalent creep factors. In January and February, low temperatures were recorded and the equivalent creep factors are quite high, though lower than those of March and December. July came with highest ambient temperatures and lowest

equivalent creep factor for all the months considered. Judging engine life consumption for the entire period based on January data will lead to overestimation of engine life since the equivalent creep factor of the 8 months of engine operation (overall equivalent creep factor, denoted as OE) is lower than the value obtained in January. Also, using July data for engine life estimation will give lower values compared to the overall equivalent. The overall equivalent creep factor is representative of all the data employed in the analysis.

The equivalent creep factors for each month of engine operation are different from the overall equivalent creep factor for all the 8 months under review. Figure 6.7 shows the percentage difference between the equivalent creep factor of each month and the overall equivalent creep factor. Absolute values are used in the percentage evaluation. The percentage differences are highest in March followed by December- the two months of most favourable engine operation where the equivalent creep factor is much greater than the reference creep life.

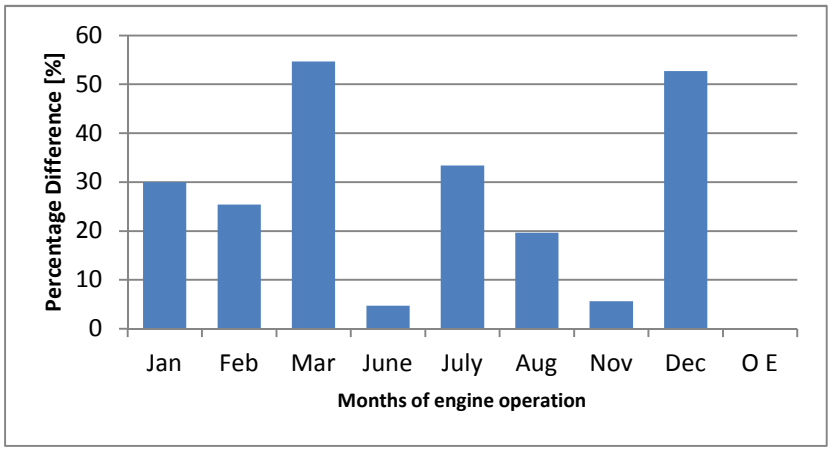

Figure 6.7: Percentage Difference between Monthly Equivalent Creep Factors and Overall Equivalent Value

The percentage differences are lowest in June and November which equivalent creep factors are very close to that of the overall equivalent. The percentage difference in July is quite high as its equivalent creep factor is the lowest in all the months of engine operation under review. Comparing the percentage difference in July with those of January and February, it is clear that the equivalent creep factors in January and February are closer to the overall equivalent value compared to the equivalent creep

factor value in July. The overall equivalent creep factor value is also included in Figure 6.7 for the purpose of completeness. The percentage difference at this point is zero since the percentage difference is calculated based on the deviation of the equivalent creep factor of each month of engine operation from the overall equivalent value.

The equivalent creep life based on each month of engine operation is given in Figure 6.8. The equivalent creep lives are in the same order with the equivalent creep factors in terms of magnitude. The equivalent creep lives are highest in March and December but lowest in July. In January, February, March and December, the creep lives estimated are each higher than the overall equivalent value; estimating engine life using the results of any of these months will lead to over-estimation of engine life with respect to the overall equivalent value. In June, July, August and November, the creep lives are each lower than the overall equivalent value; thus, estimating life using any of these months will lead to under-estimating of life compared to the overall equivalent value. Using the July result for life estimation will lead to the highest under-estimated value while March value will give the highest over-estimated life value.

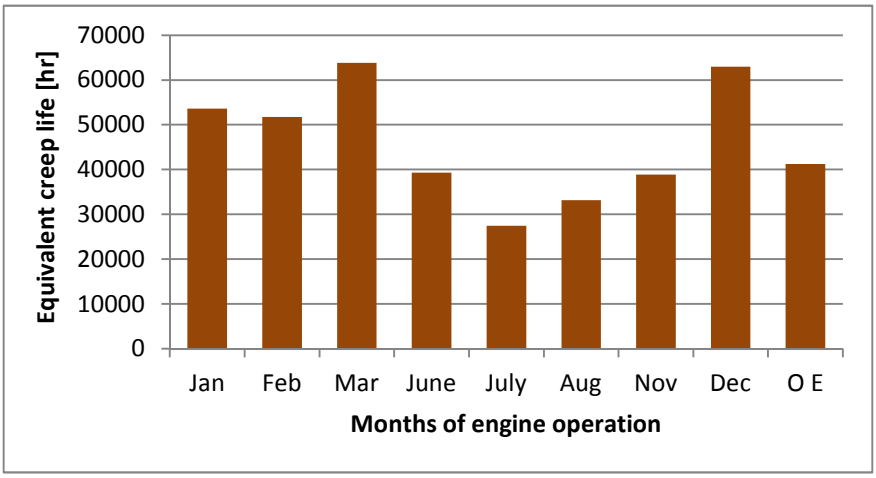

Figure 6.8: Equivalent creep life for each Month of Engine Operation

The overall equivalent creep life of the 8 months analysed is close to the values in June and November, hence June gave the lowest value of percentage difference followed by November. It is clear from the creep life values that accurate life estimation involves using much data. Using the code developed in this work, analysing many data for engine life consumption is possible within a short time. The remaining life based on each month of engine operation could be estimated. The remaining life is the difference

between the equivalent creep life and the number of hours the engine has been in operation for the period considered. The smaller the equivalent creep life, the faster the rate of engine creep life consumption, and vice-versa.

Table 6.1: Engine Operation Data

S/N	Month	Period of engine operation	Equivalent creep factor
1	January	631.17	1.9858
2	February	498.50	1.9163
3	March	471.92	2.3633
4	June	619.92	1.4553
5	July	616.08	1.0180
6	August	683.58	1.2280
7	November	375.75	1.4412
8	December	328.16	2.3329
9	Overall	**4211.08**	**1.5278**

Table 6.1 shows the months of engine operation with the total hours engine was operated in each month. The equivalent creep factors for each month are also included. In the period considered, the engine was operated for a period of 421.08 hours and the equivalent creep factor for the whole period is estimated as 1.5278. The creep lives and the remaining lives predicted may not be very accurate, but the values in each case are related to the actual values which are always difficult to predict. This formed the decision for relative life analysis using the creep factors and the equivalent creep factors. This enables the engine operator to ascertain the wellness of engine operation. In all, the life tracking procedure developed in this research can clearly distinguish between a set of engine operating conditions the level of wellness of engine operation in each condition. Also, the remaining lives predicted will certainly give the engine operators some idea of when engine component will fail and enable them to make decisions concerning maintenance and replacement of affected parts.

6.3 Effects of Ambient Temperature and Shaft Power on Creep Life

From the previous section, it is clear that ambient temperature affects the creep life of the HP turbine blades. Power also affects the creep life of the blades but the extent to which the creep life is shortened or lengthened as a result of a unit increase or drop in

ambient temperature at different power levels need to be investigated. Pinning the temperature drop or rise effect on life to power level is necessary because power influences creep life also and at different power levels the rise in ambient temperature will have different magnitude of effect on the turbine blades. Shaft power (SP) levels of 70% to maximum power level (100%) and ambient temperatures of 5^{o}C to 30^{o}C (expressed in terms of deviations from ISA condition) are employed to see the effect of temperature drop on creep life at each power level. By increasing the ambient temperature from 5^{o}C to 30^{o}C (-10 to 15 deviation from ISA)) at the various power levels, the creep factors of the engine operation are as shown in Figure 6.9.

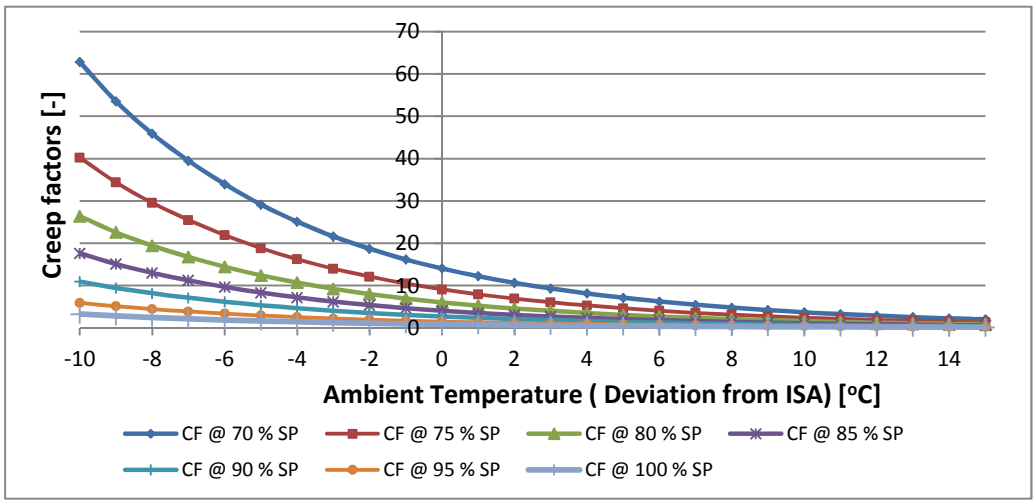

Figure 6.9: Creep Factors Variation with Ambient Temperature at different Shaft Power Levels

In investigating the effect of ambient temperature increase on creep life, the effect of unit increase in ambient temperature on creep life could be estimated by calculating the percentage decrease in creep factor. In doing this, the original temperature before the increase should be specified. Expressing the increase in ambient temperature in terms of percentage may not be inappropriate, unless a universal starting temperature is accepted. In this work, effect of ambient temperature on creep life consumption is investigated in the range -10^{o}C to 15^{o}C deviation from ISA. -10^{o}C deviation from ISA is used as a basis for calculating percentage increase in ambient temperature. Based on this, at -9^{o}C deviation from ISA, the percentage increase in ambient temperature will be 10%. Thus, a unit increase in ambient temperature or percentage increase in ambient temperature

could be used in investigating the effect of ambient temperature rise on creep life; in both cases, the starting point should be specified.

Increase in ambient temperature leads to increase in the temperature of the gases at turbine entry, and the blades are exposed to higher creep life consumption. The rate of life consumption depends on the power level of the engine. The creep factors decrease with increase in ambient temperature at all power levels. This is because an increase in ambient temperature leads to corresponding increase in the temperature of the gases the blades are exposed to. The rate of decrease in creep factors with ambient temperature at each power level is higher in the lower temperature band. This is because in the lower temperature band the gases are more compressible and change in ambient temperature in that range will produce more noticeable change in the properties of the gases at the combustion exit compared to the higher ambient temperature band. Also, ambient temperature has much influence on creep factor and hence creep life at lower power levels than at higher power levels; this is understandable since at higher power levels an increase in ambient temperature may not lead to too much significant increase in the combustor exit gases. Higher values of creep factors are gotten in lower ambient temperatures and lower shaft power levels, thus at each power level, higher percentage decrease in creep factors are obtainable at lower ambient temperatures.

Figure 6.10 shows the average percentage decrease in creep factors with ambient temperature at different power levels. The percentage decreases in creep factors with ambient temperature for all the range of ambient temperatures considered are used in getting the average value at each power level. For instance, at 70 % power level and -10^{o}C the creep factor is estimated; when the ambient temperature increases from -10^{o}C to -9^{o}C, the creep factor drops by a certain percentage based on the original -10^{o}C creep factor value. As ambient temperature increases by a single step at a given power level, the percentage decrease in creep factor is estimated in each case. The average value of all the percentage decreases in creep factors due to ambient temperature increase at a given power level is computed and this represents a single bar in Figure 6.10. The mean value of the average percentage decreases for all the power levels is about 12.33 %. Based on this value the creep factor of the hot section turbine blades will be reduced by a factor of 2 (to half the original value at set temperature and power level) when the

ambient temperature is increased by 8.11 units. In terms of percentage increase in ambient temperature, 1% increase in ambient temperature leads to about 1.23% drop in creep factor. On the other hand, the creep factor will double when the ambient temperature drops by 8.11 units at the power levels considered. This value though not be taken as a global value but to a large extent portrays how engine creep life consumption varies with ambient temperature increase and decrease.

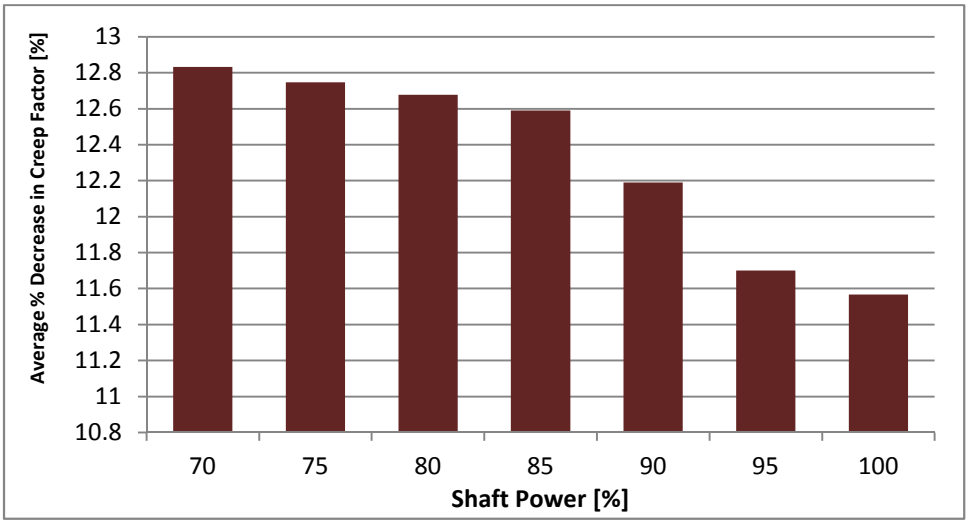

Figure 6.10: Average Percentage Decrease in Creep Factors with Ambient Temperature at Different Power Levels

A major consideration in industrial gas turbine operation is to consider operating at high power level or low power level. Creep life increases with decrease in shaft power and the rate of increase is higher in the higher power band (that is when power is dropped from say 100 % 95 % the increase in creep life is higher compared to when power is dropped from 75 % to 70 % at any prevailing ambient temperature).

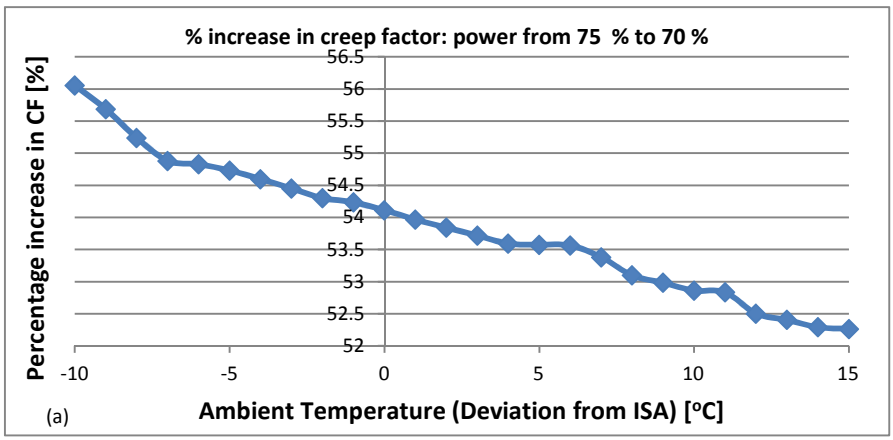

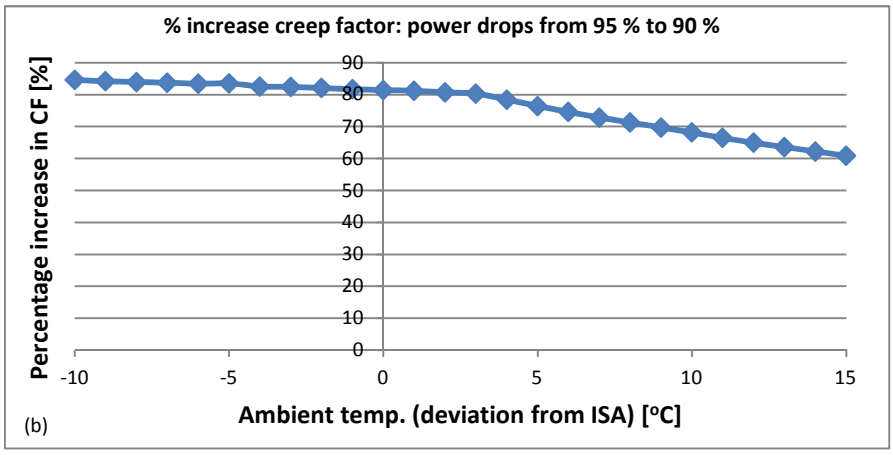

Figure 6.11: Percentage Increase in Creep Factor with Shaft Power Drop at different Ambient Temperatures

The increase in creep factors due to drop in power from 75 % power level to 70 % power level and from 95 % power level to 90 % power level for different ambient temperatures are shown in Figure 6.11. At a particular power drop, the increase in creep factor is lower at higher ambient temperatures. At a particular ambient temperature, increase in creep factor with power drop is higher in the higher power band. That is, benefits in terms of increasing creep life from power drop are more pronounced at lower ambient temperatures in the higher power band. This is because at higher ambient temperatures the turbine efficiency drops hence lowering the power has less effects at this poor operation region compared to the comfortable lower ambient temperature operations.

The increase in creep factors with power drop increases to a peak and later drops as the power drop occurs at lower power levels. Below 90 % power level, the values of increase in creep factor with power drop are lower but with no proper trend. This is shown in Figure 6.12; the mean values of the percentage increase in creep factor as power drops from one level to another at different ambient temperatures are used in the figure.

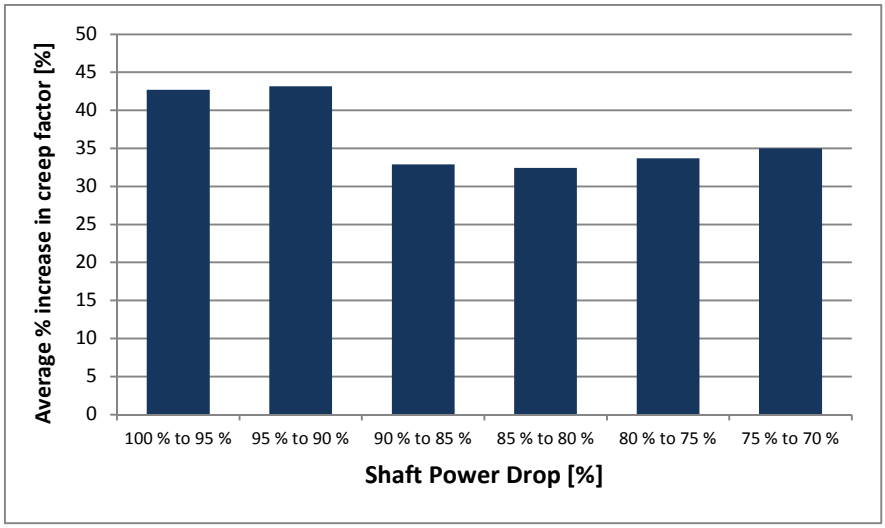

Figure 6.12: Average Percentage Increase in Creep Factor with Shaft Power Drop

The trend in the increase in creep factor with power drop tends to show that operating the engine far away from peak power conditions does not translate to faster saving in creep life. Operating the engine in this case between 100% and 90% power levels will mean lower engine life in terms of gains in dropping the shaft power. The results also depict favourable engine operation close to peak power level as against peak power level operation and operations far removed from peak power level. Although, the HP compressor turbine blade life is higher at the lower power band, but the benefits in increasing creep life with power drop are higher in the higher power band. A mean value of 36.66% increase in creep factor with power drop is recorded in all power drops and all ambient temperatures considered in this research. In terms of a unit drop in shaft power, creep factor increases by 24.44% while creep factor increases by 7.33 % for 1% drop in shaft power. Going by the last value, the blade life will double when power is dropped by 13.64%. This value, like the value obtained in increase in ambient temperature at different power levels, is not a global value, but tends to portray the effect power drop has on creep life at different ambient temperatures. It is pertinent to point out that shaft power drop has positive effect on creep life in the same magnitude shaft power increase does negatively to creep life.

From the foregoing, power variation has more effect on creep life than ambient temperature variation does. Since we have some control on the power level of engine operation, it is of advantage to the operators of gas turbines. The magnitudes in the

increase in creep life with power drop serve as guides to the gas turbine operator, deciding whether it is necessary to operate at a reduced power level based on the power demand. Operating at lower power levels may be necessary during periods of low power demand and high ambient temperatures, but the benefits in dropping the power at high temperatures are not much pronounced compared to the lower temperature range. The decision to dropping power may not be taken solely on the need to increase creep life, but at periods of low power demand, any decision to drop engine shaft power will equally lengthen the creep life of turbine blades.

6.4 Effect of Engine Degradation on Creep Life

Although, in this work direct field data is employed in the engine life analysis and the results obtained are those of the actual state of the engine, but there is the need to investigate the nature of the results by planting degradation in the major engine components. This is necessary because gas turbine components undergo degradation with time, and degraded engine components will lead to changes in creep life consumption when the engine is operated under the same ambient temperature and other operating conditions. Three components in gas turbine are usually considered in engine degradation. These are the compressor, combustor, and compressor turbine. In this research, the effect of compressor and compressor turbine degradations on the creep life of compressor turbine blades is investigated.

Methods of investigating degradation of gas turbine components have been extensively studied [159]–[162], [206], also the effects of engine degradation on engine performance has been looked at by several researchers [163], [164]; but the effect of degradation of engine health parameters on the life of engine components has not been thorough investigated. Compressor degradation comes in the form of compressor fouling and compressor erosion leading to reduction in non-dimensional mass flow (flow capacity), reduction in compressor isentropic efficiency, and reduction in compressor pressure ratio. Turbine degradation on the other hand may result from turbine fouling and turbine erosion. Turbine fouling leads to drop in both turbine flow capacity and isentropic efficiency while turbine erosion leads to rise in turbine flow capacity but drop in turbine isentropic efficiency. Turbine degradation also leads to

change in enthalpy drop and its magnitude is assumed to be inversely proportional to flow capacity change. Li[159] defined the component degradations in terms of engine health parameter degradation indices (degradation scaling factors). These indices for the compressor are the flow capacity index, isentropic efficiency index, and the pressure ratio index. The pressure ratio index is assumed to be equal to the flow capacity index. For the turbine, the indices are the flow capacity index, isentropic efficiency index and enthalpy drop index. The enthalpy drop index is assumed to be the inverse of the flow capacity index. Thus, flow capacity index and isentropic efficiency index are used to represent both compressor and turbine degradations, as the other index in each case is implicit. The flow capacity index and the isentropic efficiency index are independent of each other in both compressor and turbine degradations. The health parameter index in each case is as the ratio between the degraded engine parameter and the clean engine parameter and this is given by Equation (6.1),

$$I_{\phi,\varphi} = \frac{\lambda_{\deg}}{\lambda_{clean}} \tag{6.1}$$

$I_{\phi,\lambda}$ is the degradation index, ϕ stands for the component degraded (compressor or turbine), λ represents the parameter degraded, while $\lambda_{\deg}$ and λ_{clean} denote the parameter in the degraded and non-degraded (clean) conditions respectively. The clean engine condition for any engine that has been operated for a while has to be specified and its gas path properties noted. This is then used as a reference point with which further engine gas path properties are compared with to estimate component degradations.

Both compressor and turbine degradations lead to changes in the component maps. Figure 6.13 shows the compressor maps for clean as well as degraded compressor while the turbine maps for a clean turbine and a degraded turbine respectively are shown in Figure 6.14.

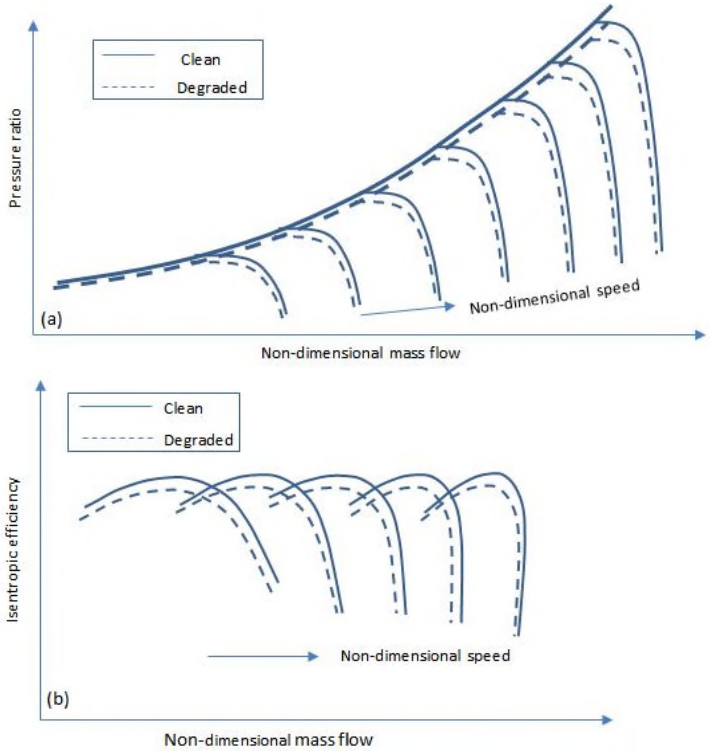

Figure 6.13: Compressor Characteristics Maps for Clean and Degraded Engines

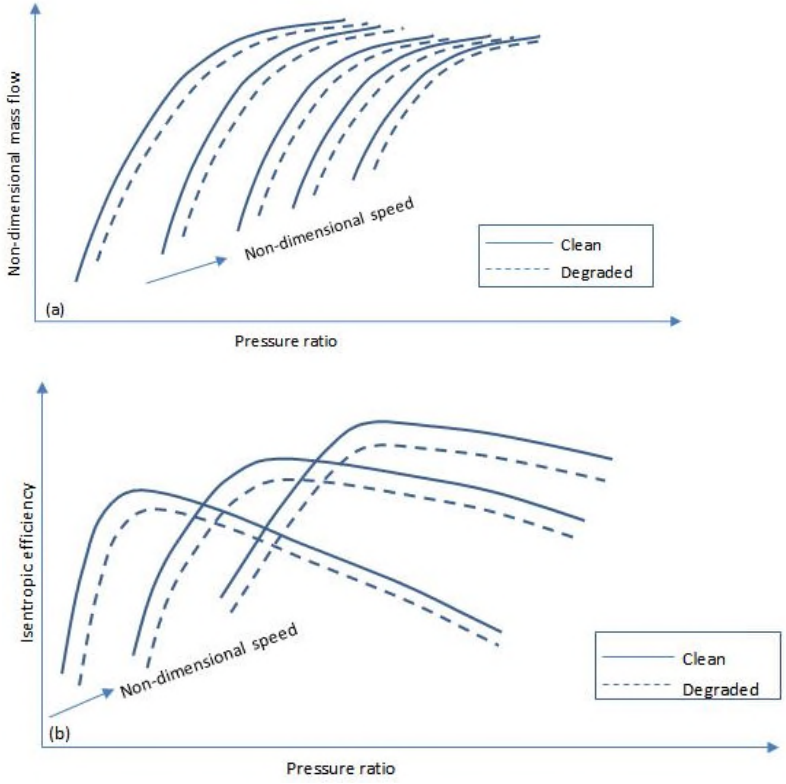

Figure 6.14: Turbine Characteristics Maps for Clean and Degraded Engines

The changes in the component maps due to degradation affect the overall engine performance. The gas path properties at the various stations along the engine components vary with components degradation. In life analysis, the temperatures and pressures at the compressor exit and the turbine inlet/exit affect the life of the turbine blades. Considering an engine with compressor efficiency degradation, the temperature of the gases at the compressor exit is increased. This is shown in the temperature-entropy (T-S) diagram of the compression process in Figure 6.15.

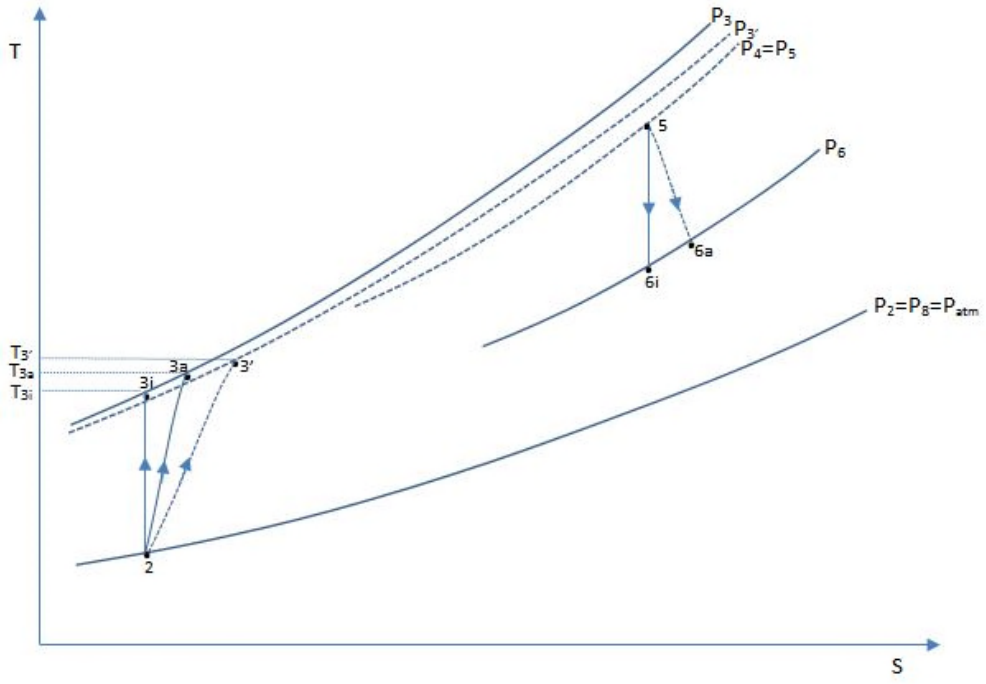

Figure 6.15: Temperature-Entropy Diagram of Compression Process with Isentropic Efficiency Degradation

The numbering in Figure 6.15 is based on the LM2500+ engine performance model given in Figure 4.1. The pressure at the exit of the combustor (P_4=P_5 in Figure 4.1) is lower than P_3 due to pressure loss in the combustion process as shown in Figure 6.15. P_6 is the pressure at the exit of the compressor turbine. The isentropic compression process without degradation in isentropic efficiency is process 2- 3i, while the actual compression process without degradation in isentropic efficiency is process 2-3a. The compressor isentropic efficiency η_{ci} is defined by Equation (6.2),

$$\eta_{ci} = \frac{T_{3i} - T_2}{T_{3a} - T_2} \tag{6.2}$$

The compression work $\dot{W}_c$ (in J/s) is given by Equation (6.3),

$$\dot{W}_c = \dot{m}_a C_{p,a} \left(T_{3a} - T_2 \right) \tag{6.3}$$

$\dot{m}_a$ (in kg/s)is the flow rate of the air , while $C_{p,a}$ (in J/kgK) is the specific heat capacity of the air at constant pressure. From Equation (6.2), $T_{3a} - T_2 = \frac{T_{3i} - T_2}{\eta_{ci}}$; substituting in Equation (6.3), the compression work is as given by Equation (6.4),

$$\dot{W}_c = \frac{\dot{m}_a C_{p,a}}{\eta_{ci}} \left(T_{3i} - T_2 \right) \tag{6.4}$$

From Equation (6.4), when the compressor isentropic efficiency η_c decreases, the compression work $\dot{W}_c$ increases. To maintain the same compression work, the compression process will not get to P_3. Pressure drops from P_3 to $P_{3'}$. The actual compression process follows the path 2-3'. $T_{3'}$ is greater than T_{3a}. Thus in a compression process with isentropic efficiency reduction, to maintain the required compression work as in non-degraded engine condition, the pressure at the compressor exit decreases while the temperature at the compressor exit increases. Since the compressor exit air serves as the cooling air for the turbine stage, if the compressor turbine entry temperature (TET) is the same as in non-degraded engine (TET will equally increase with compressor degradation), the temperature of the compressor turbine blades will be higher. This will lead to failure of the compressor turbine blades in less time compared to a clean engine. Compressor flow capacity reduction also leads to increase in compressor exit gas temperature. The gas temperature at the compressor exit (T_3 in this case), and the compressor turbine entry temperature (TET) are the two major parameters which influence the temperature of the compressor turbine blade material and hence the life of the blades under different cases of engine components degradation.

Both T_3 and TET increase with ambient temperature and shaft power. Figures 6.16 and 6.17 show respectively T_3 and TET values for two different power levels with clean engine, engine with compressor flow capacity reduction, and engine with compressor

isentropic efficiency reduction. The temperatures are expressed relative to a reference point of engine operation. The temperatures are obtained at 90% power level and maximum power level (100%) at different ambient temperatures expressed in terms of deviations from ISA. Aside the clean engine, designated as CE, 1% reduction in compressor flow capacity (FCR-flow capacity reduction) and 1% reduction in compressor isentropic efficiency (EffR- Efficiency reduction) were implanted in the engine performance model to obtain temperatures in the degraded case.

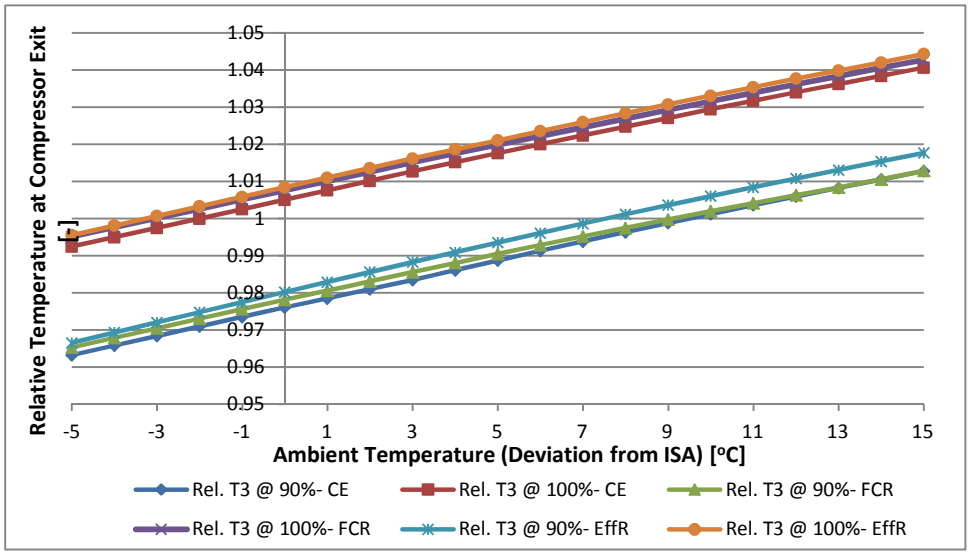

Figure 6.16: Relative Temperature at Compressor Exit at different Power Levels and different Engine Conditions

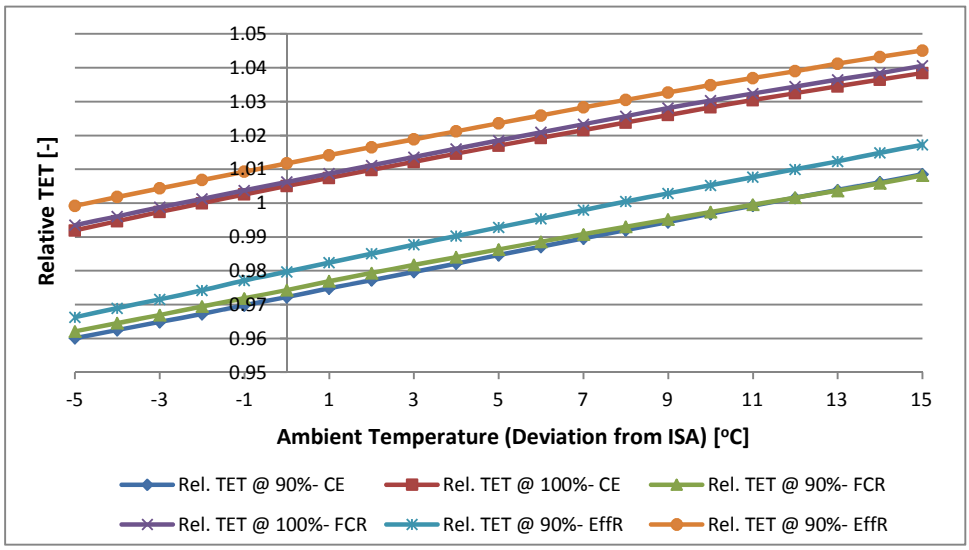

Figure 6.17: Relative TET at different Power Levels and different Engine Conditions

Comparing the compressor exit temperature for the clean engine with either case of compressor degradation, the compressor exit temperature is higher for the degraded cases at the two power levels. For the two cases of degradation, compressor isentropic efficiency reduction leads to greater increase in compressor exit temperature at the two power levels considered. A similar trend occurs in the turbine entry temperature; but in this case, compressor isentropic efficiency reduction leads to relatively greater increase in turbine entry temperature. From the above trend, one can conclude that for the engine under consideration, compressor efficiency deterioration will lead to faster compressor turbine blades creep life consumption compared to compressor flow capacity reduction. The actual life analysis results due to engine degradation carried out later in this chapter will confirm the above observation.

The gas turbine health status estimation process has been implemented in PYTHIA by Li[159], thus in this research, PYTHIA is used to estimate the gas path properties of degraded engine and the results are used the life analysis models developed in this research to see the effect of various engine component degradation cases on creep life consumption of the compressor turbine blades of the engine considered. Several cases of degradation are considered. Table 6.2 shows the various cases of degradation considered in this research. The first six cases have to do with degradation in single health parameter in a single component and both components (compressor and compressor turbine), while the remaining cases deal with degradation of combinations of health parameters. The first six of cases will enable comparison of the effect of the different health parameters on creep life in individual components and both components. The last three cases will show which component degradation has more effect on creep life. In addition, the last three cases will also show if increase in magnitude of degradation of the health parameter index will have corresponding decrease in engine creep life. It is pertinent to point out that flow capacity index reduction in compressor also implies reduction in pressure ratio index, but, in compressor turbine, flow capacity index reduction implies increase in enthalpy drop index.

Table 6.2: Degradation Cases for Creep Life Analysis

Case	Component	Degraded Parameter	
		Efficiency Index [%]	Flow capacity Index [%]
I	Compressor	-1	0
II	Compressor	0	-1
III	Compressor Turbine	-1	0
IV	Compressor Turbine	0	-1
V	Both Components	-1	0
VI	Both Components	0	-1
VII	Compressor	-1 &-2	-1 &-2
VIII	Compressor Turbine	-1 &-2	-1 &-2
IX	Both Components	-1 &-2	-1 &-2

Percentage Decrease in Creep factors

To assess the relative effect of each degradation case on creep life, the percentage decrease in creep factor at each power level and ambient temperature due to engine degradation will be evaluated. The percentage decrease in creep factors due to engine degradation could be obtained using Equation (6.5),

$$PD_{CF} = \frac{CF_{CE} - CF_{DE}}{CF_{CE}} \times 100 \qquad (6.5)$$

PD_{CF} is the percentage decrease in creep factor, CF_{CE} is the creep factor for the clean engine while CF_{DE} is the creep factor for the degraded engine. At a given power level, the creep factors changes with ambient temperatures for both the clean and degraded condition. Thus, at a given power level, different creep factors are obtained for both the clean and degraded engines, and the percentage decrease in creep factor could be expressed for creep factors at each ambient temperature as given by Equation (6.6).

$$PD_{CF,i} = \frac{CF_{CE,i} - CF_{DE,i}}{CF_{CE,i}} \times 100 \qquad (6.6)$$

The percentage decrease in creep factor depends on the shaft power level and the ambient temperature since creep factors vary with both shaft power level and ambient temperature. The value of the percentage decrease in creep factor due to degradation

obtained at a specified power level and ambient temperature indicates the magnitude of the impact the degradation has on creep life. Larger values of percentage decrease in creep factor portray greater impact of degradation on creep life and vice-versa. At a given power level, the percentage decrease in creep factor could be evaluated at different ambient temperatures and the mean value could be used to represent the impact of degradation at that power level. This is given by Equation (6.7),

$$PD_{CF\_m} = \frac{\sum_{i=1}^{n} PD_{CF,i}}{n} \tag{6.7}$$

PD_{CF_m} is the mean value of the percentage decreases in creep factor at a given power level, and n is the number of ambient temperature levels where creep factors are estimated for both clean and degraded engines.

6.4.1 Effects of Compressor Isentropic Efficiency and Flow Capacity Degradations on Creep Life Consumption

To estimate the relative effects of compressor efficiency index and flow capacity index reductions on creep life, 1% degradation in compressor efficiency index was implanted in the engine performance model and simulated; thereafter, 1% degradation in compressor flow capacity index was implanted in the engine performance model and simulated, and the results are used in the creep life analysis models. Figure 6.18 shows the creep factors for compressor efficiency index reduction and compressor flow capacity index reduction for two different power levels and a number of ambient temperatures. The results of the clean engine for same power levels are also included. The trends of the creep factors for the degraded engines are similar to those of the clean engine. The clean engine (CE) creep factors as should be expected are higher than those of the degraded engine at the two power levels and the ambient temperatures considered. More appreciable difference between the creep factors for the clean and degraded engines occur at lower ambient temperatures and lower power levels. This is because large values of creep factors are obtainable from both engines at low ambient temperatures and low shaft power levels.

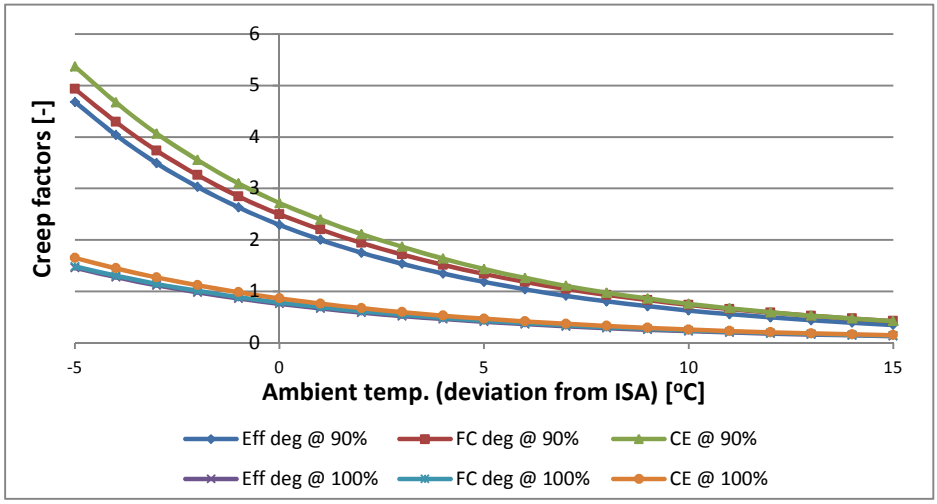

Figure 6.18: Comparison of the Effects Compressor Efficiency and Flow Capacity Indices Degradation on Creep Factors at Different Power Levels and Ambient Temperatures

From Figure 6.18, Eff deg @ 90% represents isentropic efficiency index degradation at 90% power level while FC deg at 90% represent flow capacity index degradation at 90% power level. The other notations follow similar convention. The creep factors for the engine with compressor flow capacity index degradation are higher than those with compressor efficiency index degradation (confirming the observations made in Figures 6.16 and 6.17); with very clear difference at the lower power level and lower ambient temperatures. At the peak power operation and higher ambient temperatures, the creep factors for the two degraded cases are almost the same, but those with flow capacity degradation are still higher. This means for the engine under consideration, compressor efficiency index degradation will lead to blade failure faster compared to compressor flow capacity index degradation. Also, at peak power and higher ambient temperature operations, the effects due to compressor efficiency index degradation and compressor flow capacity degradation are almost the same and minimal.

The average percentage decreases in creep factors due to compressor isentropic efficiency index reduction at 90% and 100% power levels are 16.34% and 12.46% respectively. This shows that compressor isentropic efficiency index reduction has more impact on creep life at lower power levels. This is because the compression process is

more efficient in the lower power band, and reduction in efficiency in lower power levels will have more noticeable effect on creep life at that power band. Compressor flow capacity index reduction on the other hand produces 5.38% and 8.50% as the average percentage reductions in creep factors at 90% and 100% power levels; the value increases with power level. This is because flow capacity reduction also leads to pressure loss which value is high at higher power levels, and hence the effect of degradation has greater impact as power level increases. Comparing these values with those of compressor isentropic efficiency reduction shows that compressor isentropic efficiency reduction has more impact on creep life than compressor flow capacity index reduction, especially at lower power levels.

6.4.2 Effects of Compressor Turbine Efficiency and Flow Capacity Degradations on Creep Life Consumption

The operation of the compressor is controlled by the operating conditions of the compressor turbine. Degradation of the compressor turbine changes the operation of the compressor turbine, and this in turn affects the gas path properties which determine the life of the compressor turbine blades. The effect of 1% degradation in compressor turbine flow capacity index on the compressor turbine blade life is compared with the effect produced by 1% degradation in compressor turbine isentropic efficiency index in Figure 6.19.

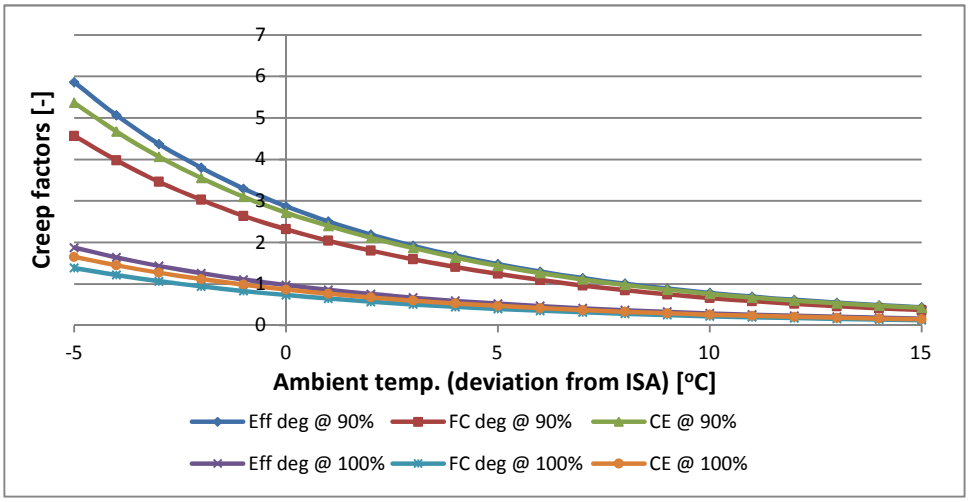

Figure 6.19: Comparison of the Effects of Compressor Turbine Efficiency and Flow Capacity Indices Reduction on Creep Factors at Different Power Levels and Ambient Temperatures

In Figure 6.19, compressor turbine flow capacity index degradation gives creep factors that are lower than those from the clean engine and the engine with isentropic efficiency index degradation at all ambient temperatures. Like in the case of compressor degradation, more noticeable difference in the creep factors occur at lower power level and lower ambient temperatures. A strange occurrence in Figure 6.21 is that the engine with compressor turbine isentropic index degradation gives creep factors that are higher than those of the clean engine, indicating that the engine with compressor turbine isentropic index reduction will have blades which will last longer than that of the clean engine operating under same conditions. This occurrence is explained here. From Figure 6.15, the compressor turbine isentropic efficiency η_{ti} is defined by Equation 6.8,

$$\eta_{ti} = \frac{T_5 - T_{6a}}{T_5 - T_{6i}} \tag{6.8}$$

T_5 is the turbine entry temperature (TET), T_{6i} is the turbine exit temperature under isentropic expansion while T_{6a} is the actual temperature at the turbine exit. From Equation (6.8), T_{6a} is given by Equation (6.9),

$$T_{6a} = T_5 - \eta_{ti}\left(T_5 - T_{6i}\right) \tag{6.9}$$

The turbine work $\dot{W}_t$ (in J/s) is given by Equation (6.10),

$$\dot{W}_t = \dot{m}_t C_{pt}\left(T_5 - T_{6a}\right) = \dot{m}_t C_{pt}\eta_{ti}\left(T_5 - T_{6i}\right) \tag{6.10}$$

$\dot{m}_t$ is the total mass of the hot gases at the point of expansion in the turbine while C_{pt} is the specific heat capacity at constant pressure of the gases. From Equations (6.9) and (6.10), when the isentropic efficiency drops, T_{6a} increases while $\dot{W}_t$ reduces. The compressor turbine is meant to run the compressor for the set power level, thus additional fuel is burn to increase the turbine entry temperature, but the compressor also responds by reducing the pressure ratio and the temperature at the compressor exit. Although there is increase in TET, the reduction in the compressor exit temperature is greater, hence the relatively lower cooling air temperature extracted from towards the last stage of the compression process leads to lower blade temperature and longer blade life. This is only feasible for cooled blades. The overall thermal efficiency of the plant

drops as a result of reduction in the turbine efficiency; this means increase in fuel cost compared to the clean engine, this is not desirable in practice.

Compressor turbine flow capacity index reduction has more negative effect on creep life than compressor flow capacity index reduction. The average percentage reductions in creep factors due to compressor turbine flow capacity index reduction evaluated at 90% and 100% power levels are 13.77 and 15.25%. These values are higher than those due to compressor flow capacity index reduction which are 5.38% and 8.50% respectively. The impact of the compressor turbine flow capacity reduction on creep life is less than compressor isentropic efficiency index reduction at 90% power level but it is greater at 100% power level judging from the values of the average percentage decrease in creep factors.

6.4.3 Effects of Efficiency and Flow Capacity Degradations of Compressor and Compressor Turbine on Creep Life Consumption

The effect of isentropic efficiency index reduction in both compressor and compressor turbine on creep life is compared with the effect of flow capacity index reduction in both components on creep life in this section. The comparisons are made at two power levels and several ambient temperatures as shown in Figure 6.20.

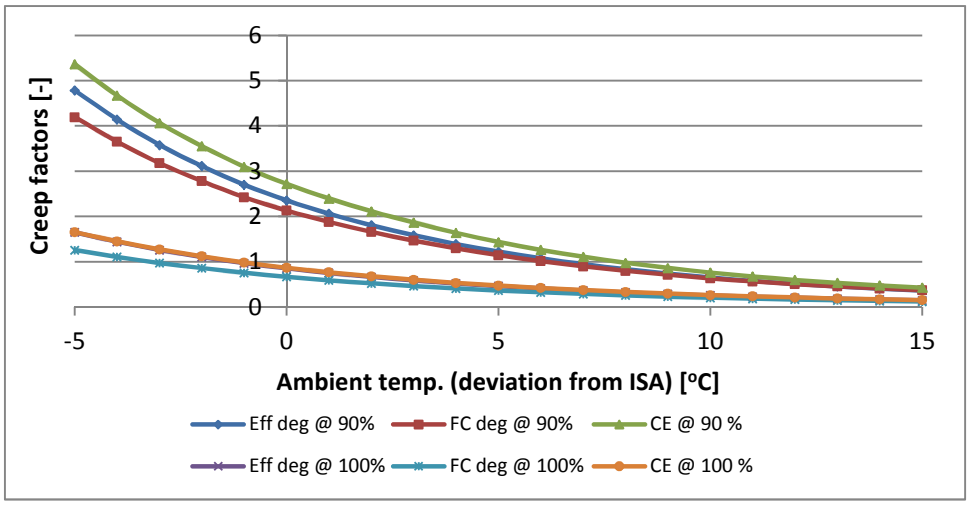

Figure 6.20: Comparison of the Effects of Isentropic Efficiency Index Degradation and Flow Capacity Index Degradation in both Compressor and Compressor Turbine on Creep Life Consumption

Isentropic efficiency index reduction in both components has less effect on creep life with average percentage decreases in in creep factors of 13.93% and 2.14% respectively at 90% and 100% power levels compared to flow capacity index reduction which gives average percentage decrease in creep factors of 19.07% and 22.52% respectively at the two power levels. The creep factors for both degradation cases are lower than those of the clean engine at the two power levels and ambient temperatures. At the 100% power level, efficiency degradation gives very little reduction in creep factors at all ambient temperatures. The effect of isentropic efficiency index reduction in both components on creep life is lower than the effect compressor isentropic index reduction has on creep life. This is because the compressor turbine isentropic efficiency reduction affects creep life positively, thus the combined effect of isentropic efficiency degradation in both components on creep life is less than the effect from only compressor isentropic efficiency index reduction. The average percentage decrease in creep factors due to compressor isentropic efficiency index reduction at 100% power level is 12.46% as stated earlier, and this is much higher than the value gotten from both components degradation which is 2.14%. Table 6.3 summarises the effect of the reduction of different health parameters on creep life using the values of the average percentage decrease in creep factors evaluated at 90% and 100% power levels.

Table 6.3: Comparison of Effects of Health Parameter Reductions on Creep Life

SN.	Component	Degraded Parameter		Average Percentage Decrease in Creep Factor [-]	
		Eff. Index [%]	FC Index [%]	90%	100%
1	Compressor	-1	0	16.34	12.46
2	Compressor	0	-1	5.38	8.50
3	Compressor Turbine	-1	0	-4.36	-11.78
4	Compressor Turbine	0	-1	13.77	15.25
5	Both Components	-1	0	13.93	2.13
6	Both Components	0	-1	19.07	33.52

All the components health parameter degradation cases lead to life reduction except compressor turbine isentropic efficiency reduction which leads to increase in creep factor. The positive effect of compressor turbine isentropic efficiency reduction on creep life accounts for lower values of average percentage decrease in creep factor in both components compared to the values in compressor isentropic efficiency reduction.

6.4.4 Effect of Compressor Degradation on Creep Life Consumption

Two cases of compressor degradation are considered. These are 1% reduction in compressor isentropic efficiency and compressor flow capacity indices, and 2% reduction in compressor isentropic efficiency and compressor flow capacity indices. The respective effects of engine degradation on creep life were carried out at 70% to 100% power levels and ambient temperatures in the range 10°C to 30°C, expressed in term of deviations from ISA condition. The creep factors for three different power levels for the ambient temperature range are shown in Figure 6.21 (a) and (b) for the 1% and 2% degradation cases respectively.

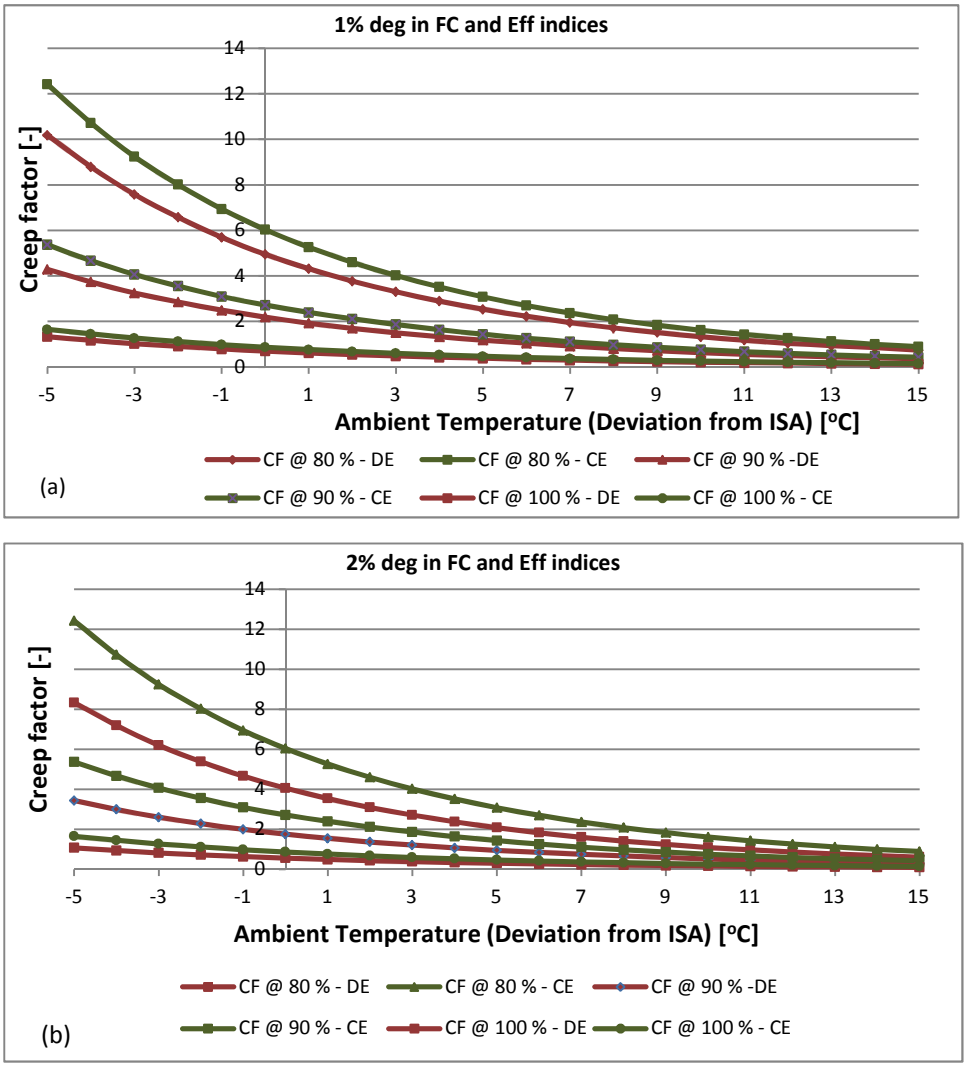

Figure 6.21: Creep Factors for Clean and Degraded Engines (Compressor Degradation) at Different Power Levels

The creep factors for the clean engine (CE) are also presented in the figures together with those of the degraded engines (DE) for the purpose of comparison. The creep factors for degraded engines are lower than those of the clean engines at the different power levels and ambient temperatures. The variation of creep factors with ambient temperature and power for the degraded engines is similar to those of the clean engines-higher at lower power level and lower ambient temperatures. Also at lower ambient temperatures, the difference between the creep factor values for the clean and degraded engines are higher compared to higher ambient temperatures.

Comparing the results of the 1% degradation with the 2% degradation, the creep factors of the 1% degradation case are higher than those of the 2% degradation case at the power levels and ambient temperatures; the degraded engine creep factors are closer to the clean engine creep factors in Figure 6.21 (a) than in Figure 6.21 (b). To make proper comparison between the two cases of degradation, average percentage decrease in creep factors at the various power levels should be estimated. The average percentage decrease in creep factors at 90% power level for 1% and 2% degradations are 18.44% and 33.71% respectively. This shows that the engine with 2% degradation has greater impact on creep life and blade failure will occur faster compared to the engine with 1% degradation. Also, the results show that doubling the values of the degradation indices (increasing by 100%) does not double the rate of life reduction (the average percentage decrease in creep factors at 90% power level increased by 82.81% in this case). The average percentage decrease in creep factors increases slightly with power level, indicating that there is high tendency to reduce creep life faster if degraded engine operates at higher power levels. The average percentage decrease in creep factors for 1% degradation at 80%, 90% and 100% power levels are respectively 17.56%, 18.44% and 19.30%.

The differences between the creep factors for clean and degraded engines are higher at lower shaft power and lower ambient temperatures. This is because large creep factor values are obtainable at lower power levels and lower ambient temperatures and the effect of degradation which will lead to a given percentage decrease in creep factors will lead to large reductions in creep factors at lower power levels and lower ambient temperatures. The decreases in the creep factors due to compressor degradation (1%

reduction in flow capacity and isentropic efficiency indices) at 80% and 100% power levels for different ambient temperatures are shown in Figure 6.22.

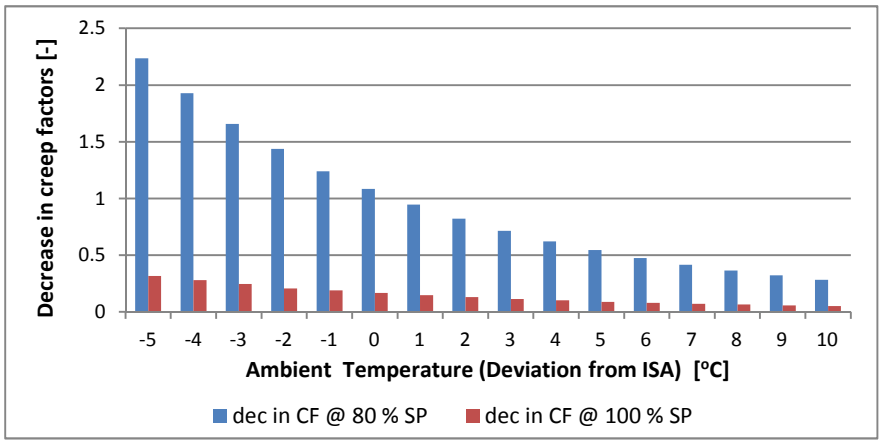

Figure 6.22: Decrease in Creep Factors Due to Compressor Degradation at different Power Levels

Larger decrease in creep factors occur in lower ambient temperatures and and lower shaft power levels, and the reason for this has already been adduced. In terms of percentage decrease in creep factor, on the average, the percentage decrease in creep factor due to compressor degradation considering all ambient temperatures is almost the same at lower power levels, but increases greatly towards peak power operation. This is shown in Figure 6.23. This is because towards peak power operations of the engine the compression process becomes less efficient and relative increase in hot gases with degradation is higher.

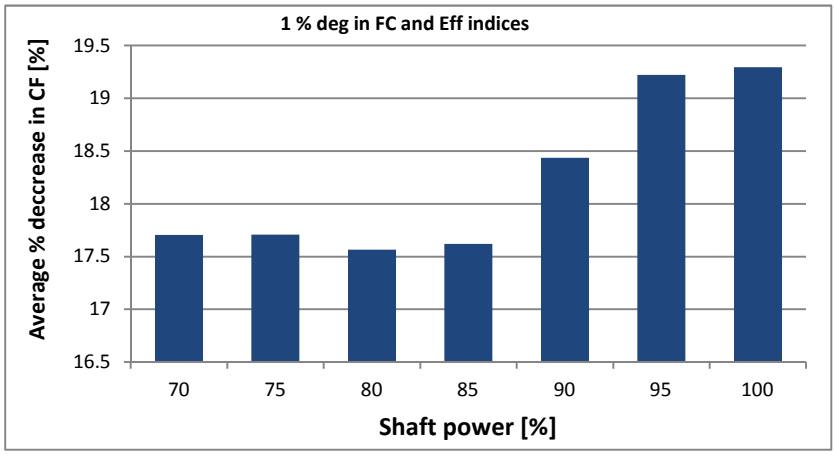

Figure 6.23: Average Percentage Decrease in Creep Factors with Compressor Degradation at Different Power Levels

The 2% reduction in compressor flow capacity and isentropic efficiency indices gave percentage reduction in creep factors similar to 1% degradation case. This is shown in Figure 6.24.

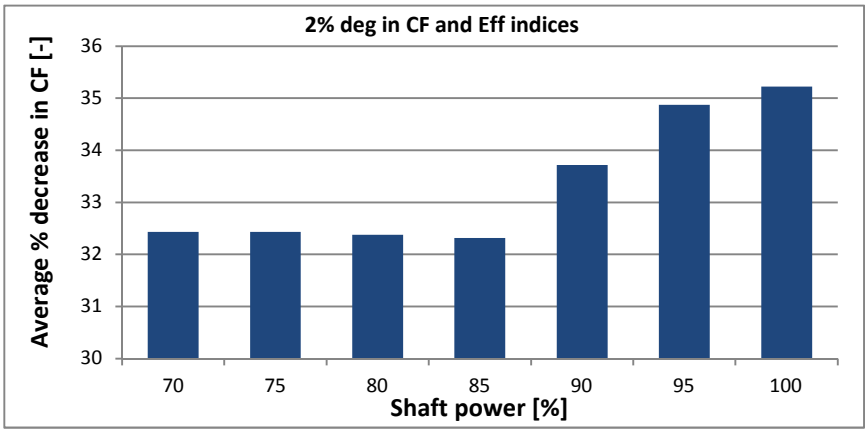

Figure 6.24: Average Percentage Decrease in Creep Factors with Compressor Degradation at different Power Levels - 2% Deg. in FC and Eff. Indices

The average percentage decrease in creep factors for both cases of degradation increases with shaft power. It is pertinent to point out that the values of the average percentage decreases in creep factors at 2% degradation case do not double those of the 1% degradation case for all the power levels considered.

6.4.5 Effect of Compressor Turbine Degradation on Creep Life Consumption

The effect of compressor turbine degradation on creep life is similar to that of compressor degradation on creep life but of less magnitude. Figure 6.25 shows the creep factors obtained for 1% reduction in compressor turbine flow capacity and isentropic efficiency indices at different temperatures for three power levels together with the creep factors of the clean engine for the purpose of comparison. At any ambient temperature, the difference in creep factors between the degraded engine and the clean gets smaller at higher shaft power levels. At 100% power level, the creep factors for the degraded engine are almost the same as those of the clean engine. Also, at any power level, the difference between the creep factors of the degraded engine and the clean engine reduces with increase in ambient temperature. The average percentage decrease in creep factors for 1% degradation case at 80%, 90% and 100% power levels are 11.99%, 10.35%, and 4.93% respectively; these values are much lower than the values

obtained in compressor degradation. Compressor turbine degradation has less effect on the creep life of the hot section blades compared to compressor degradation because what goes on in the later stages of the turbine as the required power is set is basically influenced in the compression stage. Also, compressor turbine isentropic efficiency reduction has positive effect on creep life.

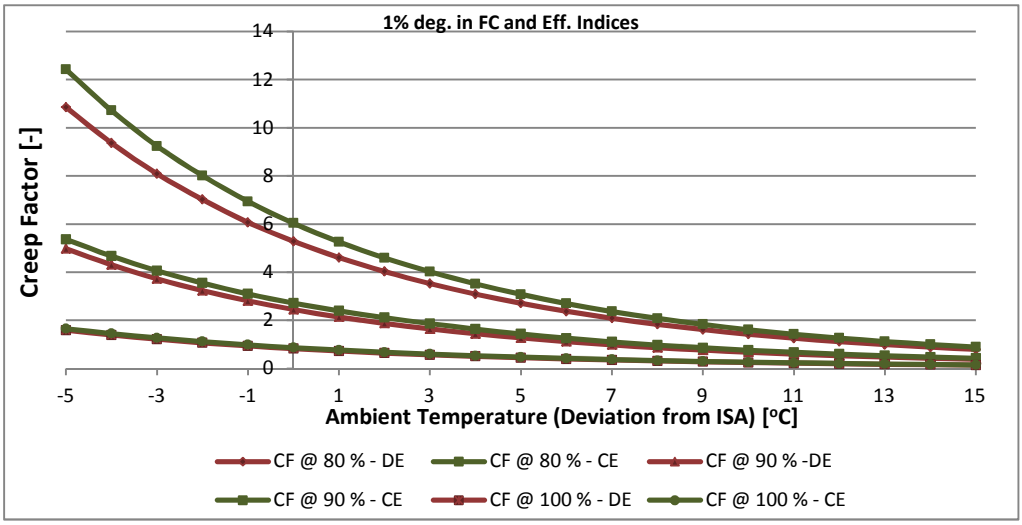

Figure 6.25: Creep Factors for Clean and Degraded Engines (HP Turbine Degradation) at different Power Levels

The 2% reduction in HP turbine flow capacity and isentropic efficiency indices produces creep factors which trend is like that of the clean engine with average percentage decreases in creep factors of 24.31%, 23.42% and 9.74% respectively at the three power levels (80%, 90% and 100%). The average percentage decrease in creep factors obtained at 80% and 90% power levels are more than twice the values obtained for 1% reduction in the health parameter indices of the compressor turbine, unlike the case of compressor degradation. Unlike compressor degradation, the average percentage decrease in creep factor with turbine degradation is higher in the lower power band but has no regular trend. This is shown in Figure 6.26 for 1% reduction in compressor turbine flow capacity and isentropic efficiency indices.

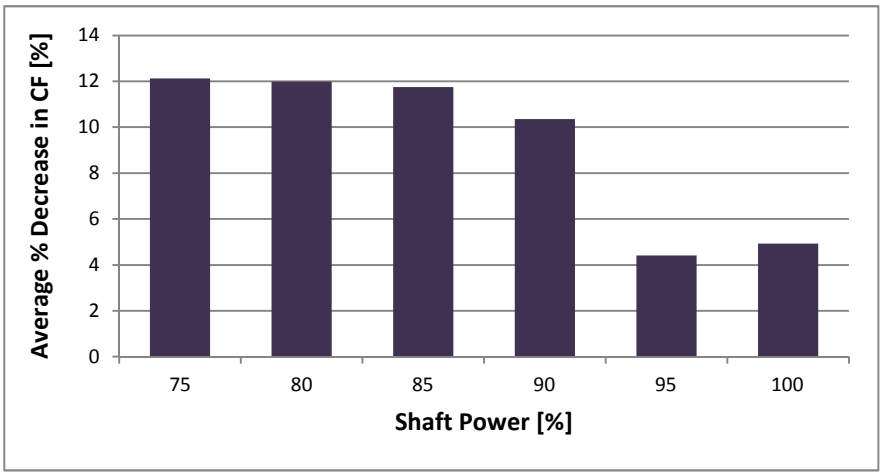

Figure 6.26: Average Percentage Decrease in Creep Factors with Compressor Turbine Degradation at different Power Levels

The above occurrence is because turbine is more efficient in the higher power band and the effects introduced by degradation of the turbine are less in the more efficient operating region of the turbine.

6.4.6 Effects of Compressor and Compressor Turbine Degradations on Creep Life Consumption

The combined effect of compressor and compressor turbine degradations on creep life as may be expected is similar to the effect either component degradation has on creep life but of higher magnitude.

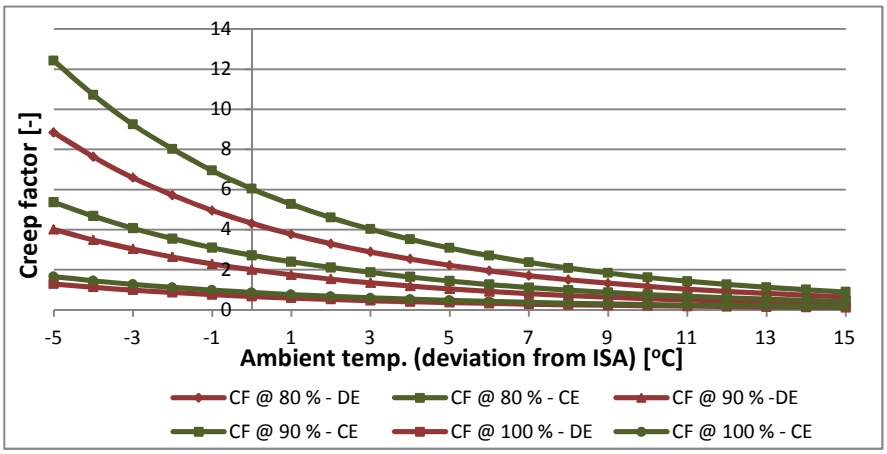

Figure 6.27: Creep Factors for Clean and Degraded Engines (Compressor and Compressor Turbine Degradation) at different Power Levels

Figure 6.27 compares the creep factors due to degradation of both compressor and compressor turbine degradation with the creep factors of the clean engine at three different power levels. The creep factors due to degradation of both compressor and compressor turbine are lower than those of the clean engine at all ambient temperatures and shaft power levels considered; like in the cases of individual component degradations, the difference between the creep factors are more noticeable at lower ambient temperatures and lower shaft power levels. The manner in the percentage decrease in creep factors with shaft power is skewed towards that of turbine degradation as shown in Figure 6.28. This should be expected as the operation of the compressor turbine influences the operation of the compressor.

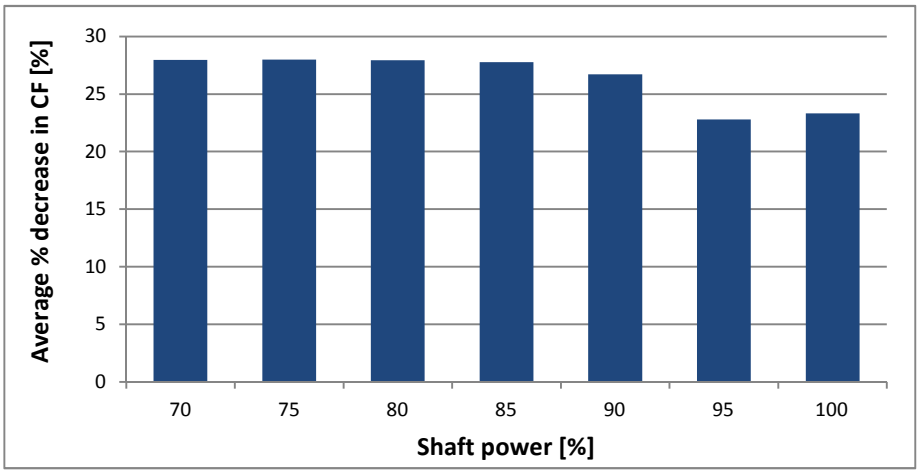

Figure 6.28: Average Percentage Decrease in Creep Factors with Compressor and Compressor Turbine Degradations at Different Power Levels

The average percentage decreases in creep factors for the 1% degradation case at 80%, 90% and 100% power levels are 27.94%, 26.70% and 23.32% respectively. The respective values for the 2% degradation case are 49.33%, 48.86% and 41.70. Like in the case of compressor degradation, increasing the degradation indices by a factor of two does not increase the average percentage decrease in creep factors by a factor of two. 2% degradation in the health parameters of both components at the operating conditions considered nearly reduced the creep life to half the value in clean engine operation. Comparison of the effects on creep life due to degradation of the various components will suffice.

6.4.7 Comparisons of Parameters in the various cases of Components Degradations

The average percentage decrease in creep factors at all ambient temperatures at the different power levels due to degradation of the various components could be compared to reveal the relative influence the degradation of each component has on creep life. Figure 6.29 shows decreases in creep factors due to compressor degradation, turbine degradation and degradation of both components (for 1% degradation in the respective health parameter indices) at 80% power level while Figure 6.30 shows the respective values at 100% power level.

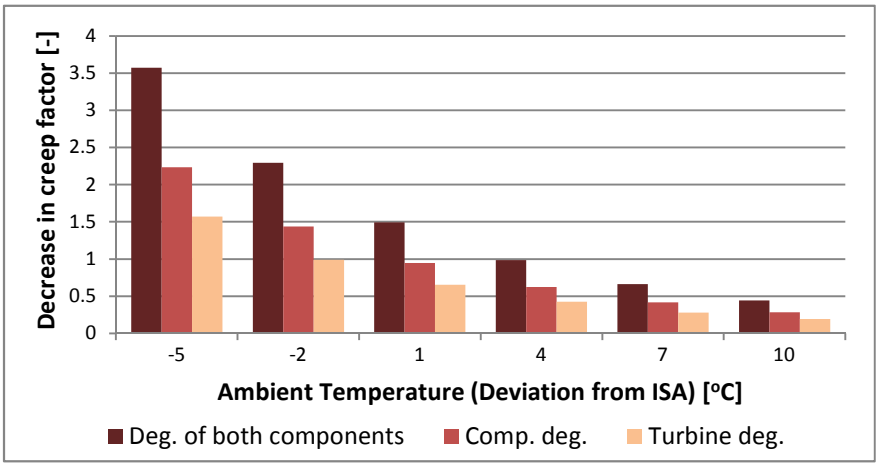

Figure 6.29: Comparison of Decreases in Creep Factor Values with different Components Degradations at 80% Power Level

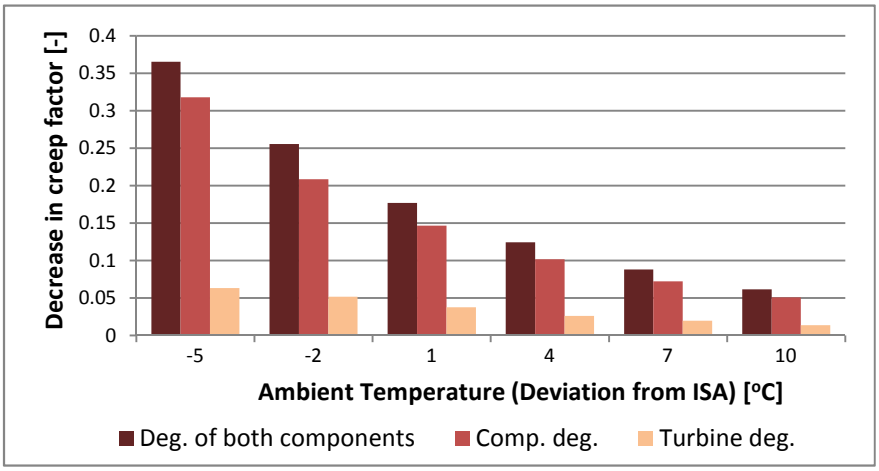

Figure 6.30: Comparison of Decreases in Creep Factor Values with Different Components Degradations At 100% Power Level

At all ambient temperatures, degradation of each component leads to higher reduction in creep factor and hence creep life at lower ambient temperatures and lower shaft powers, and the reasons for these occurrences have been given in previous sections. The sums of the reductions in creep factors due to degradations in each component are slightly higher than those of both components degradations at all ambient temperatures. The sum of the average percentage decrease in creep factors due to degradations in each component is also slightly higher than the average percentage decrease in creep factors due to both components degradations at any power level for both 1% and 2% degradation cases. For 1% degradation case at 90% power level, the average percentage decrease in creep factors due to compressor degradation, compressor turbine degradation, and both components degradations are respectively 18.44%, 10.35% and 26.70%. The sum of the average percentage decrease in creep factors due to compressor and compressor turbine degradations is 28.79% which is a bit higher than 26.70%. Compressor degradation has more effect on creep life than compressor turbine degradation at all power levels and ambient temperatures as shown by the values of average percentage decrease in creep factors.

Only 1 % and 2% degradations in flow capacity and isentropic efficiency is considered respectively in each of the components- compressor, compressor turbine, and both compressor and compressor turbine. The effect of degradation of each component on creep life has been investigated and significant reduction in creep life is obtainable due to components degradation. Higher percentage degradation in flow capacity and isentropic efficiency in each of the components leads to higher rate of reduction in creep life, although not shown in this work. Compressor degradation has more effect on creep life than turbine degradation as noted previously. Compressor degradation also comes more often than turbine degradation. Compressor degradation may occur in the form of compressor fouling (deposition of debris in the airstream on compressor blades and disc) which is a very common occurrence. Compressor fouling is a recoverable degradation and it is corrected by either online washing or offline washing or combination of both methods. The debris comes from the air and irrespective of the efficiency of the air filtering system, compressor fouling will occur, the nature of the environment playing a key role. In online washing, it is difficult to prevent all the debris dislodged from the early stages of the compressor stage from settling in the latter stages.

Operators of turbines often view the negative effect of degradation in terms of additional energy cost in maintaining same power, but this work reveals that blade life consumption is faster with engine components degradations and operators should worry about that as well.

6.5 Comparison of the Various Effects on Creep Life Consumption

The effect of ambient temperature variation on creep life is expressed in terms of percentage decrease in creep factors with ambient temperature increase. In doing this, ambient temperature of 5^{o}C (expressed in terms of deviation from ISA condition) is used as a base temperature. Results of average percentage decrease in creep factors with unit increase in ambient temperature are also expressed. In investigating the effect of ambient temperature on creep life, at a given power level, percentage decreases in creep factors due to unit ambient temperature increase are evaluated for a range of ambient temperatures and the average value taken at the specified power level. The effect of shaft power increase on creep life could be examined by computing the average percentage decrease in creep factors with shaft power increase at different ambient temperatures. For degradation, the values of average percentage decrease in creep factors are computed by comparing the creep factor values of the clean engine with those of the degraded engine at the different ambient temperatures and power levels.

To have a complete or holistic view of the various effects on creep life, the manner of obtaining the average percentage decrease in creep factor should be specified. The average percentage decrease in creep factors due to power increase is obtained at a particular ambient temperature; this could be obtained at the different ambient temperatures (-10^{o}C to 15^{o}C deviation from ISA) where the range and the mean value could be gotten. The average percentage decrease in creep factors due to power variation reduces with ambient temperature, Figure 6.31; this is because air becomes less compressible at higher ambient temperatures and changes in the properties of air reduce with increase in ambient temperature.

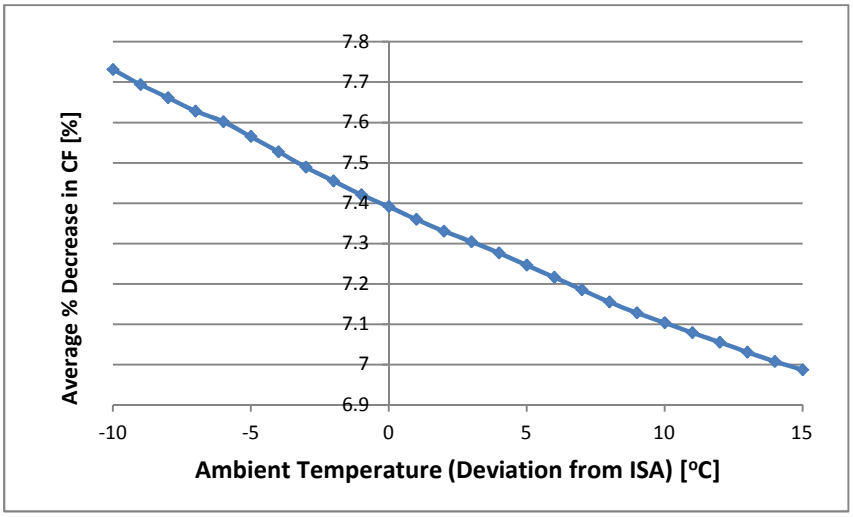

Figure 6.31: Average Percentage Decrease in Creep Factors due to Shaft Power Increase at different Ambient Temperatures

Considering the effects of ambient temperature variation, shaft power variation, the different cases of engine degradation and the average percentage decrease in creep factors defined for the various effect on creep life, the impact of the various effects on creep life could be presented in their respective distinct forms and comparisons made should indicate the ambient temperatures and the power levels at which the results are obtained. Table 6.4 summarises the impact of the various effects on creep life. In each effect, a range of the average percentage decrease in creep factors is given, together with a mean value. For instance, in a unit drop in ambient temperature, the average percentage decreases in creep factors are evaluated at 70% to 100% power levels. The range indicates the smallest value and the highest value, while the mean value is calculated using all the average percentage decreases in creep factors at the different power levels. For the component degradations, results are shown for 1% and 2% degradations in the health parameter indices of the respective components (cases VII, VIII and IX in Table 6.2).

Table 6.4: Summary of Various Effects on Creep Life Consumption

SN.	Effect	Average % Decrease in Creep Factors [-]	
		Range	Mean Value
1	Unit increase in ambient temperature	11.56-12.83	12.33
2	1% increase in shaft power	6.49-8.64	7.33
3	Unit increase in shaft power	21.64-28.81	24.44
4	Compressor degradation (1%)	17.62-19.30	18.22
5	Compressor degradation (2%)	32.31-35.22	33.34
6	Compressor turbine degradation (1%)	4.41-12.19	9.68
7	Compressor turbine degradation (2%)	9.74-24.38	20.26
8	Both components degradation (1%)	22.81-28.00	26.36
9	Both components degradation (2%)	41.70-49.42	47.21

The effects of ambient temperature, shaft power, and engine degradation on creep life presented in Table 6.4 are applicable for the ambient temperatures and shaft power levels used in analysing the creep life consumption of the LM2500+ engine used in this research. For unit increase in ambient temperature, the lower value in the range occurs at the highest power level while the higher value occurs at the lowest power level. For 1% increase in shaft power, the lower value in the range occurs at the highest ambient temperature considered while the higher value occurs at the lowest ambient temperature. In compressor degradation, the highest average percentage decrease in creep factors considering all ambient temperatures occurs at the highest power level while in compressor turbine degradation, the highest average percentage decrease in creep factors is obtained at the lowest power level considered. In both components degradation, the lowest average percentage decrease in creep factors is obtained at the highest power level. Comparing the various effects on creep life, 1% increase in shaft power has the lowest impact on creep life, but it should be made clear that power variation is made in terms of unit percentage increase. A unit increase in shaft power has more effect 1% degradation in any component. If ambient temperature increase is expressed in terms of percentage increase, its effect on creep life will be the lowest. The above results are only comparable at the specified changes in the quantities concerned.

6.6 Chapter Conclusions

Creep life consumption, creep life tracking and the influences of shaft power variation, ambient temperature variation, and engine degradation on creep life are considered in this chapter. The Larson-Miller Parameter method is used for creep life analysis. The blade material temperature and stresses at different sections along the blade are provided by the blade thermal and stress models presented in Chapter 4. The LMP value is read based on the stress value estimated at each point of engine operation. Robinson life fraction rule is applied to accumulate the creep life consumption for different periods of engine operation, and to estimate the equivalent creep life for the same periods of engine operation. Absolute creep life estimated may not be very accurate. Thus relative creep life analysis is carried out using the creep factor concept. Equivalent creep factor is introduced to assess the severity of engine operation over any period of time - this is the creep life estimation methodology presented in chapter 3. An integrated creep life assessment system is developed and engine creep life at different periods of engine operation could be estimated.

Engine creep life tracking is carried out by using data of 8 months of engine operation to illustrate how engine creep life could be tracked using the developed algorithms in this research. The creep life tracking produces results which are comparable with those in real engine operation conditions thus confirming the accuracy of the life tracking algorithms developed in this research.

In investigating the influences of shaft power variation, ambient temperature variation and engine degradation on creep life, the following are the basic findings:

- Creep life generally reduces with an increase in shaft power, but increases with reduction in shaft power at all ambient temperatures.
- The increase in creep life as power drops from higher levels to lower levels increases initially and later drops- more favourable life increase occurs towards peak power operation of the engine at any ambient temperature.
- Creep factor / creep life decreases with an increase in ambient temperature. At a given power level, the rate of decrease in creep factors with ambient temperature is smaller at higher ambient temperatures.

- Creep life increases with ambient temperature drop in the same magnitudes as ambient temperature increase does to creep life reduction.
- Judging by the values of the average percentage decrease in creep factors due to engine components degradation:
    - Compressor isentropic efficiency index reduction has more impact on engine life than compressor flow capacity index reduction.
    - Compressor turbine isentropic efficiency index reduction has little positive effect on creep life.
    - Compressor turbine flow capacity index reduction has more impact on creep life than compressor flow capacity index reduction.
    - Flow capacity index reduction in both components has more impact on creep life than isentropic efficiency index reduction.
- For 1% and 2% reductions in efficiency and flow capacity indices of compressor and compressor turbine respectively, the creep life / creep factors are reduced. The trends of the creep life / creep factors are similar to those of the clean engines.
- Increasing the engine health parameter reduction by 100% does not increase the average percentage decrease in creep factors by 100% for compressor degradation, but the average percentage decrease in creep factors is increased by more than 100% at lower power levels for compressor turbine degradation.
- The reduction in creep life due to engine degradation is more pronounced in lower ambient temperatures and lower shaft power levels.
- From the values of the average percentage decrease in creep factors:
    - Compressor degradation has more impact on creep life than compressor turbine degradation.
    - A unit increase in ambient temperature has more impact on creep life than 1% degradation of compressor turbine but has less impact compared to 1% degradation of compressor.
    - 1% increase in engine shaft power has less impact on creep life compared to unit increase in ambient temperature, but a unit increase in shaft power has more impact on creep life than 1% degradation of compressor.

7 LOW CYCLE FATIGUE (LCF) LIFE ANALYSIS

Low cycle fatigue life analysis involves the strain-life approach to fatigue life analysis, where a component in most cases is believed to undergo plastic deformation before failing. Fatigue life consumption analysis of a component involves the determination of the number of cycles to failure at a given stress amplitude, and the number of stress cycles corresponding to a given block of load defined by the stress amplitude. The stress amplitudes at different engine operation points are obtained from the stress model presented in Chapter 4. The equivalent fatigue or stress cycles accumulated at any point of engine operation is estimated from the values of the stress amplitudes. In this research, a low cycle fatigue model is adopted to calculate the cycles to fatigue failure at a given stress amplitude while a new cycle counting method is developed to estimate the equivalent stress cycles (fatigue cycles) in each block of load. The methodologies employed in the fatigue life consumption analysis of the HP turbine blades of the LM2500+ engine used in this research is presented in chapter 3. The developed methodolies are applied to real engine operation data in this chapter. Before considering the application of the developed fatigue life consumption methodolies, the fatigue cycles counting model presented in Chapter 3 is applied to real engine operation data to estimate the fatigue cycles.

7.1 Application of Fatigue Cycles Counting Model

Figure 7.1 shows four different days of engine operation and the equivalent fatigue cycles recorded using the proposed model with $k = 0.95$. The equivalent number of cycles depends on the transition of shaft speed from one point to the other. Comparing Figure 7.1 (a) and (b), the shaft speed variation from point to point is more pronounced in Figure 7.1 (a) than in Figure 7.1 (b), hence the equivalent number of fatigue cycles is higher in Figure 7.1 (a). In Figure 7.1 (c) and (d), more uniform shaft speed levels are recorded leading to lower equivalent fatigue cycles compared to Figure 7.1 (a) and (b). The respective results from the aircraft model where only type 3 speed transitions are obtainable are approximately 2.875, 2.675, 1.975 and 1.850 respectively. The two sets of results are comparable but the proposed model accounts for stress variations not accounted for in the air-craft model hence the larger values.

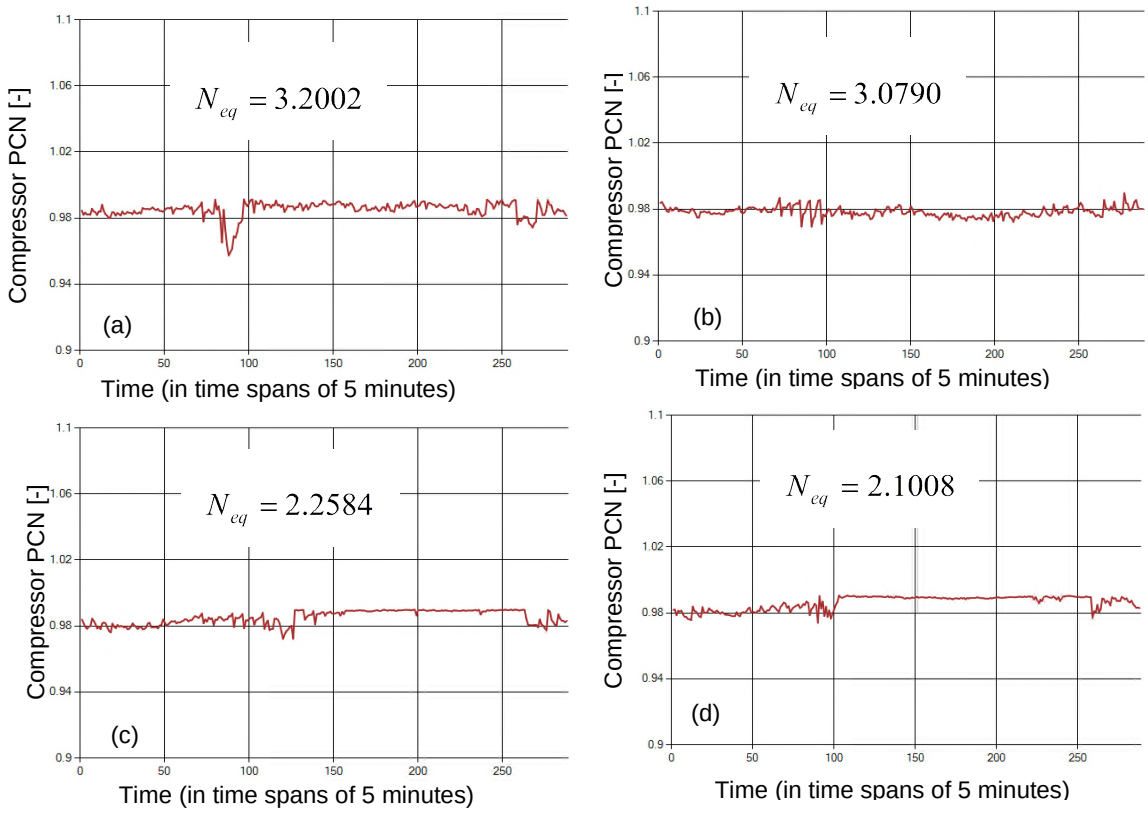

Figure 7.1: Shaft Speed Variation and Equivalent Number of Fatigue Cycles with Proposed Model

7.2 Low Cycle Fatigue Life Tracking: A Case Study

In life tracking for gas turbine that is shut down daily, the equivalent fatigue factors will indicate how engine life is consumed due to fatigue as a result of frequent engine shut down. In the absence of engine shut down, the cycle counting model developed accumulates the fatigue cycles experienced as a result of variations in the stresses imposed on rotating engine components with time. The fatigue life algorithm developed in this research is applied to 8 months of engine operation using real engine field data to ascertain the applicability of the developed algorithms. Figure 7.2 shows the equivalent daily fatigue factors for 8 months of engine operation. It is same data used for the creep life tracking. The equivalent fatigue factors are lower in January, February and March of engine operation compared to the values obtained in June, July and August. This is because fatigue life depends on the stresses on the blades which arise from engine shaft

speed and momentum changes. The latter depends on the amount of air intake. In January, February and March, lower ambient temperatures are recorded leading to higher air intake (due to increase in air density with temperature drop). Even if shaft speed is constant, only the centrifugal stress component will be constant, but the increase in intake air leads to increase in the momentum change stresses and hence higher alternating stress amplitude on the blades.

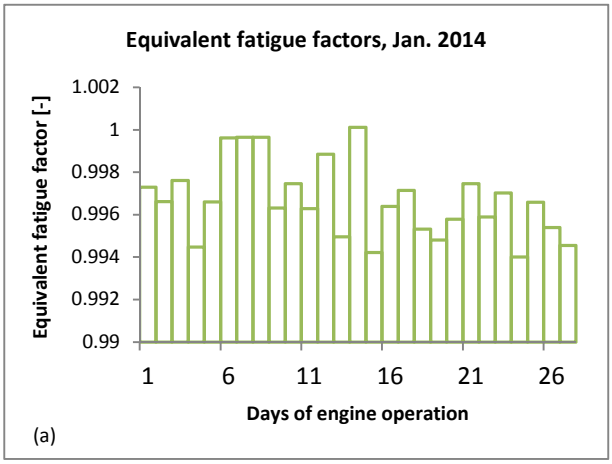

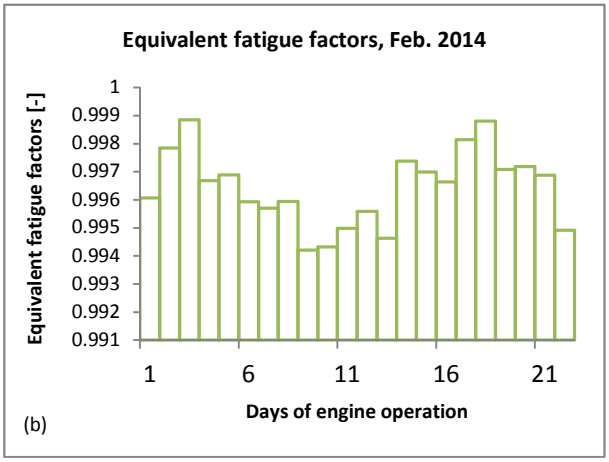

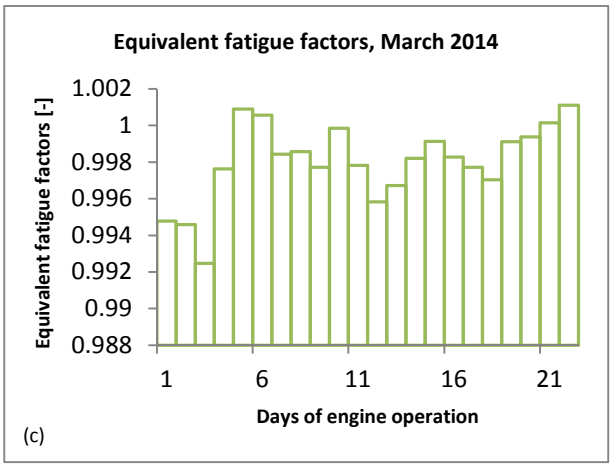

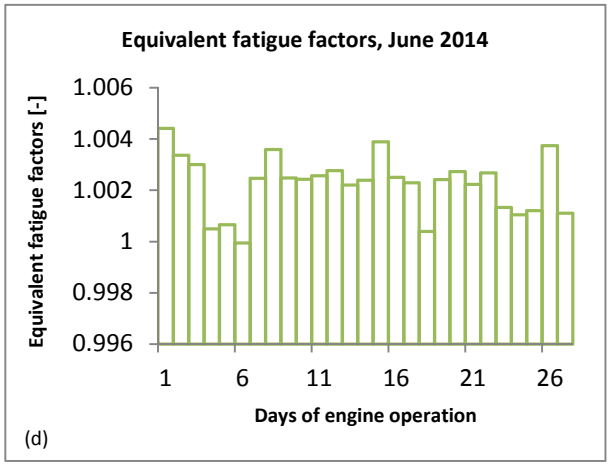

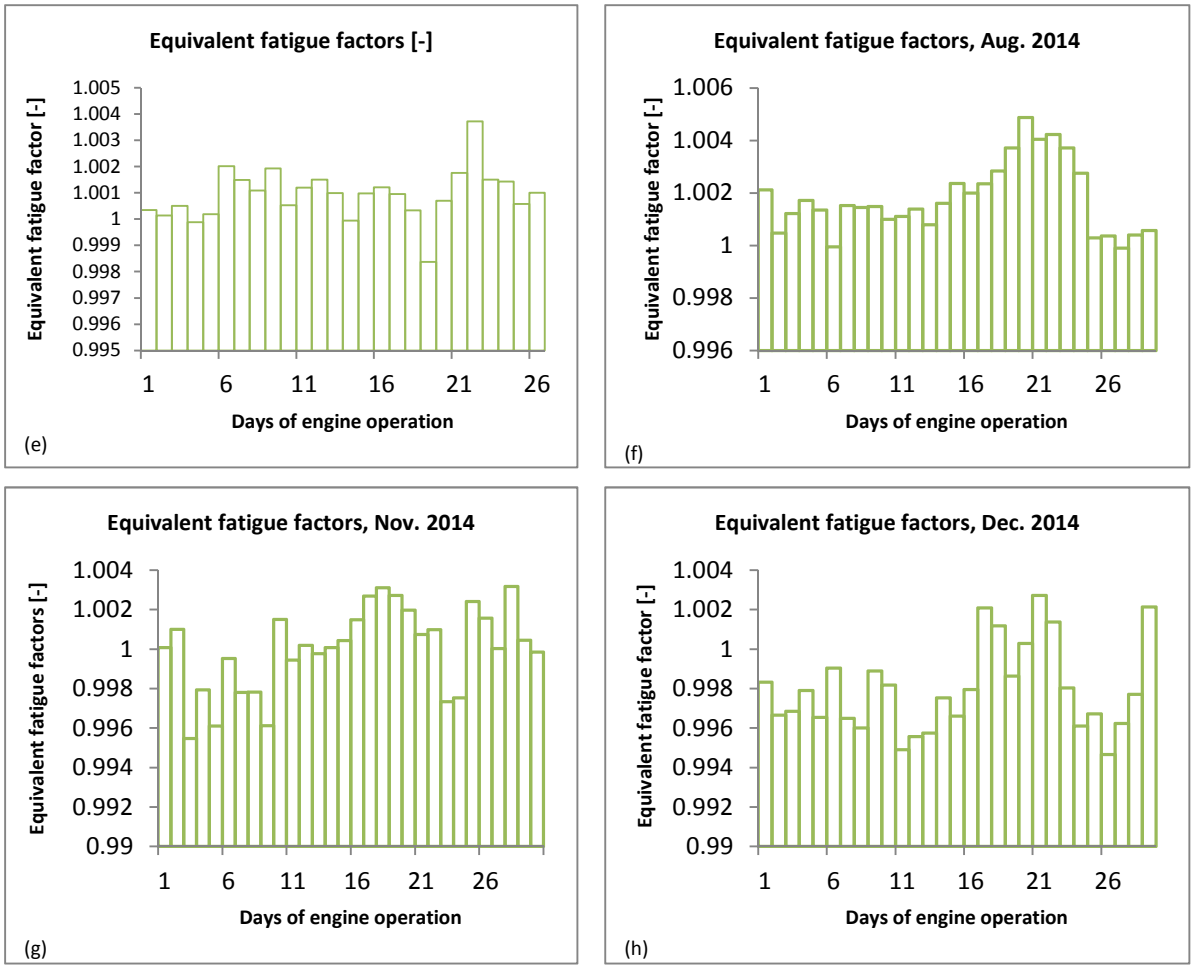

Figure 7.2: Equivalent Fatigue Factors for Different Months of Engine Operation

If engine is shut down from high levels of alternating stress amplitudes in each day of engine operation, fatigue life consumption is faster, and the equivalent fatigue factor which indicates the wellness of engine operation due to fatigue is lower. The equivalent fatigue factors are thus lower in the months of January, February and March compared to the months of June, July and August of engine operation. Higher fatigue factors indicate lower risk to fatigue failure. November engine operation is also safe in terms of fatigue life consumption as the equivalent fatigue factor is greater than unity for a number of days. In December, lower ambient temperatures were recorded with increased air mass intake and hence higher alternating stress amplitudes on the blades like in January, February and March of engine operation; the equivalent fatigue factors are thus quite low in many of the days.

The equivalent fatigue factor for each month of engine operation will give a general picture of how engine fatigue life is consumed in each of the months of engine operation. Figure 7.3 shows the monthly equivalent fatigue factors for each of the months of engine operation. The monthly equivalent fatigue factors are highest in June, July and August, while lower values are recorded in January, February, March and December. The overall equivalent fatigue factor (indicated as OEFF) is also included in Figure 7.3. The overall equivalent fatigue factor is a little above unity. This means the fatigue life consumption of the blades is favourable in the period of engine operation. The equivalent fatigue factor for each month of engine operation is different from the overall equivalent fatigue factor. The closest monthly equivalent fatigue factor to the overall equivalent value is the value in November. Engine fatigue life tracking, like creep life tracking, requires the usage of large amount of engine operation data especially when the results are to be relied on for future life consumption predictions.

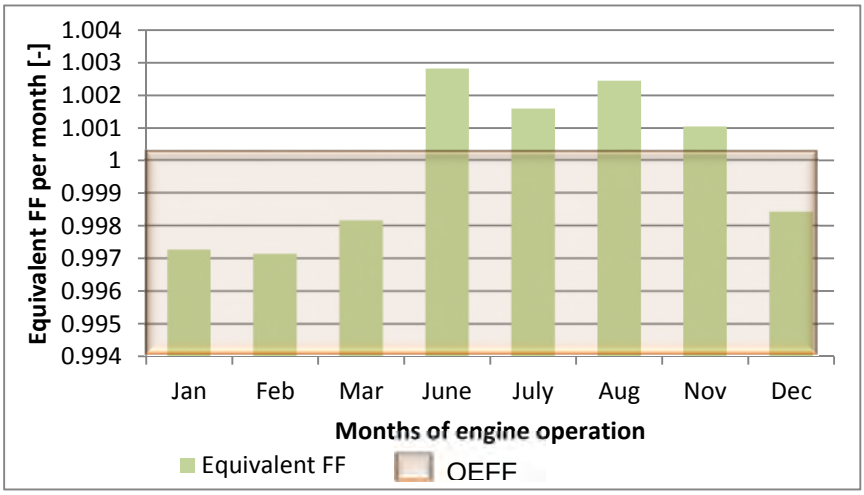

Figure 7.3: Equivalent Fatigue Factors for each month of Engine Operation

The fatigue cycles accumulated per period of engine operation using the cycle counting model developed in this research reveals the extent of stress variations, but this does not tell the level of the maximum stresses experienced. Thus the fatigue factors do not have similar trend with the mean fatigue cycles per day recorded for the various months, Table 7.1. From Table 7.1, smoothest engine operation was recorded in November.

Table 7.1: Engine Operation Data and Mean Fatigue Cycles per Day

S/N	Month	Number of days of Engine Operation	Mean Fatigue Cycles Per Day
1	January	27	5.03
2	February	22	4.87
3	March	22	5.35
4	June	27	6.13
5	July	26	5.48
6	August	29	6.56
7	November	30	2.07
8	December	29	2.37

The equivalent fatigue factors obtained for the different months of engine operation clearly shows the manner in which ambient temperature and engine shaft power affects fatigue life. This goes to show that the algorithms developed for fatigue life tracking predicts engine fatigue life consumption accurately. This validates the models and the life tracking technique could be employed in tracking the life of other engine models. The use of the fatigue factors and the equivalent fatigue factor in fatigue life tracking also evades the excessive accuracy factor required in real fatigue life estimation and provides a means for predicting the manner/trend of engine fatigue life consumption.

7.3 Effects of Ambient Temperature and Shaft Power Variation on Fatigue Life

From the results of fatigue life tracking, it is clear that fatigue life consumption is higher if the engine is shut down from high load level. Thus fatigue life consumption appears higher during the months of low ambient temperatures where as a result of increased intake air density and hence increased intake mass, the resulting momentum stresses imposed on the blades are increased and even in cases of almost constant centrifugal stresses, the resulting stress amplitude is increased leading to shorter fatigue cycles to failure and lower equivalent fatigue factors. In investigating the effect of ambient temperature on fatigue factor, the engine power level is pinned and the engine is assumed to be operating at a constant ambient temperature before it is short down. At the prevailing ambient temperature and power level, the stress amplitude is calculated from where the cycles to failure based on the stress amplitude are estimated. The cycles to failure are compared with the cycles to failure at a reference operating point to obtain

the fatigue factor in each case. Like in the case of creep life analysis, shaft power levels of 70% to 100% of maximum power, and ambient temperatures of 5°C to 30°C (expressed in terms of deviations from ISA condition) are employed to see the effect of temperature on fatigue life at different power levels.

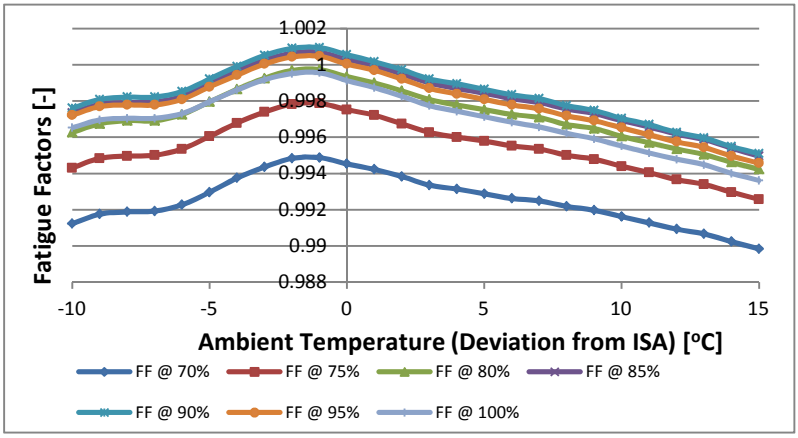

Figure 7.4: Fatigue Factors Variation with Ambient Temperature at different Shaft Power Levels

Figure 7.4 shows the effect of ambient temperature on fatigue life consumption at different power levels. At a given power level, the fatigue factors increases with ambient temperature, reach a peak value and then drops. The peak value occurs around ISA temperature deviation of -2°C (13°C). Thus at ambient temperatures between 0°C and 13°C, the fatigue factors appear to increase, indicating that failure due to fatigue decreases with ambient temperature increase in this temperature band. The above occurrence is explained here. As ambient temperature increases, the density of air drops. In the lower temperature band, the drop in air density with ambient temperature is greater leading to high drop in intake airflow. This leads to large reduction in momentum change stresses, and also tend to reduce the shaft power. To keep the shaft power constant, the compressor shaft speed increases. The increase in the shaft speed leads to increase in the centrifugal stress. The reduction in the momentum change stress is greater than the increase in the centrifugal stress in the lower ambient temperature band. The result is reduction in stress and lower alternating stress amplitude. Reduction in stress amplitude leads to increase in the number of fatigue cycles to failure and hence increase in fatigue factors. The stress amplitude reduces until ambient temperature of about -2°C ISA deviation, beyond which the centrifugal stress increase is greater than

the reduction in the momentum change stresses. The stress amplitude thus increases at the higher temperature band, defined by temperatures beyond -2^{o}C ISA deviation. This leads to the decrease in the fatigue cycles to failure and reduction in fatigue factors.

At any given power level, increasing the ambient temperature through the range of temperatures considered lead to a decrease in the fatigue factor on the average. Higher values of percentage decrease in fatigue factors due to increase in ambient temperature for the specified ambient temperature range occur at higher shaft power levels. This is shown in Figure 7.5. The trend in Figure 7.5 shows that on the average, ambient temperature has much influence on engine fatigue life at higher shaft power levels. This is because at higher shaft power levels, the stress amplitude resulting from the centrifugal stresses and the momentum change stresses are higher and the tendency to fatigue failure when engine is shut down increases.

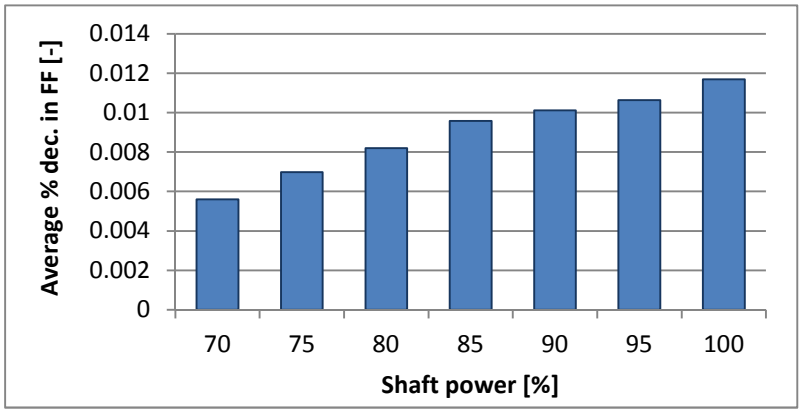

Figure 7.5: Average Percentage Decrease in Fatigue Factors with Ambient Temperature at different Power Levels

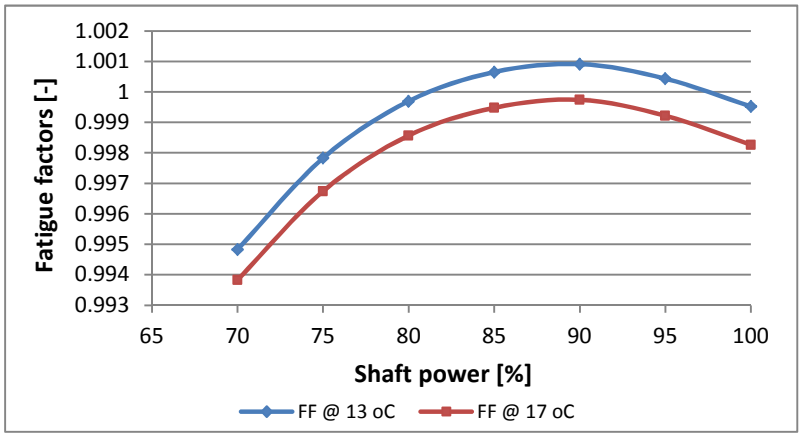

Figure 7.6: Fatigue Factor Variation with Shaft Power at Specified Ambient Temperatures

At a particular ambient temperature, the fatigue factors increases with shaft power, reaches a peak and drops. This is shown in Figure 7.6 for ambient temperatures of 13^{o}C and 17^{o}C respectively (-2^{o}C and 2^{o}C deviation from ISA).

Starting at a part load of 70%, at all ambient temperatures, fatigue factors increase as power is increased to 90%, but fatigue factors drop with further increase in shaft power. At peak load operation (100% power level), the fatigue factors are higher than those at 75% power level at all ambient temperatures. The trend in the fatigue factor variation with shaft power indicates that low part load and peak load operation exposes the engine to faster fatigue life consumption if the engine is shut down often. Engine seems to operate more efficiently around 90% power level. In this favourable region, the shaft speed needs to change only a little to maintain the required power level. In the lower power band and peak operations, changes in intake airflow will force large increase in shaft speed to maintain the required power. This leads to much increase in the alternating stress amplitude and lower cycles to fatigue failure and lower fatigue factors. At any given ambient temperature level, increasing shaft power from 70% to peak power level leads to an increase in fatigue factor on the average. The average percentage increase in fatigue factor with shaft power increase (in the specified range) decreases with increase in ambient temperature; this is shown in Figure 7.7. The average percentage increase in fatigue factors with power increase in the specified range decreases with increase in ambient temperatures because at higher ambient temperatures intake air becomes less compressible and changes in the properties of the air are less pronounced.

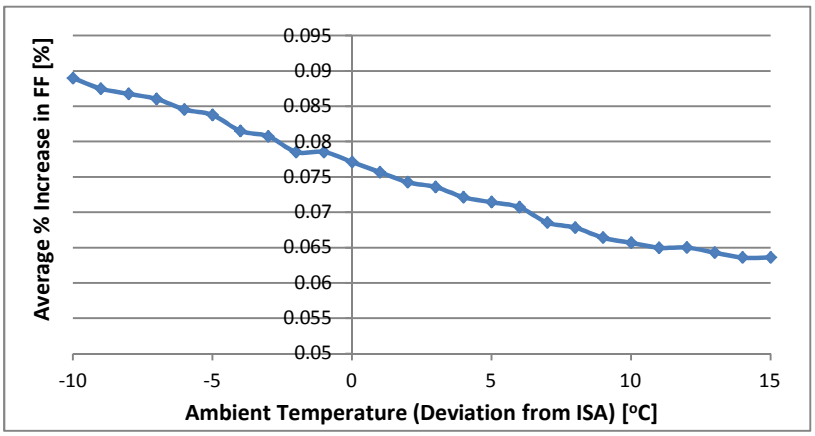

Figure 7.7: Average Percentage Increase in Fatigue Factors with Power Increase at different Ambient Temperatures

In practice, in most periods, the engine is operated between 90% power levels to peak power level; in this case, operating the engine beyond 90% leads to faster engine fatigue life consumption if engine is often shut down.

7.4 Effect of Engine Degradation on Fatigue Life

When any of the engine components is degraded, it will have effect on the fatigue life consumption, especially when the engine is often shut down. The alternating stress amplitude at any operating condition will be affected hence engine degradation will affect fatigue life consumption. Compressor is the most commonly degraded component in the gas turbine. Thus, only the effect of compressor degradation on fatigue life consumption at different power levels and ambient temperatures is considered in this research. Two cases of compressor degradation are looked at. These are 1% and 2% reductions respectively in compressor health parameter indices as shown in Table 7.2. Flow capacity index reduction in compressor also implies reduction in compressor pressure ratio (as in creep life analysis under engine degradation).

Table 7.2: Degradation Cases for Fatigue Life Analysis

Case	Component	Degraded Parameter	
		Efficiency Index [%]	Flow capacity Index [%]
I	Compressor	-1	-1
II	Compressor	-2	-2

Analyzing the fatigue life consumption under 1% and 2% reductions in compressor health parameter indices will show the extent to which the degradations affect fatigue life, and in addition, reveal the effect of doubling the health parameter indices on fatigue life. The effect of each degradation case on fatigue life will be investigated separately and the results will be compared. The sensitivity of engine life to engine component degradation, expressed in terms of percentage decrease in fatigue factors with degradation will be used to assess the effect of degradation on engine fatigue life. The fatigue factors for the clean and the degraded engines respectively will be employed in estimating the percentage decreasess in fatigue life. At each power level and the various ambient temperatures, the percentage decreases in fatigue factors is given by Equation (7.1),

$$PD_{FF,i} = \frac{FF_{CE,i} - FF_{DE,i}}{FF_{CE,i}} \times 100 \qquad (7.1)$$

$PD_{FF,i}$ is the percentage decrease in fatigue factor at each power level and at the various ambient temperatures, $FF_{CE,i}$ is the fatigue factor for the clean engine at a given power level and temperature counter i, while $FF_{DE,i}$ is the fatigue factor for the degraded engine at same power level and temperature. The value of the percentage decrease in fatigue factor indicates how engine fatigue life responds to engine degradation at the given power level and ambient temperature. Higher values of percentage decrease in fatigue factor indicate greater impact of degradation on fatigue life and vice-versa. Results of the fatigue factors of the clean and degraded engines at different power levels and ambient temperatures will be presented for comparisons.

7.4.1 Effect of 1% Reduction in Compressor Health Parameter Indices on Fatigue Life

In implanting 1% degradation in compressor isentropic efficiency index and flow capacity index respectively in the engine performance model, simulations are carried out to obtain results for the fatigue life analysis sub-model. The fatigue factors obtained at the various power levels and ambient temperatures are similar to those of the clean engine in terms of their trend, but less than those of the clean engine in terms of magnitude. Figure 7.8 shows the fatigue factors of the degraded engine together with those of the clean engine at two different power levels and various ambient temperatures. The fatigue factors of the degraded engine (DE) are lower than the fatigue factors of the clean engine (CE) at all power levels and ambient temperatures because in the degraded engine the compressor work reduces which will lead to reduced shaft power output; to keep the power output at the required level (power is used as the engine handle), the compressor speed is increased leading to greater centrifugal stresses on the blades and hence lower fatigue life and fatigue factor. The momentum stresses may reduce a little in the process with reduction in flow capacity, but the contribution from the increase in centrifugal stresses is dominant. The difference between the fatigue factors of the clean and degraded engines is slightly higher at lower power levels because the compression process is more efficient at lower power levels and also responds more to changes in the compressor health parameters at lower power levels.

The difference between the fatigue factors is almost independent of ambient temperature. This shows that fatigue failure is influenced mainly by engine shaft power and not ambient temperature. But if thermal stresses are considered also, ambient temperature will also influence fatigue failure, but not as much as shaft power does.

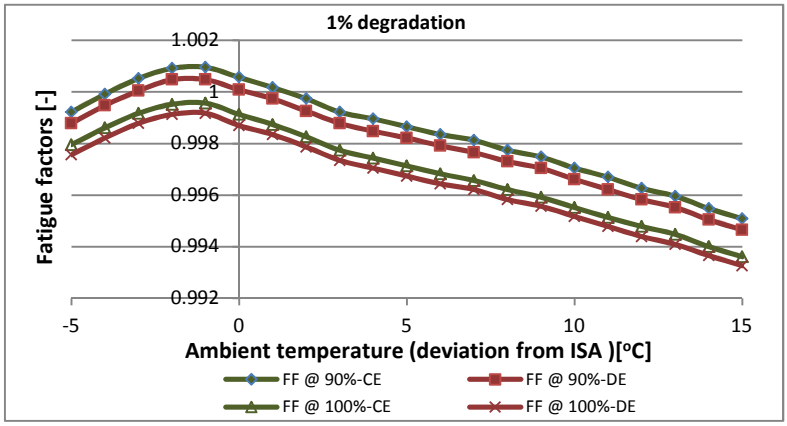

Figure 7.8: Fatigue Factors of Degraded and Clean Engines at different Power Levels and Ambient Temperatures -1% Reduction in Compressor Health Parameters

The percentage decrease in fatigue factors due to compressor degradation at each power level and various ambient temperatures is low. The average value of the percentage decrease in fatigue factors at each power level and for the specified temperature range is shown in Figure 7.9. The average percentage decrease in fatigue factors is higher at lower power levels. The percentage decrease in fatigue factors at the different power levels and various ambient temperatures are low, but, noting that fatigue cycles to failure runs into thousands, this will lead to large reduction in fatigue cycles to failure. The occurrence in Figure 7.9 depicts that compressor health parameters reduction has more impact on fatigue life reduction at lower power levels than at higher power levels. This is because of more efficient compression process at lower power levels. The average percentage decrease in fatigue factors are evaluated at each power level and ambient temperatures between -10^{o}C to 30^{o}C, expressed in terms of deviation from ISA. The results are applicable at the given power levels and the ambient temperatures where engine fatigue life is investigated. Also, the results may be slightly different for different engine models, but the trends will be the same. Noting that fatigue failure is stochastic, some level of confidence should be applied in using the results for engine condition monitoring.

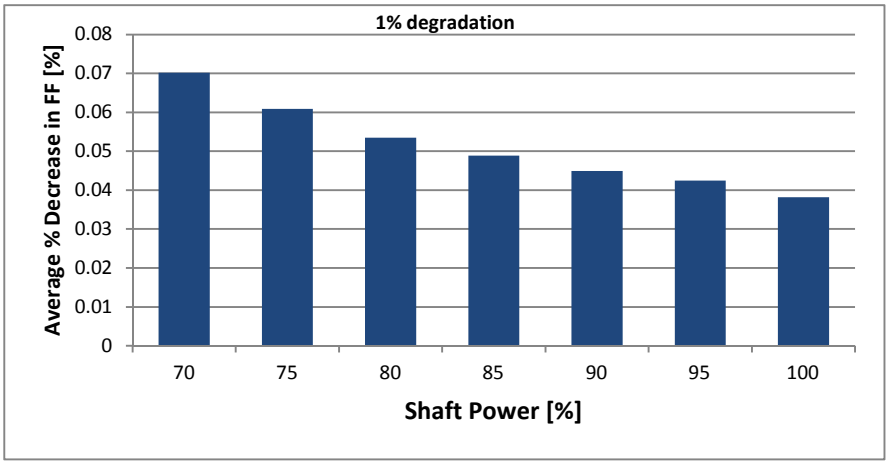

Figure 7.9: Average Percentage Decrease in Fatigue Factors at different Power Levels - 1% Reduction in Compressor Health Parameter Indices

At a given power level, the percentage decrease in fatigue factors does not form a regular trend with ambient temperature, but on the average, the value decreases with shaft power as shown in Figure 7.9. At a given ambient temperature, the percentage decrease in fatigue factors decreases with increase in shaft power. This is shown in Figure 7.10 for two different ambient temperatures. The trend shows that engine degradation has less effect on fatigue life at higher power levels. This is because at the higher power levels, changes in the intake air properties responds less to the degradation effect. The percentage decrease in fatigue factors does not form a proper trend with ambient temperature hence the nature of the two lines in Figure 7.10.

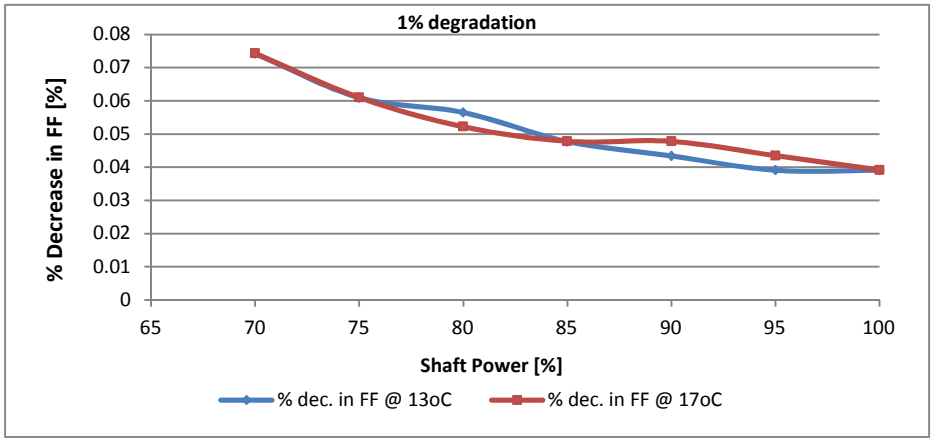

Figure 7.10: Trend of Percentage Decrease in Fatigue factors with Shaft Power at different Ambient Temperatures – 1% Reduction in Compressor Health Parameter Indices

7.4.2 Effect of 2% Reduction in Compressor Health Parameter Indices on Fatigue Life

2% reduction in compressor health parameter indices produces fatigue factors similar to those of the clean engine and the 1% degradation case in terms of trend but of lower magnitude at all shaft power levels and ambient temperatures. The fatigue factors of the degraded engine and the clean engine are shown in Figure 7.11. Like in the case of 1% reduction in compressor health parameter indices, the difference between the fatigue factors of the clean engine and the degraded engine is slightly higher at lower shaft power level but not influenced by ambient temperature.

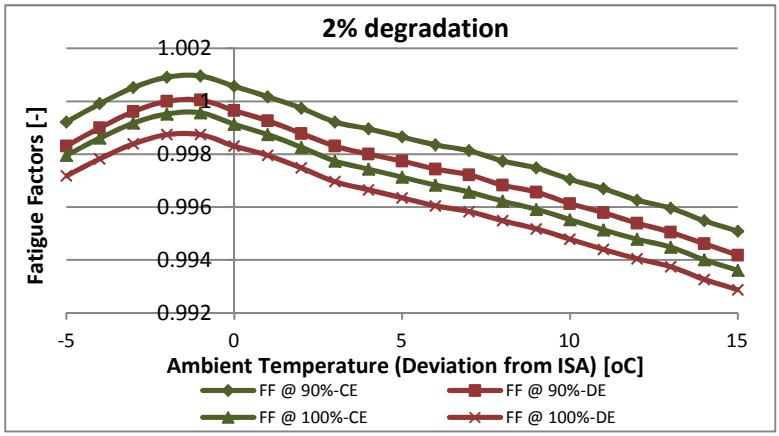

Figure 7.11: Fatigue Factors of Degraded and Clean Engines at Different Power Levels and Ambient Temperatures -2% Reduction in Compressor Health Parameter Indices

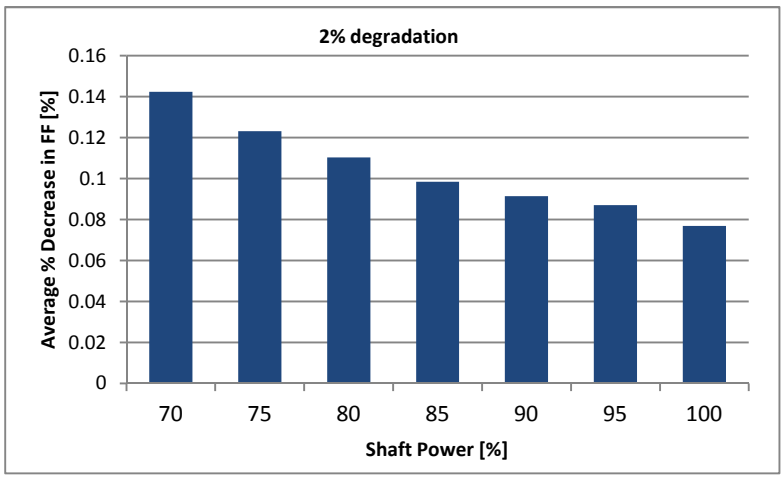

Figure 7.12: Average Percentage Decrease in Fatigue Factors at different Power Levels - 2% Reduction in Compressor Health Parameter Indices

The percentage decreases in fatigue factors at each power level and different ambient temperatures are higher than those of 1% degradation. The average percentage decrease in fatigue factor, like in the case of 1% degradation, decreases with increase in shaft power as shown in Figure 7.12. At each power level, the average percentage decrease is greater than the value obtained in the case of 1% degradation.

At a given ambient temperature, the percentage decrease in fatigue factors, like in the case of 1% degradation, decreases with increase in shaft power but of greater magnitude. This is shown in Figure 7.13 for same ambient temperature levels considered for the 1% degradation. In both degradation cases, the impact on fatigue life is more pronounced in lower shaft power levels and is not being influenced by ambient temperature. The trend in the percentage decrease in fatigue factors only indicates that the impact of compressor degradation on fatigue life consumption is higher at lower power levels, but for both clean and degraded engines, fatigue factors decrease close to peak operation of the engine.

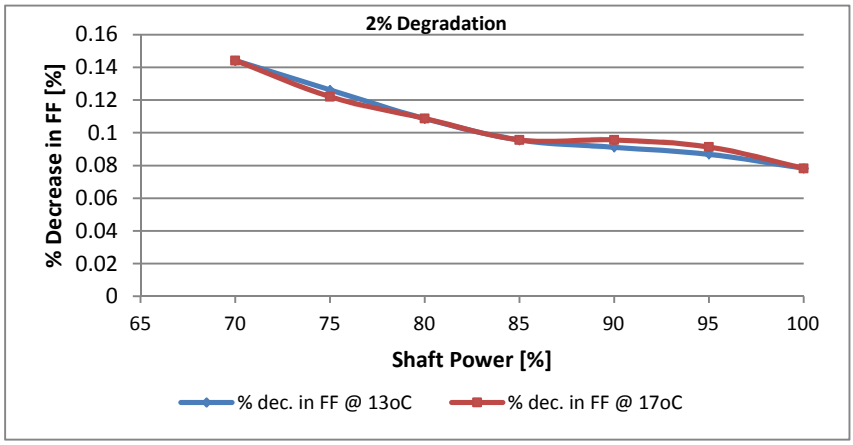

Figure 7.13: Trend of Percentage Decrease in Fatigue factors with Shaft Power at different Ambient Temperatures – 2% Reduction in Compressor Health Parameter Indices

7.4.3 Comparison of the Impacts of the two Degradation Cases on Fatigue Life

From the values of the average percentage decrease in fatigue factors with compressor degradation at the different power levels, 2% reduction of compressor health parameter indices has more than double impact on fatigue life than 1% degradation. This means doubling the compressor health parameter indices has more than double impact on

fatigue life consumption. For instance, at 70% power level, the average percentage decrease in fatigue factors for the 1% and 2% degradation cases are 0.0702% and 0.1423% respectively (0.1423 > 2x0.0702). In both degradation cases, percentage decrease in fatigue factors reduce with shaft power at a given ambient temperature. But, it is worth mentioning that even in the degraded engine, fatigue failure will occur faster if engine is shut down from higher power levels at any ambient temperature, in line with Figure 7.6. This trend is shown in Figure 7.14 for both degradation cases at 13^{o}C (-2^{o}C deviation from ISA).

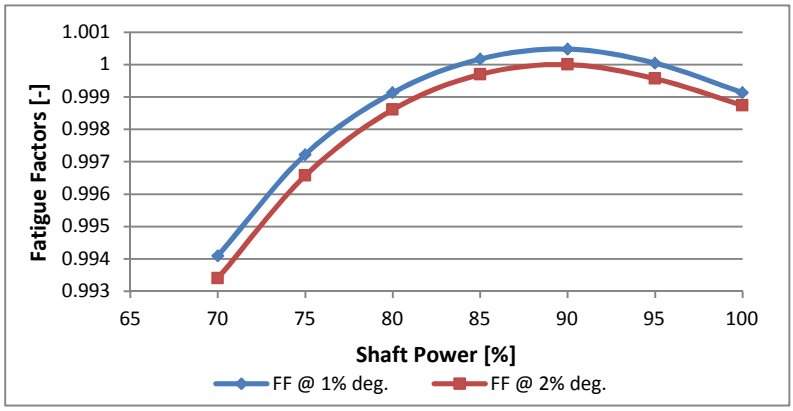

Figure 7.14: Fatigue Factor Variation with Shaft Power for Degraded Engines at a Given Ambient Temperature

Aside showing that in the degraded engines, the fatigue factors vary with shaft power in a similar trend as in the clean engine, Figure 7.14 also depicts that the engine with 2% degradation case has fatigue factors lower than the engine with 1% degradation case at a given ambient temperature and at all power levels.

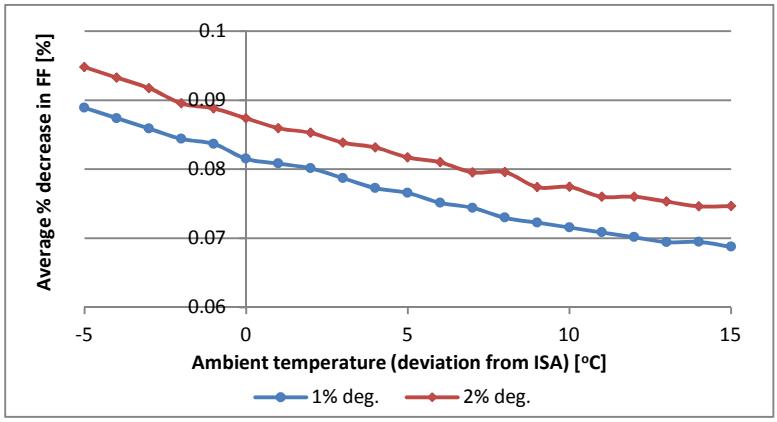

Figure 7.15: Average Percentage Increase in Fatigue Factors with Power Increase for Degraded Engines at a Given Ambient Temperature

At a given ambient temperature, like in the case of the clean engine, increasing shaft power from 70% to maximum power on the average leads to increase in fatigue factors. The average percentage increase in fatigue factors due to power increase decreases with ambient temperature; this is shown in Figure 7.15 for the two cases of degradation. From Figure 7.18, the average percentage decrease in fatigue factors due to power increase in the specified range is greater in the 2% degradation case at all ambient temperatures. This should be expected since at 2% degradation the compressor health parameters are reduced further compared to the case of 1% degradation and the compressor speed has to be increased more than the 1% degradation case to maintain the set shaft power level.

7.5 Chapter Conclusions

Low cycle fatigue life analysis is carried out in this chapter. The fatigue life model used is the modified universal slopes method, as this method fits low cycle fatigue data better, compared to many other methods. The stress required in this model is obtained from the stress model developed in Chapter 4. In industrial gas turbine operation, a bit steady operations are assumed and hence steady stress levels are obtainable, and a fatigue cycle is counted when engine is shut down. Knowing that there are minor variations in stresses from time to time, a cycle counting method is developed, similar to what the US Air Force apply to Aero engines. The fatigue cycles to failure are estimated using the low fatigue life model, while the actual fatigue cycles experienced are estimated using the cycle counting model developed. Palmgren-Miner damage summation rule is applied to estimate the fatigue life consumption and the equivalent fatigue life at any given period of engine operation. The low fatigue life model, the cycle counting model, and the damage summation model are implemented in PYTHIA to ensure engine life analysis is executed on a common platform. The fatigue life analysis methodologies are developed and presented in Chapter 3.

Since fatigue failure is stochastic, and some assumptions are made in arriving at the various models, absolute results of fatigue failure may not be too reliable. In the light of the above, in this research, the concept of fatigue factor is introduced, where fatigue life obtained at any time frame of engine operation is compared to the fatigue life at a

reference time frame of engine operation, both governed by the stress variations. Considering complicated engine operation where several different time frames of engine operations are involved, the equivalent fatigue factor is used to represent the fatigue life consumption. Equivalent fatigue factor of unity means the complicated engine operation process consumes the engine fatigue life in the same rate as the reference time frame of engine operation. If the equivalent fatigue factor is greater than unity, the engine operation in that time frame is favourable compared to the reference time frame and vice-versa.

The fatigue life models are applied to 8 different months of engine operation to track the fatigue life consumption of the engine for the entire period, and to also test the feasibility of the life tracking process. The models predict life consumption in a manner similar to what is obtainable in real engine operation. The effects of ambient temperature, shaft power and engine degradation on fatigue life consumption were investigated. The basic findings are summarized below:

- At a given shaft power level, in the ambient temperature range 5^{o}C to 30^{o}C, fatigue factors increases to about 13^{o}C and then drop. On the average, there is decrease in the fatigue factors for the entire temperature range at all power levels.
- At a given ambient temperature, beyond 90% power level, fatigue factors decrease with increase in shaft power.
- For an engine with compressor health parameter indices reduction, the fatigue factors trend is similar to that of the clean engine, but lower in terms of magnitude at all ambient temperatures and shaft power levels.
- The average percentage decrease in fatigue factors due to compressor degradation decreases with increase in shaft power, where the average value is evaluated at each power level for the different ambient temperatures
- Doubling the compressor health parameter indices reduction has more than double impact on fatigue life consumption.

8 CREEP-FATIGUE INTERACTION LIFE ANALYSIS

When a gas turbine engine is often shut down, especially for peak load operations, failure may result from the both creep and fatigue. In this, the time to failure due to creep estimated at any point of engine operation will be higher than the actual time the engine component concerned will fail. Even if engine is operated without frequent shut down, operating conditions bring about variations in engine speed and stresses in components from time to time. The stress variations in rotating components lead to the accumulation of stress cycles (fatigue cycles) and failure of such components may result from the combined effects of creep and fatigue.

The methodologies involved in carrying out creep-fatigue interaction life analysis were developed in Chapter 3. Taira's linear accumulation method was adopted for creep-fatigue interaction life analysis. The apparent shortcomings in the model were evaded with the utilization of relative life analysis. The model takes input from both the results of creep life analysis and fatigue life analysis, necessitating the life estimation to be carried out at the same sections of the blade where both creep life and fatigue life consumption were estimated. All the developed algorithms are inputed in PYTHIA hence the creep-fatigue life consumption analysis is carried out in the same platform as the creep life and the fatigue life analyses. In this chapter, developed methodologies are applied to real engine operation data in order to track the creep-fatigue interaction life consumption of the industrial gas turbine blades under review in this study. Failure due to creep-fatigue interaction is compared with creep failure under similar engine operating conditions and the contribution of fatigue to creep-fatigue interaction failure is investigated. Also, the effects of engine shaft power variation, ambient temperature variation and compressor degradation on creep-fatigue interaction failure are examined.

8.1 Creep-Fatigue Interaction Life Tracking: A Case Study

To test the feasibility and the applicability of the developed creep-fatigue interaction algorithms in this research, the developed algorithms are applied to 8 months real engine operation field data. It is the same data used for testing both the creep life and the fatigue life analysis algorithms. Figure 8.1 shows the equivalent creep-fatigue interaction factors (ECFF) of the 8 months of engine operation under review.

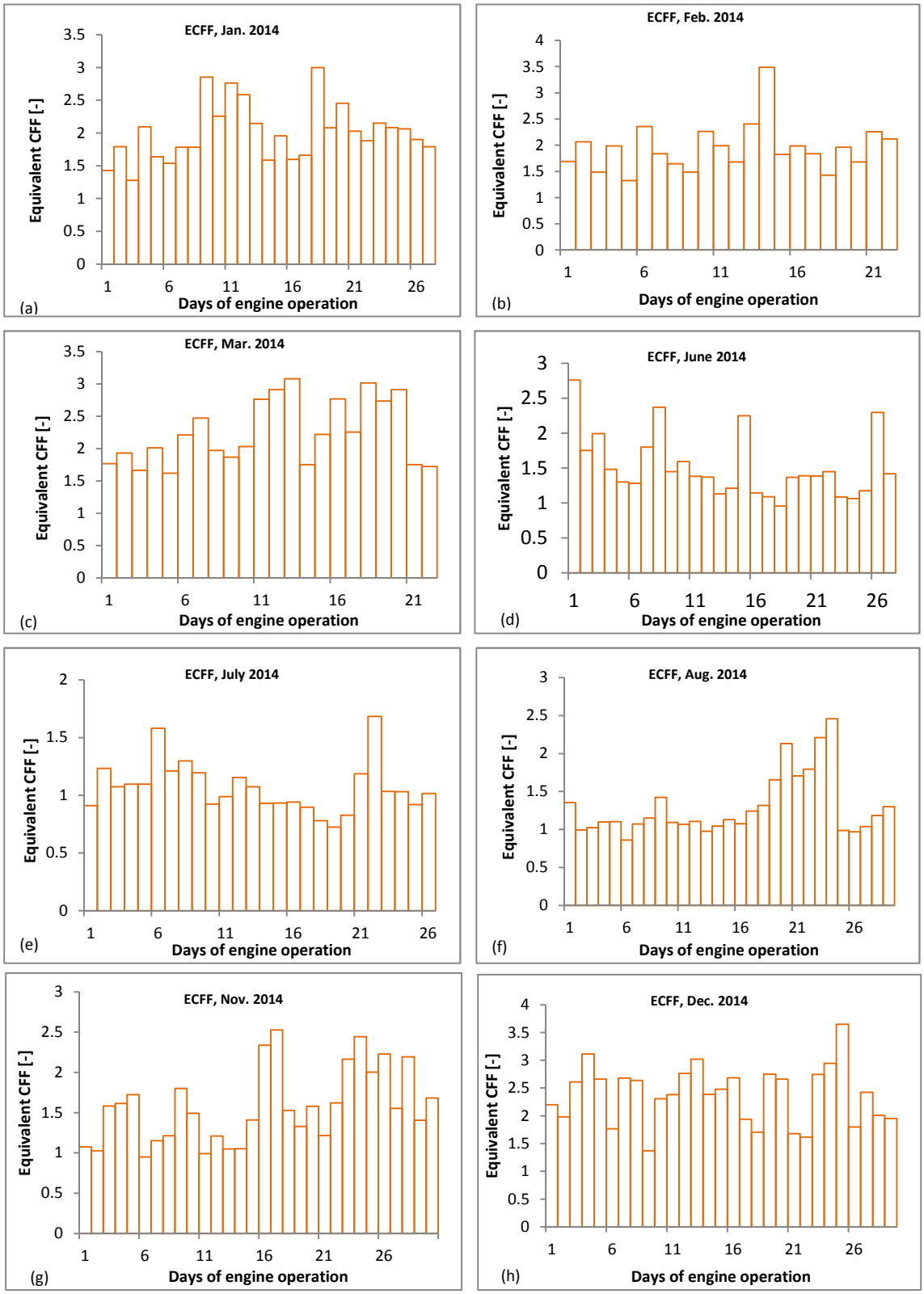

Figure 8.1: Equivalent Creep-Fatigue Factors for Different Months of Engine Operation

The equivalent creep-fatigue interaction factors are higher during the months of low ambient temperature engine operation where the creep factors are also higher. These are in the months of January, February, March, and December. Lower values of equivalent creep-fatigue factors are gotten in June, July and August, which come with high ambient temperatures. The results in November are also low, as a bit high temperatures were recorded in many days of engine operation. Higher equivalent creep-fatigue factors are obtained in the months with low ambient temperatures because in industrial turbine failure is more prone to creep as against fatigue failure. The contribution of creep to the creep-fatigue interaction failure for daily shut down of engine is much higher compared to the fatigue contribution.

To have a global view of the equivalent creep fatigue factors, the monthly equivalent creep-fatigue factors are presented in Figure 8.2. The equivalent creep-fatigue factor for each month is greater than 1, this means favourable engine operation in the entire period with respect to creep-fatigue interaction failure at a reference operation point. The lowest equivalent creep-fatigue factor, 1.03 was recorded in July, a bit safe operation. This is the month with highest ambient temperatures and lowest creep factor values.

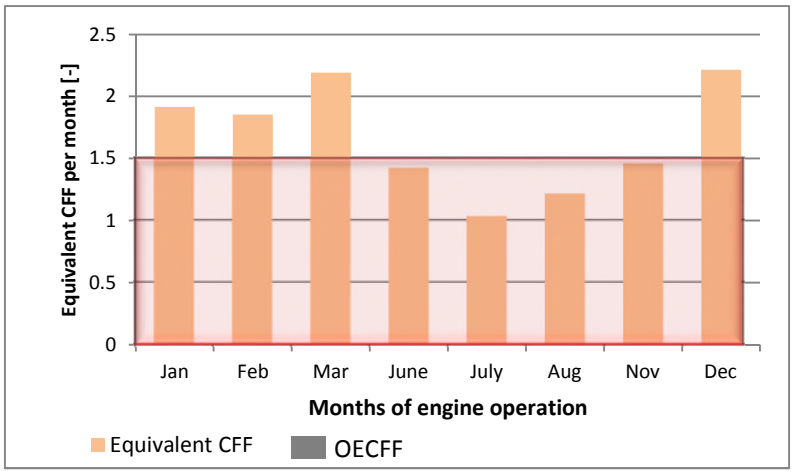

Figure 8.2: Equivalent Creep - Fatigue Factors for each Month of Engine Operation

The equivalent creep-fatigue factor of the entire period of engine operation is also included in Figure 8.2, designated as OECFF (overall equivalent creep-fatigue factor). The overall equivalent creep-fatigue factor for the entire period of engine operation is 1.5. This indicates that the life consumption rate due to creep-fatigue interaction is 50%

less compared to the reference engine operation condition. The engine operation in the entire period is thus favourable.

The results of the creep-fatigue interaction are similar to those of creep because creep contributes more to creep-fatigue interaction failure than fatigue. To have a proper view of the larger contributions of creep to creep-fatigue interaction failure, the equivalent creep factors and the equivalent creep-fatigue factors for two different months of engine operation are presented in Figure 8.3 as data points. A month with low ambient temperatures, January and a month with high ambient temperatures, July is used for the comparisons. In both months of engine operation, the equivalent creep-fatigue interaction factors closely approximate the equivalent creep factors for each day of engine operation. The contribution of creep becomes more dominant in periods of high ambient temperatures. The equivalent creep factors are closer to the equivalent creep-fatigue factors in July of engine operation (Figure 8.3 (b)) than in January (Figure 8.3(a)).

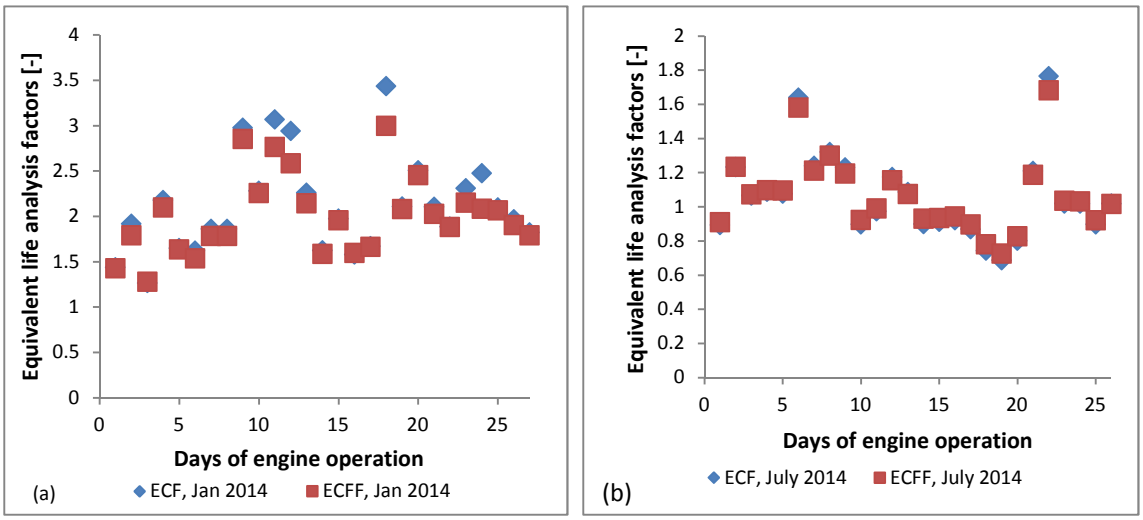

Figure 8.3: Comparison of Equivalent Creep Factors and Equivalent Creep-Fatigue Factors in two Months of Engine Operation

The equivalent creep-fatigue factor values are closer to the creep factor values in July than in January because in July the tendency of fatigue failure is lower due to low intake air and reduced momentum change stresses. Failure of the HP turbine blades is thus more dominated by creep during periods of high ambient temperatures, which do result in low shaft powers. If engine is often shut down from high shaft power levels, the

contribution of creep to creep-fatigue interaction failure will be reduced compared to shutting down from low power levels.

8.1.1 Low Cycle Fatigue Contribution to Creep-Fatigue Interaction

The contribution of the low cycle fatigue life consumption to the creep-fatigue life consumption can be expressed as life reduction due to fatigue life consumption in this work. That is, under creep life consumption, the time to failure is estimated. As the engine is operated for a given number of hours per day, say 12 hours and shut down, the engine life consumption due to creep ought to be reduced by a factor of about 2. If shutting down the engine constitutes a low cycle fatigue, the life consumption will be reduced by a factor of less than 2. This may be viewed as life reduction as low cycle fatigue interacts with creep. The average values of percentage reduction in life due to fatigue interaction with creep for the 8 different months of engine operation are given in Figure 8.4.

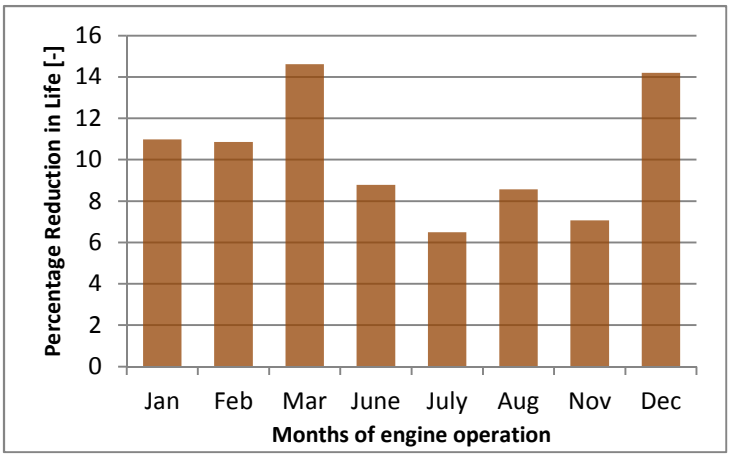

Figure 8.4: Percentage Reduction in Life due to Fatigue Interaction with Creep

The percentage reduction in life is evaluated taking creep life as the base life. As creep interacts with fatigue, the resultant life is less than the creep life and the decrease in life due to fatigue contribution decreases with an increase in fatigue factors. The reduction in life is highest in the months with low ambient temperatures where fatigue contributions are highest. At the conditions where creep dominance is more paramount, the results of creep life consumption is not much different from those of creep-fatigue interaction life consumption. Thus in such engine operation conditions, estimating only creep life consumption is sufficient.

8.2 Effects of Ambient Temperature and Shaft Power on Creep-Fatigue Life

The results of creep-fatigue interaction show that the creep term dominates in the creep-fatigue interaction failure. Thus, it is very likely creep-fatigue interaction failure will respond to ambient temperature and power changes similar to creep. In this section, the effects of ambient temperature and shaft power variations on creep-fatigue interaction failure of the compressor turbine blades of LM2500+ engine is investigated. In investigating the effect of ambient temperature on the creep-fatigue interaction life consumption, the power level will be specified while creep-fatigue factors at different ambient temperatures of engine operation are recorded. At a given ambient temperature and power level, the maximum stress the blades are exposed is estimated. If the engine is shut down from that power level and ambient temperature, assumed to operate at that point for a defined time before shutting down, the creep life consumption as well as the fatigue life consumption assuming one fatigue cycle is experienced could be estimated. Shutting down the engine at same power level and different ambient temperatures will generate different creep-fatigue factors which will show the trend of creep-fatigue factors with ambient temperature.

To investigate the effect of shaft power on creep-fatigue life consumption, the ambient temperature will be fixed while the engine is operated at different power levels before shut down. The above analyses are made possible with the engine performance model and the life analysis models developed in this research. Like in creep life and fatigue life analysis, the effects of ambient temperature and shaft power on creep-fatigue interaction analysis are carried out at 70% to 100% power levels and ambient temperatures of 5^{o}C to 30^{o}C (expressed in terms of deviations from ISA condition). Figure 8.6 shows the effect of ambient temperature variation on creep-fatigue interaction at different power levels. The creep-fatigue factors, like the creep factors, decrease with ambient temperature increase at all power levels. This is because the creep failure contributes majorly to creep-fatigue failure. At higher ambient temperatures, the creep-fatigue factors trend is closer to the creep trend as creep contribution to creep-fatigue failure is more in higher ambient temperatures. At lower ambient temperatures, the fatigue contribution increases but still far less than the creep

contribution; the creep-fatigue factors trend is less similar to the creep factors trend in this temperature band. Both creep and fatigue contributions to creep-fatigue interaction failure at a given ambient temperature increases with increase in shaft power, but creep contribution increases faster; the creep-fatigue factors trend thus behaves more closely with the creep factors trend at higher shaft power levels.

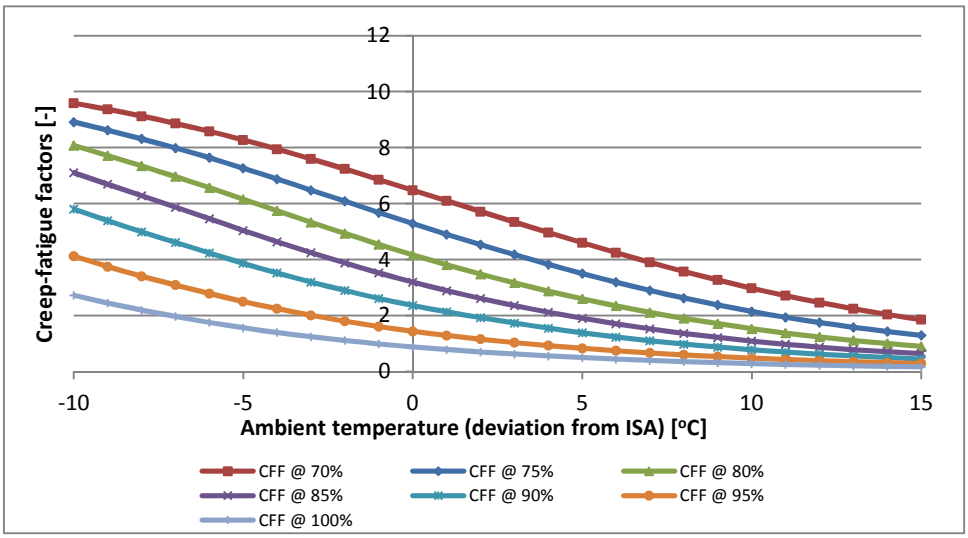

Figure 8.5: Creep -Fatigue Factors Variation with Ambient Temperature at different Shaft Power Levels

At any given power level, increasing the ambient temperature through the range of temperatures considered lead to a decrease in the creep-fatigue factors as shown in Figure 8.5. At lower ambient temperatures, the decrease in creep-fatigue factors with temperature increase is small compared to same occurrence at higher temperature band. This is because of the increase in fatigue contribution at lower ambient temperatures and fatigue factors responds poorly to temperature increase. At the higher temperature band, creep contribution increases leading to increase in creep-fatigue interaction factors when temperature increase occurs at higher temperature band. Higher values of percentage decrease in creep-fatigue factors due to increase in ambient temperature for the specified ambient temperature range occur at higher shaft power levels, Figure 8.6. The trend in Figure 8.6 shows faster engine creep-fatigue life consumption with temperature increase at higher power levels. This is because at higher shaft power levels, the contributions of both creep and fatigue to creep-fatigue life increases, and

increase in ambient temperatures thus has more impact on the creep-fatigue failure at higher power levels.

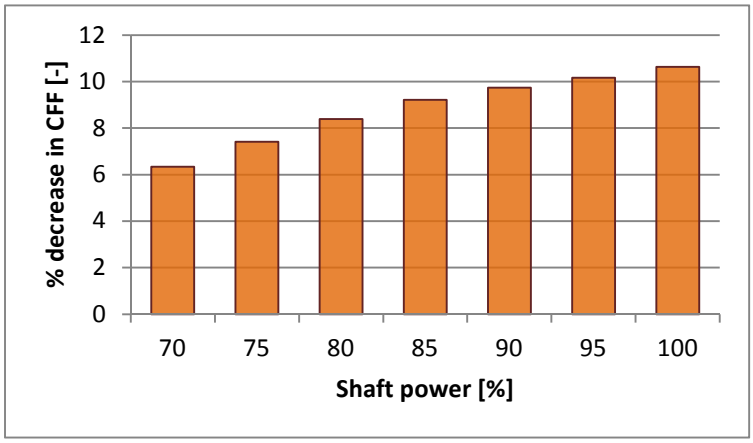

Figure 8.6: Average Percentage Decrease in Creep-Fatigue Factors with Ambient Temperature at different Power Levels

At a given ambient temperature, the creep-fatigue factors decrease with increase in shaft power. This is shown in Figure 8.7 for ambient temperatures of 13^{o}C and 17^{o}C respectively (-2^{o}C and 2^{o}C deviation from ISA).

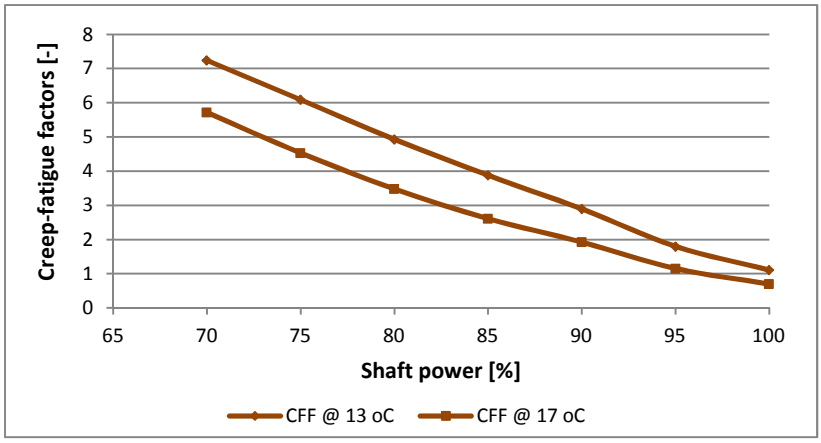

Figure 8.7: Creep-Fatigue Factors Variation with Shaft Power at Given Ambient Temperatures

Creep life decreases with increase in shaft power at all ambient temperature, also towards peak operations fatigue life decreases with increase in shaft power. With creep dominating creep-fatigue interaction at all ambient temperatures and power levels, increase in shaft power at any ambient temperatures leads to decrease in creep-fatigue factors at all ambient temperatures as shown in Figure 8.7.

At a given ambient temperature, increase in shaft power leads to decrease in creep-fatigue factors as in Figure 8.7. On the other hand, increase in creep-fatigue factors occur with power drop, in the same magnitudes as increase in shaft power does to creep-fatigue factors decrease. Greater values of percentage increase in creep-fatigue factors are obtained when power drop occurs at higher power levels. By estimating the increase in creep-fatigue factors with power drop at different ambient temperatures, the mean value is obtained at each power drop as shown in Figure 8.8. The results in Figure 8.8 are a bit similar to those obtained in creep life analysis where larger increase in creep factors is obtained when power drop occurs at higher power levels. The large contribution of creep to creep-fatigue interaction failure makes most of the creep-fatigue results to be similar to the creep results.

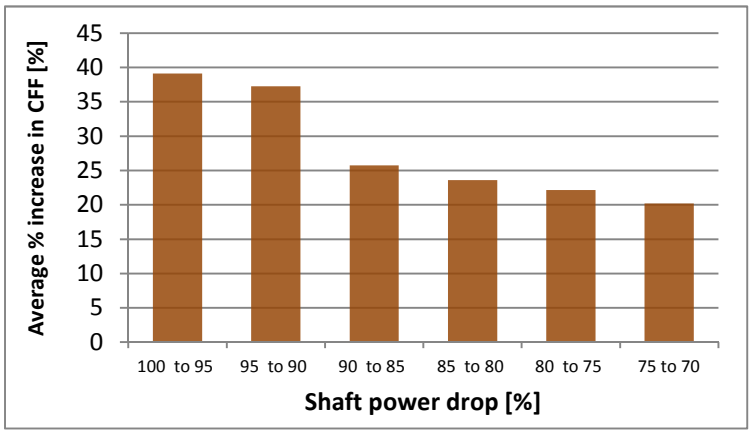

Figure 8.8: Average Percentage Increase in Creep-Fatigue Factors with Shaft Power Drop

High values of increase in creep-fatigue factors are obtained when power drop occurs around peak operation. Also, when shaft power increase occurs close to peak power operation, creep-fatigue life consumption will be faster. In practice, in most periods of engine operation, engine operates at part load, often gets to peak power levels. Operating at part loads will lead to elongating engine life, but other considerations such as specific fuel consumption at part load, power demand, etc. will be considered by engine operators in making such decisions. For the sake of elongating engine life, in high ambient temperatures, operating close to peak power should be avoided, unless it becomes very necessary to do so.

8.3 Effect of Engine Degradation on Creep-Fatigue Life Consumption

Degradation of any engine component affects the properties of the gas and hence the life of the hot section components. Only the effect of compressor degradation on creep-fatigue interaction life consumption is looked at here since compressor is the most commonly degraded component in the gas turbine engine. Two cases of compressor degradation will be considered: 1% and 2% reductions respectively in compressor health parameter indices and these are shown in Table 8.1. The effect of each case of engine degradation on creep-fatigue life consumption will be examined at different power levels (70% to 100% power levels) and various ambient temperatures (10^{o}C to 30^{o}C expressed in terms of deviations from ISA condition).

Table 8.1: Degradation Cases for Creep-Fatigue Interaction Life Analysis

Case	Component	Degraded Parameter	
		Efficiency Index [%]	Flow capacity Index [%]
I	Compressor	-1	-1
II	Compressor	-2	-2

The extent to which engine compressor degradation affect creep-fatigue interaction life consumption will be revealed by examining the sensitivity of creep-fatigue interaction factors to compressor degradation at different engine operating conditions; that is, the response of creep-fatigue interaction factors to compressor degradation will be investigated at different conditions of engine operation. This is best presented in terms of the percentage decrease in creep-fatigue factors due to compressor degradation, and it is given by Equation (8.1),

$$PD_{CFF,i} = \frac{CFF_{CE,i} - CFF_{DE,i}}{CFF_{CE,i}} \times 100 \qquad (8.1)$$

$PD_{CFF,i}$ is the percentage decrease in creep-fatigue factor at each power level and at the various ambient temperatures, $CFF_{CE,i}$ is the creep-fatigue factor for the clean engine at a given power level and temperature counter i, while $CFF_{DE,i}$ is the creep-fatigue factor for the degraded engine at same power level and temperature. The value of the percentage decrease in creep-fatigue factor indicates how engine creep-fatigue life responds to engine degradation at the given power level and ambient temperature.

Higher values of percentage decrease in creep-fatigue factor indicate greater impact of degradation on creep-fatigue life and vice-versa. Results of the creep-fatigue factors of the clean and degraded engines at different power levels and ambient temperatures are presented for comparisons.

8.3.1 Effect of 1% Reduction in Compressor Health Parameter Indices on Creep-Fatigue Interaction Life

When the compressor health parameter indices are reduced by 1% each, the creep-fatigue factors are reduced at each condition of engine operation. Figure 8.9 shows the creep-fatigue factors for 90% and 100% power levels and at different ambient temperatures for both the clean engine (CE) and the degraded engine (DE).

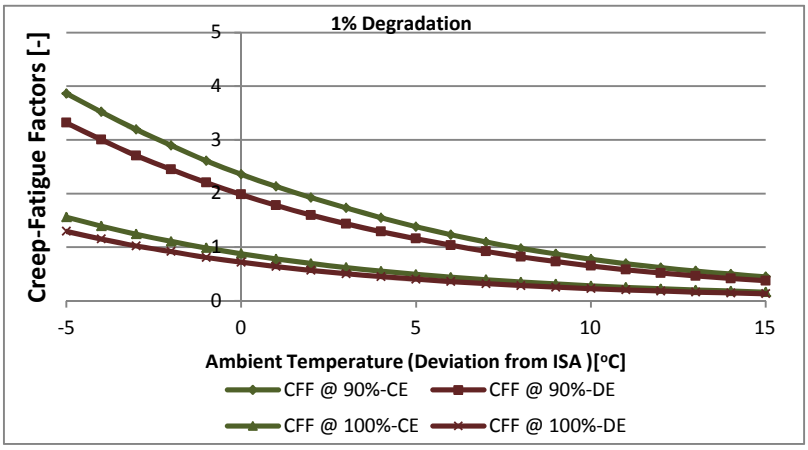

Figure 8.9: Creep- Fatigue Factors of Degraded and Clean Engines at different Power Levels and Ambient Temperatures -1% Reduction in Compressor Health Parameter Indices

The creep-fatigue factors of the clean engine are greater than those of the degraded engine at the two power levels and the different ambient temperatures. Like in the case of the creep factors variation with compressor degradation, the creep-fatigue factors for the degraded engine are much lower than those of the clean engine at lower ambient temperatures and lower power levels (this is on numerical scale since high values of creep-fatigue factors are recorded at low shaft power and low ambient temperatures). At 100% power level and higher ambient temperatures, the creep-fatigue factors of the two engines are almost the same. The compression process is more efficient at lower power levels and lower ambient temperatures and any change in compressor health parameter indices will lead to more noticeable change in the creep-fatigue factors at lower ambient

temperatures and lower shaft powers as larger values of creep-fatigue factors are obtained in these regions. In terms of percentage decrease in creep-fatigue factors, larger values are recorded at higher power levels and higher ambient temperatures similar to the way creep factors respond to compressor degradation. Thus at a given power level, the percentage decrease in creep-fatigue factors increases with ambient temperature (though does not form a very regular trend). This is shown in Figure 8.10 for 70% and 85% power levels.

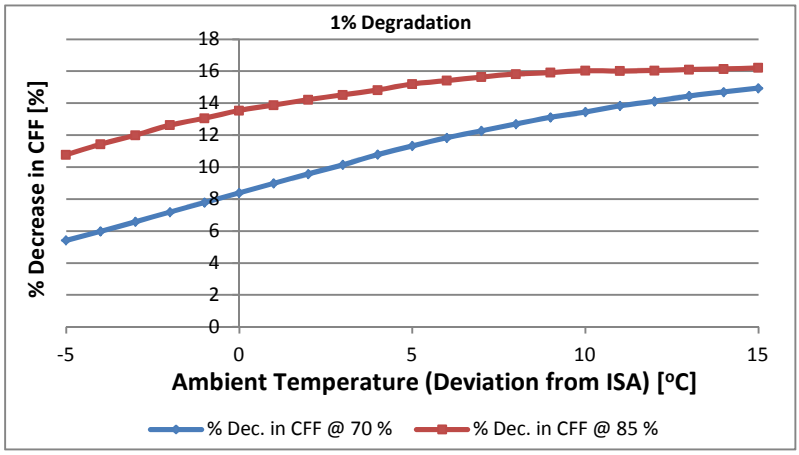

Figure 8.10: Percentage Decrease in Creep-Fatigue Factors at different Power Levels and Various Ambient Temperatures - 1% Reduction in Compressor Health Parameter Indices

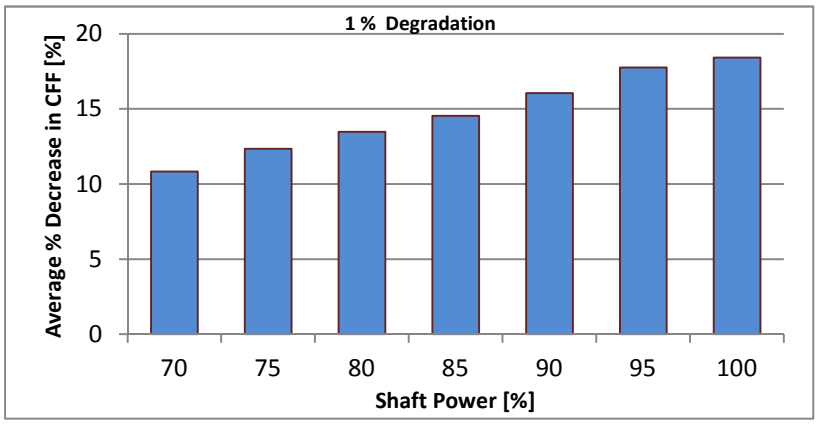

Figure 8.11: Average Percentage Decrease in Creep-Fatigue Factors at different Power Levels - 1% Reduction in Compressor Health Parameter Indices

The average percentage decrease in creep-fatigue factors are evaluated at each power level and ambient temperatures between -10°C to 30°C, expressed in terms of deviation from ISA. The average percentage decrease in creep-fatigue factors increases with shaft

power as shown in Figure 8.11. Compressor health parameters indices reduction thus has more impact on creep-fatigue life consumption at higher ambient temperatures and at higher power levels.

At a given ambient temperature, the percentage decrease in creep-fatigue factors increases with increase in shaft power. This is shown in Figure 8.12 for two different ambient temperatures, 13^{o}C and 17^{o}C. The trend shows that compressor degradation has more effect on creep-fatigue life at higher power levels. This is because at the higher power levels, the compression process is less efficient and compressor degradations lead to greater percentage increase in the temperature of gases at the turbine entry. Since creep-fatigue interaction life consumption is dominated by creep which is temperature-driven, compressor degradation has greater impact on creep-fatigue life consumption at higher power levels. The increase in percentage decrease in creep-fatigue factors does not form a uniform trend with shaft power but on the increase.

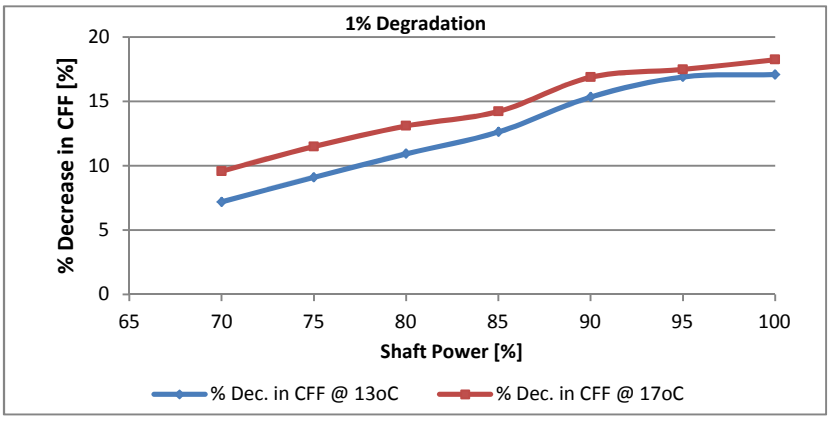

Figure 8.12: Trend of Percentage Decrease in Creep-Fatigue factors with Shaft Power at different Ambient Temperatures – 1% Reduction in Compressor Health Parameter Indices

8.3.2 Effect of 2% Reduction in Compressor Health Parameter Indices on Creep-Fatigue Interaction Life

The creep-fatigue interaction factors obtained for 2% reduction in compressor health parameter indices are similar to those of both the clean engine and the engine with 1% reduction in compressor health parameter indices in terms of trend, but less than those of 1% compressor degradation in terms of magnitude. Figure 8.13 shows the creep-

fatigue interaction factors for the engine with 2% compressor degradation and the clean engine at 90% and 100% power levels and at different ambient temperatures.

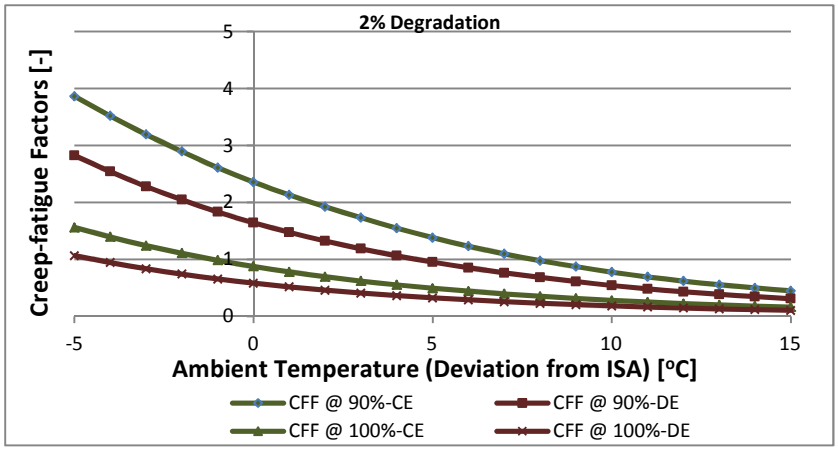

Figure 8.13: Creep-Fatigue Factors of Degraded and Clean Engines at different Power Levels and Ambient Temperatures -2% Reduction in Compressor Health Parameter Indices

The creep-fatigue interaction factors for the degraded engine, like in the case of 1% reduction in compressor health parameter indices, are much lower than those of the clean engine at lower power levels and lower ambient temperatures. In this case, at 100% power level and higher ambient temperatures, there is still noticeable difference between the creep-fatigue factors of the clean and degraded engines, signifying that 2% reduction in compressor health parameter indices led to more reduction in creep-fatigue factors than the 1% degradation case. Although more noticeable difference between the creep-fatigue factors are obtained at lower power levels and lower ambient temperatures, the percentage decrease in creep-fatigue interaction factors, like in the case of 1% compressor degradation, is higher at higher ambient temperatures and shaft powers. Thus at a given power level, the percentage decrease in creep-fatigue factors increases with increase in ambient temperature as shown in Figure 8.14 for 70% and 85% power levels. The percentage decrease values are higher than those of 1% degradation case at all ambient temperatures and shaft power levels. The average percentage decrease in creep-fatigue factors computed at each power level and at the different ambient temperatures increases with increase in shaft power like in the case of 1% degradation case but of higher magnitude, Figure 8.15.

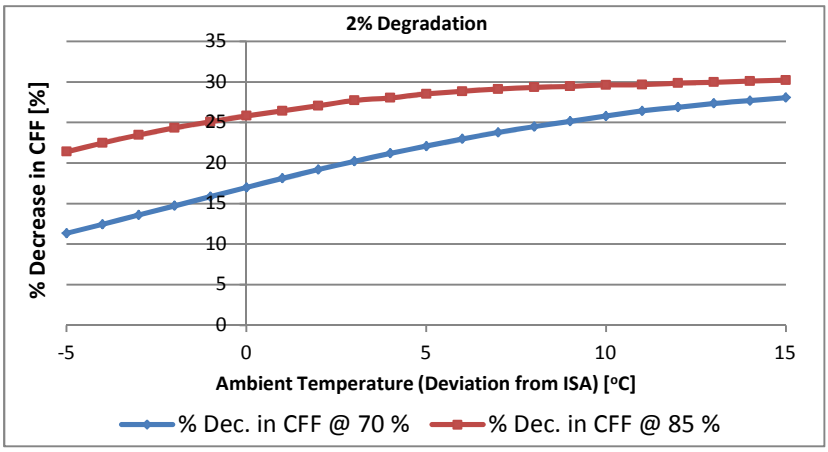

Figure 8.14: Percentage Decrease in Creep-Fatigue Factors at Different Power Levels and Various ambient temperatures - 2% Reduction in Compressor Health Parameters

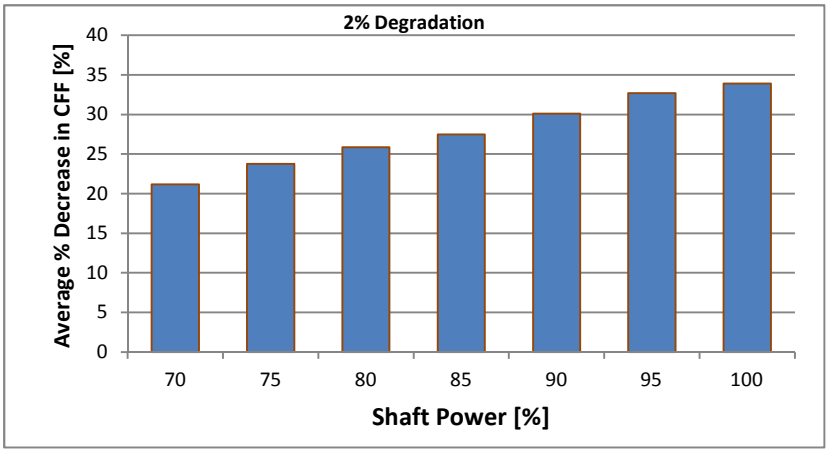

Figure 8.15: Average Percentage Decrease in Creep-Fatigue Factors at different Power Levels - 2% Reduction in Compressor Health Parameter Indices

Like in the case of 1% reduction in compressor health parameter indices, at a given ambient temperature, the percentage decrease in creep-fatigue factors increases with increase in shaft power as shown in Figure 8.16 for 13^{o}C and 17^{o}C ambient temperatures. The percentage reductions are higher than those obtained for 1% degradation. The percentage decrease in creep-fatigue factors for the engine with 2% reduction in compressor health parameter indices is higher than those of the engine with 1% degradation case at all ambient temperatures and shaft power levels. This means the engine with 2% degradation case has more impact on creep-fatigue interaction life than the engine with 1% degradation case. To know the relative impact of the 1% and 2%

degradation cases on creep-fatigue interaction life, the average percentage decrease in creep-fatigue factors at different power levels should be compared.

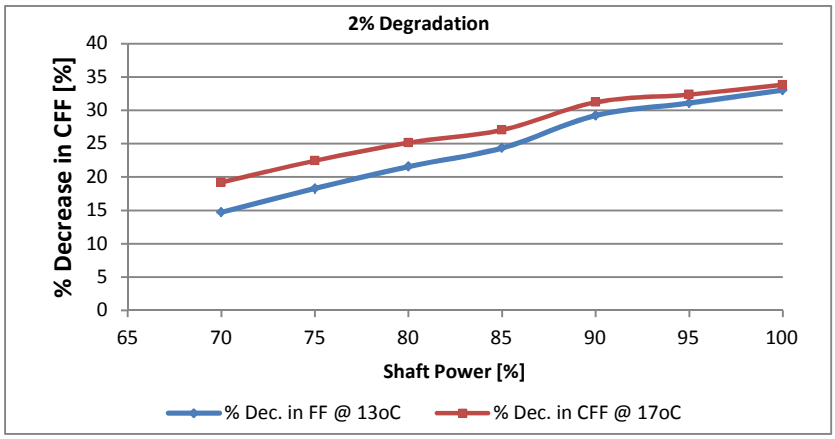

Figure 8.16: Trend of Percentage Decrease in Creep-Fatigue factors with Shaft Power at different Ambient Temperatures – 2% Reduction in Compressor Health Parameter Indices

8.3.3 Comparison of the Impacts of the two Degradation Cases on Creep-Fatigue Life

In both cases of degradation, the creep-fatigue factors behave like the creep-fatigue factor of the clean engine in terms of trend but of lower magnitude at all temperatures and shaft power levels. The creep-fatigue factors for both the clean and degraded engines decrease with increase in ambient temperature for a given power level; they also decrease with increase in shaft power for a given ambient temperature level. Figure 8.17 shows the creep-fatigue factors for the two cases of degradation at 13^{o}C (-2^{o}C deviation from ISA) and different power levels. Figure 8.17 also shows that the engine with 2% reduction in compressor health parameter indices has creep-fatigue factors lower than the engine with 1% degradation case at a given ambient temperature and at all power levels. More noticeable difference between the creep-fatigue factors is obtained at lower power levels because high values of creep-fatigue factors are gotten at lower power levels.

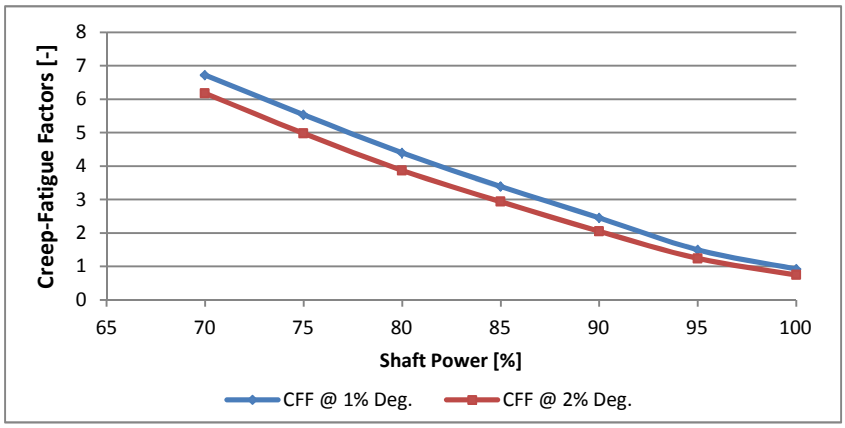

Figure 8.17: Creep-Fatigue Factor Variation with Shaft Power for Degraded Engines at a Given Ambient Temperature

Increasing the compressor health parameter index reduction from 1% to 2% nearly doubles the impact of the degradation on creep-fatigue interaction life at all ambient temperatures and shaft power levels judging from the values of the average percentage decrease in creep-fatigue factors. This means doubling the compressor health parameter indices nearly doubles impact on creep-fatigue life consumption. For instance, at 70% power level, the average percentage decrease in creep-fatigue factors for the 1% and 2% degradation cases are 10.837% and 21.155% respectively, and for 90% power level, the respective values are 16.053% and 30.096%. In both degradation cases, percentage decrease in creep-fatigue factors increases with shaft power at a given ambient temperature, and at a given ambient temperature, the percentage decrease in creep-fatigue factors increases with shaft power level. The values of the percentage decreases in creep-fatigue factors with compressor degradation obtained in this research are specific to the engine model, different engine models will give different results but the trends may be similar. Thus, the results could serve as guides to different engine operators.

8.4 Chapter Conclusions

Creep-fatigue interaction life analysis is considered in this chapter. Taira's linear creep and fatigue accumulation model is used for the creep-fatigue interaction analysis, while the limitations imposed by the linear model are evaded by exploiting relative life analysis. The creep-fatigue model gets inputs from the creep model and the fatigue model. The creep-fatigue life analysis methodology using relative life analysis make it

possible for engine operators to assess how well they operate their engines over time and makes creep-fatigue life tracking feasible. The developed models were applied to 8 different months of engine operation using same data for the creep life analysis as well as the fatigue life analysis in Chapters 6 and 7 respectively. The creep-fatigue life consumption of the engine was tracked in the process and the results obtained were in line with what is obtainable in real engine operation. Creep dominates the creep-fatigue failure at the different conditions the engine was operated. This is expected as industrial gas turbines are operated in a bit stable power conditions and fatigue cycles accumulated over time are quite few. The contribution of fatigue to creep-fatigue interaction increases with shaft power.

The effects of ambient temperature, shaft power and engine degradation on creep-fatigue life consumption were also investigated. The basic findings are presented below:

- At a given shaft power level, creep-fatigue factors decrease with increase in ambient temperature.
- At a given ambient temperature, creep-fatigue factors decrease with increase in shaft power.
- For an engine with compressor turbine health parameter indices reduction, the trend of the creep-fatigue factors is similar to that of the clean engine, but lower in terms of magnitude at all ambient temperatures and shaft power levels.
- The percentage decrease in creep-fatigue factors due to compressor degradation increases with both shaft power increase and ambient temperature increase.
- The average percentage decrease in creep-fatigue factors due to compressor degradation increases with increase in shaft power, where the average value is evaluated at each power level for the different ambient temperatures
- Doubling the compressor health parameter indices reduction nearly doubles the impact on creep-fatigue life consumption.

9 CONCLUSIONS AND FUTURE WORK

9.1 Conclusions

Gas turbines are widely used for civil/military aviation and industrial power generation and many other utilities. These machines are operated at quite high temperatures, especially the high pressure turbine blades, and are prone to failure due to creep, fatigue and creep-fatigue interaction. In this work, algorithms are developed using appropriate lifing models to simultaneously estimate the creep life consumption, fatigue life consumption and creep-fatigue interaction life consumption of the high pressure turbine blades of an industrial gas turbine using LM2500+ engine operated by Manx Utilities at Isle of Man as a case study. Relative life analysis is employed by comparing the engine life estimated to a reference life in each failure mode (where the reference life is also estimated from same algorithms in a specified engine operation condition) and the resulting life analysis factor indicates how well the engine has being operated for any given time frame. The usage of the life analysis factors lessens the excessive demand on the accuracy of the life prediction method employed but makes engine operators aware of the relative extent engine life is being consumed.

The aim of this work is to study and develop appropriate engine life estimation methods and apply same to industrial gas turbine hot section blades by making use of direct engine measurement data and make engine life tracking feasible and in less time, but at low cost to the operators of the engines. To be able to carry out the engine life estimation, an engine performance model is created in PYTHIA, Cranfield University's in-house gas turbine performance and diagnostics software. The created model is adapted to the real engine operation conditions. A data acquisition and pre-processing computer module is created while blade thermal and stress models are developed to provide temperatures and stresses at various locations along the span of the blade for life analysis. Different life analysis models are selected for the creep life analysis, fatigue life analysis and creep-fatigue interaction analysis respectively. The life analyses models and the sub-models developed to make engine life consumption analyses feasible are implemented in PYTHIA. The effects of various parameters on engine life consumption are thoroughly investigated in the different lifing modes. The various aspects of the research and some major findings in the research are are highlighted here.

The engine performance model of the LM2500+ engine created in PYTHIA is adapted to both the design and the off-design conditions of the real engine. The created and adapted engine model must behave like the real engine for its output gas path properties to be trusted for any further analysis. To ascertain the accuracy of the engine performance model, the model was applied to different conditions of engine operation and it produces results that closely matched those from the real engine. The model was thus validated and applied in the engine life analysis in this research.

To ensure transfer of data from the real engine operation to the engine performance model in PYTHIA for simulation, a data acquisition and pre-processing computer module was created. This module accepts field data in excel sheets, sends the data to the engine performance model and simulations are carried out using PYTHIA code. Shaft power and ambient temperature are used as parameters for off-design calculation (simulation) while other gas path properties available from the real engine operation are kept for comparison of results. The simulations are necessary because not all gas path properties required in the life analysis process are available from the real engine operation data; for instance TET. The results of the simulation are mainly gas path properties and components' efficiencies. The data acquisition and pre-processing module compares the simulated results with those from the real engine where results from the real engine exist, such as compressor exit temperature and ensure the results are in good agreement. Some of the simulated results are sent to the blade thermal and stress models through the data acquisition and pre-processing module. The module is able to transfer data for any period of engine operation in a given day for simulations and makes life analysis feasible.

Four thermal models are developed in this research with each blade divided into 8 equal parts and 9 nodes identifierd for life calculations. These are uniform temperature model with and without TBC, and one-dimensional temperature model with and without TBC. The one-dimensional model with TBC is used for life analysis. This model is developed assuming convective cooling of the blades and a radial temperature distribution factor of the combustor exit gases. The maximum gas temperature is assumed to occur at 62.5% distance from the blade root which varies linearly to minimum values at the blade tip and the blade root respectively. The blade material temperature is assumed to be the

same at every point in each nodal location. Although, a number of assumptions were made in obtaining the thermal model, the temperatures of the blade material predicted are in line with results from FEA models under similar loading conditions. In the blade stress model, centrifugal stress and bending momentum stresses are considered. Other sources of stresses are identified to be minimal thus not considered in estimating the blade stresses. The centrifugal stress is the major source of stress and it is highest in the blade root. The bending momentum stresses arise from velocity change bending moments and pressure change bending moments. Stresses are estimated at three chord-wise sites (leading edge, trailing edge, and furthest point at the suction surface of the blade) in each of the 9 nodes and the maximum value is used for life analysis in each node. The evaluation of the stresses in the three sites is because maximum stress is likely to occur in any of those sites.

The Larson-Miller Parameter method is used for creep life analysis. This model was chosen for its accuracy and availability of material master curve of the blade material. This model requires blade material temperature, Larson-Miller Parameter (LMP) value, and Larson-Miller Parameter constant which is known. The blade material temperature is gotten from the blade thermal model while the LMP value is read from the master curve based on the stress value gotten from the blade stress model. The LMP value is obtained by interpolation from a numerical equivalent of the master curve. An integrated creep life estimation system is built as a separate module in PYTHIA for creep life consumption analysis.

Relative creep life consumption analysis is carried out by dividing the creep life obtained with a reference creep life to give the creep factor. The creep factor stands for the severity of engine operation at each engine operation point. If creep factor is greater than one, it means favourable engine operation and vice-versa. Since the engine is being operated in different conditions, the concept of equivalent creep factor is introduced in this research to assess the wellness of engine operation in any time frame. Robinson's life fraction rule is applied to obtain the equivalent creep life in any period of engine operation, and the ratio of the equivalent creep life to the reference life gives the equivalent creep factor. If the equivalent creep factor is greater than unity, this portrays favourable engine operation for the given period, and vice-versa. If the equivalent creep

factor is unity, the cumulative engine creep life consumption is the same as operating the engine in the reference condition for the entire period.

Engine creep life consumption could be tracked from the values of the equivalent creep factors of engine operation which are easily gotten from the integrated creep life estimation system. The creep life analysis algorithms were applied to 8 different months of engine operation to illustrate how engine creep life could be tracked and to test the feasibility and the applicability of the creep life tracking process. The creep life tracking of the 8 months of engine operation produces results which are comparable with those in real engine operation (high equivalent creep factors obtained during low ambient temperatures and lower shaft power levels and lower equivalent creep factors obtained during periods of high ambient temperatures and high shaft power operations) thus confirming the accuracy of the life tracking algorithms developed in this research.

The influences of shaft power variation, ambient temperature and engine components degradations on creep life consumption were also investigated in this research. Components degradations come in the form of reduction of isentropic efficiency indices and flow capacity indices. The salient findings about the various effects on engine creep life consumption are summarized below:

- Generally, creep life reduces with an increase in shaft power.
- More favourable life increase with shaft power drop occurs towards peak power operation of the engine at any ambient temperature.
- Creep life increases with shaft power drop in the same magnitudes as shaft power increase does to reduction in creep life.
- Creep life decreases with an increase in ambient temperature. At a given power level, the rate of decrease in creep life with ambient temperature is smaller at higher ambient temperatures
- Creep life increases with ambient temperature drop in the same magnitudes as ambient temperature increase does to creep life reduction.
- Engine components degradations lead to decrease in creep life.
- Considering the reductions in isentropic efficiency and flow capacity reductions in components:

    - Compressor isentropic efficiency index reduction has more impact on engine creep life than compressor flow capacity index reduction
    - Compressor turbine flow capacity index reduction has more impact on creep life than compressor flow capacity index reduction
- For 1% and 2% reductions in efficiency and flow capacity indices of compressor and HP turbine respectively, the creep life / creep factors are reduced. The trends of the creep life / creep factors are similar to those of the clean engines, but less in magnitude.
- Compressor degradation has more influence on creep life than HP turbine degradation
- A unit increase in ambient temperature has more impact on creep life than 1% degradation of compressor turbine but has less impact compared to 1% degradation of compressor
- 1% increase in engine shaft power has less impact on creep life compared to unit increase in ambient temperature.
- A unit increase in engine shaft power has more impact on creep life than 1% reduction in health parameter indices of either the compressor or the HP turbine.

Fatigue life analysis is carried out in this research. The fatigue life estimation process requires a model for estimating the fatigue cycles to failure and another model for calculating the fatigue cycles accumulated in any period of engine operation. The Palmgren-Miner rule is then applied to estimate the fraction of fatigue life consumed from different blocks of loads obtained from engine operation, and thus estimate the equivalent fatigue life which is usually in terms of the number of fatigue cycles to failure for the different conditions of engine operation. The modified universal slopes method is used for calculating the fatigue cycles to failure at any condition of engine operation in this research. A low cycle fatigue life counting model suitable for analysing the cycles accumulated in industrial gas turbine operation was developed. This model was developed by considering the model the US Air Force use in accumulating fatigue cycles in air-craft operation. The developed model accounts for every variation of engine shaft speed. The development and the application of the fatigue cycles counting model ensures that fractional fatigue cycles accumulated in the course of engine

operation are generated and cycle counting does not depend on when engine is shut down to represent one fatigue cycle as practiced in many circumstances.

Like in the case of creep life, absolute results are not depended on, thus the concept of fatigue factor is introduced to assess the severity of operation at any time frame of engine operation. The fatigue factor is the ratio of the fatigue cycles to failure at any time frame of engine operation to the fatigue cycles to failure at a reference engine operation condition. Equivalent fatigue factor, which is the ratio of the equivalent fatigue life to the fatigue cycles to failure at a reference engine operation condition, is used to represent the wellness of engine operation considering different time frames of engine operation. If the equivalent factor is greater than one, this indicates slower rate of fatigue life consumption with respect to the reference engine operation condition, and vice-versa.

Fatigue life tracking of the engine is possible, and this was carried out for 8 different months of engine operation to track the fatigue life consumption of the engine for the period, and to also test the feasibility and the applicability of the life tracking process. The fatigue life tracking results are similar to what is obtainable in real engine operation. Also, the effects of shaft power variation, ambient temperature variation, and engine degradation on fatigue life consumption were investigated. It was observed that fatigue life is greatly affected by power level, while ambient temperature has only little effect on fatigue life consumption. The basic observations concerning the various effects on fatigue life consumption are presented below:

- At a given shaft power level, in the temperature range 5^{o}C to 30^{o}C, fatigue factors increase to about 13^{o}C and then drop. This stems from changes in the air density which leads to decrease in the mass of the compressor intake air, the shaft speed increases to balance the reduction in the momentum change stresses leading to increase in stresses and lower cycles to fatigue failure beyond 13^{o}C.
- For shaft power level above 90%, fatigue factors decrease with further increase in shaft power at any ambient temperature
- .Fatigue factors decrease with compressor degradation at all ambient temperatures and shaft power levels. Greater decrease in fatigue factors with compressor degradation is obtainable at lower power levels.

- When the compressor health parameter indices reductions are doubled (increased by 100%) the impact on fatigue life consumption increases more than 100%.

Creep-fatigue life analysis is carried out in this research using Taira's linear accumulation method. The creep-fatigue interaction model gets inputs from both the outputs of the creep life model and the fatigue life model. Creep-fatigue interaction life is estimated at the same locations in the blade where both creep life and fatigue life consumption are evaluated. The creep-fatigue interaction life could be expressed in terms of both time to failure and cycles to failure. The concept of creep-fatigue interaction factor is introduced to assess the severity of engine operation in any time frame, while equivalent creep-fatigue interaction factor is introduced to assess the severity of engine operation in different time frames. The use of the creep-fatigue interaction factor overcomes the apparent shortcomings in the Taira's linear accumulation model.

The contributions of creep and fatigue to creep-fatigue interaction life consumption are expressed in terms of creep and fatigue damage parameters respectively, which represent the fraction of creep life and the fraction of fatigue life consumed respectively in any period of engine operation. Considering the contributions of creep and fatigue to the creep-fatigue interaction life at different conditions of engine operation, it is observed that creep contribution dominates at all power levels and ambient temperatures but more dominance occurs in high ambient temperatures and lower power levels. At such conditions where creep dominance is more paramount, the results of creep life consumption is not much different from those of creep-fatigue interaction life consumption. Fatigue failure never dominates but contributes more in higher power levels of engine operation because it is driven by stress amplitude.

The creep-fatigue interaction life estimation methodology was applied to 8 months of engine operation using same data for the creep life consumption analysis as well as the fatigue life consumption analysis. The creep-fatigue life consumption of the engine was tracked in the process and the results obtained were in line with what is obtainable in real engine operation. On investigating the effects of shaft power variation, ambient

temperature variation, and engine degradation on creep-fatigue life consumption, the following are the basic findings:

- Creep-fatigue factor decreases with increase in ambient temperature at a given shaft power level.
- Creep-fatigue factor decreases with increase in shaft power at a given ambient temperature.
- Creep-fatigue factor decreases with engine components degradation.
- The percentage decrease in creep-fatigue factors with compressor degradation is higher at higher ambient temperatures and higher power levels.
- When the compressor health parameter indices reduction is doubled, the impact on the creep-fatigue life consumption is nearly doubled.

Apart from developing algorithms that could be applied in engine life consumption analysis exploiting different lifing modes, the developed lifing algorithms could be applied to engine life tracking. Engine operators could use the developed life consumption methodologies in monitoring the wellness of their engine operations. Also, the results of the various effects on engine life consumption will be of immense help to engine operators, especially, decisions concerning operating at part when with a view to extending engine life. Generally, these results will help engine operators in their condition monitoring and condition-based maintenance.

The aim of this research has been achieved and this research has contributed to the existing body of knowledge in a number of areas. These are summarized below:

- A platform has been created to simultaneously determine creep life, low cycle fatigue life and creep-fatigue interaction life consumptions using relative life analysis. The use of relative life analysis ensures having accurate trend in the engine life consumption irrespective of any minor shortcomings in the life estimation models.
- A means of quick assessment of engine life consumption has been created and engine life tracking is possible using direct engine measurement data.

- A low fatigue cycles counting model suitable for industrial turbines operation is developed. This model has the advantage of accounting for any minor variation of compressor shaft speed which brings about variations in stress levels. With this model, waiting for engine to be shut down to count one fatigue cycle is avoided.
- In this research, by investigating the low cycle fatigue contributions to creep-fatigue interaction life consumption at different engine operation conditions, safety margins have been developed where creep contribution to creep-fatigue interaction life is very dominant. At such margins, engine life consumption analysis could be wholly creep and the results are not much different from those of creep-fatigue interaction life consumption.
- In-depth analysis of the relative extent in which various factors affect engine life has been carried out. These results will meet many needs of engine operators.

9.2 Suggestions for Future Research

Gas turbine life estimation methods and life monitoring algorithms are successfully developed in this research thus achieving the aim and the objectives set out from the beginning. Inspite of this, there is still much room for improving the present work and there is need to look at other similar areas of research that will add to the present work and widen the scope of its applications. Improvements in some of the models developed and the life estimation methodlogy are first highlighted here, and this is followed by some future areas of research that will add value to the present work.

Improvements Required

Improvements are required in different aspects of the present work. These include improvements in blade thermal model, improvements in the blade stress model, and improvements in the entire life estimation methodlogy. Each of these is considered in turn.

Improvements in Blade Thermal Model

In the blade thermal model, temperatures are estimated at 9 nodes. To have a better temperature distribution, the nodes should be increased. Also, the maximum gas temperature is assumed to vary linear to the blade tip and blade root. The temperature variation is not actually linear; a quadratic function should be exploited to estimate the temperature variation from the maximum location to the blade tip and root. Another area of improvement in the blade thermal model is the usage of different radial temperature distribution factors (RTDF). The RTDF is assumed. Thus, to have results that represent the real situation better, which is not known, different values of RTDF should be used and the average blade metal temperature used for the life calculations.

Improvements in Blade Stress Model

The stress model considers centrifugal stresses and stresses arising from pressure change bending moments and velocity change bending moments. Stresses due to temperature gradients were not considered in the present work. Also, shear loading stresses due to gas pressure or centrifugal twisting of blades were left out. The temperature gradient stresses need to be accounted for in future works. When these stresses are included, the total stresses imposed on the blades will increase even if minor.

Improving the Life Estimation Methodology

In the present work, to estimate the engine life consumption, the engine operation data for each day is fed into the life estimation software and the engine life consumed per day or any period within the day of engine operation is estimated. When data for another day is uploaded, the life consumption for that day is estimated and the cumulative life consumed for the two days is also calculated automatically. There is no limit to the amount of data to be used for life estimation. The system calculates life consumption quickly but it is necessary to take it to the next level. Thus, a major improvement in the life estimation process developed in this research is to couple it to the real engine so that it will take the output of the engine and calculate the engine life consumption as the engine is being operated. This will enable the engine operators to monitor the rate at which the engine life is consumed while in operation. The above improvement will require some adjustments in the PYTHIA main code, the code that calls the blade thermal and stress models and the data acquisition and pre-processing module. This is achievable and I strongly recommend it is looked at in the future. Although, online engine life monitoring systems exist, but engine

operators hardly have access to such tools. Also, issues of accuracy are rarely ruled. The use of PYTHIA in this regard is therefore encouraged.

Future Areas of Research

There are several failure modes of gas turbine critical components. In this work, creep, fatigue and creep-fatigue interaction are considered. Oxidation is one very common failure mode which also acts as catalyst to the speedy occurrences of both creep and fatigue. When creep, fatigue and oxidation are brought under one umbrella, it is often termed thermo-mechanical fatigue (TMF) which mechanism is yet to be properly defined/understood. Since this work exploits analytical models for life analysis aimed at making engine life tracking feasible, in the future, I suggest the effect of oxidation should be built into it making use of the engine operation properties.

The gas turbine hot section components include nozzle guide vanes and rotor blades. In this work, the life analysis methodologies are applied to only the high pressure turbine rotor blades. The Application of the Lifing Methodology to Nozzle Guide Vanes in the future is recommended. This will be achieved by developing a thermal model and a stress model for nozzle guide vanes. The development of the thermal model will only require extracting relevant information from the blade thermal model developed in this work since the gas temperatures at the exit of the nozzle guide vanes were estimated in this work. For the nozzle guide vanes stress model, appropriate relations that model the stresses imposed on them could be exploited.

Another area I suggest should be looked at is the economics of operating at part load. Part load operation leads to burning more fuel per unit power output compared to peak power operation for most industrial gas turbine operations. But part load operation lengthens the life of the blades. If operating at a given part load extends blade life by a number of hours, thus extending both maintenance as well as replacement times, it is proper to look at different part load operations and the extent to which blade life is extended in each case. It is also important to estimate the financial gains in the life extension of the blades at each part load operation. Also, the additional fuel cost at each part load should be noted. An economic model should thus be developed covering different part load operations and determine the net gain obtained in each part load operation. This is also of interest to the author and I will likely look at it in the future.

REFERENCES

[1] H. I. H. Saravanamuttoo, G. F. C. Rogers, H. Cohen, and P. V Straznicky, *Gas Turbine Theory*, 6th ed. London: Pearson Educational Limited, 2009.

[2] M. P. Boyce, *GasTurbine Engineering Handbook*, 4th ed. Waltham: Butterworth-Heinemann, 2012.

[3] A. M. Y. Razak, *Industrial Gas Turbines: Performance and Operability*. Boca Raton, FL: Woodhead Publishing Limited, 2007.

[4] MIT Gas Turbine Lab, "Early Gas Turbine History," 2013. [Online]. Available: http://web.mit.edu/aeroastro/labs/gtl/early_GT_history.html. [Accessed: 20-Apr-2013].

[5] Y. A. Cengel and M. A. Boles, *Thermodynamics: An Engineering Approach*, 5th ed. NY: McGraw-Hill, 2009.

[6] Wikipedia, "Gas Turbines." [Online]. Available: http://en.wikipedia.org/wiki/Gas turbine. [Accessed: 12-Aug-2013].

[7] P. Pilidis and J. R. Palmer, "Gas Turbine Theory and Performance." (MSc Lecture Notes), Department of Power and Propulsion, Cranfield University, Cranfield, Bedfordshire, 2012.

[8] R. Kurz, "Introduction to Gas Turbines and Applications." Solar Turbines, 2013.

[9] E. Tsoutsanis, "Performance Adaptation of Gas Turbines for Power Generation Applications," (PhD Thesis),Cranfield University, Cranfield, Bedfordshire, 2010.

[10] GE-Marine, "LM2500+ Marine Gas Turbine," 2014. [Online]. Available: www.geaviation.com/engines/docs/marine/datasheet-lm2500plus.pdf. [Accessed: 20-Jan-2015].

[11] Energy and Environmental Analysis (an ICF International Company), "Technology Characterization : Gas Turbines," Arlington, Virginia, 2008.

[12] M. Hudson and S. Elders, "Maintenance and Support of Mature Gas Turbines." Siemens AG, 2005.

[13] G. H. Farrahi, M. Tirehdast, E. Masoumi Khalil Abad, S. Parsa, and M. Motakefpoor, "Failure Analysis of a Gas Turbine Compressor," *Eng. Fail. Anal.*, vol. 18, no. 1, pp. 474–484, Jan. 2011.

[14] M. F. Abdul Ghafir, Y. G. Li, L. Wang, and W. Zhang, "Impact Analysis of Aero-engine Performance Parameter Variation on Hot Section's Creep Life Using Creep Factor Approach," *AIAA*, vol. 16, no. 9, pp. 1–12, 2011.

[15] Z. Liu, D. N. Mavris, and V. Volovoi, “Creep Life Prediction of Gas Turbine Components Under Varying Operating Conditions,” in *ASME International Joint Power Generation Conference, June 4-7, New Orleans, Louisiana*, 2001, pp. 1–7.

[16] Y. G. Li and R. Singh, “An Advanced Gas Turbine Gas Path Diagnostic System-PYTHIA,” in *The XVII International Symposium on Air Breathing Engines, Munich, Germany*, 2005, pp. 1–12.

[17] J. Liburdi and J. Wilson, “Guidelines for Reliable Extension of Turbine Blade Life,” in *Proceedings of the 12th Turbomachinery Symposium, Texas A&M University, Texas, November*, 1983, pp. 21–29.

[18] R. Kurz and K. Brun, “Gas Turbine Performance — What Makes the Map?,” in *Proceedings of the 29th Turbomachinery Symposium, 18-21 September*, 2000, pp. 247–262.

[19] V. A. Pachidis, “Gas Turbine Simulation and Diagnostics, (MSc. Lecture Notes).” Department of Power and propulsion, Cranfield University, Cranfield, Bedfordshire, 2013.

[20] A. Diango, C. Périlhon, E. Danho, and G. Descombes, “Influence of Heat Transfer on Gas Turbine Performance,” in *Advances in Gas Turbine Technology*, E. Benini, Ed. Paris: InTech, 2011, pp. 212–236.

[21] Y. G. Li and P. Pilidis, “GA-Based Design-Point Performance Adaptation and its Comparison with ICM-Based Approach,” *Appl. Energy*, vol. 87, no. 1, pp. 340–348, Jan. 2010.

[22] R. Seleski, “Gas Turbine Efficiency Improvements Through Shroud Modifications,” PSM, Jupiter, Florida, 2013.

[23] S. Mattheij, “Repair Assessment and Modification of Gas Turbine Components and Assemblies.” Sulzer Technical Review 2, pp. 14–17, 2010.

[24] J. Petek and P. Hamilton, “Performance Monitoring Monitoring for Gas Turbines,” *ORBIT*, vol. 25, no. 1, pp. 65–74, 2005.

[25] Q. M. Jaber, J. O. Jaber, and M. A. Khawaldah, “Assessment of Power Augmentation from Gas Turbine Power Using Different Inlet Air Cooling Systems,” vol. 1, no. 1, pp. 7–15, 2007.

[26] A. Marzouk and A. Hanafi, “Thermo- Economic Analysis of Inlet Air Cooling in Gas Turbine Plants,” *Sch. J. Eng. Res.*, vol. 1, no. 15, pp. 76–84, 2012.

[27] A. Paula, P. Santos, C. R. Andrade, and E. L. Zaparoli, “Comparison of Different Gas Turbine Inlet Air Cooling Methods,” *World Acad. Sci. Eng. Technol.*, vol. 6, no. 1, pp. 40–45, 2012.

[28] A. P. Santos and C. R. Andrade, “Analysis of Gas Turbine Performance with Inlet Air Cooling Techniques Applied to Brazilian Sites,” *J. Aerosp. Technol. Manag.*, vol. 4, no. 3, pp. 341–354, 2012.

[29] W. E. Stewart, “Turbine Inlet Air Cooling,” *ASHRAE J.*, pp. 32–37, 1998.

[30] M. Chaker and C. B. Meher-homji, “Inlet Fogging of Gas Turbine Engines: Climatic Analysis of Gas Turbine Evaporative Cooling Potential of International Locations,” in *Proceedings of ASME Turbo Expo, Amsterdam, June 3-6*, 2002, pp. 1–16.

[31] J. Phillips and P. Levine, “Gas Turbine Performance Upgrade Options,” *FERN Engineering*. [Online]. Available: http://www.fernengineering.com/pdf/gt_upgrade_options.pdf. [Accessed: 02-Feb-2014].

[32] Wikipedia, “Degradation.” [Online]. Available: www.wikipedia/wiki-degradation. [Accessed: 19-Oct-2013].

[33] M. O. Vigueras Zuniga, “Analysis of Gas Turbine Compressor Fouling and Washing on Line,” (PhD Thesis), Cranfield University, Cranfield, Bedfrodshire, 2007.

[34] C. B. Meher-homji, M. A. Chaker, and H. M. Motiwala, “Gas Turbine Performance Deterioration,” in *30th Turbomachinery Symposium, Texas A&M University, Texas*, 2001, pp. 139–176.

[35] R. Kurz and K. Brun, “Degradation in Gas Turbine Systems,” in *International Gas Turbine & Aeroengine Congress Exhibition, May 8-11*, 2000, pp. 1–10.

[36] G. Cerri, M. Gazzino, F. Botta, and C. Salvini, “Production Planning with Hot Section Life Prediction for Optimum Gas Turbine Management,” *Int. J. Gas Turbine, Propuls. Power Syst.*, vol. 2, no. 1, pp. 9–16, 2008.

[37] M. F. Abdul Ghafir, “Performance Based Creep Life Estimation for Gas turbine Application,” (PhD Thesis), Cranfield University, Cranfield, Bedfordshire, 2011.

[38] S. Oakley and D. Nowell, “Prediction of the Combined High- and Low-Cycle Fatigue Performance of Gas Turbine Blades after Foreign Object Damage,” *Int. J. Fatigue*, vol. 29, no. 1, pp. 69–80, Jan. 2007.

[39] M. Wilcox, R. Baldwin, A. Garcia-Hernandez, and K. Brun, “Guidelines for Gas Turbine Inlet Air Filtration Systems, Release 1.0.” Gas Machinery Research Council, SouthWest Research Institute, San Antonio, Texas, 2010.

[40] R. Kurz and K. Brun, “Fouling Mechanisms in Axial Compressors,” *J. Eng. Gas Turbines Power*, vol. 134, no. 032401, pp. 1–9, 2012.

[41] A. Gannan, “Cascade Testing and CFD Applied to Gas Turbine Performance Improvement with Compressor Cleaning,” (PhD Thesis), Cranfield University, Cranfield, Bedfordshire, 2010.

[42] K. Brun, T. a. Grimley, W. C. Foiles, and R. Kurz, “Experimental Evaluation of the Effectiveness of Online Water-Washing in Gas Turbine Compressors,” *J. Eng. Gas Turbines Power*, vol. 137, pp. 1–15, 2015.

[43] E. A. Ogbonnaya, “Gas Turbine Performance Optimization Using Compressor Online Water Washing Technique,” *Sci. Res.*, vol. 3, pp. 500–507, 2011.

[44] E. Schneider, S. Demircioglu, S. Franco, and D. Therkorn, “Analysis of Compressor On-line Washing to Optimize Gas Turbine Power Plant Performance,” in *Proceedings of GT2009 ASME Turbo Expo 2009: Power for Land, Sea and Air, June 8-12*, 2009, pp. 1–9.

[45] M. P. Boyce and F. Gonzalez, “A Study of On-Line and Off-Line Turbine Washing to Optimize the Operation of a Gas Turbine,” *J. Eng. Gas Turbines Power*, vol. 129, pp. 114–122, 2007.

[46] P. Janardhan and N. C. M. Babu, “Effect of Foreign Object Damage on Fatigue Life of Compressor Blades in a Gas Turbine Engine,” *SASTECH*, vol. 7, no. 1, pp. 66–73, 2008.

[47] S. Suresh, *Fatigue of Materials*, 2nd ed. NY: Cambridge University Press, 2004.

[48] M. Sapsard, “Recommended Practices for Monitoring Gas Turbine Engine Life Consumption, RTO/NATO- NASA,” Canada Communication Group Inc., 2000.

[49] C. B. Meher-homji and G. George, “Gas Turbine Blade Failures: Causes, Avoidance, and Troubleshooting,” in *Proceedings of the 27th Turbomachinery Symposium, Texas A&M University*, 1998, pp. 129–180.

[50] J. Ding, S. B. Leen, E. J. Williams, and P. H. Shipway, “Finite Element Simulation of Fretting Wear-Fatigue Interaction in Spline Couplings,” *Tribol. - Mater. Surfaces Interfaces*, vol. 2, no. 1, pp. 10–24, Mar. 2008.

[51] Y. Fu, J. Wei, and A. W. Batchelor, “Some Considerations on the Mitigation of Fretting Damage by the Application of Surface-Modification Technologies,” *J. Mater. Process. Technol.*, vol. 99, pp. 231–245, 2000.

[52] “Hot Corrosion in Gas Turbines,” in *High Temperature Corrosion and Materials Application*, ASM International, 2007, pp. 249–259.

[53] A. K. Koul, A. Tiku, S. Bhanot, and B. Junkin, “Physics of Failure Modelling at the Microstructural Level for Prognostics of Creep Failure in an Engine Turbine Blade,” in *Proceedings of RTO AVT-144 Workshop on “Enhanced Aircraft*

Platform Availability Through Advanced Maintenance Concepts and Technologies", 3-5 October, 2006, pp. 1–12.

[54] H. Farhangi and A. A. Fouladi Moghadam, "Fractographic Investigation of the Failure of Second Stage Gas Turbine Blades," in *Proceedings of 8th International Fracture Conference, Istanbul, Turkey, 7-9 November*, 2007, pp. 577–584.

[55] L. Binda, "Advanced Creep Damage and Deformation Assessment of Materials Subject to Steady and Cyclic Loading Conditions at High Temperatures, (PhD Thesis)," ETH Zurich, 2010.

[56] F. R. N. Nabarro and F. de Villiers, *The Physics of Creep and Creep-Resistant Alloys*, 1st ed. CRC Press, Taylor & Francis Group, UK, 1995.

[57] T. G. Langdon, "An Analysis of Flow Mechanisms in High Temperature Creep and Superplasticity," *Mater. Trans.*, vol. 46, no. 9, pp. 1951–1956, 2005.

[58] DoITPoMS, "Creep Deformation of Metals," *University of Cambridge*. [Online]. Available: http://www.doitpoms.ac.uk/tlplib/creep/index.php. [Accessed: 15-Mar-2015].

[59] R. C. Reed, T. Tao, and N. Warnken, "Alloys-By-Design: Application to Nickel-Based Single Crystal Superalloys," *Acta Mater.*, vol. 57, pp. 5898–5913, 2009.

[60] I. M. Razumovskii, A. V Ruban, V. I. Razumovskiy, A. V Logunov, V. N. Larionov, O. G. Ospennikova, V. A. Poklad, and B. Johansson, "New Generation of Ni-Based Superalloys Designed on the Basis of First-Principles Calculations," *Mater. Sci. Eng. A*, vol. 497, pp. 18–24, 2008.

[61] T. M. Pollock and S. Tin, "Nickel-Based Superalloys for Advanced Turbine Engines: Chemistry, Microstructure and Properties," *J. Propuls. Power*, vol. 22, no. 2, pp. 361–374, 2006.

[62] M. Gell, D. N. Duhl, and A. F. Giamel, "The Development of Single Crystal Superalloy Turbine Blades," Pratt & Whitney Aircraft Group, East Hartford, 1974.

[63] Wikipedia, "Creep." [Online]. Available: www.wikipedia/wiki/creep -definition. [Accessed: 19-Oct-2013].

[64] J. L. Rhoads, "Basic Explanation of Creep Processes, CA 94720-1730," University of California, Berkeley, 2013.

[65] M. Gedeon, "Factors Affecting Stress Relaxation and Creep," no. 13. Brush Wellman Inc., Parkland Blvd, Mayfield Heights, 2010.

[66] Gas Path Analysis Ltd, “Turbine Creep Life Cycle Analysis.” [Online]. Available: http://www.gpal.co.uk/xcreep.htm. [Accessed: 17-Oct-2013].

[67] D. McLean, “The physics of High Temperature Creep in Metals,” *Reports Prog. Phys.*, vol. 29, no. 1, pp. 1–33, Jan. 1966.

[68] M. P. Hanson, “Effect of Temperature on Tensile and Creep Characteristics of PRD49 Fibre / Epoxy Composites.” NASA, Washington D C, pp. 1–13, 1972.

[69] Y. Terada and T. Sato, “Relationship between Minimum Creep Rate and Rupture Life for a Die-Cast Mg-Al-Mn Alloy,” *Mater. Trans.*, vol. 49, no. 3, pp. 439–442, 2008.

[70] Y. Terada and T. Sato, “Assessment of Creep Rupture Life of Heat Resistant Mg–Al–Ca Alloys,” *J. Alloys Compd.*, vol. 504, no. 1, pp. 261–264, Aug. 2010.

[71] “Creep and Stress Rupture.” [Online]. Available: www.materialsengineer.com-512x384-Search by image. [Accessed: 21-Oct-2013].

[72] D. Socie and B. Socie, “Thermomechanical Fatigue Made Easy.” [Online]. Available: http://www.cdm.unicas.it/files/Download/TMF_Made_Easy.pdf. [Accessed: 19-Oct-2013].

[73] P. Lowden, S. Turcott, M. Perrin, and S. Hastie, “The Role of Metallurgical Analysis in Gas Turbine Maintenance,” in *Proceedings of the 18th Symposium of the Industrial Application of Gas turbine Committee, Banff, Alberta, Canada, 19-21 October*, 2009, pp. 1–15.

[74] D. Harmon, M. Mcclure, R. Grelotti, and E. Hartford, “Unified Low Cycle Fatigue for Gas Turbine Engine Rotor Alloys,” in *Proceedings of 51st AIAA/ASME/ASCE/AHS/ASC Structures, Structural Dynamics, and Materilas Conference, Orlando, Florida, 12-15 April*, 2010, pp. 1–10.

[75] T. Nicholas, “Material Allowances for High Cycle Fatigue in Gas Turbine Engines,” in *RTO AVT Specialists’ Meeting on "Application of Damage Tolerance Principles for Improved Airworthiness of Rotorcraft*, 1999, pp. 1–9.

[76] Wikipedia, “Fatigue-(Materials).” [Online]. Available: www.wikipedia/wiki/fatigue- (materials). [Accessed: 18-Oct-2013].

[77] R. Zhang, “Reliability-Based Reassessment of Corrosion Fatigue Life,” *Struct. Saf.*, vol. 23, no. 1, pp. 77–91, Jan. 2001.

[78] A. Haslam and P. Laskaridis, “Fatigue & Fracture.” (MSc. Lecture Notes), Department of Power and Propulsion, Cranfield University, Cranfield, Bedfordshire, 2013.

[79] D. P. Deluca, “Understanding Fatigue,” *ASME*, 2013. [Online]. Available: http://files.asme.org/IGTI/Knowledge/Articles/13048.pdf. [Accessed: 07-May-2013].

[80] B. A. Cowles, “High Cycle Fatigue in Aircraft Gas Turbines — An Industry Perspective,” *Int. J. Fract.*, vol. 80, no. 2, pp. 147–163, 1989.

[81] H. Christ, A. Jung, H. J. Maier, and R. Teteruk, “Thermomechanical Fatigue – Damage Mechanisms and Mechanism-Based Life Prediction Methods,” *Sadhana*, vol. 28, no. Parts 1&2, pp. 147–165, 2003.

[82] A. García De la Yedra, A. Martín-Meizoso, R. R. Martín, and J. L. Pedrejón, “Thermo-Mechanical Fatigue Behaviour and Life Prediction of C-1023 Nickel Based Superalloy,” *Int. J. Eng. Sci. Technol.*, vol. 3, no. 6, pp. 88–101, 2011.

[83] W. Z. Zhuang and N. S. Swansson, “Thermo-Mechanical Fatigue Life Prediction : A Critical Review, DSTO-TR-0609.” DSTO Aeronautical and Marine Research Laboratory, Melbourne Victoria, Australia, 1998.

[84] S. Brookes, M. Nass, and B. Ward, “The Development of Stress Controlled Thermo-Mechanical Fatigue Testing at the Rolls-Royce Mechanical Test Operations Centre (MTOC),” Dahlewitz, Germany, 2012.

[85] S. M. Bagnail, D. L. Shaw, and J. C. Mason-Flucke, “Implications of ‘ Power by the Hour ’ on Turbine Blade Lifing,” in *RTO AVT Specialists’ Meeting on "Design for Low Cost Operation and Support, 21-22 October*, 1999, pp. 1–10.

[86] M. Villasante, “Predictive Methods for Combined Cycle Fatigue in Gas Turbine Blades,” in *Aerodays, Madrid, March 30- April 1*, 2011, pp. 1–8.

[87] R. O. Ritchie, S. Suresh, J. W. Hutchinson, and W. W. Milligan, “High-Cycle Fatigue and Time-Dependent Failure in Metallic Alloys for Propulsion Systems AFOSR F49620-96-1-0478,” in *Proceedings of 6th National Annual Conference on High-Cycle Fatigue, Jacksonville, FL, Feb*, 2000, pp. 1–16.

[88] E. Benvenuti, “Innovative Gas Turbine Performance Diagnostics and Hot Parts Life Assessment Techniques,” in *Proceedings of the 30th Turbomachinery Symposium*, 1965, pp. 23–32.

[89] L. C. Jaw, D. N. Wu, and D. J. Bryg, “Tracking and Control of Gas Turbine Engine Component Damage / Life,” in *Proceedings of RTO AVT Symposium on Ageing Mechanisms and Control: Monitoring and Management of Gas Turbine Fleets for Extended Life and Reduced Costs, Manchester , 8-11 October*, 2001, pp. 1–14.

[90] T. Goswamy, “Creep-Fatigue Interactions of Gas Turbine Materials,” *Def. Sci. J.*, vol. 38, no. 4, 1988.

[91] T. Nicholas, “High Cycle Fatigue Life Management in Gas Turbine Engines,” in *Proceedings of RTO AVT Workshop on “Quantification of Life Extension Schemes for Engine Components”, Corfu, Greece, 5-6 October*, 1998, pp. 1–10.

[92] S. Eshati, “An evaluation of Operation and Creep Life on Stationary Gas Turbine Engine,” (PhD Thesis), Cranfield University, Cranfield, Bedfordshire, 2012.

[93] M. N. Faridani, “Classification and Probabilistic Model Development for Creep Failures of Structures: Study of x-70 Carbon Steel and 7075-t6 Aluminum Alloys,” (MSc. Thesis), University of Maryland, College Park, 2012.

[94] Wikipedia, “Creep (deformation).” [Online]. Available: http://en.wikipedia.org/wiki/Creep_(deformation). [Accessed: 27-Oct-2014].

[95] “Creep / Viscoplasticity (Book Chapter).” [Online]. Available: http://www.ewp.rpi.edu/hartford/~ernesto/F2005/CINVESTAV/Notes/ch6.pdf. [Accessed: 05-May-2013].

[96] C. Schuh and D. C. Dunand, “An Overview of Power-Law Creep in Polycrystalline b -Titanium,” *Scr. Mater.*, vol. 45, pp. 1415–1421, 2001.

[97] J. A. Collins and S. R. Daniewicz, “Failure Analysis,” in *Handbook of Materals Selection*, K. Myer, Ed. New York: John Wiley & Sons, Inc., 2002, pp. 740–773.

[98] J. Shen, K. Ikeda, S. Hata, and H. Nakashima, “Transient Creep in High-Purity Aluminum at Ultra-Low Strain Rate and Room Temperature by Constant Stress and Changing-Stress Experiments,” *Mater. Trans.*, vol. 52, no. 10, pp. 1885–1889, 2011.

[99] X. He, G. Li, and Y. Ding, “Statistical Thermal Fatigue-Creep Modeling of 316 Stainless Steel Materials,” *Sci. Res. Essays*, vol. 6, no. 20, pp. 4172–4178, 2011.

[100] D. R. Eno, G. A. Young, and T. L. Sham, “A Unified View of Engineering Creep Parameters,” in *ASME Pressure Vessels and Piping Division Conference, July 21-31, Chicago, Illinois*, 2008, vol. 6, pp. 777–792.

[101] Wikipedia, “Larson-Miller Relation.” [Online]. Available: http://en.wikipedia.org/w/index.php?title=Larson? [Accessed: 19-Oct-2013].

[102] F. R. Larson and J. Miller, “Time-Temperature Relationship for Rupture and Creep Stresses,” *Trans. ASME*, vol. 74, pp. 765–771, 1952.

[103] Wikipedia, “Larson-Miller Parameter.” [Online]. Available: http://en.wikipedia.org/wiki/Larson-Miller_Parameter. [Accessed: 19-Oct-2013].

[104] L. D. O. Bueno, V. L. Sordi, and L. Marino, “Constant Load Creep Data in Air and Vacuum on 2 . 25Cr-1Mo Steel from 600 ° C to 700 ° C,” *Mater. Res.*, vol. 8, no. 4, pp. 401–408, 2005.

[105] Y. Kurata, H. Tsuji, M. Shindo, and H. Nakajima, “Creep Rupture Properties of a Ni-Cr-W Superalloy in Air Environment,” *J. Nucl. Mater.*, vol. 246, no. 2–3, pp. 196–205, 1997.

[106] E. O. Oluyede, “Fundamental impact of Firing Syngas in Gas Turbimes.” Electric Power Research Institute, Charlotte NC, University of Pittsburgh, 2006.

[107] I. Nonaka, T. Ohba, and F. Abe, “Residual Life Estimation for Long-Term Used Power Boiler Tubes,” in *Proceedings of ECCC Creep Conference, London, 12-14 September*, 2005, pp. 847–852.

[108] R. N. Ghosh, “CLIP: Computer Software for Creep Life Prediction of Engineering Materials,” *Eng. Fract. Mech.*, vol. 54, no. 1, pp. 71–73, 1996.

[109] M. F. Abdul Ghafir, Y. G. Li, R. Singh, K. Huang, and X. Feng, “Impact of Operating and Health Conditions on Aero Gas Turbine Hot Section Creep Life Using a Creep Factor Approach,” in *Proceedings of ASME Turbo Expo 2010: Power for Land, Sea and Air, June 14-16*, 2010, pp. 1–13.

[110] M. Vaezi and M. Soleymani, “Creep Life Prediction of Inconel 738 Gas Turbine Blade,” *J. Appl. Sci.*, vol. 9, no. 10, pp. 1950–1955, 2009.

[111] K. M. B. Taminger, “Analysis of Creep Behavior and Parametric Models For 2124 A L 2124 A L + Sic W Composite,” (MSc. Thesis), Virginia Polytechnic Institute and State University, 1999.

[112] A. K. Koul, “Larson-Miller Parameter and its Modified Version,” *Scr. Metall. Pergamon Press. Ltd.*, vol. 16, no. 8, pp. 947–950, 1982.

[113] F. T. Furillo, S. Purushothaman, J. K. Tien, and R. J. Dimelfi, “Comments on: ‘Understanding the Larson-Miller Parameter,’” *Scr. Metall. Pergamon Press. Inc.*, vol. 12, no. 4, pp. 327–329, 1978.

[114] F. T. Furillo, S. Purushothaman, and J. K. Tien, “Understanding the Larson-Miller Parameter,” *Scr. Metall. Pergamon Press. Inc.*, vol. 11, no. 6, pp. 493–496, 1977.

[115] J. Park, “Creep Rupture Data Analysis by Association with Large Database on Numerous Materials Tested for Long Times,” (Ph.D. Thesis), Case Western Reserve University, 1993.

[116] V. Krivenyuk, “Creep-Rupture Data for Complex Alloys at Elevated Temperatures,” *METALURGIJA*, vol. 46, no. 2, pp. 79–85, 2007.

[117] D. Šeruga, M. Fajdiga, and M. Nagode, “Creep Damage Calculation for Thermo Mechanical Fatigue,” *Strojniški Vestn. – J. Mech. Eng.*, vol. 57, no. 05, pp. 371–378, May 2011.

[118] S. S. Manson and G. R. Halford, *Fatigue and Durability of Metals at High Temperatures*. ASM International, Electronic Books, 2009.

[119] M. Aghaie-Khafri and M. Noori, "Life Prediction of a Ni-Base Superalloy," *Bull. Mater. Sci.*, vol. 34, no. 2, pp. 305–309, Aug. 2011.

[120] A. Mendelson, E. Roberts, and S. S. Manso, "Optimization of Time-Temperature Parameters for Creep and Stress Rupture, with Application to Data from German Cooperative Long-Term Creep Program." NASA, Washington D.C., 1965.

[121] H. Al-Ethari, "Creep in Metals," *University of Babylon*, 2013. [Online]. Available: http://www.uobabylon.edu.iq/eprints/publication_4_29484_1037.pdf. [Accessed: 17-Oct-2013].

[122] D. C. Dunand, B. Q. Han, and A. M. Jansen, "Monkman-Grant Analysis of Creep Fracture in Dispersion Strengthened Particulate-Reinforced Aluminum," *Metall. Mater. Trans.*, vol. 30A, pp. 829–838.

[123] M. Law, W. Payten, and K. Snowden, "Finite Element Analysis of Creep Using Theta Projection Data," *Int. J. Press. Vessel. Pip.*, vol. 75, no. 5, pp. 437–442, 1998.

[124] M. Evans, "A comparative Assessment of Creep Property Predictions for a 1CrMoV Rotor Steel Using the CRISPEN, CDM, Omega and Theta Projection Techniques," *J. Mater. Sci.*, vol. 39, no. 6, pp. 2053–2071, Mar. 2004.

[125] W. Evans, J. Screech, and S. Williams, "Thermo-Mechanical Fatigue and Fracture of INCO718," *Int. J. Fatigue*, vol. 30, no. 2, pp. 257–267, 2008.

[126] Y. Kariya, M. Otsuka, and W. J. Plumbridge, "The Constitutive Creep Equation for a Eeutectic Sn-Ag Alloy Using the Modified Theta-Projection Concept," *J. Electron. Mater.*, vol. 32, no. 12, pp. 1398–1402, Dec. 2003.

[127] C. C. Manu, "Finite Element Analysis of Stress Rupture in Pressure Vessels Exposed to Accidental Fire Loading," (MSc. Thesis), Queen's University, Ontario, Canada, 2008.

[128] J. Jelwan, M. Chowdhry, and G. Pearce, "Creep Life Processing of Weldment," *J. Solid Mech.*, vol. 3, no. 1, pp. 42–63, 2011.

[129] J. T. Yeom, J. Y. Kim, Y. S. Na, and N. K. Park, "Creep Strain and Creep-Life Prediction for Alloy 718 Using the Omega Method," *Met. Mater. Int.*, vol. 9, no. 6, pp. 555–560, Dec. 2003.

[130] J. JianPing, M. Guang, S. Yi, and X. SongBo, "A Continuum Damage Mechanics Model on Creep Rupture Life Assessment of a Steam Turbine Rotor," *J. Eng. Gas Turbines Power*, vol. 128, pp. 173–177, 2006.

[131] JobShop.com, “Nondestructive Testing Techniques on Plant Reliability.” .

[132] F. Van den Abeele and P. Goes, “Non Destructive Testing Techniques for Risk Based Inspection,” *Int. J. Sustain. Constr. Des.*, vol. 2, pp. 161–171, 2011.

[133] IAEA, “Non-Destructive Testing for Plant Life Assessment.” IAEA, Training Course Series, Vienna, pp. 1–68, 2005.

[134] M. Willcox and G. Downes, “A Brief Description of NDT Techniques,” *Insight NDT Equipment Limited*. pp. 1–22, 2000.

[135] E. Herba, “Fatigue and Damage Tolerance,” 2004. [Online]. Available: http://users.encs.concordia.ca/~mcqueen/Ed-Herba_class-lecture.pdf. [Accessed: 15-Oct-2013].

[136] J. E. Shigley and C. R. Mischke, *Mechanical Engineering Design*, 5th ed. New York: McGraw-Hill, 1989.

[137] R. Browell and A. Hancq, “Calculating and Displaying Fatigue Results.” ANSYS Inc., 2006.

[138] ASM, “Fatigue,” in *Elements of Metallurgy and Engineering Alloys*, Hitchin Hertfordshire: ASM International, 2008, pp. 243–265.

[139] V. B. Bhandari, *Design Of Machine Elements*, 3rd ed., vol. 15. NY: Tata McGraw-Hill Education, 2010.

[140] A. Ince and G. Glinka, “A Modification of Morrow and Smith-Watson-Topper Mean Stress Correction Models,” *Fatigue Fract. Eng. Mater. Struct.*, vol. 34, pp. 854–867, 2011.

[141] W. Cui, “A State-of-the-Art Review on Fatigue Life Prediction Methods for Metal Structures,” *J. Mar. Sci. Technol.*, vol. 7, pp. 43–56, 2002.

[142] M. Chaussumier, C. Mabru, M. Shahzad, R. Chieragatti, and F. Rezai-Aria, “A Predictive Fatigue Life Model for Anodized 7050 Aluminium Alloy,” *Int. J. Fatigue*, vol. 48, pp. 205–213, Mar. 2013.

[143] Y. Liu and S. Mahadevan, “Multiaxial High-Cycle Fatigue Criterion and Life Prediction for Metals,” *Int. J. Fatigue*, vol. 27, no. 7, pp. 790–800, Jul. 2005.

[144] K. S. Kim, X. Chen, C. Han, and H. W. Lee, “Estimation Methods for Fatigue Properties of Steels Under Axial and Torsional Loading,” *Int. J. Fatigue*, vol. 24, no. 1, pp. 783–793, 2002.

[145] Z. Hashin, “A Reinterpretation of Palmgren-Miner Rule,” 1979.

[146] N. E. Dowling, “Mean Stress Effects in Stress-Life and Strain-Life Fatigue,” *Soc. Automot. Eng. Inc.*, Apr. 2004.

[147] ETBX, “Strain-LifeFatigue Analysis,” *ETBX*. [Online]. Available: www.fea-optimization.com/EBTX/strainlife_help.html. [Accessed: 19-Oct-2013].

[148] J. Park and J. Song, “Detailed Evaluation of Methods for Estimation of Fatigue Properties,” *Int. J. Fatigue*, vol. 17, no. 5, pp. 365–373, 1995.

[149] Y. Liu and S. Mahadevan, “Probabilistic Fatigue Life Prediction Using an Equivalent Initial Flaw Size Distribution,” *Int. J. Fatigue*, vol. 31, no. 3, pp. 476–487, Mar. 2009.

[150] Y. S. Upadhyaya and B. K. Sridhara, “Fatigue Crack Initiation and Propagation Life Prediction of Materials,” in *Proceedings of International Conference on Mechanical, Electronics and Mechatronics Engineering (ICMEME’2012), March 17-18*, 2012, pp. 13–18.

[151] “Fatigue : Total Life Approaches, (A Presentation),” 2013. [Online]. Available: http://materials.iisc.ernet.in/~ramu/Fatigue.pdf. [Accessed: 13-Oct-2013].

[152] A. Fatemi, “Multiaxial Stresses, (Lecture Notes), University of Toledo, Ohio.” 2014.

[153] H. Mao and S. Mahadevan, “Creep Fatigue Reliability of High Temperature Materials,” in *8th ASCE Specialty Conference on Probabilistic Mechanics and Structural Reliability, University of Notre Dame, July 4-26*, 2000, pp. 1–6.

[154] V. Ogarevic, “Thermo-mechanical Fatigue, (A Presentation),” *nCode International Inc.*, 2003. [Online]. Available: http://www.fatigue.org/minutes/Fall-2003/Vladimir-Ogarevic.pdf. [Accessed: 19-Oct-2013].

[155] S. L. Robinson, “Effect of Temperature Variation on the Long Time Rupture Strength of Steels,” *Trans. ASME 74*, pp. 777–780, 1952.

[156] M. L. Weaver, “Creep-Fatigue Interaction.” (Lecture Notes), University of Alabama, Alabama, 2012.

[157] C. J. Pierce, “Creep and Fatigue Interaction Characteristics of PWA1484,” (MSc. Thesis), Air force Institute of Technology, Wright-Patterson Air Force Base, Ohio, 2009.

[158] R. Chachurski, P. Glowacki, and S. Szczecinski, “Methods of Counting Aircraft Turbine Engines Operating Cycles.” Transactions of the Institute of Aviation 217, Warsaw, pp. 5–13, 2011.

[159] Y. G. Li, “Gas Turbine Performance and Health Status Estimation Using Adaptive Gas Path Analysis,” *J. Eng. Gas Turbines Power*, vol. 132, no. 4, pp. 1–9, 2010.

[160] L. Marinai, D. Probert, and R. Singh, “Prospects for Aero Gas-Turbine Diagnostics: A Review,” *Appl. Energy*, vol. 79, pp. 109–126, 2004.

[161] R. B. Joly, S. O. T. Ogaji, R. Singh, and S. D. Probert, “Gas-Turbine Diagnostics Using Artificial Neural-Networks for a High Bypass Ratio Military Turbofan Engine,” *Appl. Energy*, vol. 78, pp. 397–418, 2004.

[162] S. O. T. Ogaji, S. Sampath, L. Marinai, R. Singh, and S. D. Probert, “Evolution Strategy for Gas-Turbine Fault-Diagnoses,” *Appl. Energy*, vol. 81, pp. 222–230, 2005.

[163] R. Kurz, K. Brun, and M. Wollie, “Degradation Effects on Industrial Gas Turbines,” *J. Eng. Gas Turbines Power*, vol. 131, 2009.

[164] R. Kurz and K. Brun, “Degradation of Gas Turbine Performance in Natural Gas Service,” *J. Nat. Gas Sci. Eng.*, vol. 1, pp. 95–102, 2009.

[165] K. Jordal, M. Assadi, and M. Genrup, “Variations in Gas-Turbine Blade Life and Cost due to Compressor Fouling – A Thermoeconomic Approach,” vol. 5, no. 1, pp. 37–47, 2002.

[166] S. Eshati, A. Abu, P. Laskaridis, and A. Haslam, “Investigation into the Effects of Operating Conditions and Design Parameters on the Creep Life of High Pressure Turbine Blades in a Stationary Gas Turbine Engine,” vol. 15, no. 3, pp. 237–247, 2011.

[167] G. Marahleh, A. R. I. Kheder, and H. F. Hamad, “Creep-Life Prediction of Service-Exposed Turbine Blades,” *Mater. Sci.*, vol. 42, no. 4, pp. 476–481, Jul. 2006.

[168] D. G. Ullman, *The Mechanical Design Process*, 4th ed. New York: McGraw-Hill Companies, Inc., 2010.

[169] C. O. C. Oko, “Solution Tree Problem Solving Procedure for Engineering Analysis Problems,” *J. Model. Des. Manag. Eng. Syst.*, vol. 4, no. 1, 2006.

[170] R. L. Hartung, “Low Cycle Fatigue Damage Counter,” 1977. [Online]. Available: http://www.google.com/patents/US4031366. [Accessed: 11-Jan-2015].

[171] S. Downing and D. Socie, “Simple Rainflow Counting Algorithms,” *Int. J. Fatigue*, pp. 31–40, 1982.

[172] G. Glinka and J. Kam, “Rainflow Counting Algorithm for Very Long Stress Histories,” *Int. J. Fatigue*, vol. 9, no. 3, pp. 223–228, 1987.

[173] N. Hong, “A Modified Rainflow Counting Method,” *Int. J. Fatigue*, vol. 13, no. 6, pp. 465–469, 1991.

[174] S. H. Baek, S. S. Cho, and W. S. Joo, “Fatigue Life Prediction Based on the Rainflow Cycle Counting Method for the End Beam of a Freight Car Bogie,” *Int. J. Automot. Technol.*, vol. 9, no. 1, pp. 95–101, 2008.

[175] R. A. Cookson and A. S. Halsam, “Fatigue and Fracture.” (MSc Lecture Notes), Cranfield University, Cranfield, Bedfordshire, 2013.

[176] Y. G. Li, P. Pilidis, and M. A. Newby, “An Adaptation Approach for Gas Turbine Design-Point Performance Simulation,” *J. Eng. Gas Turbines Power*, vol. 128, no. 4, pp. 789–795, 2006.

[177] J. Blinstrub, Y. G. Li, M. Newby, Q. Zhou, G. Stigant, P. Pilidis, and H. Honen, “Application of Gas Path Analysis to Compressor Diagnostics of an Industrial Gas Turbine Using Field Data,” in *Proceedings of ASME Turbo Expo 2014: GT2014, June 16-20, Dusseldorf, Germany*, 2014, pp. 1–12.

[178] Y. G. Li, M. F. Abdul Ghafir, L. Wang, R. Singh, K. Huang, X. Feng, and W. Zhang, “Improved Multiple Point Nonlinear Genetic Algorithm Based Performance Adaptation Using Least Square Method,” *J. Eng. Gas Turbines Power*, vol. 134, pp. 1–9, 2012.

[179] Y. G. Li, M. F. A. Ghafir, L. Wang, R. Singh, K. Huang, and X. Feng, “Nonlinear Multiple Points Gas Turbine Off-Design Performance Adaptation Using a Genetic Algorithm,” *J. Eng. Gas Turbines Power*, vol. 133, pp. 1–9, 2011.

[180] Y. G. Li, L. Marinai, V. Pachidis, E. Lo Gatto, and P. Pilidis, “Multiple-Point Adaptive Performance Simulation Tuned to Aeroengine Test-Bed Data,” *J. Propuls. Power*, vol. 25, no. 3, pp. 635–641, 2009.

[181] A. Stamatis, K. Mathioudakis, and K. D. Papailiou, “Adaptive Simulation of Gas Turbine Performance,” *J. Eng. Gas Turbines Power*, vol. 112, no. 2, pp. 168–175, 1990.

[182] J. K. Suraweera, “Off-Desin Performance Prediction of Gas Turbines without the Use of Compressor or Turbine Characteristics,” (MSC. Thesis), Department of Mechanical and Aerospace Engineering, Carleton University, Ottawa, Ontario, 2011.

[183] I. Griffiths, *Programming C# 5.0*. O’Reilly Media, 2012.

[184] Manx Electricity Authority, “Borescope Inspection Report,” Isle of Man, 2014.

[185] D. G. Wilson, “The Design of High-Efficiency Turbomachinery and Gas Turbines.” MIT Press, Cambridge, Massachusetts, pp. 487–492, 1991.

[186] H. Mousthapha, M. F. Zelesky, N. C. Baine, and D. Japikse, *Axial and Radial Turbines*. Vermont: Concepts NREC, 2003.

[187] P. A. Rubini, "Turbine Blade Cooling." (MSc Lecture Notes), Cranfield University, Cranfield, Bedfordshire, 2014.

[188] L. Torbidoni and J. H. Horlock, "A New Method to Calculate the Coolant Requirements of a High-Temperature Gas Turbine Blade," *J. Turbomach.*, vol. 127, pp. 191–199, 2005.

[189] M. J. Holland and T. F. Thake, "Rotor Blade Cooling in High Pressure Turbines," *J. Aircr.*, vol. 17, no. 6, pp. 412–418, 1980.

[190] A. Feuerstein, N. Hitchman, T. A. Taylor, and D. Lemen, "Process and Equipment for Advanced Thermal Barrier Coatings," *CESR*, vol. 29, no. 4, pp. 107–122, 2008.

[191] D. R. Clarke and S. R. Phillpot, "Thermal Barrier Coating Materials," *Materialstoday*, pp. 22–29, 2005.

[192] X. Q. Cao, R. Vassen, and D. Stoever, "Ceramic materials for thermal barrier coatings," *J. Eur. Ceram. Soc.*, vol. 24, pp. 1–10, 2004.

[193] "Properties of Dry Air," *The Engineering ToolBox*. [Online]. Available: http://www.engineeringtoolbox.com/dry-air-properties-d_973.html. [Accessed: 07-May-2014].

[194] D. G. Ainley, "Internal Air-Cooling for Turbine Blades - A General Design Survey," R&M 3013, Aeronautic Research Council, 1957.

[195] Wikipedia, "Sutherland Equation." [Online]. Available: http://en.wikipedia.org/wiki/Viscosity. [Accessed: 12-Mar-2014].

[196] E. V. Klapdor, "Simulation of Combustor –Turbine Interaction in a Jet Engine," (MSc Thesis), Institute of Energy and Power Plant Technology, TU Darmstadt, 2010.

[197] T. C. Lieuwen and Y. Vigor, *Gas Turbine Emissions*. New York: Cambridge University Press, 2013.

[198] A. H. Lefebvre, *Gas Turbine Combustion*, 2nd ed. Phiadelphia: Taylor and Francis, 1999.

[199] P. Walsh and P. Fletcher, *Gas Turbine Performance*, 2nd ed. Oxford: Blackwell Publishing Company, 2004.

[200] A. O. Abu, "Integrated Approach for Stress Based Lifing of Aero Gas Turbine Blades," (PhD Thesis), Cranfield University, Cranfield, Bedfordshire, 2013.

[201] R. A. Cookson and A. S. Haslam, “Mechanical Design of Turbomachinery.” (MSc Lecture Notes), Cranfield University, Cranfield, Bedford, 2011.

[202] F. Saedi, “Gas Turbine Diagnostics Analysis for Manx Electricity Authority,” (MSc Thesis), Cranfield University, Cranfield, Bedfordshire, 2013.

[203] D. S. Aziaka, “Gas Turbine Performance Adaptation,” (MSc Thesis), Cranfield University, Cranfield, Bedfordshire, 2013.

[204] D. Buggins, “Gas Turbine Diagnostics Analysis Using Gas Path Analysis for Manx Electricity Authority,” (MSc Thesis), Cranfield University, Cranfield, Bedfordshire, 2013.

[205] W. L. Macmillan, “Development of a Modular Type Computer Program for Calculation of Gas Turbine Off Design Performance,” (PhD Thesis), Cranfield University, Cranfield, Bedfordshire, 1974.

[206] R. Salamat, “Gas Path Diagnostics for Compressors,” (PhD Thesis), Cranfield University, Cranfield, Bedfordshire, 2012.

[207] J. H. Wood, D. A. Shores, and N. R. Lindblad, “Cast Nickel-Base Alloy , US Patent (US 6416596 B1),” 2002. [Online]. Available: http://www.google.co.uk/patents/US6416596. [Accessed: 12-May-2014].

APPENDICES

APPENDIX A : Program Details and Functionalities

Cranfield University in-house gas turbine performance and diagnostics software, PYTHIA is used as the core program in this work. The capabilities of PYTHIA in carrying out off-design performance calculation are exploited in this research. This work entails engine life consumption estimation and monitoring. The life consumption analysis algorithms developed are incorporated in PYTHIA and this makes it possible for engine like tracking. New interfaces or program windows are created and program codes provided to make the life consumption analysis feasible. The new interfaces created and the functions of the engine life consumption modules incorporated in PYTHIA to form a modified version of the software are presented briefly in this appendix. The provision of this appendix here is only to show what I have done regarding putting my work in a software for the usage of the company that co-sponsored my research, Manx Utilities (MU). The product of my research is the property of Manx Utilities, thus, much details about the software will not be given. Details regarding to the forms created and those of academic importance are presented here.

A.1 Program Windows/Interfaces

The interfaces or windows that are relevant to the lifing analysis in this research could be put into three categories. These are the Engine Design window, Life Setting windows and Life Analysis windows. Each of these windows is presented in the following sub-sections.

A.1.1 Engine Design Window

The engine design window is part of original version of PYTHIA but it is modified here and serves as the means of communicating with the new windows created for life analysis. Figure A.1 shows the engine design window. The engine design window links with the life analysis modules through “Build Lifing” and the “Lifing Analysis” Menu items at the top of the window. The “Lifing Analysis” Menu is not ‘Enabled’ until data is uploaded for simulation. The engine performance model is loaded in the system through the file menu (sub-menu “Open Existing Engine Model”). Also, engine data for simulation is uploaded through the file menu (sub-menu “Upload Engine Measurement

Data") while files uploaded are displayed in the "Files Uploaded" frame, Figure A.2. One file is uploaded at a time and simulations are carried out before a second file is uploaded for simulations. There is no limit to the number of files to be uploaded for simulation.

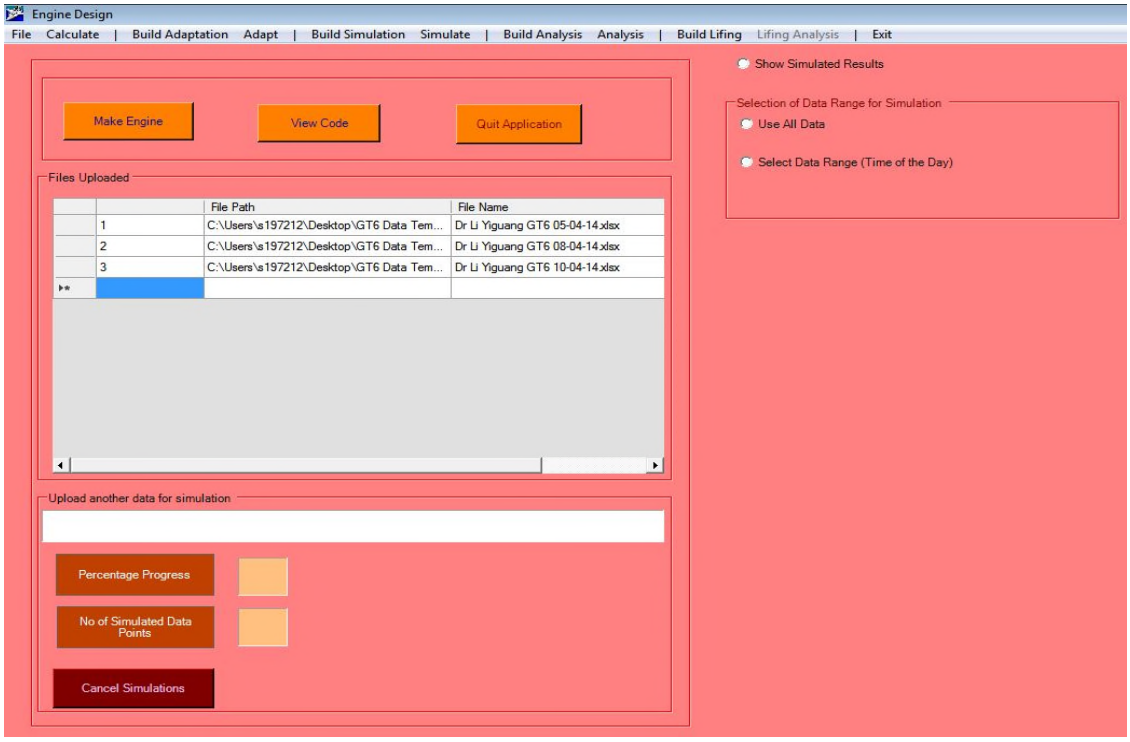

Figure A.1: Engine Design Window

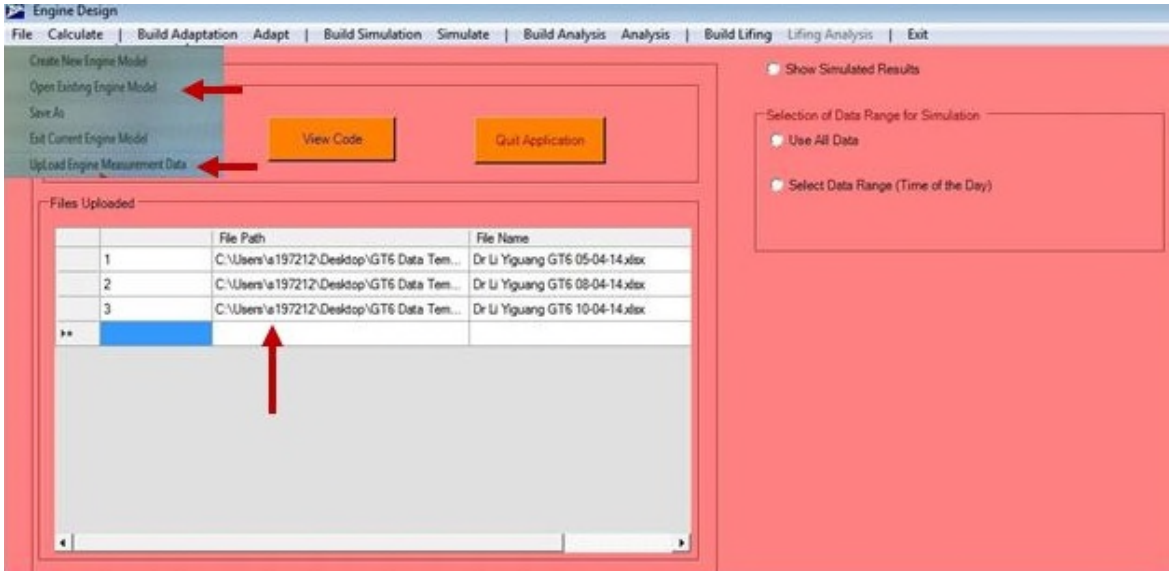

Figure A.2: Engine Model Upload and Measurement Data Upload from Engine Design Window

In selecting data for simulation, engine operators may like to know how well the engine was operated in different periods of the day. Thus, two radio buttons are created in the Selection of Data Type for Simulation Frame: “Use All Data” and “Select Data Range (Time of the Day)”. By Default, all data of the day operation of the engine is selected. When the “Select Data Range (Time of the Day)” radio button is checked, two combo boxes are made visible for the operator to select the period of the day. In Figure A.3, 00:10am and 12:02pm are selected and the engine operation data between these periods will be used for life consumption analysis. To select all the data, the “Use All Data” radio button should be checked. When the engine performance model and engine operation data are uploaded, off-design performance calculations or simulations are carried out by clicking the “Simulate Engine Performance” sub-menu (not shown) in the Build Lifing Menu. When simulations are completed, the operator may like to view some simulated results. This is achieved by checking the “Show Simulated Results” radio button as in Figure A.3.

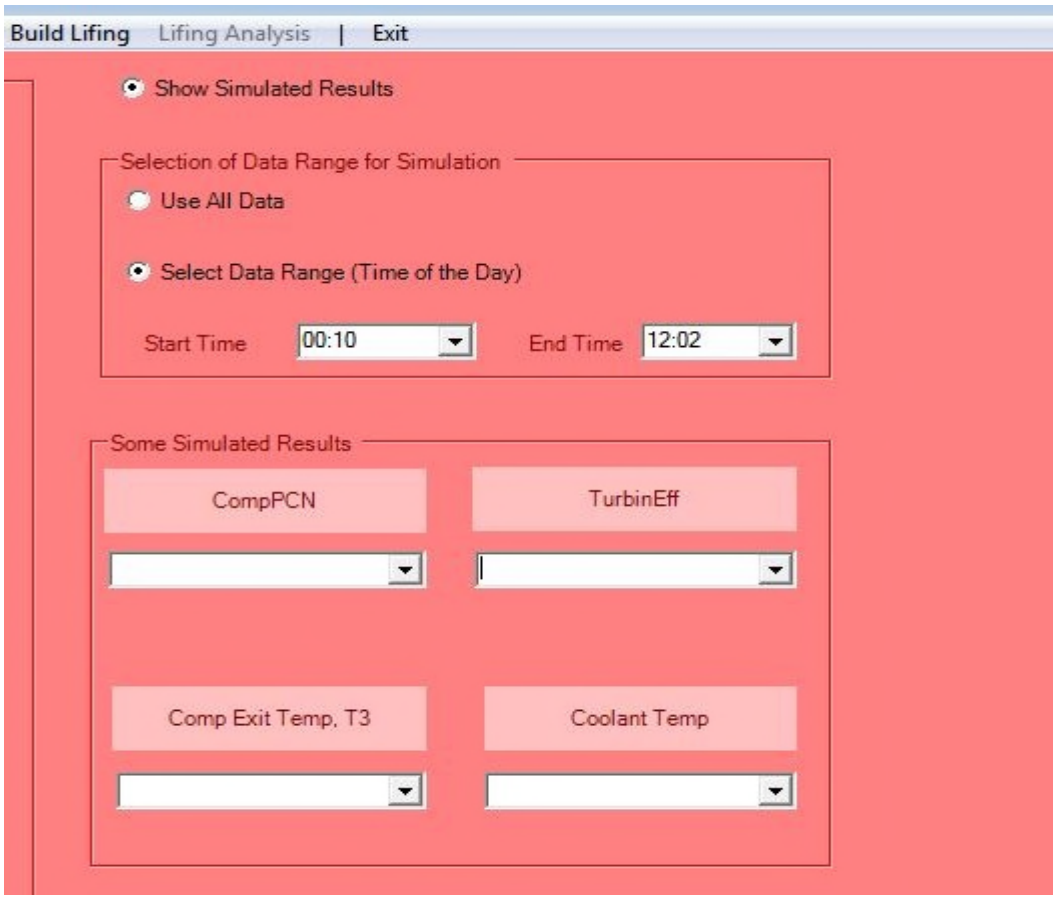

Figure A.3: Selection of Data for Simulation and Simulated Results View

The engine design window also has a frame ("Upload another data for simulations") for monitoring the progress of simulations. The simulations could also be cancelled at any point. When simulations are going on, the text changes to "Simulations in Progress" and on completion of Simulations, it changes to "Simulations Completed Successfully", Figure A.4. When the program is not running, the frame display text is "Display Progress"

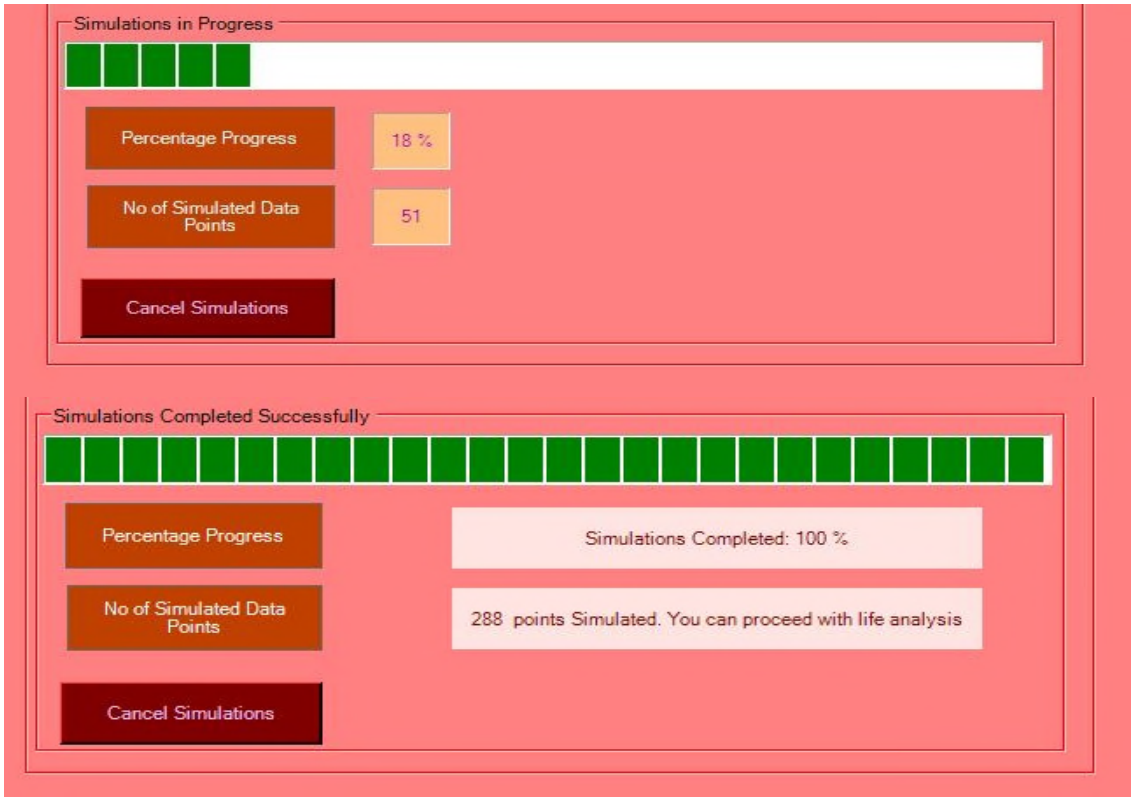

Figure A.4: Simulations Progress Display

In the Engine Design window, other menus that are not relevant to the life consumption analysis carried out in this research are also shown. The Life Setting Windows and the Life Analysis windows are accessed from the Engine Design window and these are considered next.

A.1.2 Life Setting Windows

The Life Setting Windows are assessed from the Building Lifing Menu in the Engine Design window. Three life setting windows are created to enable life consumption analysis. These are the Blade Parameters Setting window, Creep Life Setting window, and Fatigue and Creep-Fatigue Interaction Setting window.

Blade Parameters Setting Window

Figure A.5 shows the Blade Parameters Setting window. Data about blade geometry, blade cooling and thermal barrier coating are provided. The values pertaining to the engine used for this research are already stored in the program. Some data for the blade parameter setting is given in Appendix G. The operator does not need to change anything if dealing with same engine. For a different engine, there is provision for the operator to supply new set of data and save such data in a required location or change those of the original engine used. These provisions are made available by sub-menu items under the file menu in the window. Also, the thermal model to be used is selected. By default, the one-dimensional thermal model is selected.

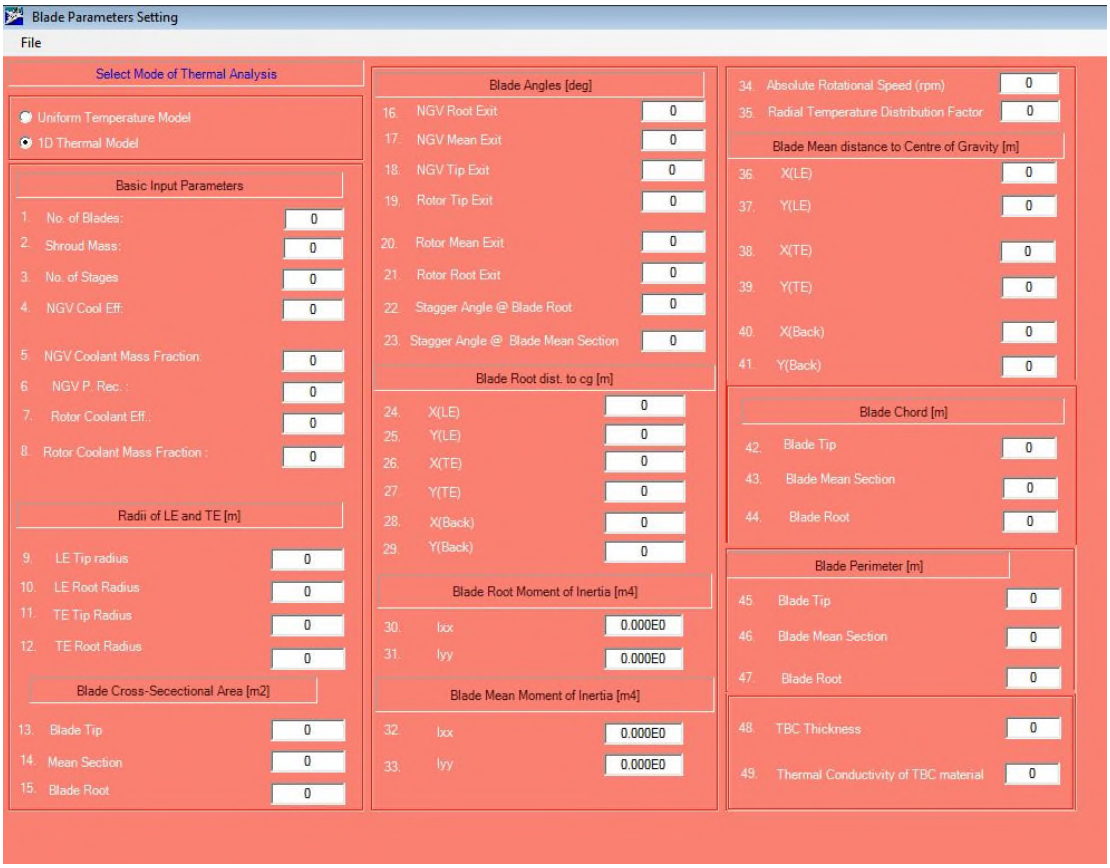

Figure A.5: Blade Parameters Setting Window

Creep Life Setting Window

In the creep life setting window, Figure A.6, the blade material Larson-Miller parameter data consisting of stress and LMP values are inputted. The Larson-Miller Parameter constant C and the blade material density are also supplied in this window. The data

could be stored in any location or in the program. The required data is already stored in the system for life analysis hence the operator has nothing to do here unless a new engine is considered. Data about LMP values is provided in Appendix G.

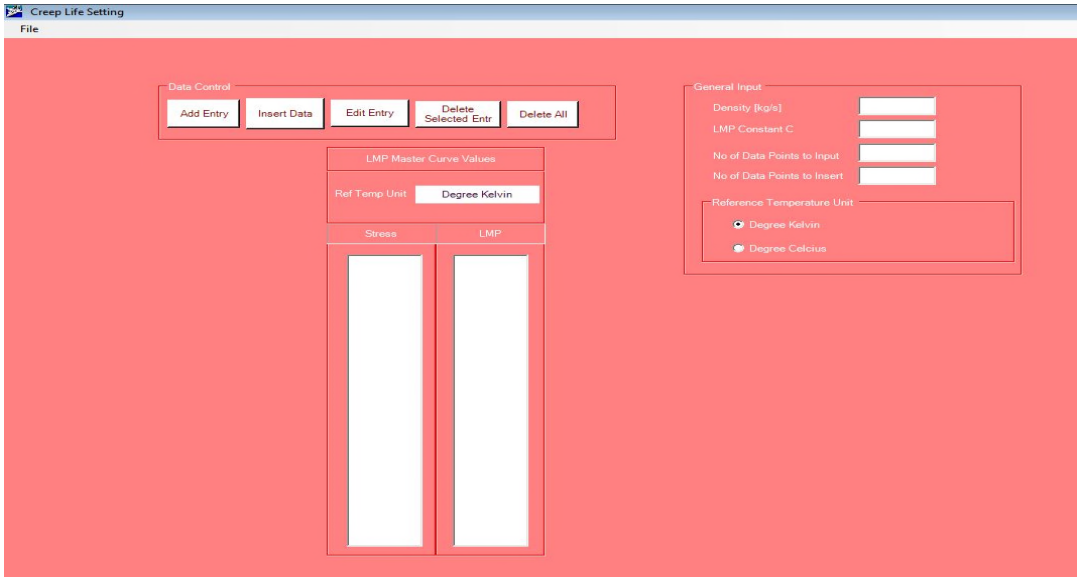

Figure A.6: Creep Life Setting Window

Fatigue and Creep-Fatigue Interaction Setting Window

Figure A.7 shows the fatigue and creep-fatigue interaction setting window. In this window, the Young's modulus, the ultimate tensile strength and the true fracture ductility of the material are inputted. Also, a low cycle definition is supplied here. The relevant values are already stored in the system.

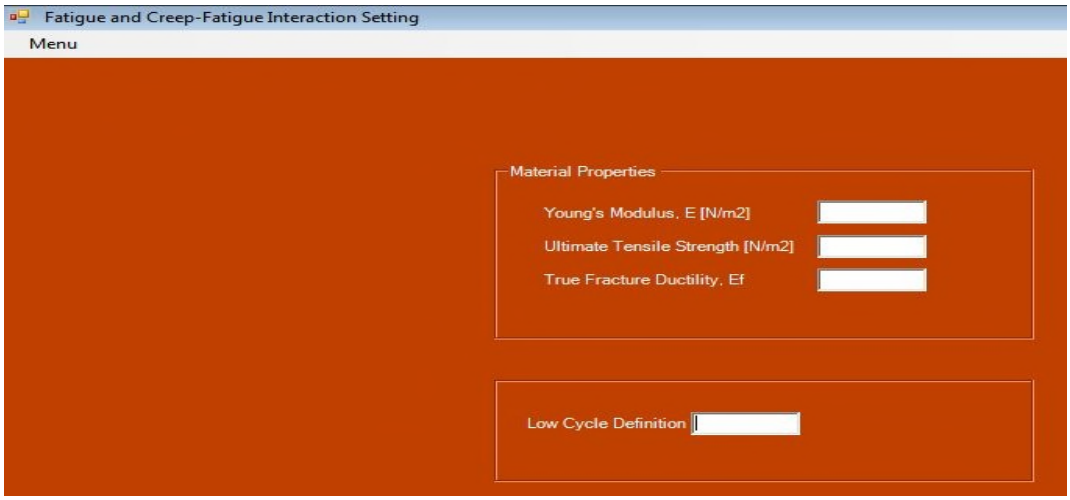

Figure A.7: Creep and Creep-Fatigue Interaction Setting Window

A.1.3 Life Analysis Windows

The life analysis windows are two in number. These are the creep life analysis window and the fatigue and creep-fatigue interaction life analysis window. Each of these is presented here. These windows are accessed through the Lifing Analysis menu in the Engine Design window.

Creep Life Analysis Window

The creep life analysis window is shown in Figure A.8. Here, the creep life consumption of the engine is estimated. The creep lives and the creep factors at each operation point of the last data simulated are given. The time in hours of each data used for life analysis, the creep life due to each data and the creep factor for each data used for life analysis are also obtained here. The overall equivalent creep life and equivalent creep factor due to every data of engine operation are obtained also.

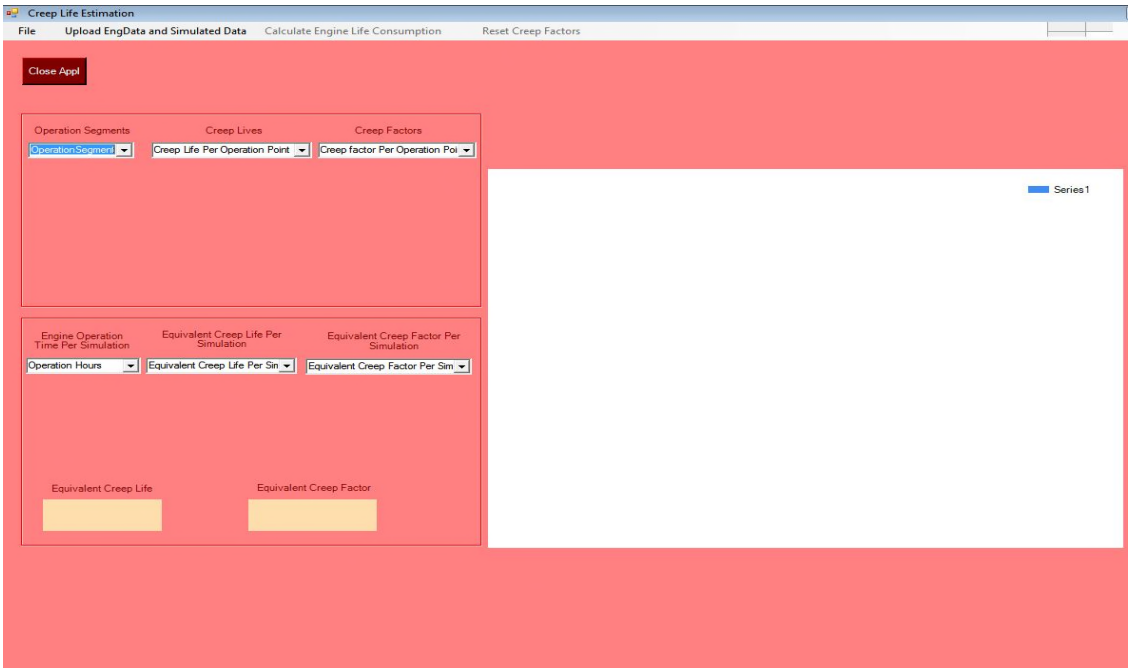

Figure A.8: Creep Life Analysis Window

There is also a graphical plotting area where the operator can visualize any engine operation property or creep life analysis property. The creep factors and the equivalent creep factor for the last data could be plotted against time of engine operation. The equivalent creep factors per data simulated and the overall equivalent creep factor could be plotted against time. Also, the trend of the equivalent creep factors could be

displayed as in Chapter 6. The plot selection panel is visible when the “Upload EnData and Simulated Data” menu is clicked followed by “Calculate Engine Life Consumption” menu, Figure A.9. The creep life analysis results could be saved and the data analysed could be deleted from the system through sub-menus provided in the file menu.

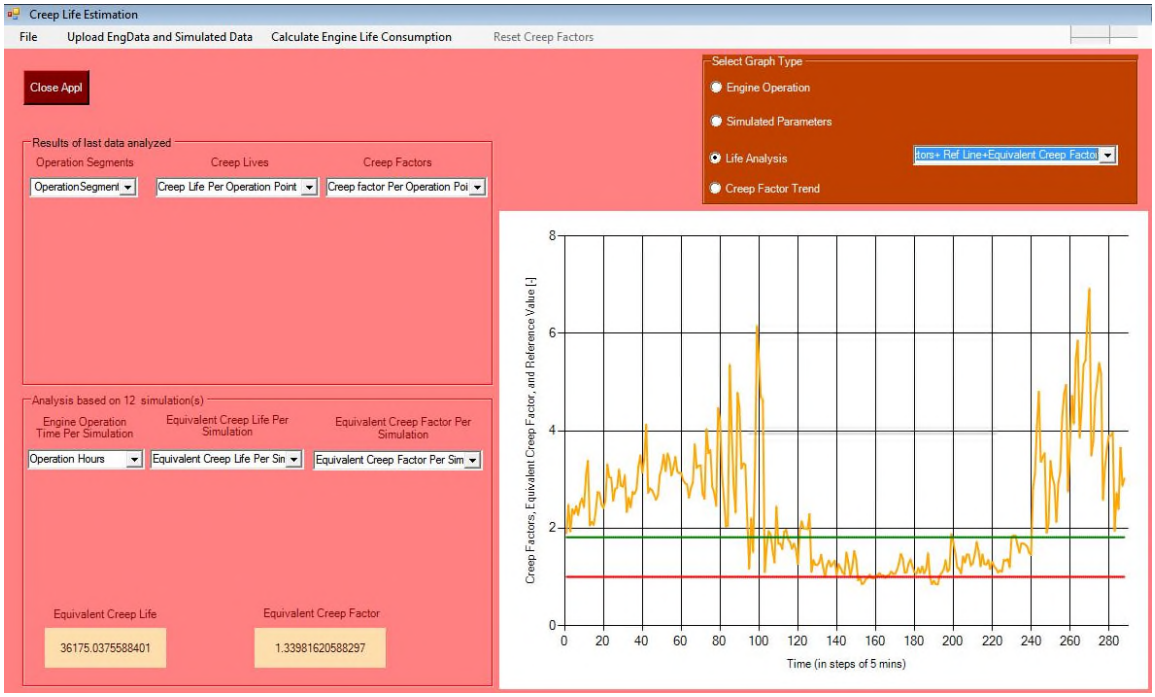

Figure A.9: Plotting of Creep Life Results

Fatigue and Creep-Fatigue Interaction Life Analysis Window

Fatigue life consumption and creep-fatigue interaction life consumption is displayed in the fatigue and creep-fatigue interaction life analysis window shown in Figure A.10. Fatigue life analysis is carried out for the last simulated data by clicking the “Run Fatigue Life Estimation” menu. The “Run Creep-Fatigue Estimation” menu carries out creep-fatigue interaction life analysis. Life analysis data could be saved in excel file if the “Save Data in Excel Sheet” radio button is checked. The equivalent fatigue factor per simulated data and the overall equivalent fatigue factor for all simulated data are obtained. Also, the fatigue cycles accumulated are estimated. Results of creep-fatigue interaction in the form of equivalent creep-fatigue factor per simulated data and overall equivalent creep-fatigue factor for all simulated data are presented. Results could be plotted in the plot area provided. A plot selection panel is visible when creep-fatigue

interaction life analysis is carried out, Figure A.11. Fatigue and creep-fatigue life consumption results could be saved in any desired location from sub-menus provided under the file menu.

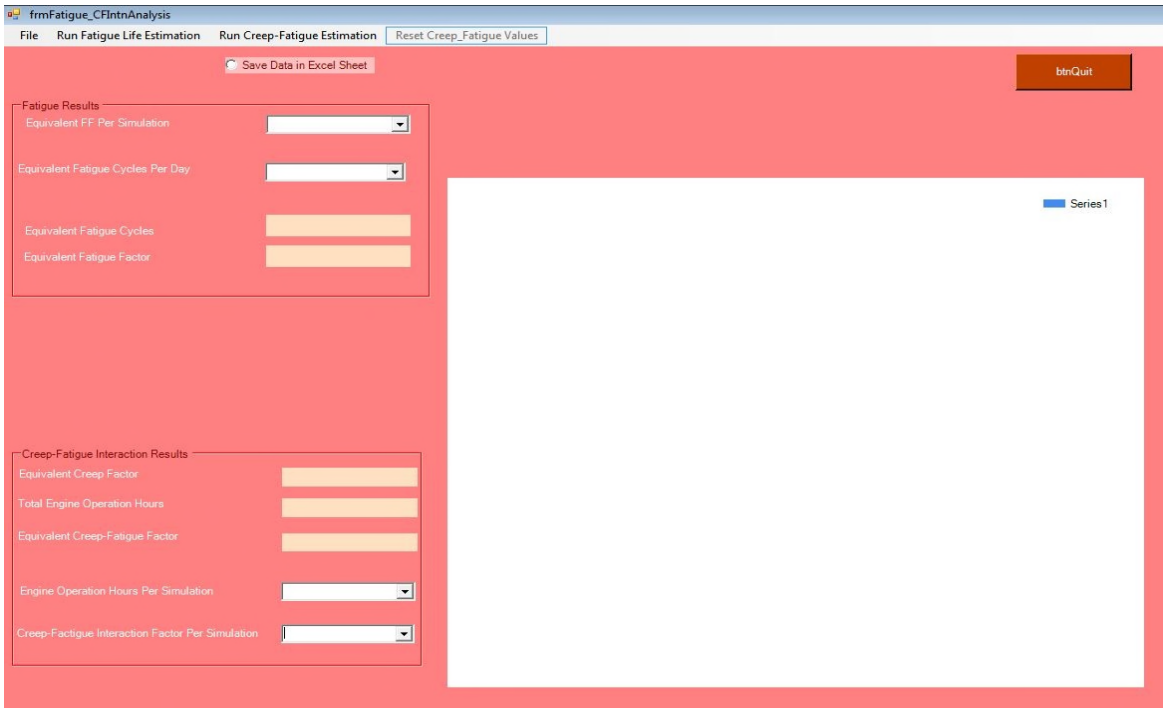

Figure A.10: Fatigue and Creep-Fatigue Interaction Life Analysis Window

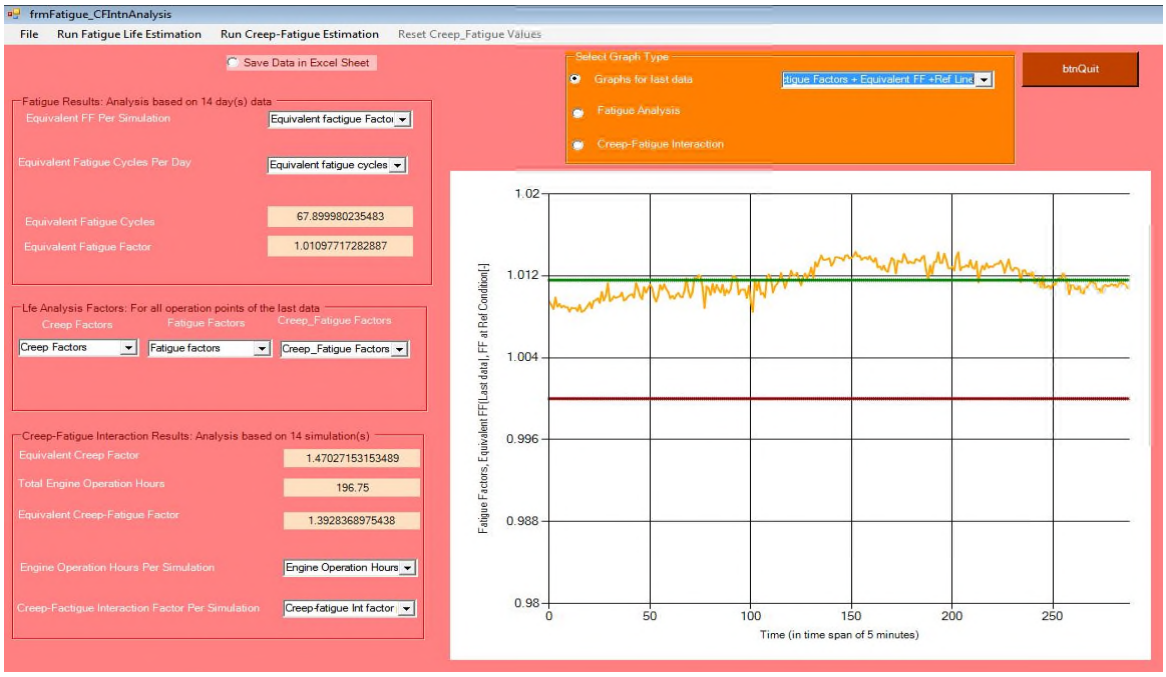

Figure A.11: Plotting of Fatigue and Creep-Fatigue Life Results

APPENDIX B : Larson-Miller Equation

Creep failure is determined by the amount of plastic strain a material undergoes. Thus, the creep rate is represented by the amount of plastic strain a material undergoes in a given time and it is referred to as creep strain rate. Steady state creep dominates the creep behaviour and occurs by diffusion and dislocation, with diffusion creep dominating at relatively high homologous temperatures. The creep strain rate $\dot{\varepsilon}$ therefore has Arrhenius dependence on temperature and it is given by the Arrhenius Equation given by Equation (B-1),

$$\dot{\varepsilon} = A.\exp\left(-\frac{Q}{RT}\right) \qquad \text{(B-1)}$$

A is a constant, of the same unit as the creep strain rate, Q (in J/mol) is the activation energy, R (in J/mol.K) is the universal gas constant, and T (in K) is the absolute temperature. Taking the natural logarithm of both sides of Equation (B-1), we obtain,

$$\ln\dot{\varepsilon} = \ln A - \frac{Q}{RT} \qquad \text{(B-2)}$$

Assumptions:

- The creep strain is steady state creep,
- The creep strain to rupture ε_r is constant over range of temperature considered.

From the above assumptions, the creep strain rate is replaced by the creep strain to rupture and the time to rupture t_r given by Equation (B-3),

$$\dot{\varepsilon} = \frac{\varepsilon_r}{t_r} \qquad \text{(B-3)}$$

Substituting for the creep strain rate in Equation (B-2) and simplifying, Equation (B-4) is obtained,

$$\ln A - \ln\varepsilon_r + \ln t_r = \frac{Q}{RT} \qquad \text{(B-4)}$$

Rearranging Equation (B-4), we obtain,

$$T\left(C+\ln t_r\right)=LMP \tag{B-5}$$

where $C=\ln A-\ln \varepsilon_r$ is the Larsson-Miller constant, $LMP=\frac{Q}{R}$ is the Larsson-Miller Parameter. The Larsson-Miller constant is of the order of 46. Equation (B-5) could be expressed in terms of logarithm to base 10, in which case the Larsson-Miller constant is of the order of 20,

$$T\left(C+\log t_r\right)=LMP \tag{B-6}$$

The time to creep failure is obtained from Equation (B-6) and it is given by Equation (B-7),

$$t_r=10^{\left(\frac{LMP}{T}-C\right)} \tag{B-7}$$

The higher the value of the Larsson-Miller parameter, the longer time it will take for creep failure to occur. The Larsson-Miller Parameter is stress dependent. At higher stress levels, the activation energy required to obtain a given creep strain rate reduces- the LMP value reduces as such. Therefore, higher stresses will lead to faster creep failure. The Larsson-Miller constant C represents two constants and it is material dependent. From Equation (B-7), larger values of C will lead to smaller time to creep failure while smaller values of C will lead to longer time to creep failure. The magnitude of C thus stands for the level of susceptibility of a given material to creep failure, where larger values portend higher susceptibility to creep failure.

APPENDIX C : Derivations and Details of Some Parameters in Development of Lifing Sub-Models

C.1 Polytropic Efficiency

Taking T_{in} , T_{ex} , P_{in} and P_{ex} as the temperature at turbine inlet, temperature at turbine exit, pressure at turbine inlet and pressure at turbine exit respectively, the polytropic efficiency η_p could be obtained from Equation (C-1) [7],

$$\frac{P_{in}}{P_{ex}} = \left(\frac{T_{in}}{T_{ex}} \right)^{\frac{\gamma_h}{(\gamma_h - 1)\eta p}} \qquad \text{(C-1)}$$

γ_h is the ratio of specific heat capacities of the hot gases. The expansion process in the turbine is shown in the temperature- entropy (T-S) diagram in Figure C.1. This will aid in obtaining an expression of the polytropic efficiency in terms of the turbine isentropic efficiency η_{ti} and pressure ratio only.

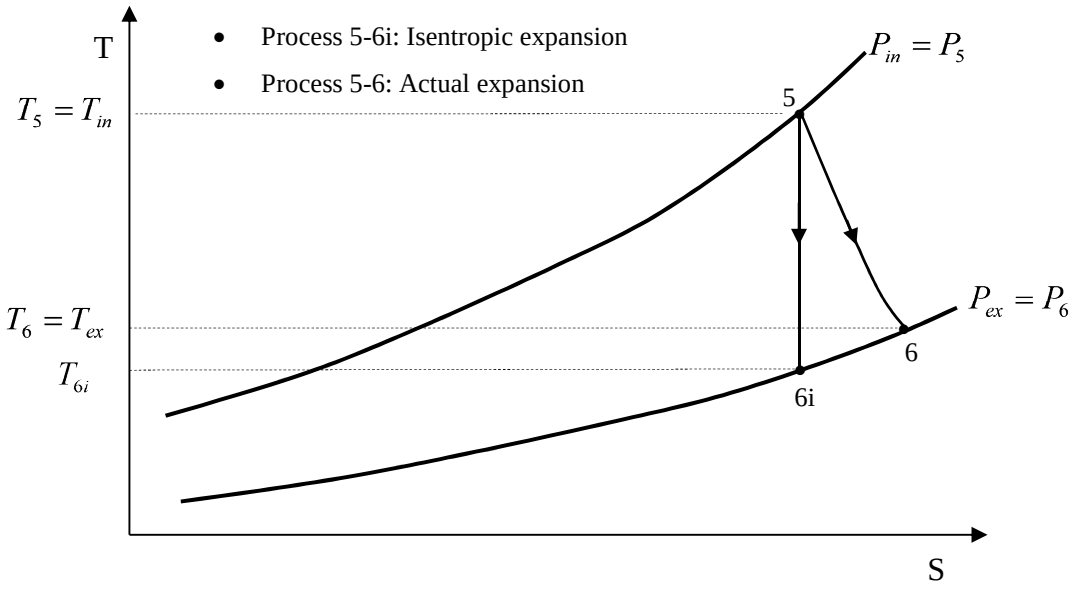

Figure C.1: Expansion Process in Turbine Stage

Taking the natural logarithm of both sides of Equation (C-1) and simplifying, we obtain the polytropic efficiency in terms of other parameters in the form,

$$\eta_p = \frac{\ln\left(\frac{T_{in}}{T_{ex}}\right)}{\left(\frac{\gamma_h - 1}{\gamma_h}\right)\ln\left(\frac{P_{in}}{P_{ex}}\right)} \tag{C-2}$$

The isentropic efficiency of the turbine expansion process is defined by Equation (C-3),

$$\eta_{ti} = \frac{T_5 - T_6}{T_5 - T_{6i}} \tag{C-3}$$

Simplifying, we obtain the ratio of T_5 to T_6 in the form,

$$\frac{T_5}{T_6} = \frac{1}{1 - \eta_{ti}\left(1 - \frac{T_{6i}}{T_5}\right)} \tag{C-4}$$

The temperatures and the pressures in the isentropic process are related in the form,

$$\frac{T_{6i}}{T_5} = \left(\frac{P_6}{P_5}\right)^{\left(\frac{\gamma_h - 1}{\gamma_h}\right)} \tag{C-5}$$

From Figure C.1, $P_5 = P_{in}$ and $P_6 = P_{ex}$, thus making these substitutions in Equation (C-5), we obtain,

$$\frac{T_{6i}}{T_5} = \left(\frac{P_{ex}}{P_{in}}\right)^{\left(\frac{\gamma_h - 1}{\gamma_h}\right)} \tag{C-6}$$

From Figure C.1 also, $T_5 = T_{in}$ and $T_6 = T_{ex}$, therefore, making all relevant substitutions in Equation (C-4), we obtain,

$$\frac{T_{in}}{T_{ex}} = \frac{1}{1 - \eta_{ti}\left[1 - \left(\frac{P_{ex}}{P_{in}}\right)^{\left(\frac{\gamma_h - 1}{\gamma_h}\right)}\right]} \tag{C-7}$$

$$\frac{T_{in}}{T_{ex}} = \left\{1-\eta_{ti}\left[1-\left(\frac{P_{ex}}{P_{in}}\right)^{\left(\frac{\gamma_h-1}{\gamma_h}\right)}\right]\right\}^{-1} \tag{C-8}$$

Substituting the value of $\frac{T_{in}}{T_{ex}}$ in Equation (C-2), the polytropic efficiency is obtained as,

$$\eta_p = \frac{\ln\left\{1-\eta_{ti}\left[1-\left(\frac{P_{ex}}{P_{in}}\right)^{\left(\frac{\gamma_h-1}{\gamma_h}\right)}\right]\right\}^{-1}}{\left(\frac{\gamma_h-1}{\gamma_h}\right)\ln\left(\frac{P_{in}}{P_{ex}}\right)} \tag{C-9}$$

$$\eta_p = \frac{\ln\left\{1-\eta_{ti}\left[1-\left(\frac{P_{ex}}{P_{in}}\right)^{\left(\frac{\gamma_h-1}{\gamma_h}\right)}\right]\right\}}{(-1)\left(\frac{\gamma_h-1}{\gamma_h}\right)\ln\left(\frac{P_{in}}{P_{ex}}\right)} \tag{C-9a}$$

$$\eta_p = \frac{\ln\left\{1-\eta_{ti}\left[1-\left(\frac{P_{ex}}{P_{in}}\right)^{\left(\frac{\gamma_h-1}{\gamma_h}\right)}\right]\right\}}{\left(\frac{\gamma_h-1}{\gamma_h}\right)\ln\left(\frac{P_{in}}{P_{ex}}\right)^{-1}} \tag{C-9b}$$

Therefore,

$$\eta_p = \frac{\ln\left\{1-\eta_{ti}\left[1-\left(\frac{P_{ex}}{P_{in}}\right)^{\left(\frac{\gamma_h-1}{\gamma_h}\right)}\right]\right\}}{\left(\frac{\gamma_h-1}{\gamma_h}\right)\ln\left(\frac{P_{ex}}{P_{in}}\right)} \tag{C-10}$$

Equation (C-10) is the relation given in Equation 4.26. The polytropic efficiency is used in determining the intermediate temperatures and pressures in turbine with multi-stage design.

C.2 Gas Temperatures at Blade Nodal Points

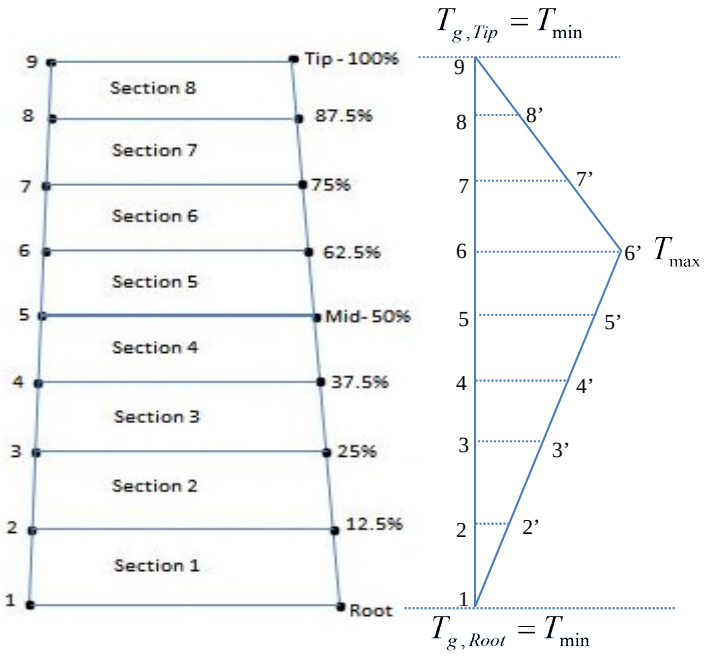

Figure C.2: Radial Temperature Distribution along Blade Span

In Figure C.2, the gas temperatures at the blade root and blade tip are the minimum temperatures $T_{\min}$. The gas temperature at the blade root is also denoted as $T_{g,Root}$ while at the blade tip it is denoted as $T_{g,Tip}$. The maximum temperature occurs at 62.5% distance from the blade root. In terms of linear distance, the maximum temperature occurs at 5 steps away from the blade root and 3 steps away from the blade tip. The maximum gas temperature is equivalent to the distance 66'. Based on this, the gas temperatures at 12.5%, 25%, 37.5%, 50%, 75%, and 87.5% distance respectively from the blade root are equivalent to the respective distances 22', 33', 44', 55', 77' and 88'. These temperatures are denoted as $T_{g,12.5\%Rt}$, $T_{g,25\%Rt}$, $T_{g,37.5\%Rt}$, $T_{g,Mid}$, $T_{g,75\%Rt}$ and $T_{g,87.5\%Rt}$ respectively. The nodal temperatures can equally be represented as $T_{g,i}$, where $1 \le i \le 9$. From similar triangles, the following relations are obtained:

- At 12.5% distance from the blade root:

$$\frac{T_{\max} - T_{g,Root}}{T_{g,12.5\%Rt} - T_{g,Root}} = \frac{6-1}{2-1} = \frac{5}{1} \qquad \text{(C-11)}$$

Simplifying,

$$T_{g,12.5\%Rt} = \frac{4T_{g,Root} + T_{\max}}{5} = \frac{4T_{\min} + T_{\max}}{5} \quad \text{(C-12)}$$

NB: $T_{g,12.5\%Rt} = T_{g,2}$

- At 25% distance from the blade root:

$$\frac{T_{\max} - T_{g,Root}}{T_{g,25\%Rt} - T_{g,Root}} = \frac{6-1}{3-1} = \frac{5}{2} \quad \text{(C-13)}$$

Simplifying,

$$T_{g,25\%Rt} = \frac{3T_{g,Root} + 2T_{\max}}{5} = \frac{3T_{\min} + 2T_{\max}}{5} \quad \text{(C-14)}$$

- At 37.5% distance from the blade root:

$$\frac{T_{\max} - T_{g,Root}}{T_{g,37.5\%Rt} - T_{g,Root}} = \frac{6-1}{4-1} = \frac{5}{3} \quad \text{(C-15)}$$

Simplifying,

$$T_{g,37.5\%Rt} = \frac{2T_{g,Root} + 3T_{\max}}{5} = \frac{2T_{\min} + 3T_{\max}}{5} \quad \text{(C-16)}$$

- At the blade mid:

$$\frac{T_{\max} - T_{g,Root}}{T_{Mid} - T_{g,Root}} = \frac{6-1}{5-1} = \frac{5}{4} \quad \text{(C-17)}$$

Simplifying,

$$T_{Mid} = \frac{T_{g,Root} + 4T_{\max}}{5} = \frac{T_{\min} + 4T_{\max}}{5} \quad \text{(C-18)}$$

- At 75% distance from the blade root:

$$\frac{T_{\max} - T_{g,Tip}}{T_{g,75\%Rt} - T_{g,Tip}} = \frac{6-9}{7-9} = \frac{3}{2} \quad \text{(C-19)}$$

Simplifying,

$$T_{g,75\%Rt} = \frac{T_{g,Tip} + 2T_{\max}}{3} = \frac{T_{\min} + 2T_{\max}}{3} \quad \text{(C-20)}$$

- At 87.5% distance from the blade root:

$$\frac{T_{\max} - T_{g,Tip}}{T_{g,87.5\%Rt} - T_{g,Tip}} = \frac{6-9}{8-9} = \frac{3}{1} \qquad \text{(C-21)}$$

Simplifying,

$$T_{g,75\%Rt} = \frac{2T_{g,Tip} + T_{\max}}{3} = \frac{2T_{\min} + T_{\max}}{3} \qquad \text{(C-22)}$$

The gas temperatures at all the nodal points of the blade are now obtained, but in terms of the maximum and minimum temperatures. The maximum gas temperature is obtained from Equation (4.42), also given here in Equation (C-23),

$$T_{\max} = T_{Bur\_Mean} + RTDF\left(T_{Bur\_Mean} - T_{Bur\_In}\right) \qquad \text{(C-23)}$$

T_{Bur_Mean} is the burner exit mean temperature. Thus, the mean value of all the gas temperatures at the 9 nodal points of the blade will give T_{Bur_Mean}. Therefore,

$$T_{Bur\_Mean} = \frac{T_{g,1} + T_{g,2} + T_{g,3} + T_{g,4} + T_{g,5} + T_{g,6} + T_{g,7} + T_{g,8} + T_{g,9}}{9} \qquad \text{(C-24)}$$

Substituting for each of the nodal temperatures and simplifying, we obtain,

$$9T_{Bur\_Mean} = 5T_{\min} + 4T_{\max} \qquad \text{(C-25)}$$

The minimum gas temperature is thus obtained in terms of the mean burner exit temperature and the maximum gas temperature in the form,

$$T_{\min} = \frac{9T_{Bur\_Mean} - 4T_{\max}}{5} \qquad \text{(C-26)}$$

These gas temperatures are used in the one-dimensional blade thermal model where the temperature of the blade material is estimated at 9 nodal points.

C.3 Details in Pressure Change Bending Moment Estimation

In the pressure change bending moment estimation, the change in static pressure across the blade is first evaluated; the force at each blade section is estimated using the annulus area of the blade section and the force is used to calculate the pressure change bending moments at the base of each blade section, Equations (4.72) to (4.77). The static pressures are estimated at the blade mid-section and the change in static pressure is assumed to be the same for all the sections of the blade. Obtaining the static pressure at the inlet and the exit of each blade stage is much involved hence the details are provided here in the appendix.

C.3.1 Basic Nomenclature

The following nomenclature will be useful in the analysis.

Symbol	Meaning
A	Flow Area
C_p	Specific Heat Capacity at Constant Pressure
C_v	Specific Heat Capacity at Constant Volume
H	Total or Stagnation Enthalpy
M	Mach Number of Gas Flow
M_{Guess}	Guessed Mach Number
NGV	Nozzle Guide Vane(s)
P	Total or Stagnation Pressure
R	Gas Constant
T	Total or Stagnation Temperature
U	Blade Speed
V	Velocity of gas Flow
V_{Abs}	Absolute Velocity of gas Flow
V_{Abs_in}	Absolute Velocity of gas Flow at Blade Inlet
V_{Abs_ex}	Absolute Velocity of gas Flow at Blade Exit

V_{Ax}	Axial Velocity of Gas Flow
V_{Ax_in}	Axial Velocity of Gas Flow at Blade Inlet
V_{Ax_ex}	Axial Velocity of Gas Flow at Blade Exit
V_r	Relative Velocity of Gas Flow
V_{r_in}	Relative Velocity of Gas Flow at Blade Inlet
V_{r_ex}	Relative Velocity of Gas Flow at Blade Exit
V_ω	Whirl Velocity
V_{ω_in}	Whirl Velocity at Blade Inlet
V_{ω_ex}	Whirl Velocity at Blade Exit
c	Speed of Sound
h	Static Enthalpy
$\dot{m}$	Mass Flow Rate of Gas
$\dot{m}_{in}$	Mass Flow Rate of Gas at Blade Inlet
$\dot{m}_{ex}$	Mass Flow Rate of Gas at Blade Exit
p	Static Pressure of Gas
p_{in}	Static Pressure of Gas at Blade Inlet
p_{ex}	Static Pressure of Gas at Blade Exit
Δp	Change in static pressure
r	Radial Distance from Blade Nodal Point to Blade Axis of Rotation
t	Static Temperature
Γ	Non-Dimensional Flow Parameter
Γ_{in}	Non-Dimensional Flow Parameter at Blade Inlet
Γ_{ex}	Non-Dimensional Flow Parameter at Blade Exit
Γ_{Guess}	Guessed Non-Dimensional Flow Parameter
Γ_{Cal}	Calculated Non-Dimensional Flow Parameter
Γ_{Cal_in}	Calculated Non-Dimensional Flow Parameter at Blade Inlet
Γ_{Cal_ex}	Calculated Non-Dimensional Flow Parameter at Blade Exit
α	Flow Angle

β	Relative Flow Angle or Blade Angle
ρ	Density of gas
γ	Ratio of Specific Heat capacities
ω	Angular Velocity of Compressor Shaft

Subscripts	**Meaning**
in	Blade Inlet
ex	Blade Exit

C.3.2 Static Pressures at Turbine Inlet and Exit

The change in static pressure between the turbine inlet and exit is given by Equation (C-27),

$$\Delta p = p_{in} - p_{ex} \tag{C-27}$$

The static pressures are obtained from the stagnation or total pressure. The total or stagnation enthalpy H of the gas relates with the static enthalpy h in the form,

$$H = h + \frac{V^2}{2} \tag{C-28}$$

Here, V is the absolute velocity of the gas and could be denoted as V_{Abs} . The enthalpy depends on temperature. Thus Equation (C-28) is expressed as,

$$C_p T = C_p t + \frac{V_{Abs}^{\ 2}}{2} \tag{C-29}$$

The static temperature is thus obtained as,

$$t = T - \frac{V_{Abs}^{\ 2}}{2C_p} \tag{C-30}$$

The stagnation properties are obtained by bringing the fluid to zero velocity isentropically. Thus, the process of moving from static condition to stagnation condition is an isentropic process. The stagnation and static pressures therefore relate with their respective temperatures as in Equation (C-31),

$$\frac{P}{p} = \left(\frac{T}{t}\right)^{\frac{\gamma}{\gamma-1}} \tag{C-31}$$

$$p = P / \left(\frac{T}{t}\right)^{\frac{\gamma}{\gamma-1}} \tag{C-32}$$

The stagnation temperatures and pressures were obtained in previous analysis. The static temperature could be obtained from Equation (C-30), but the absolute velocity of the fluid is not yet known. The absolute velocity is obtained by considering the flow of the fluid at the inlet and the exit of the blade stage. Figure C.3 will aid in calculating the absolute velocities at the inlet and the exit of the blade.

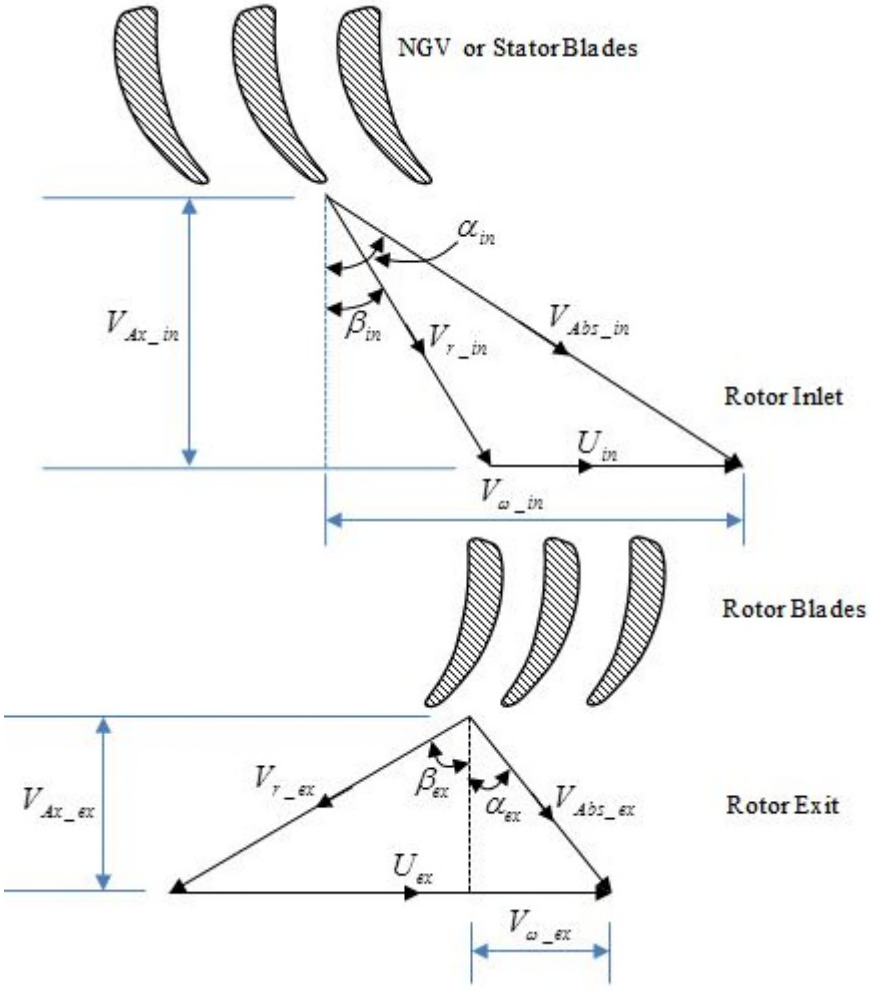

Figure C.3: Velocity Triangles for Turbine Stage

From Figure C.3, the absolute velocity is given as,

$$V_{Abs} = \sqrt{V_{Ax}{}^2 + V_{\omega}{}^2} \tag{C-33}$$

V_{ω} is the tangential component of the absolute velocity, referred to as whirl velocity which at the inlet V_{ω_in} and exit V_{ω_ex} are given respectively by Equations (C-34a) and (C-34b),

$$V_{\omega\_in} = U_{in} + V_{Ax\_in} \tag{C-34a}$$

$$V_{\omega\_ex} = U_{ex} - V_{Ax\_ex} \times \tan\beta_{ex} \tag{C-34b}$$

And the change in whirl velocity which is required in the velocity change bending moment evaluation is,

$$\Delta V_{\omega} = V_{\omega\_ex} - V_{\omega\_in} \tag{C-35c}$$

The flow angles at inlet and outlet are estimated using Equations (C-35a) and (C-35b) respectively,

$$\alpha_{in} = \tan^{-1}\left(\frac{V_{\omega\_in}}{V_{Ax\_in}}\right) \tag{C-35a}$$

$$\alpha_{ex} = \tan^{-1}\left(\frac{V_{\omega\_ex}}{V_{Ax\_ex}}\right) \tag{C-35b}$$

The blade speed at any section of the turbine at inlet and exit could be estimated using Equation (C-36),

$$U = \omega r \tag{C-36}$$

ω is the angular speed of the compressor shaft in rad/s, and r is the radial distance from the axis of rotation of the turbine to the nodal point (root, mid-section, tip etc.) of the blade. This is equivalent to $h_{n,i}$ in Figure 4.13, but expressed for both the inlet (LE) and exit (TE) of the blade. The flow angles at the blade inlet and outlet α_{in} and α_{ex} (denoted in some literatures as α_1 and α_2) could be obtained when the axial velocities

at blade inlet and exit (V_{Ax_in} and V_{Ax_ex}) and the blade angles at inlet and exit (β_{in} and β_{ex}) same as the relative flow angles are known. The blade angles are gotten from the blade geometry. The axial velocities at the blade inlet and the blade exit have to be estimated. To do this, we consider the non-dimensional flow parameter Γ at the turbine inlet and exit. This is given by Equation (C-37),

$$\Gamma = \frac{\dot{m}\sqrt{T}}{PA} \tag{C-37}$$

$\dot{m}$ is the mass flow rate, T is the total temperature, P is the total pressure and A is the flow area. The parameters $\dot{m}$, T and P at inlet and the exit of each turbine stage has been estimated. The flow area is the annulus area which can be calculated for any blade section for both the inlet and exit, Equation (4.75). At the inlet and exit of the blade for any blade section, the non-dimensional flow parameter will be given respectively by Equations (C-38a) and (C-38b),

$$\Gamma_{in} = \frac{\dot{m}_{in}\sqrt{T_{in}}}{P_{in}A_{in}} \tag{C-38a}$$

$$\Gamma_{ex} = \frac{\dot{m}_{ex}\sqrt{T_{ex}}}{P_{ex}A_{ex}} \tag{C-38b}$$

The non-dimensional flow parameter here is calculated hence it can be denoted as Γ_{Cal} (Γ_{Cal_in} for turbine inlet and Γ_{Cal_ex} for turbine exit). The mass flow rate $\dot{m}$ (either at the blade inlet or exit) could also be computed from the flow area A, the density of the gas ρ and the axial velocity V of the flow in the form,

$$\dot{m} = \rho AV \tag{C-39}$$

The density of the gas is given by Equation (C-40),

$$\rho = \frac{p}{Rt} \tag{C-40}$$

p is the static pressure, t is the static temperature and R is the gas constant. Substituting in Equation (C-39), we obtain,

$$\dot{m} = \frac{pAV}{Rt} \tag{C-41}$$

From Equation (C-30), here the velocity is the axial velocity,

$$\frac{T}{t} = 1 + \frac{V^2}{2C_p t} \tag{C-42}$$

Introducing the Mach number M of the flow, where c is the speed of sound, we obtain,

$$M = \frac{V}{c} = \frac{V}{\sqrt{\gamma Rt}} \tag{C-43}$$

$$V = M\sqrt{\gamma Rt}\,; \;\; V^2 = M^2 \times \gamma Rt \tag{C-44a, b}$$

But,

$$\gamma = \frac{C_p}{C_v} \text{ and } R = C_p - C_v \text{, thus } \gamma R = \frac{C_p}{C_c}\left(C_p - C_v\right) = C_p(\gamma - 1) \tag{C-45 a, b, c}$$

Therefore,

$$V^2 = M^2 \times C_p(\gamma - 1)t \tag{C-46}$$

Substituting for V^2 in Equation (C-42), the ratio of the stagnation and static temperature is obtained as,

$$\frac{T}{t} = 1 + \frac{\gamma - 1}{2} M^2 \tag{C-47}$$

Thus,

$$t = \frac{T}{\left(1 + \frac{\gamma - 1}{2} M^2\right)} \tag{C-48}$$

$$V = M\sqrt{\gamma Rt} = M\sqrt{\gamma R \times \frac{T}{\left(1 + \frac{\gamma - 1}{2} M^2\right)}} \tag{C-49}$$

$$\frac{V}{\sqrt{T}} = \frac{M\sqrt{\gamma R}}{\left(1+\frac{\gamma-1}{2}M^2\right)^{\frac{1}{2}}} \tag{C-50}$$

From Equations (C-32) and (C-47), the static pressure is obtained as,

$$p = \frac{P}{\left(1+\frac{\gamma-1}{2}M^2\right)^{\frac{\gamma}{\gamma-1}}} \tag{C-51}$$

Substituting for p, t and V in Equation (C-41),

$$\dot{m} = \frac{PA\left(1+\frac{\gamma-1}{2}M^2\right)}{RT\left(1+\frac{\gamma-1}{2}M^2\right)^{\frac{\gamma}{\gamma-1}}} \times \frac{M\sqrt{\gamma RT}}{\left(1+\frac{\gamma-1}{2}M^2\right)^{\frac{1}{2}}} \tag{C-52}$$

Simplifying,

$$\dot{m} = \frac{PAM}{\sqrt{T}} \times \sqrt{\frac{\gamma}{R}} \times \left(1+\frac{\gamma-1}{2}M^2\right)^{-\frac{(\gamma+)}{2(\gamma-1)}} \tag{C-53}$$

Therefore,

$$\frac{\dot{m}\sqrt{T}}{PA} = M\sqrt{\frac{\gamma}{R}} \times \left(1+\frac{\gamma-1}{2}M^2\right)^{-\frac{(\gamma+)}{2(\gamma-1)}} \tag{C-54}$$

The LHS of Equation (C-54) is the non-dimensional flow parameter as in Equation (C-37). The RHS of the equation consists of constants except one variable which is the Mach number. Thus by guessing a value of the Mach number, we can compute the value of the non-dimensional flow parameter, denoted as Γ_{Guess}, which for blade inlet becomes Γ_{Guess_in} and for blade exit designated as Γ_{Guess_ex}.

$$\Gamma_{Guess} = \frac{\dot{m}\sqrt{T}}{PA} = M\sqrt{\frac{\gamma}{R}} \times \left(1+\frac{\gamma-1}{2}M^2\right)^{-\frac{(\gamma+)}{2(\gamma-1)}} \tag{C-55}$$

This value will be compared to the calculated value at both blade inlet and exit and the Mach number will be adjusted until the two values are equal. When this is obtained, the Mach number at which the guess non-dimensional flow parameter is equal to the calculated non-dimensional flow parameter is used to estimate the axial velocity of the flow and hence every other parameter required. Traditionally, the percentage error between the calculated and the guessed non-dimensional flow parameters is calculated using an equation in the form,

$$Error\ (\%) = \frac{\Gamma_{Cal} - \Gamma_{Guess}}{\Gamma_{Cal}} \times 100 \qquad \text{(C-56)}$$

If the percentage error is smaller than a pre-defined value, then the guess Mach number is used for further calculations. An alternative approach is explored here to ease computations in computer programming. Γ_{Guess} increases with Mach number and reaches a peak when the Mach number is unity ($M = 1$). Figure C-4) shows how Γ_{Guess} (Non-Dimensional Flow Parameter) varies with Mach number for $\gamma = 1.33$ [-] and $R = 287$ [J/kg.K].

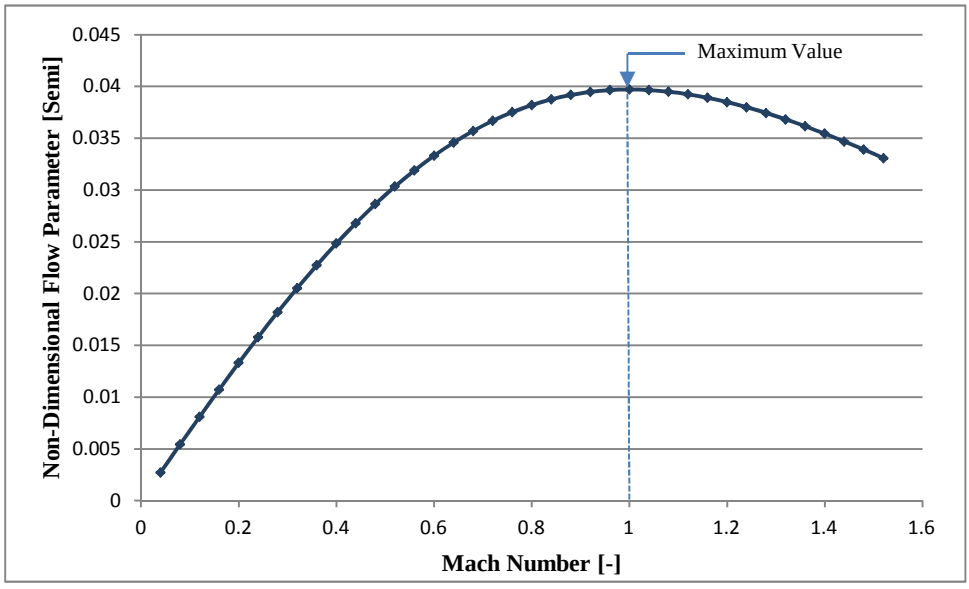

Figure C.4: Variation of Guessed Non-Dimensional Flow Parameter with Mach Number

With the above knowledge, starting with a small value of M, say $M = 0.01$, we increase it by small steps say by 0.001 and the final value greater than 1. From the

several Mach number values generated, the same numbers of values of Γ_{Guess} are obtained. The Mach number (M_{Guess}) at which $\Gamma_{Guess} > \Gamma_{Cal}$ is obtained (for both blade inlet and exit) and used in estimating the axial velocity at blade inlet and exit respectively.

The axial velocity is obtained from Equation (C-50), as in Equation (C-57),

$$\frac{V_{Ax}}{\sqrt{T}} = \frac{M_{Guess}\sqrt{\gamma R}}{\left(1+\frac{\gamma-1}{2}M_{Guess}{}^{2}\right)^{\frac{1}{2}}} \qquad \text{(C-57)}$$

Therefore,

$$V_{Ax} = \frac{M_{Guess}\sqrt{\gamma R}}{\left(1+\frac{\gamma-1}{2}M_{Guess}{}^{2}\right)^{\frac{1}{2}}} \times \sqrt{T} \qquad \text{(C-58)}$$

The temperature here is the stagnation temperature and it has been obtained in previous analysis for both blade inlet and exit. The axial velocity is obtained at both blade inlet and blade exit at any section of the blade and the values are used in obtaining other parameters leading to the static pressure difference given by Equation (C-27).

APPENDIX D : Sequential Solution-Algorithm Trees (SSAT) of Lifing Sub-Models

A sequential solution-algorithm tree of any model is a tree-like representation of the basic steps involved in getting the required parameter(s) in the model. It is a clear way of showing how the various formulas involved in getting the required parameter(s) are related and the sequence of execution of each formula. The determination of any parameter is represented by a node defined by a cycle, Figure D.1. The terms (variables/constants) required to obtain the parameter are put in bracket, with the parameter outside the bracket, in the form of a function representation. If any of the terms is unknown, it is represented by another cycle and connected to the first cycle by a single line which may be straight or not with an arrow pointing in the direction of the second cycle. The terms required to estimate the unknown term are put in a bracket like in the first case. The sequence continues until all the terms are connected with their respective formulas.

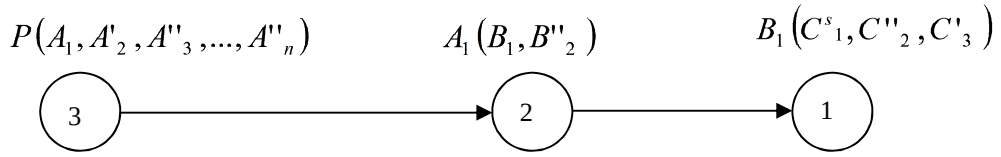

Figure D.1: Calculation of a Parameter in SSAT Method

In Figure D.1, P is the parameter to be evaluated while $A_1, A'_2, A''_3, ...,$ and A''_n are the terms in a given formula with which the parameter P could be obtained. The terms in the bracket are distinguished with primes. Table D.1 defines the type of terms used in the SSAT method. Based on the definition of the terms, to evaluate P, the only term that is unknown is A_1. Thus A_1 is placed on top of node 2 with the terms required to evaluate it (B_1 and B_2'') placed inside round brackets. B_2 is read from tables (it has two primes placed above it) while B_1 is unknown and hence brought forward and placed on top of another node (cycle). B_1 depends on C_1, C_2, and C_3 which are obtained from simulations, read from tables and assumed respectively. The numbering of the nodes is in the reverse direction as the evaluation of the terms starts from the last node in the

reverse direction. Thus, from Figure D.1, B_1 will be evaluated before A_1 and A_1 will be evaluated before P.

Table D.1: Definition of Terms used in SSAT Method

Terms	Illustration	Definition
Without Prime	A	Unknown term
With Single Prime	A'	Known or assumed
With Double Prime	A''	Read from Tables
With Double Prime	$A''(B)$	Read from tables as a function of B
With Superscript b	A^b	Obtained from blade geometry
With Superscript i	A^i	Obtained through iterations
With Superscript s	A^s	Obtained from simulations

If the SSAT does not fit into a single page, parameters taken to a new page are represented with a dotted circle and a dotted line with an arrow branching from the dotted circle. Such parameters are fully represented in the SSAT in the next page. The Sequential Solution-Algorithm Trees of the various life analysis sub-models are presented below.

D.1 SSAT of Blade Thermal Model with Uniform Temperature, without TBC

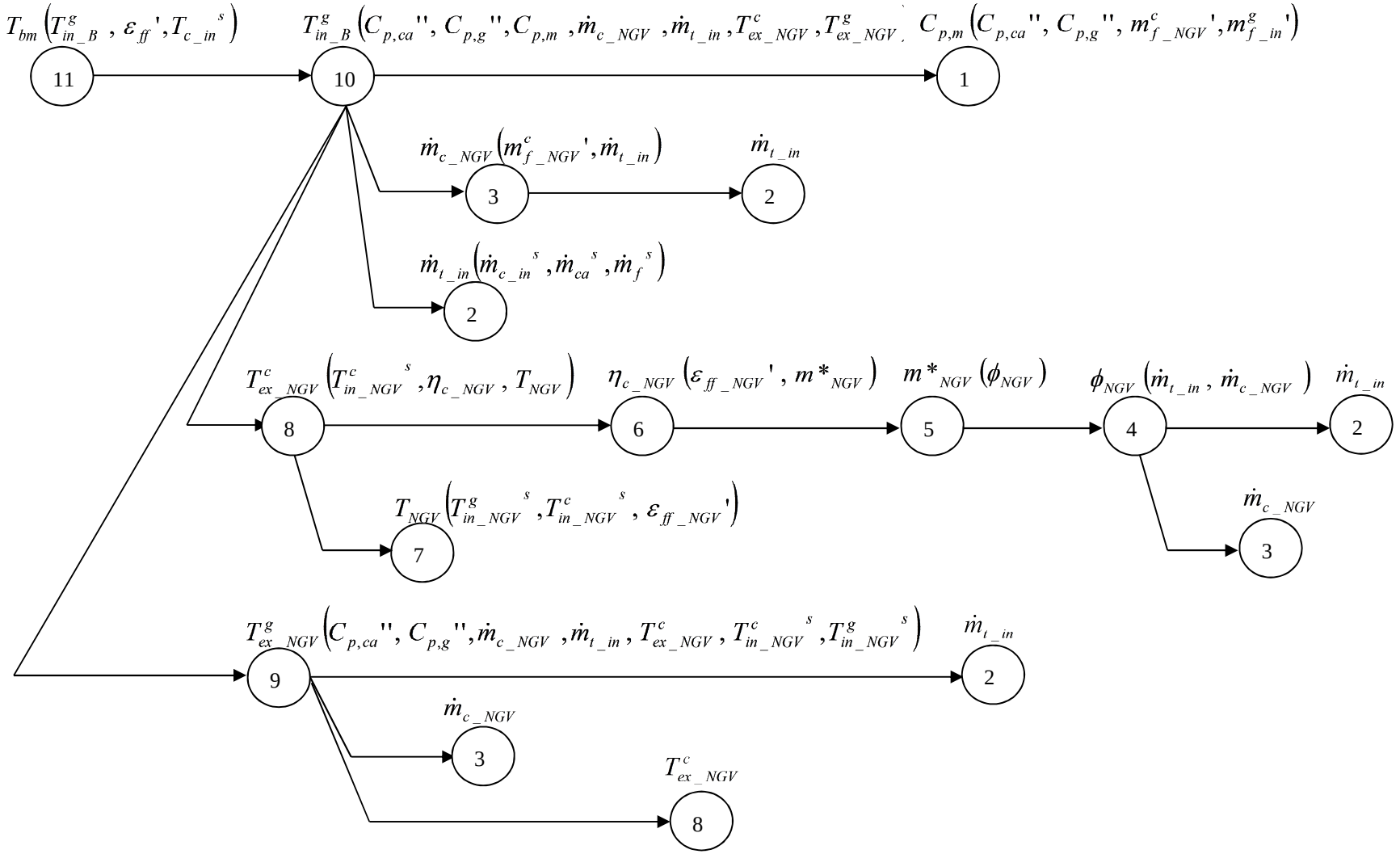

Figure D.2: SSAT of Blade Thermal Model with Uniform Temperature, without TBC

D.2 SSAT of Blade Thermal Model with Uniform Temperature, with TBC

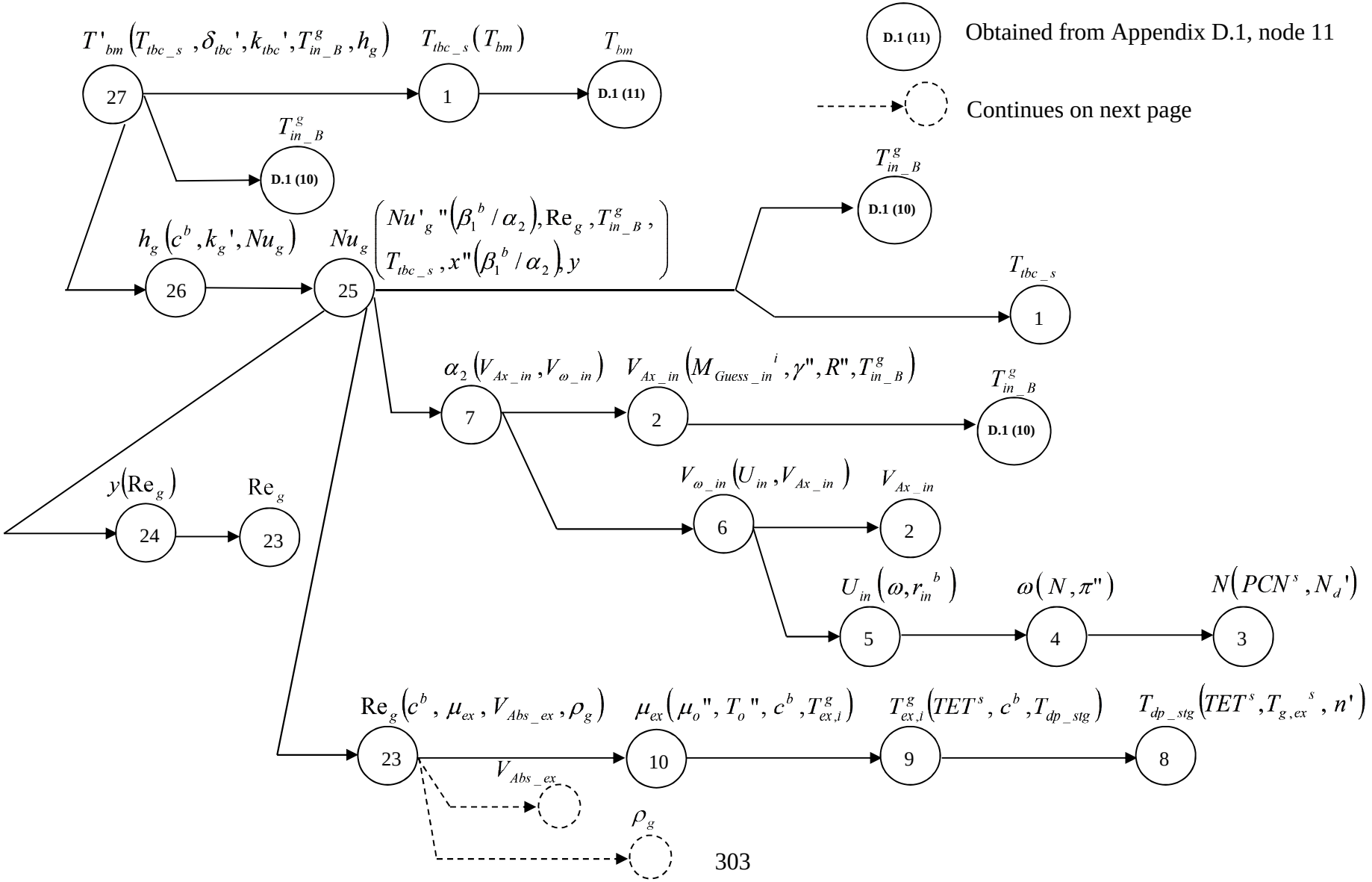

SSAT of Blade Thermal Model with Uniform Temperature, with TBC- continuation

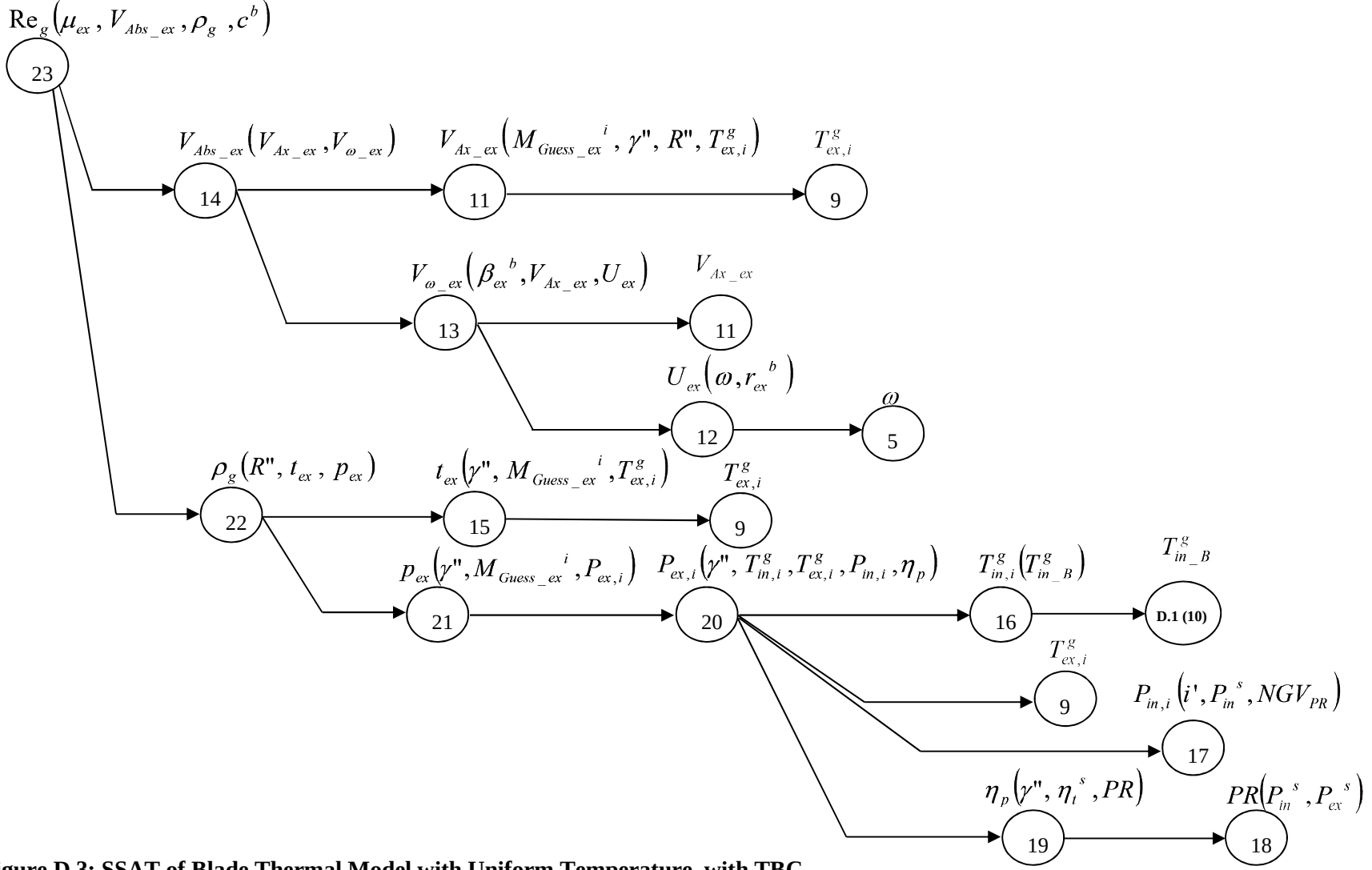

Figure D.3: SSAT of Blade Thermal Model with Uniform Temperature, with TBC

D.3 SSAT of One-Dimensional Blade Thermal Model without TBC

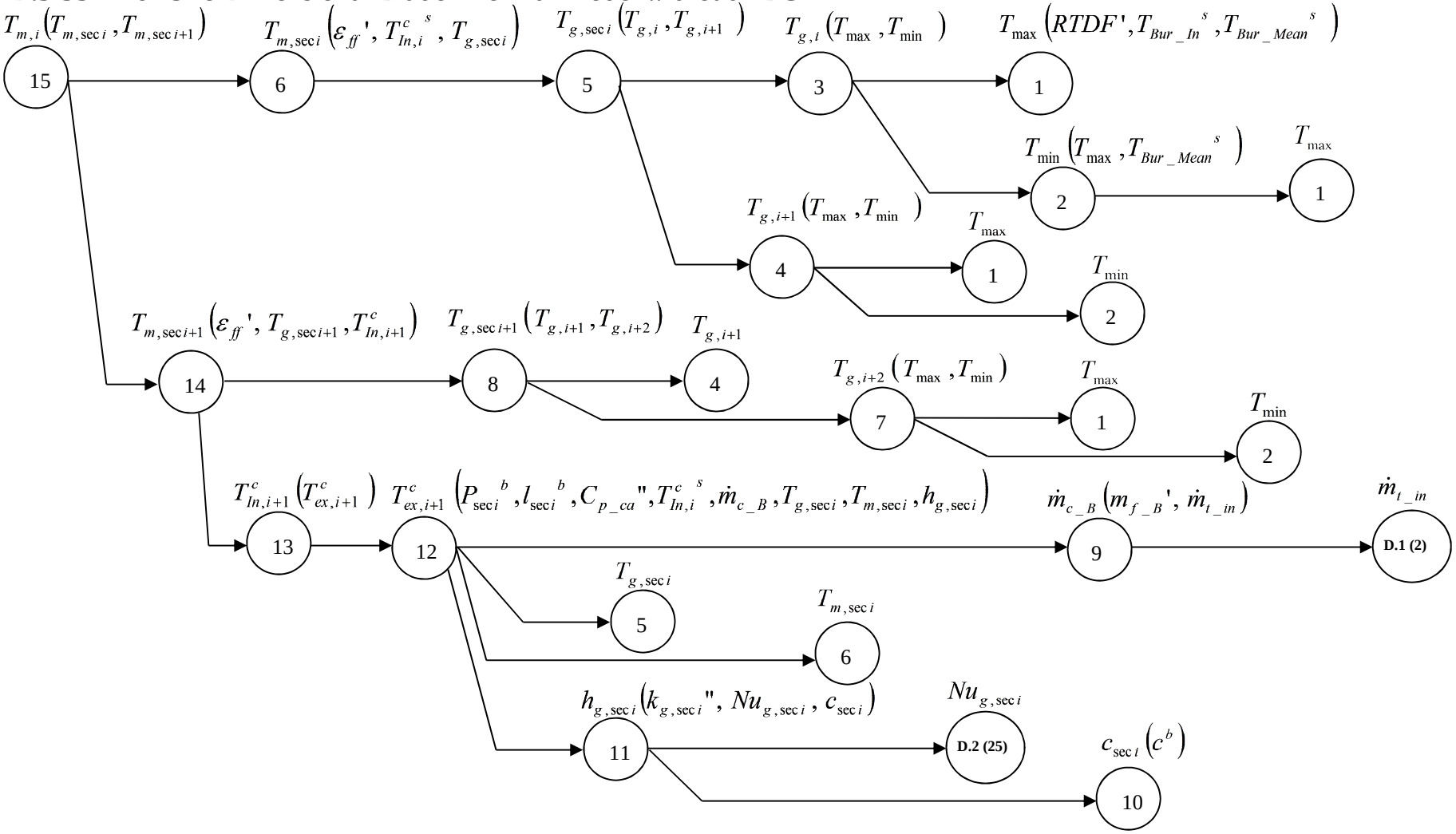

Figure D.4: SSAT of One-Dimensional Blade Thermal Model without TBC

D.4 SSAT of One-Dimensional Blade Thermal Model with TBC

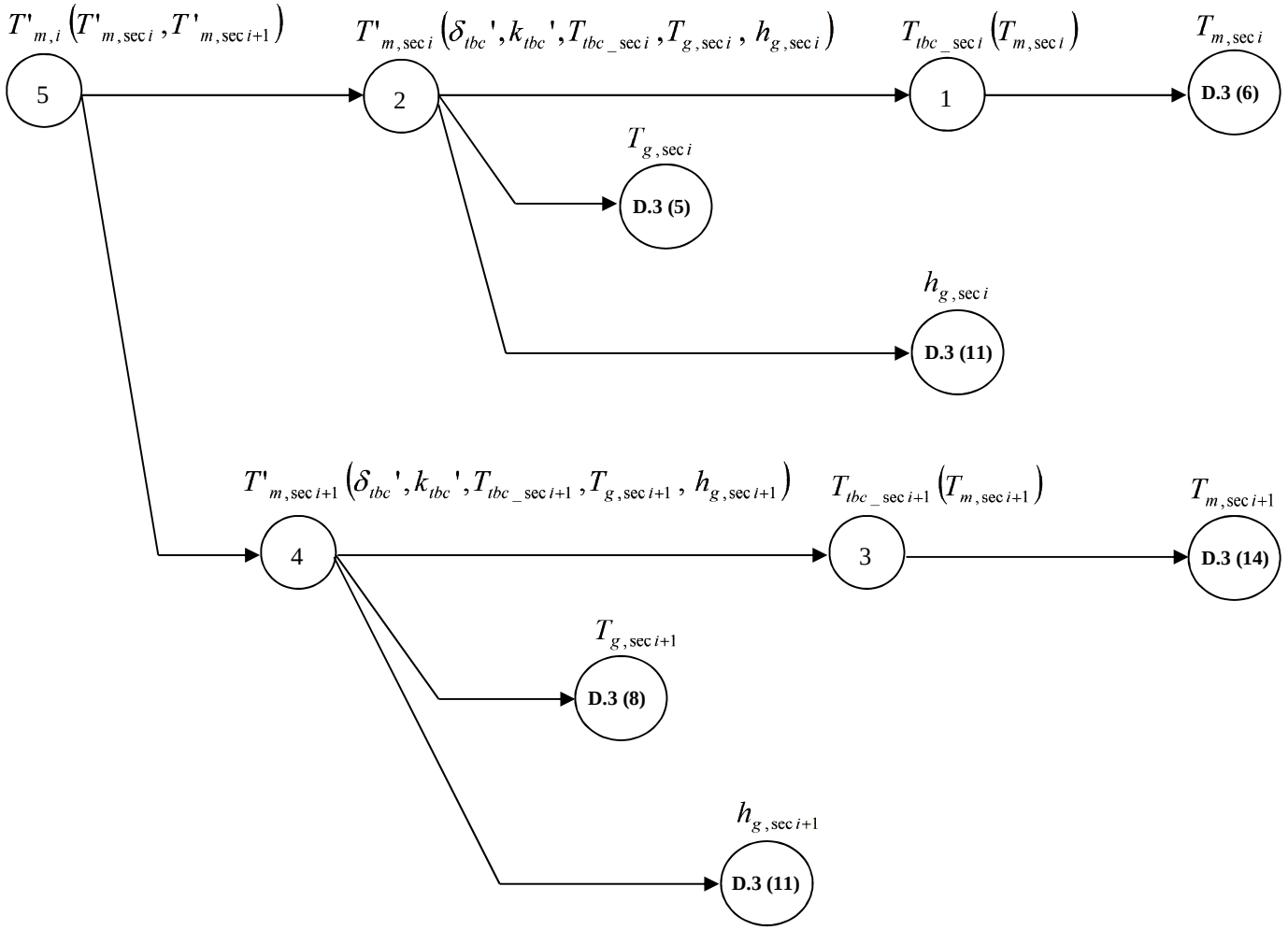

Figure D.5: SSAT of One-Dimensional Blade Thermal Model with TBC

D.5 SSAT of Blade Stress Model

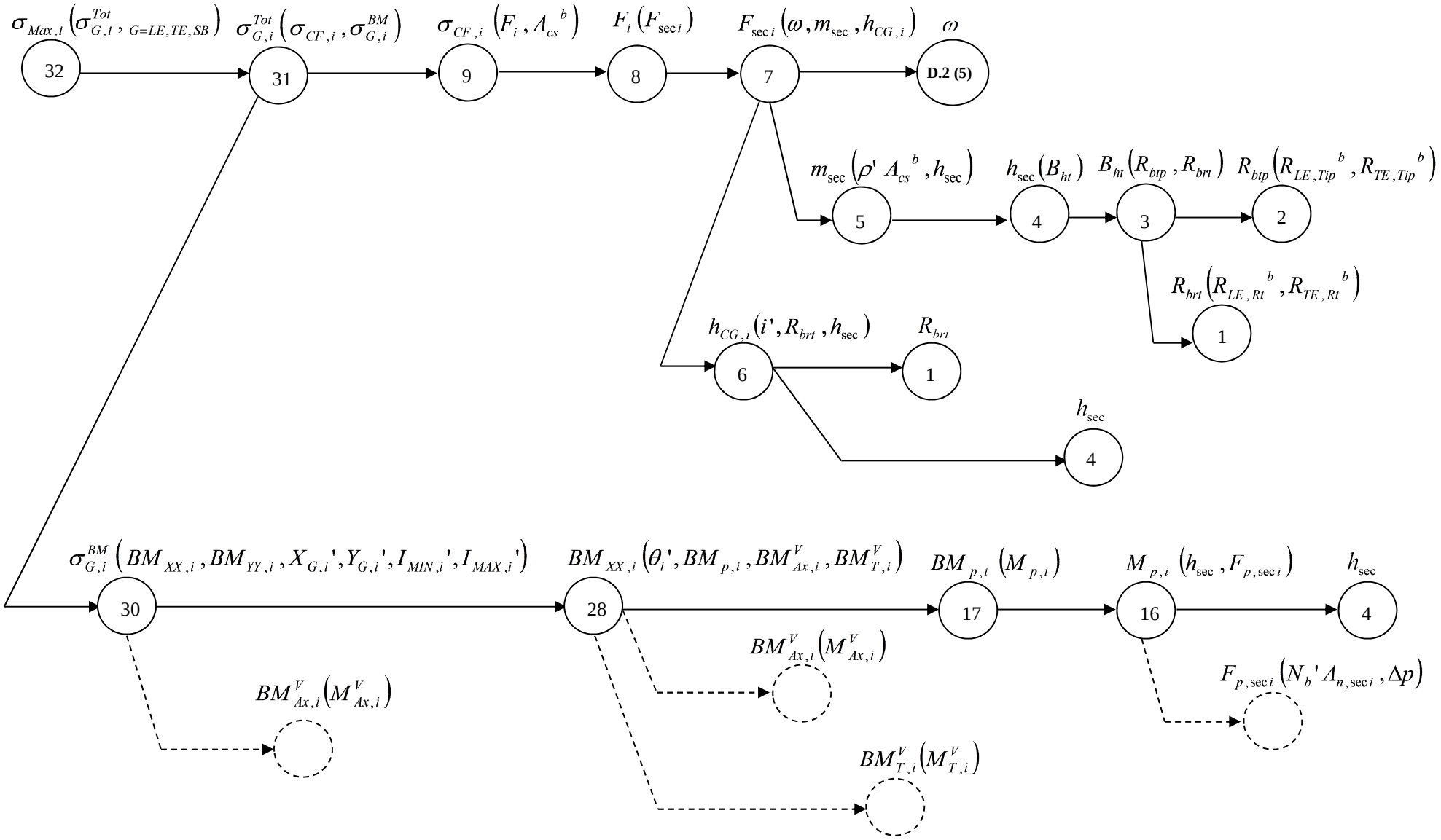

SSAT of Blade Stress Model - Continuation

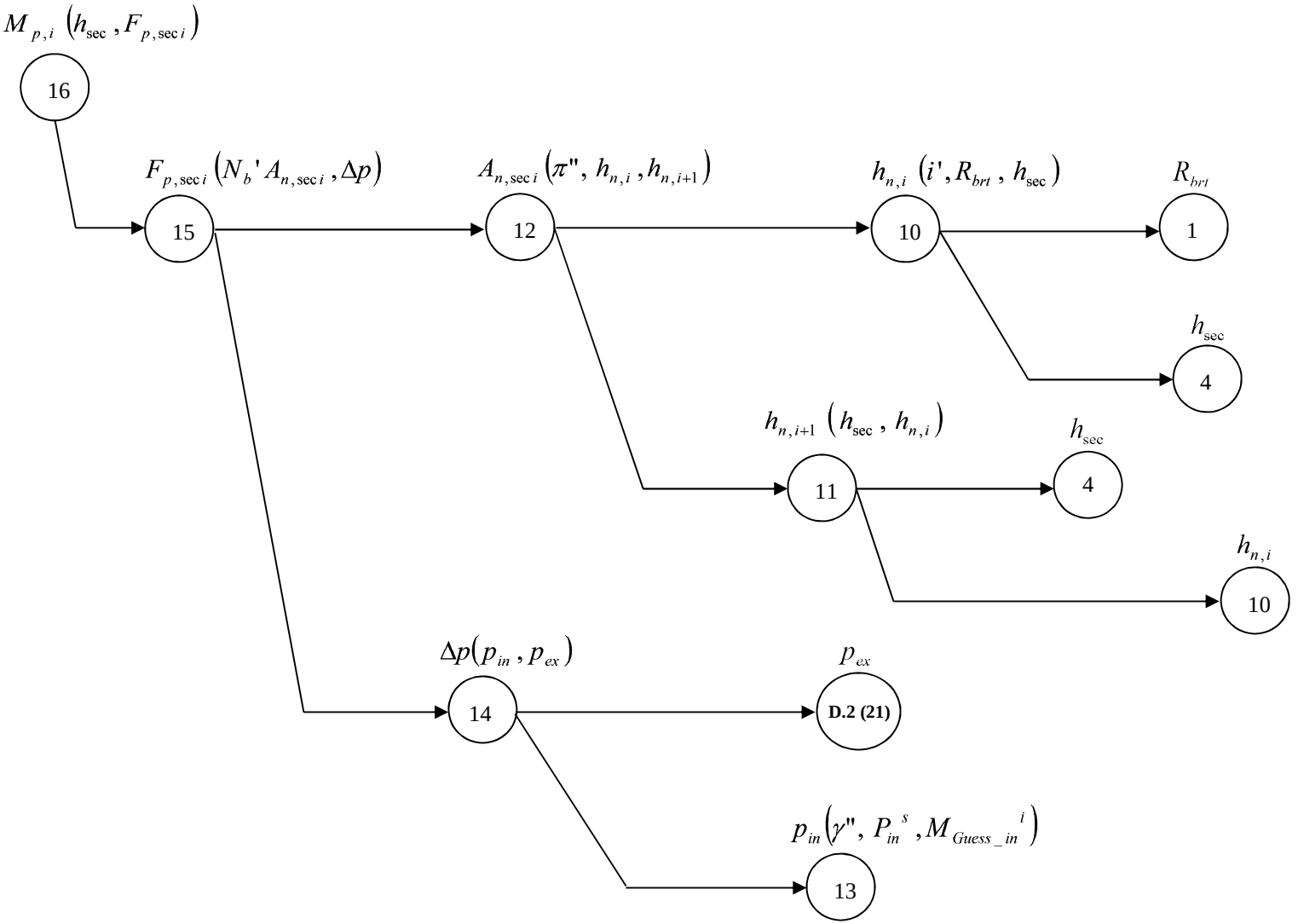

SSAT of Blade Stress Model - Continuation

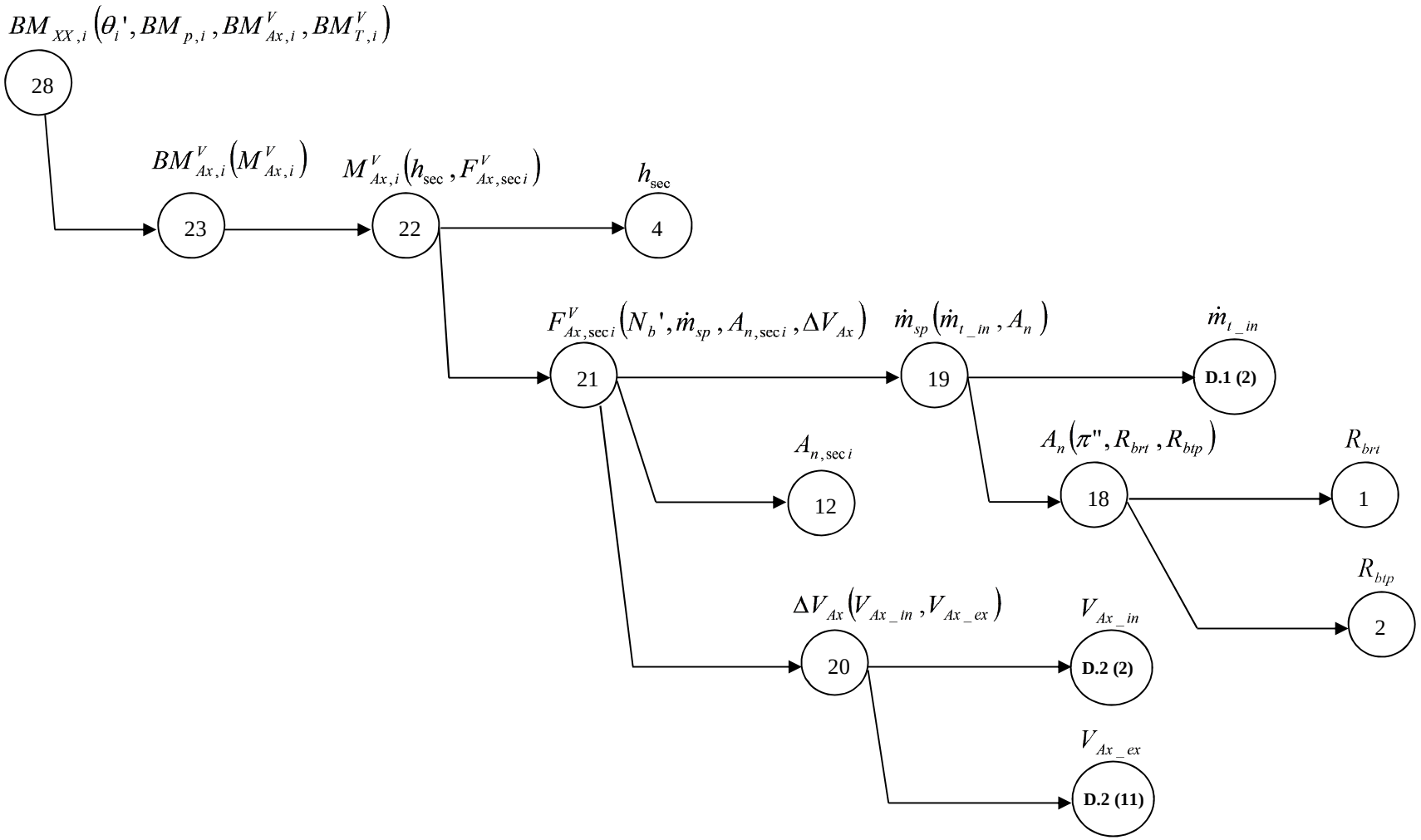

D.5 SSAT of Blade Stress Model - Continuation

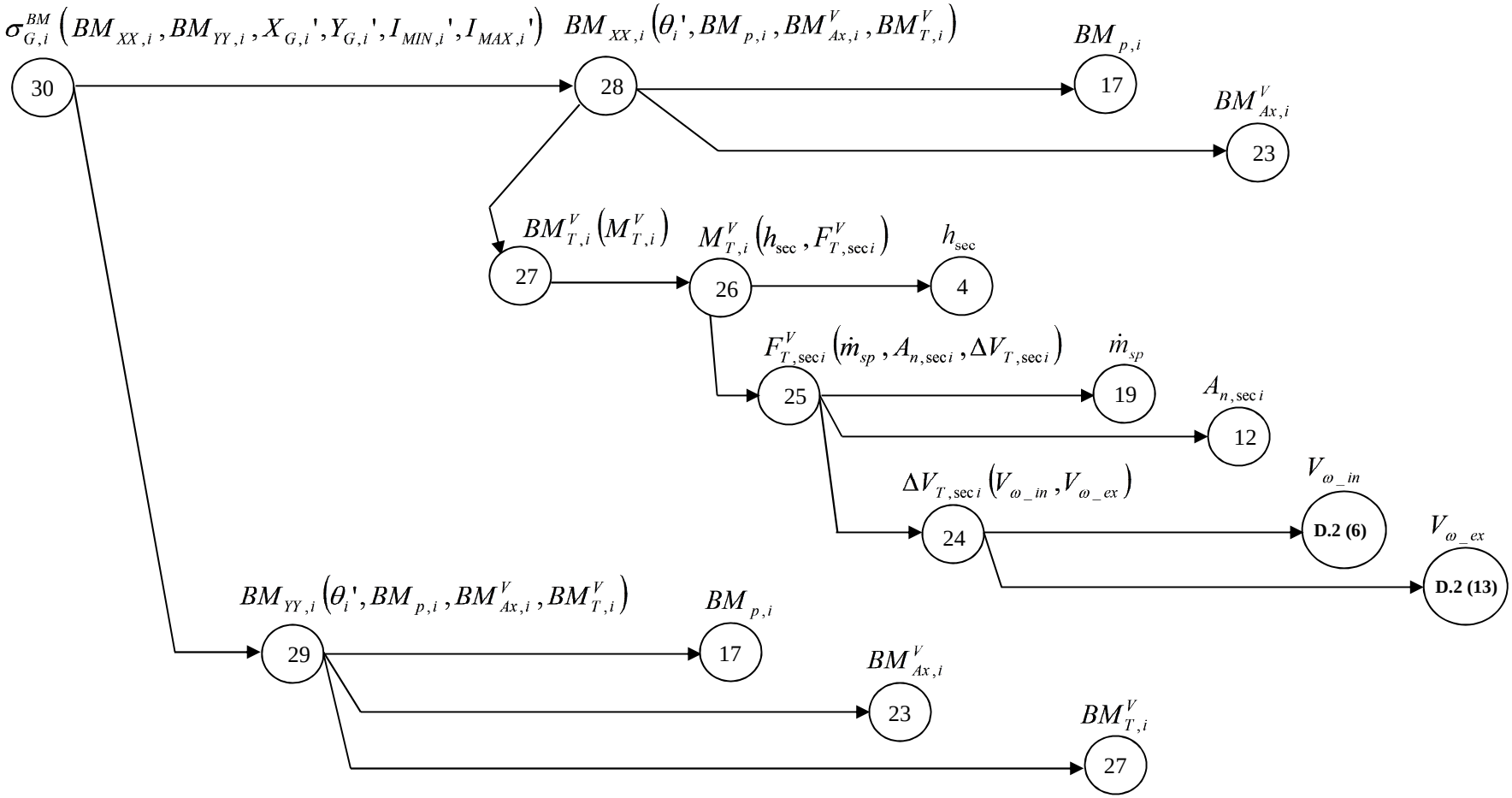

Figure D.6: SSAT of Blade Stress Model

APPENDIX E : Sequential Solution-Algorithm Trees of Lifing Models

E.1 SSAT of Creep Life Estimation Process

The Equivalent creep factor (ECF) for a given period of engine operation is estimated.

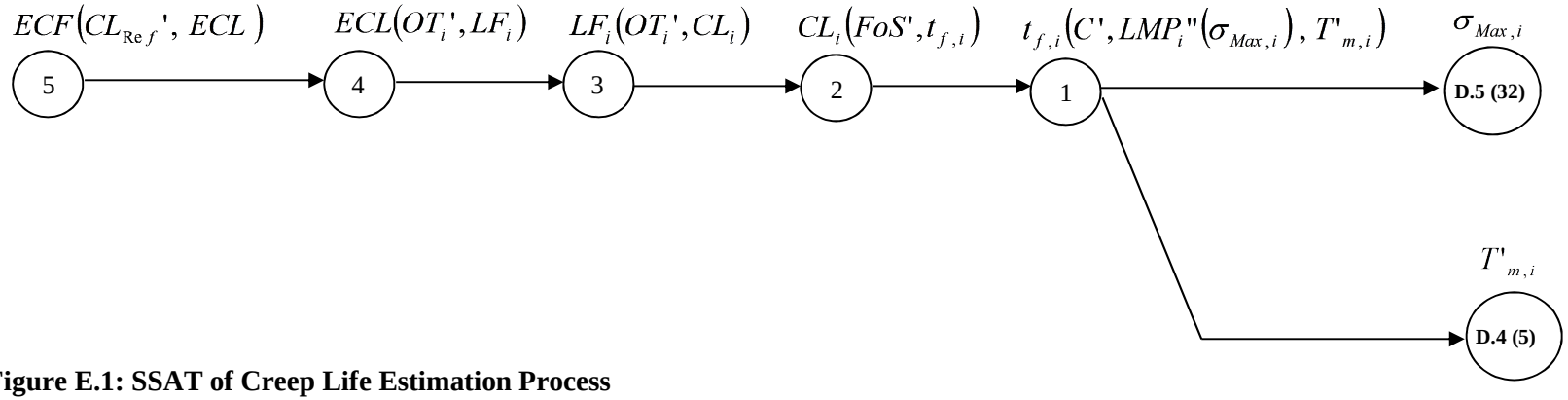

Figure E.1: SSAT of Creep Life Estimation Process

E.2 SSAT of Fatigue Life Estimation Process

The Equivalent fatigue factor (EFF) for a given period of engine operation is estimated.

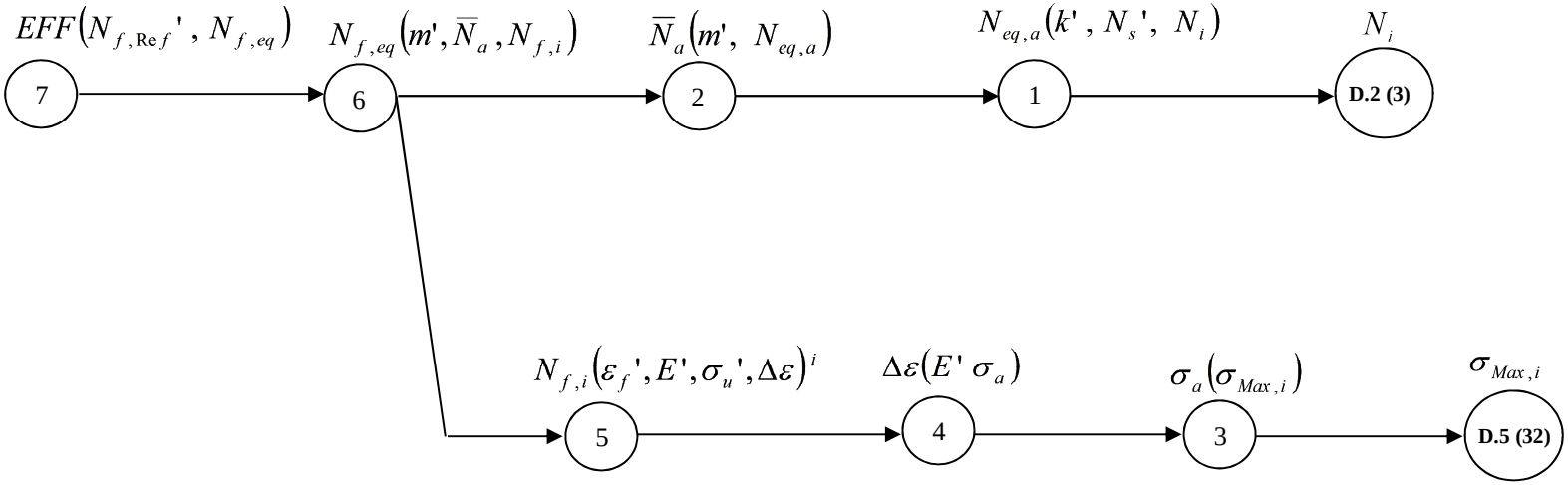

Figure E.2: SSAT of Fatigue Life Estimation Process

E.3 SSAT of Creep-Fatigue Interaction Life Estimation Process

The Equivalent creep-fatigue factor (ECFF) for a given period of engine operation is estimated.

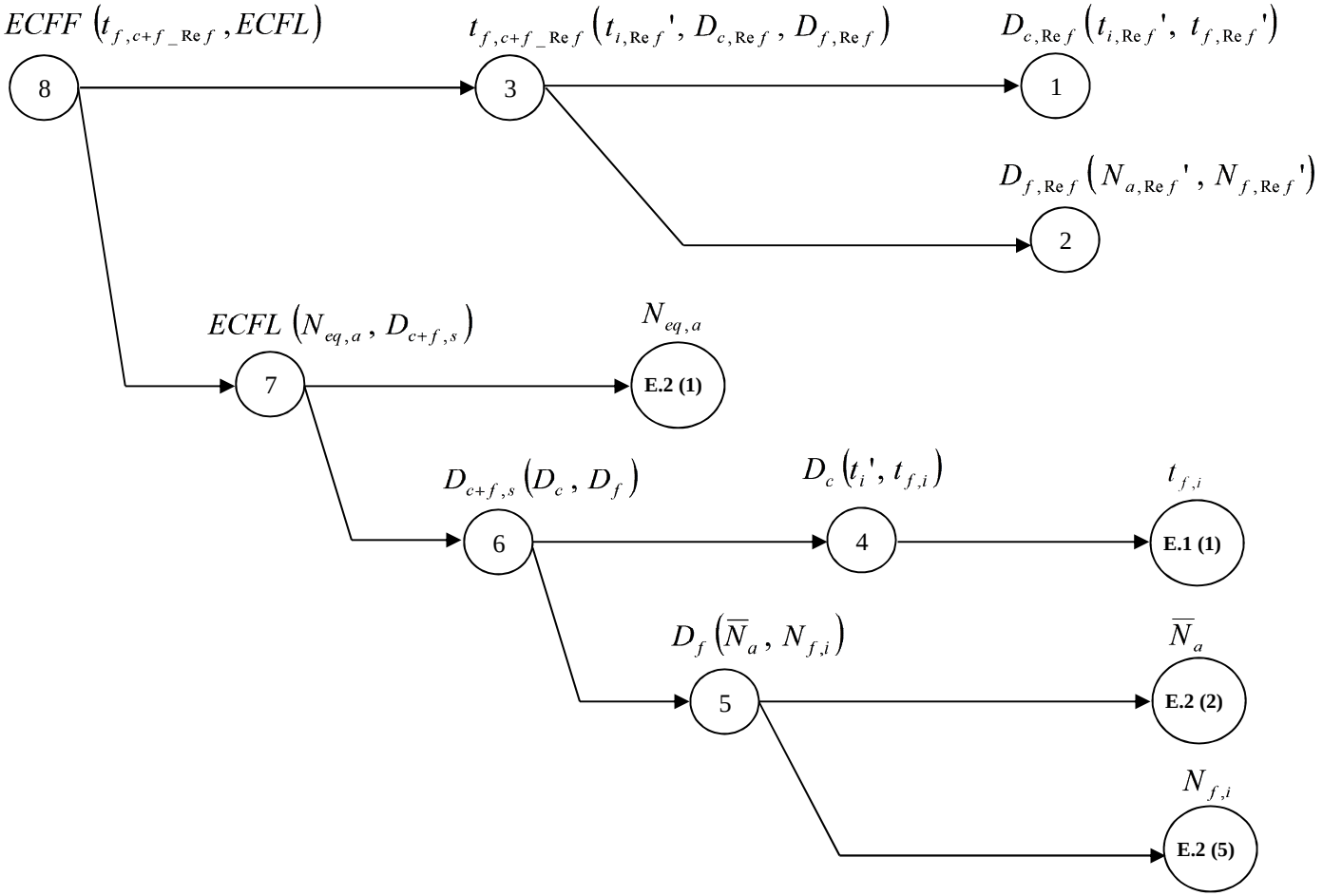

Figure E.3: SSAT of Creep-Fatigue Interaction Life Estimation Process

APPENDIX F : Fatigue Life and Creep-Fatigue Interaction Life Expressions

F.1 Fatigue Life Expressions

The fatigue life consumed is estimated by dividing the equivalent cycles by the number of cycles to failure as in Equation (F-1),

$$D_f = \frac{N_{eq}}{N_f} \tag{F-1}$$

D_f is the fatigue damage parameter, N_{eq} is the equivalent fatigue cycles accumulated, and N_f is number of stress cycles or fatigue cycles to failure. For a given period of engine operation, the mean cycles accumulated at each engine operation point could be obtained and the fatigue damage parameter is evaluated at each operation point using Equation (F-2),

$$D_{f,i} = \frac{\overline{N}_j}{N_{f,i}} \tag{F-2}$$

$D_{f,i}$ is the fatigue damage parameter at each operation point, $N_{f,i}$ is the fatigue cycles to failure at each operation point, and $\overline{N}_a$ is the mean cycles accumulated at each operation point, the same for all operation points and is given by Equation (F-3),

$$\overline{N}_a = \frac{N_{eq,a}}{m} \tag{F-3}$$

m is the number of engine operation points, and $N_{eq,a}$ is the number of fatigue cycles accumulated for the engine operation period. The sum of the fatigue damage parameters for the period, denoted as $D_{f,s}$ is given by Equation (F-4),

$$D_{f,s} = \sum_{i=1}^{m} D_{f,i} = \sum_{i=1}^{m} \frac{\overline{N}_a}{N_{f,i}} \tag{F-4}$$

At each operating point, the engine is operated for t_i hours. Based on Palgrem-Miner linear accumulation rule, failure occurs when the damage parameters are accumulated to

unity. Using the result of a single operation point, in time t_i hours, the damage parameter obtained is $D_{f,i} = \frac{\overline{N}_a}{N_{f,i}}$. In a unit time, say 1 hour, the damage parameter will be,

$$D_{f,t_i} = \frac{\frac{\overline{N}_a}{N_{f,i}}}{t_i} \tag{F-5}$$

Let fatigue failure occur in time t_{ff}. In time t_{ff} the damage parameter will be,

$$D_{f,t_{ff}} = \frac{\frac{\overline{N}_a}{N_{f,i}}}{t_i} \times t_{ff} \tag{F-6}$$

Since failure occurs at time t_{ff}, Equation (F-6) should be equated to 1 from which the value of t_{ff} will be obtained.

$$D_{f,t_{ff}} = \frac{\frac{\overline{N}_a}{N_{f,i}}}{t_i} \times t_{ff} = 1$$

$$t_{ff} = \frac{t_i}{\frac{\overline{N}_a}{N_{f,i}}} = \frac{t_i}{D_{f,i}} \tag{F-7}$$

In terms of number of fatigue cycles to failure N_{ff}, the relation based on single operation point is similar to Equation (F-7) where the time spent at the point is replaced by the mean cycles accumulated at the point as given by Equation (F-8),

$$N_{ff} = \frac{\overline{N}_a}{D_{f,i}} \tag{F-8}$$

From Equations (F-7) and (F-8), the relations between time to fatigue failure and cycle to fatigue failure based on the results of a single engine operation point is given by Equation (F-9),

$$t_{ff} = \frac{t_i}{\overline{N}_a} \times N_{ff} \tag{F-9}$$

For a given period of engine operation, the time to fatigue failure is expressed as equivalent time to fatigue failure since several engine operation points are considered. The relation is similar to that of the single point operation but the time is the summation of that due to all operation points as given by Equation (F-10),

$$t_{ff,eq} = \frac{\sum_{i=1}^{m} t_i}{\sum_{i=1}^{m} D_{f,i}} = \frac{\sum_{i=1}^{m} t_i}{\sum_{i=1}^{m} \frac{\overline{N}_a}{N_{f,i}}} \tag{F-10}$$

$t_{ff,eq}$ is equivalent time to fatigue failure. In terms of cycles to fatigue failure, the equivalent fatigue cycles to failure $N_{ff,eq}$ is given by Equation (F-11),

$$N_{ff,eq} = \frac{\sum_{i=1}^{m} \overline{N}_a}{\sum_{i=1}^{m} D_{f,i}} = \frac{N_{eq,a}}{\sum_{i=1}^{m} \frac{\overline{N}_a}{N_{f,i}}} \tag{F-11}$$

The relationship between the equivalent cycles to fatigue failure and the equivalent time to fatigue failure is given by Equation (F-12),

$$t_{ff,eq} = \frac{\sum_{i=1}^{m} t_i}{\sum_{i=1}^{m} \overline{N}_a} \times N_{ff,eq} \tag{F-12}$$

Considering daily operation of the engine, the fatigue damage parameter for each operation point is given by Equation (F-13),

$$D_{f,i} = \frac{\overline{N}_j}{N_{f,i}} \tag{F-13}$$

$\overline{N}_j$ is the mean value of the equivalent cycles evaluated per day of engine operation (the same for all operating points), and it is given by Equation (F-14),

$$\overline{N}_j = \frac{N_{eq,j}}{n} \tag{F-14}$$

$N_{eq,j}$ is the equivalent cycles accumulated for day j of engine operation, and n is the number of operation points recorded. In one day operation of the engine, the sum of the fatigue damage parameters D_{f,d_1} (represented generally for each day as D_{f,d_j}) will be,

$$D_{f,d\_j} = \sum_{i=1}^{n} D_{f,i} = \sum_{i=1}^{n} \frac{\overline{N}_j}{N_{f,i}} \tag{F-15}$$

$$D_{f,d\_1} = \sum_{i=1}^{n} D_{f,i} = \sum_{i=1}^{n} \frac{\overline{N}_1}{N_{f,i}} \tag{F-16}$$

Based on the results of one day operation of the engine, the number of days to fatigue failure is given by Equation (F-17),

$$t_{ff,d} = \frac{1}{D_{f,d\_1}} = \frac{1}{\sum_{i=1}^{n} \frac{\overline{N}_1}{N_{f,i}}} \tag{F-17}$$

$t_{ff,d}$ is the time to fatigue failure in days of engine operation. If the engine is operated for t_h hours per day, the time to fatigue failure in hours based on day 1 data is given by Equation (F-18),

$$t_{ff,h} = t_{ff,d} \times t_h = \frac{t_h}{\sum_{i=1}^{n} \frac{\overline{N}_1}{N_{f,i}}} \tag{F-18}$$

$t_{ff,h}$ is the time to fatigue failure in hours of engine operation. In terms of fatigue cycles to failure, Equation (F-17) will take the form of Equation (F-19),

$$N_{ff} = \frac{N_{eq,1}}{\sum_{i=1}^{n} \frac{\overline{N}_1}{N_{f,i}}} = \frac{N_{eq,1}}{D_{f,d\_1}} \tag{F-19}$$

N_{ff} is the cycles to failure based on daily data, $N_{eq,1}$ is the equivalent cycles fatigue cycles accumulated for day 1. The time to fatigue failure relates with the cycles to fatigue failure as given by Equations (F-20) and (F-21),

$$t_{ff,d} = \frac{1}{N_{eq,1}} \times N_{ff} \tag{F-20}$$

$$t_{ff,h} = \frac{t_h}{N_{eq,1}} \times N_{ff} \tag{F-21}$$

Considering a number of days of engine operation, say j days, the total or equivalent fatigue damage parameter, denoted as D_{f,s_j} is given by Equation (F-22),

$$D_{f,s\_j} = \sum_{j=1}^{j} D_{f,d\_j} = \sum_{j=1}^{j}\sum_{i=1}^{n} \frac{\overline{N}_{j,i}}{N_{f\_j,i}} \tag{F-22}$$

$N_{f\_j,i}$ is the number of cycles to failure for the j^{th} day and at the i^{th} operation point, and $\overline{N}_{j,i}$ is the mean value of the equivalent cycles evaluated for the j^{th} day and at the i^{th} operation point. The time to fatigue failure in days based on the data for the j days of engine operation is given by Equation (F-23),

$$t_{ff,d} = \frac{j}{\sum_{j=1}^{j} D_{f,d\_j}} = \frac{j}{\sum_{j=1}^{j}\sum_{i=1}^{n} \frac{\overline{N}_{j,i}}{N_{f\_j,i}}} \tag{F-23}$$

If mean time in hours the engine was operated per day is $\bar{t}_h$, the time to fatigue failure in hours based on the j days of engine operation is given by Equation (F-24),

$$t_{ff,h} = \frac{j \times \bar{t}_h}{\sum_{j=1}^{j}\sum_{i=1}^{n} \frac{\overline{N}_{j,i}}{N_{f\_j,i}}} \tag{F-24}$$

Using the actual times the engine was operated per day, Equation (F-24) will take the form of Equation (F-25),

$$t_{ff,h} = \frac{\sum_{j=1}^{j} t_{h,j}}{\sum_{j=1}^{j}\sum_{i=1}^{n} \frac{\overline{N}_{j,i}}{N_{f\_j,i}}} \tag{F-25}$$

$t_{h,j}$ is the time in hours the engine was operated for the j^{th} day. In terms of cycles to failure, Equation (F-25) takes the form of Equation (F-26),

$$N_{ff} = \frac{\sum_{j=1}^{j} N_{eq,j}}{\sum_{j=1}^{j}\sum_{i=1}^{n} \frac{\overline{N}_{j,i}}{N_{f\_j,i}}} \tag{F-26}$$

The time to fatigue failure and the cycles to fatigue failure for data for j days of engine operation is given by Equation (F-27),

$$t_{ff,h} = \frac{\sum_{j=1}^{j} t_{h,j}}{\sum_{j=1}^{j} N_{eq,j}} \times N_{ff} \tag{F-27}$$

The time to fatigue failure in this case is best represented as equivalent time to fatigue failure (ETFF, $t_{ff,eq}$), and the cycles to fatigue failure termed equivalent cycles to fatigue failure (ECFF, $N_{ff,eq}$).

The fatigue factor (FF) is the ratio between the numbers of cycles to fatigue failure at any point of engine operation to the numbers of cycles to fatigue failure at a reference point of engine operation. It could also be expressed in terms of time to fatigue failure. The fatigue factor is applicable to a given point of engine operation and is given by Equations (F-28) and (F-29),

$$Fatigue\ Factor\ (FF) = \frac{N_{ff}}{N_{ff,\mathrm{Re}f}} \tag{F-28}$$

$$Fatigue\ Factor\ (FF) = \frac{t_{ff}}{t_{ff,\mathrm{Re}f}} \tag{F-29}$$

$N_{ff,\mathrm{Re}f}$ and $t_{ff,\mathrm{Re}f}$ are the number of cycles to fatigue failure and the time to fatigue failure respectively at a reference engine operation point. For any time frame of engine operation, the equivalent fatigue factor (EFF) is used to characterize the engine operation, and it is given by Equations (F-30) and (F-31),

$$Equivalent\ Fatigue\ Factor\ (EFF) = \frac{N_{ff,eq}}{N_{ff,\mathrm{Re}f}} \tag{F-30}$$

$$Equivalent\ Fatigue\ Factor\ (EFF) = \frac{t_{ff,eq}}{t_{ff,\mathrm{Re}\,f}} \tag{F-31}$$

The equivalent cycles to fatigue failure $N_{ff,eq}$ and the equivalent time to fatigue failure $t_{ff,eq}$ is obtained for any time frame of engine operation. For a number of days of engine operation, the equivalent fatigue factor is expressed by Equations (F-32) and (F-33), presented in terms of cycles to failure and time to failure respectively,

$$EFF = \frac{N_{ff,eq}}{N_{ff,\mathrm{Re}\,f}} = \frac{1}{N_{ff,\mathrm{Re}\,f}} \times \frac{\sum_{j=1}^{j} N_{eq,j}}{\sum_{j=1}^{j}\sum_{i=1}^{n} \frac{\overline{N}_{j,i}}{N_{f\_j,i}}} \tag{F-32}$$

$$EFF = \frac{t_{ff,eq}}{t_{ff,\mathrm{Re}\,f}} = \frac{1}{t_{ff,\mathrm{Re}\,f}} \times \frac{\sum_{j=1}^{j} t_{h,j}}{\sum_{j=1}^{j}\sum_{i=1}^{n} \frac{\overline{N}_{j,i}}{N_{f\_j,i}}} \tag{F-33}$$

For any period of engine operation, the equivalent fatigue factors are as given by Equations (F-34) and E-35),

$$EFF = \frac{N_{ff,eq}}{N_{ff,\mathrm{Re}\,f}} = \frac{1}{N_{ff,\mathrm{Re}\,f}} \times \frac{N_{eq,a}}{\sum_{i=1}^{m} \frac{\overline{N}_a}{N_{f,i}}} \tag{F-34}$$

$$EFF = \frac{t_{ff,eq}}{t_{ff,\mathrm{Re}\,f}} = \frac{1}{t_{ff,\mathrm{Re}\,f}} \times \frac{\sum_{i=1}^{m} t_i}{\sum_{i=1}^{m} \frac{\overline{N}_a}{N_{f,i}}} \tag{F-35}$$

From the above relations, the fatigue life consumption at any point of engine operation could be estimated. The code written accepts data about engine operation on daily basis and estimates fatigue life consumption at any point of engine operation based on the available data fed to the system.

F.2 Creep-Fatigue Interaction Life Expressions

The creep-fatigue damage parameter at each point of engine operation is given by Equation (F-36),

$$D_{c+f,i} = D_{c,i} + D_{f,i} = \frac{t_i}{t_{f,i}} + \frac{N_i}{N_{f,i}} \qquad \text{(F-36)}$$

$D_{c,i}$ is the creep damage parameter, $D_{f,i}$ is the fatigue damage parameter, t_i is the time spent in each operation point, and N_i is the number of cycles experienced at each point of engine operation, usually expressed as the mean value ($\overline{N}_a$) for a given period of engine operation, and it is given by Equation (F-37),

$$N_i = \overline{N}_a = \frac{N_{eq,a}}{m} \qquad \text{(F-37)}$$

$N_{eq,a}$ is the equivalent fatigue cycles accumulated, and m is the number of engine operation points. The sum of the fatigue damage parameters for the period, denoted as $D_{c+f,s}$ is given by Equation (F-38),

$$D_{c+f,s} = \sum_{i=1}^{m} D_{c,i} + \sum_{i=1}^{m} D_{f,i} = \sum_{i=1}^{m} \frac{t_i}{t_{f,i}} + \sum_{i=1}^{m} \frac{\overline{N}_a}{N_{f,i}} \qquad \text{(F-38)}$$

Using the results of each point of engine operation, and following similar reasoning from Equations (F-5) to (F-7), the time to creep fatigue interaction failure $t_{f,c+f}$ is given by Equation (F-39),

$$t_{f,c+f} = \frac{t_i}{D_{c+f,i}} = \frac{t_i}{\frac{t_i}{t_{f,i}} + \frac{N_i}{N_{f,i}}} = \frac{t_i}{\frac{t_i}{t_{f,i}} + \frac{\overline{N}_a}{N_{f,i}}} \qquad \text{(F-39)}$$

In terms of cycles to failure $N_{f,c+f}$, the relation will be as given by Equation (F-40),

$$N_{f,c+f} = \frac{N_i}{D_{c+f,i}} = \frac{N_i}{\frac{t_i}{t_{f,i}} + \frac{N_i}{N_{f,i}}} \qquad \text{(F-40)}$$

From Equations (F-39) and (F-40), the time to creep-fatigue interaction failure and the number of cycles to creep-fatigue interaction failure obtained as given by Equation (F-41),

$$t_{f,c+f} = \frac{t_i}{N_i} \times N_{f,c+f} \tag{F-41}$$

Considering daily operation of the engine, the creep-fatigue damage parameter for each operation point is given by Equation (F-42),

$$D_{c+f,i} = D_{c,i} + D_{f,i} = \frac{t_i}{t_{f,i}} + \frac{\overline{N}_j}{N_{f,i}} \tag{F-42}$$

$\overline{N}_j$ is the mean value of the equivalent cycles evaluated per day of engine operation (the same for all operating points), and it is given by Equation (F-43),

$$\overline{N}_j = \frac{N_{eq,j}}{n} \tag{F-43}$$

In one day operation of the engine, the sum of the creep-fatigue damage parameters D_{c+f,d_1} (represented generally for each day as D_{c+f,d_j}) will be,

$$D_{c+f,d\_j} = \sum_{i=1}^{n} D_{c,i} + \sum_{i=1}^{n} D_{f,i} = \sum_{i=1}^{n} \frac{t_i}{t_{f,i}} + \sum_{i=1}^{n} \frac{\overline{N}_j}{N_{f,i}} \tag{F-44}$$

$$D_{c+f,d\_1} = \sum_{i=1}^{n} D_{c,i} + \sum_{i=1}^{n} D_{f,i} = \sum_{i=1}^{n} \frac{t_i}{t_{f,i}} + \sum_{i=1}^{n} \frac{\overline{N}_1}{N_{f,i}} \tag{F-45}$$

Based on the results of one day operation of the engine, the number of days to creep-fatigue failure $t_{f,c+f\_d}$ is given by Equation (F-46),

$$t_{f,c+f\_d} = \frac{1}{D_{c+f,d\_1}} = \frac{1}{\sum_{i=1}^{n} \frac{t_i}{t_{f,i}} + \sum_{i=1}^{n} \frac{\overline{N}_1}{N_{f,i}}} \tag{F-46}$$

If the engine is operated for t_h hours per day, the time to fatigue failure in hours $t_{f,c+f\_h}$ based on day 1 data is given by Equation (F-47),

$$t_{f,c+f\_h} = t_{f,c+f\_d} \times t_h = \frac{t_h}{\sum_{i=1}^{n} \frac{t_i}{t_{f,i}} + \sum_{i=1}^{n} \frac{\overline{N}_1}{N_{f,i}}} \tag{F-47}$$

In terms of fatigue cycles to failure $N_{f,c+f}$, Equation (F-47) will take the form of Equation (F-48),

$$N_{f,c+f} = \frac{N_{eq,1}}{D_{c+f,d\_1}} = \frac{N_{eq,1}}{\sum_{i=1}^{n} \frac{t_i}{t_{f,i}} + \sum_{i=1}^{n} \frac{\overline{N}_1}{N_{f,i}}} \qquad \text{(F-48)}$$

The time to creep-fatigue failure relates with the cycles to creep-fatigue failure as given by Equations (F-49) and (F-50),

$$t_{f,c+f\_d} = \frac{1}{N_{eq,1}} \times N_{f,c+f} \qquad \text{(F-49)}$$

$$t_{f,c+f\_d} = \frac{t_h}{N_{eq,1}} \times N_{f,c+f} \qquad \text{(F-50)}$$

Considering a number of days of engine operation, say j days, the total or equivalent creep-fatigue damage parameter, denoted as D_{c+f,s_j} is given in by Equation (F-51),

$$D_{c+f,s\_j} = \sum_{j=1}^{j} \left(\sum_{i=1}^{n} \frac{t_{j,i}}{t_{f\_j,i}} + \sum_{i=1}^{n} \frac{\overline{N}_{j,i}}{N_{f\_j,i}} \right) \qquad \text{(F-51)}$$

$t_{f\_j,i}$ is the time to failure for the j^{th} day and at the i^{th} operation point, and $t_{j,i}$ is the time spent at the i^{th} operation point for the j^{th} day. The time to creep-fatigue interaction failure in days based on the data for the j days of engine operation is given by Equation (F-52),

$$t_{f,c+f\_d} = \frac{j}{D_{c+f,s\_j}} = \frac{j}{\sum_{j=1}^{j} \left(\sum_{i=1}^{n} \frac{t_{j,i}}{t_{f\_j,i}} + \sum_{i=1}^{n} \frac{\overline{N}_{j,i}}{N_{f\_j,i}} \right)} \qquad \text{(F-52)}$$

In terms of hours to failure, the relation is as given by Equation (F-53),

$$t_{f,c+f\_h} = \frac{\sum_{j=1}^{j} t_{h,j}}{\sum_{j=1}^{j} \left(\sum_{i=1}^{n} \frac{t_{j,i}}{t_{f\_j,i}} + \sum_{i=1}^{n} \frac{\overline{N}_{j,i}}{N_{f\_j,i}} \right)} \qquad \text{(F-53)}$$

$t_{h,j}$ is the time the engine was operated for the j^{th} day. In terms of cycles to failure, Equation (F-53) takes the form of Equation (F-54),

$$N_{f,c+f} = \frac{\sum_{j=1}^{j} N_{eq,j}}{\sum_{j=1}^{j}\left(\sum_{i=1}^{n}\frac{t_{j,i}}{t_{f\_j,i}} + \sum_{i=1}^{n}\frac{\overline{N}_{j,i}}{N_{f\_j,i}}\right)} \quad \text{(F-54)}$$

The time to fatigue creep-failure and the cycles to creep-fatigue failure are related as given by Equation (F-55),

$$t_{f,c+f\_h} = \frac{\sum_{j=1}^{j} t_{h,j}}{\sum_{j=1}^{j} N_{eq,j}} \times N_{f,c+f} \quad \text{(F-55)}$$

For a given time frame of engine operation other than a single engine operation point, the time to creep- fatigue failure and the cycles to creep-fatigue failure best referred to as the equivalent time to creep-fatigue failure (ETCFF, $t_{f,c+f\_eq}$) and equivalent cycles to creep fatigue failure (ECCFF, $N_{f,c+f\_eq}$) respectively. For any period of engine operation, using Equation (F-38), the equivalent time to creep-fatigue failure and the equivalent cycles to creep-fatigue failure are given respectively by Equations (F-56) and (F-57),

$$t_{f,c+f\_eq} = \frac{\sum_{i=1}^{m} t_i}{D_{c+f,s}} = \frac{\sum_{i=1}^{m} t_i}{\sum_{i=1}^{m}\frac{t_i}{t_{f,i}} + \sum_{i=1}^{m}\frac{\overline{N}_a}{N_{f,i}}} \quad \text{(F-56)}$$

$$t_{f,c+f\_eq} = \frac{\sum_{i=1}^{m} \overline{N}_a}{D_{c+f,s}} = \frac{\sum_{i=1}^{m} \overline{N}_a}{\sum_{i=1}^{m}\frac{t_i}{t_{f,i}} + \sum_{i=1}^{m}\frac{\overline{N}_a}{N_{f,i}}} \quad \text{(F-57)}$$

The creep-fatigue interaction factor is used to assess the severity of engine operation under creep-fatigue interaction life consumption. It is the ratio of the time to creep-fatigue failure for a given time frame of engine operation to the time to creep-fatigue failure for a reference condition of engine operation. It could be defined in terms of the cycles to failure. For a single point of engine operation, the relation is given by Equations (F-58) and (F-59) for time to failure and cycles to failure respectively:

$$CFF = \frac{t_{f,c+f}}{t_{f,c+f\_\mathrm{Re}f}} \tag{F-58}$$

$$CFF = \frac{N_{f,c+f}}{N_{f,c+f\_\mathrm{Re}f}} \tag{F-59}$$

CFF is the creep-fatigue interaction factor or creep-fatigue factor for short, $t_{f,c+f\_\mathrm{Re}f}$ and $N_{f,c+f\_\mathrm{Re}f}$ are time to creep-fatigue failure and the cycles to creep-fatigue failure at a reference point. Substituting for the time to creep-fatigue failure and the cycles to creep-fatigue failure respectively in Equations (F-58) and (F-59), the relations are as given by Equations (F-60) and (F-61),

$$CFF = \frac{t_{f,c+f}}{t_{f,c+f\_\mathrm{Re}f}} = \frac{1}{t_{f,c+f\_\mathrm{Re}f}} \times \frac{t_i}{\frac{t_i}{t_{f,i}} + \frac{N_i}{N_{f,i}}} \tag{F-60}$$

$$CFF = \frac{N_{f,c+f}}{N_{f,c+f\_\mathrm{Re}f}} = \frac{1}{N_{f,c+f\_\mathrm{Re}f}} \times \frac{N_i}{\frac{t_i}{t_{f,i}} + \frac{N_i}{N_{f,i}}} \tag{F-61}$$

For any time frame of engine operation, in days or any given period of engine operation, the equivalent creep-fatigue factor (ECFF) is used to characterize the engine operation, and it is given by Equations (F-62) and (F-63),

$$ECFF = \frac{t_{f,c+f\_eq}}{t_{f,c+f\_\mathrm{Re}f}} \tag{F-62}$$

$$ECFF = \frac{N_{f,c+f\_eq}}{N_{f,c+f\_\mathrm{Re}f}} \tag{F-63}$$

Here, the equivalent time to creep-fatigue failure replaces the time to creep-fatigue failure for a given time frame of engine operation, while the equivalent cycles to creep-fatigue failure replaces the cycles to creep-fatigue failure. For a day of engine operation, the equivalent creep-fatigue factor is given by Equations (F-64) and (F-65)

$$ECFF = \frac{t_{f,c+f\_eq}}{t_{f,c+f\_\mathrm{Re}f}} = \frac{1}{t_{f,c+f\_\mathrm{Re}f}} \times \frac{t_h}{\sum_{i=1}^{n} \frac{t_i}{t_{f,i}} + \sum_{i=1}^{n} \frac{\overline{N}_1}{N_{f,i}}} \tag{F-64}$$

$$ECFF = \frac{N_{f,c+f\_eq}}{N_{f,c+f\_\mathrm{Re}f}} = \frac{1}{N_{f,c+f\_\mathrm{Re}f}} \times \frac{N_{eq,1}}{\sum_{i=1}^{n} \frac{t_i}{t_{f,i}} + \sum_{i=1}^{n} \frac{\overline{N}_1}{N_{f,i}}} \quad \text{(F-65)}$$

For a number of days of engine operation, the equivalent creep-fatigue factor is expressed by Equations (F-66) and (F-67), presented in terms of time to failure and cycles to failure respectively,

$$ECFF = \frac{t_{f,c+f\_eq}}{t_{f,c+f\_\mathrm{Re}f}} = \frac{1}{t_{f,c+f\_\mathrm{Re}f}} \times \frac{\sum_{j=1}^{j} t_{h,j}}{\sum_{j=1}^{j} \left(\sum_{i=1}^{n} \frac{t_{j,i}}{t_{f\_j,i}} + \sum_{i=1}^{n} \frac{\overline{N}_{j,i}}{N_{f\_j,i}} \right)} \quad \text{(F-66)}$$

$$ECFF = \frac{N_{f,c+f\_eq}}{N_{f,c+f\_\mathrm{Re}f}} = \frac{1}{N_{f,c+f\_\mathrm{Re}f}} \times \frac{\sum_{j=1}^{j} N_{eq,j}}{\sum_{j=1}^{j} \left(\sum_{i=1}^{n} \frac{t_{j,i}}{t_{f\_j,i}} + \sum_{i=1}^{n} \frac{\overline{N}_{j,i}}{N_{f\_j,i}} \right)} \quad \text{(F-67)}$$

For any period of engine operation, the equivalent creep-fatigue factors are as given by Equations (F-68) and E-69),

$$ECFF = \frac{t_{f,c+f\_eq}}{t_{f,c+f\_\mathrm{Re}f}} = \frac{1}{t_{f,c+f\_\mathrm{Re}f}} \times \frac{\sum_{i=1}^{m} t_i}{\sum_{i=1}^{m} \frac{t_i}{t_{f,i}} + \sum_{i=1}^{m} \frac{\overline{N}_a}{N_{f,i}}} \quad \text{(F-68)}$$

$$ECFF = \frac{N_{f,c+f\_eq}}{N_{f,c+f\_\mathrm{Re}f}} = \frac{1}{N_{f,c+f\_\mathrm{Re}f}} \times \frac{\sum_{i=1}^{m} \overline{N}_a}{\sum_{i=1}^{m} \frac{t_i}{t_{f,i}} + \sum_{i=1}^{m} \frac{\overline{N}_a}{N_{f,i}}} \quad \text{(F-69)}$$

Relationship between the life analysis factors

The creep-fatigue fatigue at a single engine operation point using cycles to failure is given by Equation (F-61), and presented below in Equation (F-70),

$$CFF = \frac{N_{f,c+f}}{N_{f,c+f\_\mathrm{Re}f}} = \frac{1}{N_{f,c+f\_\mathrm{Re}f}} \times \frac{N_i}{\frac{t_i}{t_{f,i}} + \frac{N_i}{N_{f,i}}} \quad \text{(F-70)}$$

Knowing that $t_{f,i} = CF \times t_{f,\mathrm{Re}f}$ and $N_{f,i} = FF \times N_{f,\mathrm{Re}f}$, and making the necessary substitutions to Equation (F-70) and simplifying, we obtain the relation between the three life analysis factors at each engine operation point as,

$$CFF = \frac{N_i}{N_{f,c+f\_\mathrm{Re}f}} \times \frac{CF \times FF \times t_{f,\mathrm{Re}f} \times N_{f,\mathrm{Re}f}}{(FF \times N_{f,\mathrm{Re}f} \times t_i) + (CF \times t_{f,\mathrm{Re}f} \times N_i)} \qquad \text{(F-71)}$$

In terms of time to failure, the relationship between the life analysis factors will be in the form given by Equation (F-72),

$$CFF = \frac{t_i}{t_{f,c+f\_\mathrm{Re}f}} \times \frac{CF \times FF \times t_{f,\mathrm{Re}f} \times N_{f,\mathrm{Re}f}}{(FF \times N_{f,\mathrm{Re}f} \times t_i) + (CF \times t_{f,\mathrm{Re}f} \times N_i)} \qquad \text{(F-72)}$$

At the reference point, the time to creep-fatigue failure is given by Equation (F-73),

$$t_{f,c+f\_\mathrm{Re}f} = \frac{t_i}{D_{f,c+f\_\mathrm{Re}f}} = \frac{t_i}{\frac{t_i}{t_{f,\mathrm{Re}f}} + \frac{N_i}{N_{f,\mathrm{Re}f}}} \qquad \text{(F-73)}$$

Simplifying,

$$t_{f,c+f\_\mathrm{Re}f} = \frac{t_i \times t_{f,\mathrm{Re}f} \times N_{f,\mathrm{Re}f}}{t_i \times N_{f,\mathrm{Re}f} + N_i \times t_{f,\mathrm{Re}f}} \qquad \text{(F-74)}$$

Substituting the value of $t_{f,c+f\_\mathrm{Re}f}$ in Equation (F-72) and simplifying, the relationship between the life analysis factors is gotten as in Equation (F-75),

$$CFF = CF \times FF \times \frac{t_i \times N_{f,\mathrm{Re}f} + N_i \times t_{f,\mathrm{Re}f}}{(FF \times N_{f,\mathrm{Re}f} \times t_i) + (CF \times t_{f,\mathrm{Re}f} \times N_i)} \qquad \text{(F-75)}$$

The relation between the life analysis factors holds for complicated engine operation process.

APPENDIX G : Input Data for Life Analysis

The input data for the life analysis is presented here. These include the blade parameters setting data, data for creep life estimation setting, especially the data about the Larson-Miller Parameter Master Curve of the blade material, data for fatigue life estimation setting, and some material properties. For material data that depends on temperature, a single value will be given here usually at 25^{o}C, but in the program, the data is supplied in the form of a table and interpolations are carried out to read the required value against the temperature. Any data that has to do with blade material properties and blade geometry, only approximate values are given, besides, not all parameters are presented here for the reason that the author does not have the right to publish the actual data. For blade geometry where dimensions are provided, values at the blade root, blade tip and blade mean section are given in most of the cases.

G.1 Blade Parameters Setting Data

Table G.1 presents approximate values of some of the data used in the blade parameters setting form (window) presented in Appendix A and some blade material properties.

Table G.1: Some Input Data for Blade Setting and Blade Material Properties

SN.	Parameter	Unit	Value
1.	Number of Blades	-	81
2.	Number of stages	-	2
3.	NGV coolant effectiveness	-	0.55
4.	NGV coolant mas fraction	-	0.4
5.	NGV pressure recovery	-	0.99
6.	Rotor coolant mass fraction	-	0.6
7.	LE tip radius	m	0.17599
8.	LE root radius	m	0.10339
9.	TE tip radius	m	0.17565
10.	TE root radius	m	0.10329
	Blade cross-sectional area at:		
11.	- Blade tip	m^2	1.7863×10^{-5}
12.	- Blade mean section	m^2	2.8103×10^{-5}
13.	- Blade root	m^2	5.8173×10^{-5}

Table G.1- Continuation

	Blade angles at:		
14.	- Rotor tip exit	deg.	61
15.	- Rotor mean exit	deg.	60
16.	- Rotor root exit	deg.	59
17.	Stagger angle at blade root	deg.	21
18.	Stagger angle at blade mean section	deg.	33
19.	Shaft speed at engine model design point	rpm	9780
20.	Radial temperature distribution factor	-	0.12
21.	Blade chord at tip	m	0.0340
22.	Blade chord at mean section	m	0.0345
23.	Blade chord at root	m	0.0350
24.	Blade perimeter at tip	m	0.042
25.	Blade perimeter at mean section	m	0.045
26.	Blade perimeter at root	m	0.049
27.	Thickness of thermal barrier coating	m	0.0002
28.	Thermal conductivity of thermal barrier coating	W/m.K	1.56
	Blade Material Properties		
29.	Density	kg/m^3	7800
30.	Ultimate tensile strength	MN/m^2	515
31.	Young's modulus	MN/m^2	190,000-210.000
32.	True fracture ductility	-	0.9938

G.2 Larson-Miller parameter Master Curve

The Larson-Miller parameter curve of the blade material is presented in Figure G.1. In the program, numerical data is used. Thus, effort is being made to extract data from the curve and make extrapolation to obtain data not covered by the curve. The data fit into a polynomial of order 3 given by Equation (G-1) with $R^2 = 0.9998$.

$$y = -4\times10^{-8}x^3 + 6\times10^{-5}x^2 - 0.0502x + 56.291 \qquad \text{(G-1)}$$

In Equation (G-1), x represents the stress value and y stands for the LMP value. The LMP value depends on the stress value and it decreases with increase in stress value. The numerical data extracted from the curve is presented in Table G.2. The Larson-Miller parameter constant C of the material is 20.

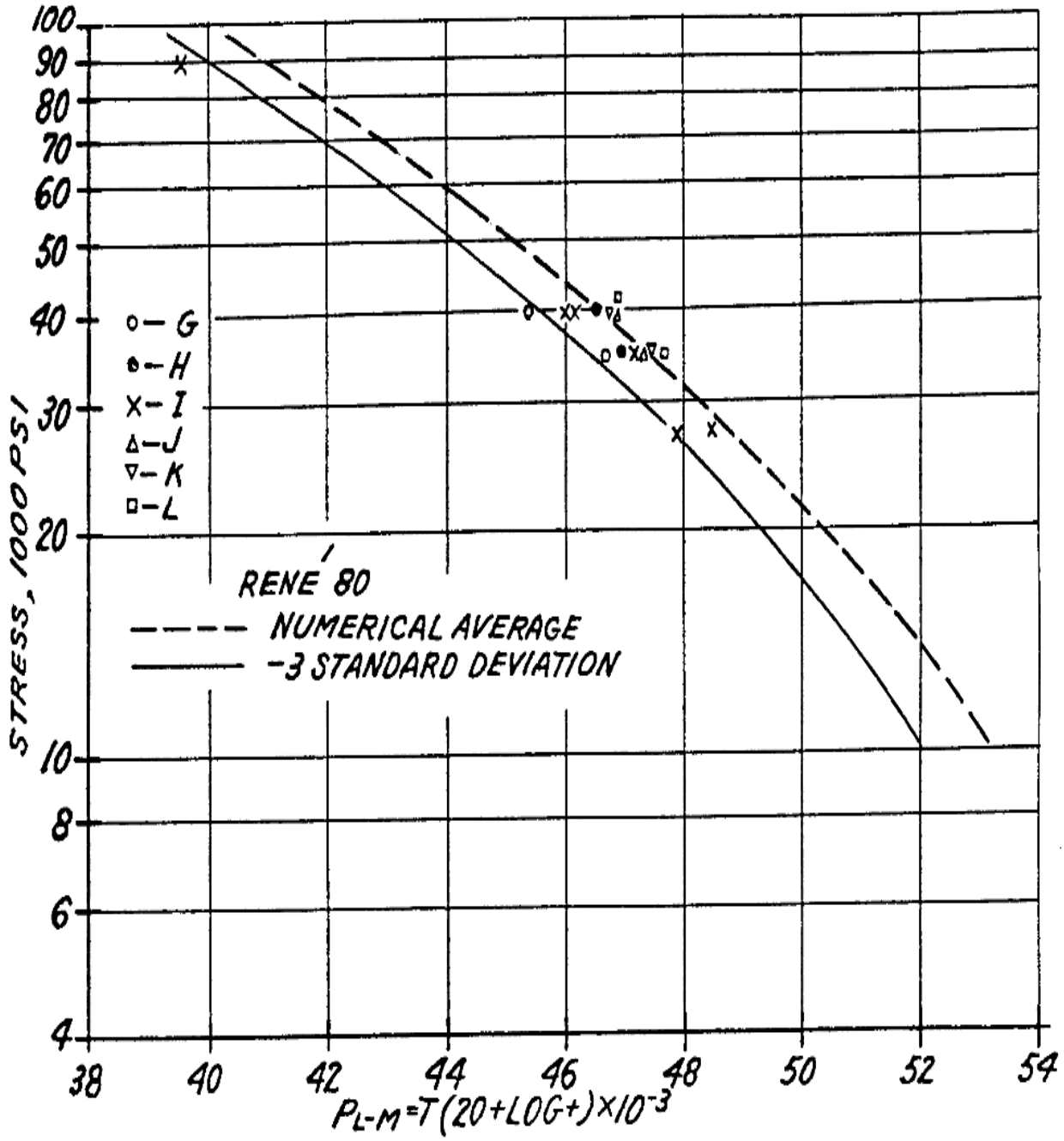

Figure G.1: LMP Master Curve of Blade Material [207]

Table G.2: LMP Values Generated from LMP Master Curve

SN.	Stress [MPa]	LMP Value [-]
1	50	53.92600
2	70	53.05728
3	90	52.22984
4	110	51.44176
5	130	50.69112
6	150	49.97600
7	170	49.29448
8	190	48.64464
9	210	48.02456
10	230	47.43232
11	250	46.86600
12	270	46.32368
13	290	45.80344
14	310	45.30336
15	330	44.82152
16	350	44.35600
17	370	43.90488
18	390	43.46624
19	410	43.03816
20	430	42.61872
21	450	42.20600
22	470	41.79808
23	490	41.39304
24	510	40.98896
25	530	40.58392
26	550	40.17600
27	570	39.76328
28	590	39.34384
29	610	38.91576
30	630	38.47712
31	650	38.02600
32	670	37.56048
33	690	37.07864
34	710	36.57856
35	730	36.05832
36	750	35.51600
37	770	34.94968
38	790	34.35744
39	810	33.73736
40	830	33.08752